Titre: Title:	Optimization of antioxidant additives in carbon-containing castables
Auteur: Author:	Huiqing He
Date:	2002
Type:	Mémoire ou thèse / Dissertation or Thesis
Référence: Citation:	He, H. (2002). Optimization of antioxidant additives in carbon-containing castables [Thèse de doctorat, École Polytechnique de Montréal]. PolyPublie. https://publications.polymtl.ca/7049/

UNIVERSITÉ DE MONTRÉAL

OPTIMIZATION OF ANTIOXIDANT ADDITIVES IN CARBON-CONTAINING CASTABLES

HUIQING HE

DÉPARTEMENT DE MATHÉMATIQUES APPLIQUÉES

ET DE GÉNIE INDUSTRIEL

ÉCOLE POLYTECHNIQUE DE MONTRÉAL

THÈSE PRÉSENTÉE EN VUE DE L'OBTENTION

DU DIPLÔME DE PHILOSOPHIAE DOCTOR (Ph.D.)

(GÉNIE MÉTALLURGIQUE)

AVRIL 2002

UNIVERSITÉ DE MONTRÉAL

ÉCOLE POLYTECHNIQUE DE MONTRÉAL

Cette thèse intitulée:

OPTIMIZATION OF ANTIOXIDANT ADDITIVES IN CARBON-CONTAINING CASTABLES

Présentée par: HE Huiqing

En vue de l'obtention du diplôme de: Philosophiae Doctor

A été dûment acceptée par le jury d'examen constitué de:

Mr. ALLAIRE, Claude. Ph.D., président

Mr. RIGAUD, Michel. D.Sc.A., membre et directeur de recherche

Mr. AJERSCH, Frank. Ph.D., membre

Mr. MOSTAGHACI, Hamid. Ph.D., membre

ACKNOWLEDGEMENTS

I would like to express my sincere gratitude to my supervisor, Prof. Michel Rigaud for his expert guidance, valuable advice and constructive criticism throughout this work. I really appreciate his constant support and encouragement during this Ph.D. program at École Polytechnique de Montréal.

I sincerely thank Dr. Claud Allaire, chairman of the jury, Dr. Ajersch, Frank and Dr. Mostaghaci, Hamid, members of the jury, and for their constructive feedbacks on this thesis.

I gratefully acknowledge Prof. Nan Li for his constant encouragement and enlightening advice and Prof. Gongquan Yuan for his kindly allowing me study at CIREP.

Special thanks go to Dr. S. Palco for his valuable help on microscopy observation and discussion, to Mr. V. Kovac for his kindly support on experimental set-up and some sample preparation, and to Dr. E. Paransky for his aid with SEM analysis. Grateful thanks also go to my colleagues at CIREP, Prof. C. Allaire, Dr. S. Afshar, Dr. Z. Guo, Dr. N. Zhou, Dr. X. Cheng, Dr. C. Feng, Dr. R. Pelletier, E. Divry, E. Planque, N. Ntakaburimvo, Dr. J. Sebbani, C. Gaubert, E. Kosc, M. Zhang, J. Gao and X. Zhou for their friendship and helpful discussion.

My particular thanks are due to J. P. Bouchard and H. Rioux at CIREP for their technical and secretarial helps.

Finally, I would like to express my deepest appreciation to my parents, my husband and my son for their love, sacrifice, encouragement and constant support.

RÉSUMÉ

Les bétons réfractaires contenant du carbone sont de plus en plus considérés au niveau de leur utilisation commerciale. L'oxydation du carbone demeure un des inconvénients majeurs, d'autant plus que les bétons sont de façon inhérente plus poreux que les briques à liaison carbone, de composition équivalente. Il est donc impérieux d'améliorer la résistance à l'oxydation de ces bétons pour qu'ils soient performants au point de vue corrosion, pénétration et résistance aux chocs thermiques, lorsqu'on vise à les utiliser dans les poches d'aciers. Les bétons à base de magnésie devant avoir a priori une bonne tenue à la ligne de laitier dans de telles poches, ont été retenus comme système à étudier dans cette thèse. Surmonter les difficultés inhérentes à l'insertion de paillettes de graphite naturel dans ces bétons et protéger ce carbone contre l'oxydation ont constitué les deux buts principaux de ce travail.

Deux catégories de bétons à base de magnésie et de graphite ont été élaborées : une avec une liaison spinelle dans le système $MgO\text{-}MgAl_2O_4\text{-}C$ et l'autre avec une liaison forsterite dans le système $MgO\text{-}Mg_2SiO_4\text{-}C$. Plus de quarante compositions différentes ont été caractérisées en termes de coulabilité, eau de gâchage, temps de prise, propriétés physiques et mécaniques, distribution des pores et bien sûr résistance à l'oxydation. Ce dernier aspect a été considéré comme le plus important.

Il a été démontré que les facteurs importants pour minimiser l'oxydation du carbone dans ces bétons sont: la nature de la source de carbone, les antioxydants utilisés et la densité des matériaux en fonction de la température d'utilisation. L'optimisation de la résistance à l'oxydation a été menée en sélectionnant la source de carbone adéquate, en agglomérant les paillettes de graphite, en utilisant des ensembles d'antioxydants répartis uniformément et un défloculant approprié ainsi que des fines de magnésie et des fines de carbone, de façon à maximiser la densité des bétons.

Il découle de ce travail et des résultats obtenus sur l'ensemble des bétons que :

1. La méthode d'insertion du graphite dans les bétons joue un rôle décisif. Les bétons avec des agglomérats de graphite obtenus par extrusion (EG) et par revêtement (CG) sont plus performants, car ils exigent une quantité d'eau de gâchage moindre, avec des pores plus petits, une densité accrue après séchage des modules de rupture à froid (CMOR) et une résistance aux chocs thermiques et à l'oxydation nettement supérieures en rapport avec des bétons contenant des paillettes non traitées.

2. En agglomérant le graphite, tout en incorporant dans ces agglomérats des antioxydants et des oxydes de support dans les micro-boulettes extrudées (EG), ceci améliore la densification, la distribution porosimétrique, favorise la formation de composés intermédiaires et améliore leur résistance à l'oxydation.

Il a été utile d'optimaliser la composition de micro-boulettes pour les 2 catégories de bétons MgO-MA-C et MgO-M_2S-C, à partir d'une quinzaine d'essais différents. Avec les additions d'antioxydants appropriées, le diamètre médian des pores est passé de 8.75 µm dans les micro-boulettes sans additif (EG-O), à 2.26-1.13 µm pour les micro-boulettes $(EG\text{-}AO)_{MA}$ et 4.93-0.5 µm pour les micro-boulettes $(EG\text{-}AO)_{MS}$. Ces 2 types de micro-boulettes ont certes une résistance à l'oxydation mesurée, supérieure à celle du type EG-O.

Les micro-boulettes les plus performantes sont constituées de 80 % de graphite, 15 % d'alumine et 5 % de B_4C pour les bétons à liaison spinelle ; pour les bétons à liaison forsterite, mieux vaut utiliser des micro-boulettes contenant 80 % de graphite et 20 % de silicium ou 80 % de graphite et 20 % de carbone de silicium.

3. Les antioxydants sont efficaces tant en insertion dans les micro-boulettes que finement dispersés dans la matrice des bétons. L'addition d'aluminium directement dans les bétons pose problème. Selon les résultats de ce travail, il est essentiel d'utiliser la majorité de l'aluminium dans les micro-boulettes plutôt que dans la matrice. Il est préférable, dans tous les cas, d'ajouter des antioxydants dans les agglomérats de graphite et simultanément dans la partie matrice des mélanges des bétons. L'utilisation du B_4C en synergie avec l'aluminium réduit très efficacement la porosité et favorise la formation de spinelle. Il est ainsi possible de freiner grandement l'intrusion de l'oxygène et donc d'améliorer la résistance à l'oxydation

des bétons M-MA-C. Pour les bétons M-M_2S-C, les micro-boulettes contenant du Si ou du SiC sont les plus recommandables.

4. Les antioxydants améliorent non seulement la résistance à l'oxydation des bétons contenant du carbone, mais aussi les propriétés mécaniques et ce, pour les 2 catégories de bétons.

5. Il a été possible d'obtenir des bétons à base de magnésie, contenant 90 % de MgO, sans ciment, avec 6 % de graphite, 1 à 2 % d'antioxydants, 5.3 à 6.5 % d'eau, ayant les caractéristiques suivantes : densité 2.70 à 2.80 g/cm^3 après séchage à 110 °C, 2.70 à 2.71 g/cm^3 après cuisson à 1500 °C, porosité apparente 10-14 % (110 °C), 17-18 % (1500 °C), module de rupture à froid 5 à 15 MPa (110 °C), 6-12 MPa (1500 °C), variation dimensionnelle ± 0.5 % (1500 °C) MgO-M_2S-C, < 1.5 % (1500 °C) MgO-MA-C.

6. Pour obtenir de telles caractéristiques, il convient d'utiliser une combinaison de défloculants (de l'hexameta-phosphate de sodium, du galoryl et du citrate de sodium). La taille des fines de magnésie utilisée influence la décroissance de la coulabilité dans le temps. Il est essentiel d'ajuster la granulométrie des fines pour obtenir une bonne ouvrabilité dans tous les bétons.

7. Des deux systèmes étudiés, le système MgO-M_2S-C semble le mieux approprié pour bien concilier l'ouvrabilité et la stabilité dimensionnelle des bétons, à un niveau commercial.

ABSTRACT

Carbon containing castables attract considerable attentions and their economic potentials can be contemplated. Oxidation of carbon is a major drawback for oxide-carbon composite refractories, especially for a castable which is inherently more porous than a brick. It is imperative to maximize the oxidation resistance in every case for high performance of castables with high corrosion, penetration and thermal shock resistance, for steelmaking ladles. Magnesia-based material system hold a potential to be used in slag line of steelmaking ladles due to their high corrosion resistance to basic slag and are chosen as the material of study in this thesis. Overcoming the difficulties of introducing flake graphite into such castables and of protecting it from oxidation have constituted the principal goals of this work.

Two magnesia-based carbon containing castable systems have been elaborated: a magnesia spinel carbon system (spinel-bonded MgO-MA-C system) and a magnesia forsterite carbon system (forsterite-bonded MgO-M_2S-C system). Over 40 castable mixes have been studied in terms of their flowability, water addition, flow decay, physical and mechanical properties, pore size distribution and oxidation resistance. The study is nevertheless mainly concentrated on the oxidation behaviour.

The results have demonstrated that important factors to minimize oxidation of carbon-containing castables are the nature of carbon source, the antioxidants and the densification of the materials. The optimization of the oxidation resistance of magnesia-based carbon containing castables has been conducted through selecting carbon source, modifying flake graphite characteristics, optimizing antioxidant additives in terms of distribution, addition and combination and densifying the structure of the material using proper deflocculant, magnesia fine, suitable binder and carbon source.

In this thesis it has been shown that:

1) The mode of incorporating flake graphite into castables plays a decisive role in developing graphite containing castables. Modified flake graphite pellets by extruding (EG) and coating (CG) efficiently reduce water addition and pore size, increasing bulk density, CMOR, thermal shock parameter and oxidation resistance of the castables. Coated graphite and extruded graphite pellets exhibit better overall properties than granulated pellets (GG) in castables.

2) Packaging natural flake graphite by incorporating antioxidants and oxide fillers into extruded graphite pellets sufficiently improve densification, pore size distribution, new compound formations and oxidation resistance of the pellets.

Optimization of extruded pellets has been achieved with totally 15 different graphite pellets for two castable systems: MgO-MA-C system and MgO-M_2S-C system. The pore sizes of $(EG\text{-}A.O.)_{MA}$ and $(EG\text{-}A.O.)_{MS}$ pellets are effectively reduced through incorporating antioxidant packages into the pellets as compared to the EG pellets without any additive (EG-0). Median pore diameters of the pellets are reduced from 8.75μm for EG-0 to 2.26-1.13μm for $(EG\text{-}A.O.)_{MA}$ and to 4.93-0.50μm for $(EG\text{-}A.O.)_{MS}$. Smaller pores have higher resistance to gaseous oxygen inward diffusion and contribute to higher oxidation resistance.

The best EG pellets for the MgO-MA-C system contains 80% graphite, 15% Al_2O_3 and 5% B_4C or 80% graphite, 15%Al and 5% B_4C. The best EG pellets for the MgO-M_2S-C system contains 80% graphite and 20% Si or 80% graphite and 20% SiC.

3) Specific antioxidants sufficiently improve oxidation resistance both locally in extruded graphite pellets and overall in the matrix of the castables. The consequences of using straight aluminium powder in castables have been documented. Based upon our findings it is more appropriate to use aluminium buried in EG pellets and a minimum amount into the castable matrix part. The combination of antioxidants in the pellets and the matrix exhibits the best oxidation resistance. Furthermore, boron carbide in combination with metallic aluminium effectively reduces pore size and promotes dense spinel layer formation. Thus, oxygen inward diffusion can be sufficiently inhibited, and

oxidation resistance is effectively improved as described for the sample EG-AB pellets and MCA1B1 matrix sample and A2B05 in castable. In the forsterite system, antioxidant Si and SiC perform well in increasing oxidation resistance and exhibit better result in the recommended combination to protect the carbon from oxidation.

4) The antioxidants not only protect graphite from oxidation but also improve the mechanical properties of the EG pellets and the castables, with either spinel or forsterite bonding. Antioxidant packaging, controlling the nature, the amount and the distribution of the antioxidants in EG pellets and the matrix, has a pronounced influence on final properties of the materials.

5) It is possible to obtain MgO-based graphite-containing castables with high magnesia content up to 90% MgO, cement free, 6% of carbon, 1 to 2% metallic antioxidants with following promising properties, depending upon the system:

Water addition: 5.3 to 6.5%

Bulk density: 2.70-2.80g/cm^3 (110°C), 2.70-2.77g/cm^3 (1500°C)

Apparent porosity: 10-14% (110°C), 17-18% (1500°C)

Cold modulus of rupture: 5-15MPa (110°C), 6-12 MPa (1500°C)

Permanent linear change: (1500°C): ±0.5% (MgO-M_2S-C system)

< 1.5% (MgO-MA-C system)

6) To achieve such performances in MgO-M_2S-C system, the deflocculants used are a combination of sodium hexametaphosphate (S6P), Galoryl (G) and sodium dihydrogencitrate (SD). Flow decay needs to be considered as an important factor influencing workability of the castables. The size of magnesia fine influences flow-decay strongly. The finer the magnesia, the faster the flow-decay is. The proper combination of different magnesia fines provides an acceptable workability.

7) Among the two systems tested, the MgO-M_2S-C system seems to be the most promising to optimize, taking into consideration the hydration resistance of magnesia fines in the two systems, the workability and the permanent linear change of the castable mixes.

CONDENSÉ

Cette thèse porte sur les travaux qui ont été menés en vue d'optimiser les stratégies pour améliorer la résistance à l'oxydation de bétons à haute teneur en magnésie, sans ciment mais avec des liants hydratables, contenant du carbone et en particulier du graphite.

Ces travaux ont été amorcés il y a déjà trois ans en vue de contribuer à la mise au point de bétons « coulables » qui pourront éventuellement servir à remplacer des briques de magnésie carbone, à la ligne de laitier, dans les poches de coulée et les fours-poches, dans les aciéries. Du succès de cette entreprise dépend le futur des monolithiques en tant que matériaux de pointe dans les sidérurgies. L'enjeu principal, c'est qu'en mettant au point un tel produit, on puisse alors songer à garnir toutes les poches d'aciéries avec des bétons coulés, pompés ou projetés, et remplacer ainsi les garnissages faits de briques (solution actuelle). C'est la mise au point de tels bétons performants à la ligne de laitier qui retarde cet avènement.

Les premiers travaux sur les bétons réfractaires à base d'alumine-magnésie puis à base de magnésie avec addition d'alumine ont vite révélé le manque de performance dans la zone de laitier d'une poche, contenant des laitiers basiques classiques même peu oxydés ou des laitiers à base d'aluminate de chaux. Les premiers bétons sont trop susceptibles à la corrosion-dissolution, les bétons à base de magnésie le sont à la pénétration suivie de l'écaillage structural. Il était clair depuis longtemps qu'il faudrait pouvoir ajouter du

carbone dans ces bétons. Les premiers travaux en ce sens, effectués au Japon, avaient révélé que l'addition de paillettes de graphite conduisait à un cul-de-sac, car l'eau de gâchage nécessaire dans ce cas s'élevait à 8 à 10 % poids, ce qui est catastrophique une fois traduit en terme de porosité apparente. D'autres carbones ont pu être utilisés, mais leur résistance à l'oxydation est nettement déficiente par rapport à celle du graphite naturel. C'est alors qu'une première génération de micro-boulettes de graphite a été réalisée au CIREP, sous l'impulsion de MM. M. Kandel, N.S. Zhou et M. Rigaud (1). Les premiers essais industriels ont à leur tour révélé que malgré les progrès réalisés, il serait essentiel d'améliorer la résistance à l'oxydation de ces bétons. C'est dans ce contexte que les travaux de la présente thèse ont été entamés.

Au total, au-delà de 40 compositions différentes ont été testées. Ces bétons peuvent être divisés d'abord en deux catégories : des bétons de magnésie avec liant de silice colloïdale à température ambiante et développant des liens de forsterite après cuisson et des bétons de magnésie avec liant d'alumine hydratable à température ambiante et développant des liens de spinelle après cuisson. Tous ces bétons contiennent au moins 6 % de graphite sous forme de micro-boulettes extrudées. La contribution essentielle de cette thèse aura été d'améliorer les caractéristiques de ces agglomérats, en les rendant plus denses par addition d'oxydes d'alumine pour les bétons du système M-MA-C et de silice pour les bétons du système M-M_2S-C, et plus résistante à l'oxydation par addition d'antioxydants appropriés et spécifiques Al+B_4C pour les bétons à liaison spinelle, SiC+ B_4C pour les bétons à liaison forsterite.

La deuxième contribution importante aura été de poursuivre l'amélioration des performances de ces bétons en utilisant en plus des micro-boulettes comme agrégats, du carbone et des antioxydants finement dispersés dans la matrice de ces bétons, tout en sélectionnant les défloculants appropriés et les distributions granulométriques adéquates pour obtenir des caractéristiques de mise en œuvre adéquates : coulabilité, temps de prise et des propriétés mécaniques inégalées pour ce genre de produits.

Le document est divisé en sept chapitres. Le premier chapitre s'ouvre sur une introduction générale qui sert à situer le contexte et à préciser les objectifs de cette thèse :

1. Tester trois modes d'insertion du graphite pour minimiser l'eau de gâchage nécessaire et produite des bétons possédant des caractéristiques à l'oxydation supérieure, à partir soit de micro-boulettes extrudées EG, soit à partir de granules pressées GG, soit de paillettes enduites pour améliorer leur hydrophobicité (CG).
2. Mettre au point des bétons magnésiens, sans ciment, possédant des caractéristiques de mise en œuvre adéquates : coulabilité, temps de prise.
3. Sélectionner les meilleures combinaisons d'antioxydants, dans les agglomérats de graphite et dans la matrice des bétons.
4. Étudier l'évolution des microstructures pour préciser les mécanismes de réaction, à hautes températures

Le deuxième chapitre sert à passer en revue les mécanismes d'oxydation du graphite et de tous les carbones dans les réfractaires carbonés, puis à décrire les modes de protection du carbone contre l'oxydation à l'aide d'antioxydants. Une analyse des travaux antérieurs sur les bétons contenant du carbone sert à faire ressortir les problèmes reliés à l'usage du graphite, mais aussi des antioxydants dans les bétons. Un de ces problèmes est relié à la réactivité de l'aluminium en présence de vapeur d'eau lors du séchage des bétons, problème qui recevra une attention particulière au cours de cette thèse. Ce chapitre se termine sur un examen des méthodes expérimentales pour mesurer la résistance à l'oxydation des réfractaires à liaison carbone ou contenant du carbone.

Dans le troisième chapitre, les méthodes d'élaboration des agglomérats de graphite sont explicités en détails, tant pour la production de granules pressées GG, de graphite enduit CG, que de micro-boulettes extrudées de graphite EG, en portant l'emphase sur les micro-boulettes extrudées EG. On retrouvera dans ce chapitre les données de caractérisation des agglomérats obtenues par microscopie optique, microscopie électronique à balayage, cathodoluminescence, porosimétrie au mercure et par mesure de l'angle de mouillage de l'eau sur ces granulats.

Les mesures ayant trait à l'oxydation des matériaux dans le système M-MA-C sont cumulées dans le chapitre 4, celles concernant le système M-M_2S-C dans le chapitre 5.

Dans le chapitre 4, on retrouvera en outre une section spécifique sur le comportement de l'aluminium dans les bétons et des résultats « préliminaires » sur la possibilité de passiver cet ajout pour éviter tout risque d'explosion au séchage. Aussi, dans ce chapitre, il y a 2 sections supplémentaires, l'une portant sur la résistance à l'oxydation des micro-boulettes EG, en propre, l'autre portant sur des mélanges pressés reproduisant la composition de la partie matricielle des bétons du système M-MA-C.

C'est à partir des résultats sur la résistance à l'oxydation des bétons du système M-M_2S-C présentés au chapitre 5, qu'il a été décidé de faire porter les efforts d'optimisation sur ces bétons. On retrouvera donc dans ce chapitre 5, deux autres sections, l'une portant sur l'ouvrabilité des bétons et le choix des défloculants ainsi que de la distribution granulométrique des fines de magnésie, l'autre portant sur l'addition de carbone fin, en plus des micro-boulettes de graphite améliorées (EG) avec oxydes et antioxydants.

Le chapitre 6 est réservé à l'interprétation et la discussion des résultats, ce qui va être résumé ci-après alors que les conclusions et recommandations qui découlent de cette thèse, sont présentées au chapitre 7.

Au niveau des résultats, en ce qui concerne le système M-MA-C, il a été clairement démontré expérimentalement que l'addition de poudre d'aluminium dans un béton présente des risques puisque l'aluminium peut facilement réduire l'eau libre des bétons

et provoquer un dégagement d'hydrogène ; c'est une réaction fortement exothermique. Les essais de passivation qui ont été effectués pour minimiser cette réaction sont décrits. Les revêtements à l'aide de brais, molasse et même d'oxydes n'ont pas été probants. De ce travail, il ressort un point essentiel : la fabrication de micro-boulettes permet d'inclure l'aluminium en toute sécurité dans les bétons. C'est déjà un point très positif en soi.

Pour ce qui est de la résistance à l'oxydation des différents agglomérats EG, CF, GG, il est clair qu'en réduisant la surface spécifique exposée, on augmente cette résistance par rapport à celle des paillettes de graphite FG. En incorporant dans les micro-boulettes des oxydes et des antioxydants, la résistance à l'oxydation est encore accrue. Les résultats présentés en page 110 de cette thèse permettent de constater un gain important en comparant une micro-boulette de première génération à des micro-boulettes de deuxième génération : l'indice d'oxydation passant de 100 à 25 pour des granules pressées et de 100 à 60 pour des bétons complets avec des EG de première génération et 35 avec des EG de deuxième génération, c'est-à-dire contenant des oxydes et antioxydants. Il faut souligner que non seulement la résistance à l'oxydation est améliorée, mais aussi la distribution et la grosseur des pores, ainsi que les propriétés mécaniques des bétons, l'indice de la valeur du module de rupture à froid (CMOR) de bétons avec paillettes passe de 100 à 200 avec des micro-boulettes EG (p. 120).

Maintenant, pour les bétons du système M-M_2S-C, tous les résultats précédents sont confirmés, avec des micro-boulettes dont la composition a été ajustée pour tenir compte de la différence de systèmes. Les améliorations sont du même ordre de grandeur, 100 à 200 pour les modules, 100 à 50 pour l'oxydation. Toutefois, en poursuivant l'optimalisation, avec le choix approprié de défloculants et de fines de magnésie et avec l'ajout d'antioxydants dans la matrice, il a été possible d'améliorer l'indice CMOR de 100 à 300 et l'indice d'oxydation de 100 à 10 (à 1400 °C dans l'air).

En finale, les bétons contenant 90 % de magnésie, sans ciment, avec 6 % de carbone, 1 à 2 % d'antioxydants seulement, ont été produits avec 5.3 à 6.5 % d'eau de gâchage, 10 à 14 % de porosité après séchage à 110 °C, 17 à 18 % de porosité après cuisson à 1500 °C, des modules de rupture à froid, après séchage de l'ordre de 5 MPa à 15 MPa et après cuisson à 1500 °C, de 6 à 12 MPa.

Les valeurs maximales ont toutes été atteintes avec les bétons du système M-M_2S-C qui, par ailleurs, présentent la meilleure stabilité dimensionnelle ± 0.5 % par rapport à < +1.5 % pour les bétons M-MA-C.

Les quatre objectifs de cette thèse ont été atteints. Il est clair que l'addition de graphite dans les bétons basiques est dorénavant pleinement justifiée et que la fabrication de micro-boulettes extrudées mérite maintenant d'être lancée à une échelle préindustrielle.

Il est recommandé de tester les meilleurs bétons produits du système M-M_2S-C dans une poche de coulée, en usine, le plus rapidement possible, tout en poursuivant la mise au point d'agglomérats de graphite. Il est juste de souligner que les agglomérats GG ET CG ont permis d'atteindre des performances parfois équivalentes aux agglomérats EG, mais jamais supérieures. Il est donc peut-être prématuré de se centrer seulement sur les agglomérats EG améliorés. Toutefois, l'optimisation des GG et CG demeure possible, mais devra faire l'objet d'une autre thèse. Un autre aspect important à documenter sera la résistance à la corrosion par des scories basiques à 1600 °C. Il est, pour l'instant, accepté que si la porosité apparente et la résistance à l'oxydation sont grandement améliorées, la résistance à la corrosion doit suivre dans le même sens.

Au-delà de ces résultats, les analyses structurales des bétons après cuisson ont permis de bien interpréter les résultats obtenus et de bien juger de leur cohérence interne. Ceci est documenté au chapitre 6 de la thèse, où la discussion est centrée sur l'importance du carbone, nature, distribution et mode d'agglomération et sur l'importance des antioxydants. Il est ainsi confirmé que dans ce domaine, l'utilisation conjuguée de deux antioxydants est nettement favorable. Pour les micro-boulettes EG dans le système M-MA-C, la composition optimale est 80 % graphite, 15 % Al_2O_3, 5 % B_4C ou 80 % graphite, 15 % Al, 5 % B_4C (l'alumine jouant un rôle comparable à l'aluminium).

Pour les micro-boulettes EG dans le système M-M_2S-C, la composition optimale est 80 % graphite, 20 % Si ou 80 % graphite, 20 % SiC, mais pour ces bétons, il faudra

prévoir ajouter 1 % de B_4C au niveau de la composition globale et 2 % de SiC ou Si, au choix.

Une partie seulement des résultats présentés dans cette thèse ont déjà fait l'objet de deux publications (2). L'ensemble des résultats sera dévoilé prochainement dans deux publications en préparation.

Il est espéré que ce travail, une fois publié dans son ensemble sera rapidement adapté, pour hâter le développement de tels produits, au moins à l'échelle pilote, et probablement à l'échelle commerciale. Les ajustements requis sortent du cadre d'une thèse, mais ne semblent pas a priori insurmontables.

(1) 1.1 M. Kandel, N.S. Zhou, M. Rigaud and P. Chabry, « Use of Micropellets of Graphite in Al_2O_3-SiC-C Castables », 9th International Symposium on Industrial Ceramics, Bologne, Italie, Octobre 1998, reproduit dans Ceramica Acta, Vol. 12, No. 56, pp. 2-12, 2000.

1.2 N.S. Zhou and M. Rigaud, « Different Approaches to Incorporation of Natural Flake Graphite into Al_2O_3-SiC-C Castables », 3rd International Symposium on Refractories, Novembre 1998, Pékin, Chine, Proceedings, pp. 291-297.

(2) 2.1 H. He, V. Kovač, M. Rigaud and P. Chabry, « Oxidation Behavior of Graphite Materials Usable in Monolithic Refractories », 3rd International

Symposium on Advances in Refractories for the Metallurgical Industries, CIMM, Québec, Août 1999, pp. 69-80.

2.2 N.S. Zhou, S. Palčo, H. He, M. Rigaud, "Oxidation and Corrosion of Carbon-Containing Castables », in Fundamentals of Metallurgical Processing, J. Toguri Symposium, CIMM, Ottawa, Août 2000, pp. 207-216.

TABLE OF CONTENTS

ACKNOWLEDGEMENT ---------- iv

RÉSUMÉ ---------- v

ABSTRACT ---------- x

CONDENSÉ ---------- xv

TABLE OF CONTENTS ---------- xxv

LIST OF TABLES ---------- xxxi

LIST OF FIGURES ---------- xxxiii

LIST OF SYMBOLS AND NOMENCLATURE ---------- xli

CHAPTER 1: INTRODUCTION ---------- 1

CHAPTER 2: LITERATURE REVIEW ---------- 9

2.1 INTRODUCTION ---------- 9

2.2 CHARACTERISTICS OF CARBON MATERIALS AND NATURAL FLAKE GRAPHITE ---------- 12

2.2.1 Natural and Synthetic Graphite ---------- 13

2.2.2 Characteristics of Graphite ---------- 15

2.3 OXIDATION OF CARBON IN REFRACTORIES ---------- 20

2.4 METHODOLOGY OF PROTECTING CARBON FROM OXIDATION ---------- 24

2.4.1 Carbon Protection----------24

2.4.2 Typical Antioxidants ----------27

2.5 **CURRENT STATUS OF CARBON-CONTAINING CASTABLES**----------32

2.5.1 Carbon Material in Castables----------33

2.5.2 Graphite in Castables----------36

2.5.3 Antioxidants in Castables----------39

2.6 **REVIEW OF METHODS MEASURING OXIDATION RESISTANCE**--------39

2.61 Existing Methods ----------39

2.6.2 Comparison of Test Conditions and Outcomes----------44

CHAPTER 3: PACKAGING FLAKE GRAPHITE----------48

3.1 INTRODUCTION----------48

3.2 EXPERIMENTAL PROCUDURE TO PRODUCE EXTRUDED GRAPHITE----------49

3.2.1 Experimental Plan----------49

3.2.2 Raw Materials ----------50

3.2.3 Characterization Tools ----------51

3.2.3.1 Microscopy Observations----------51

3.2.3.2 Pore Size Distribution ----------52

3.2.3.3 Bulk Density Measurement of Extruded Graphite Pellets ----------54

3.2.3.4 Wettability of Graphite Materials ----------54

3.2.4 The Extrusion Process ----------54

3.2.4.1 The Composition Design ----------55

3.2.4.2 The Extrusion Process ----------55

3.3 CHARACTERISTICS OF EXTRUDED GRAPHITE PELLETS ----------58

3.3.1 Hydrophilic Behaviour of EG Pellets ----------59

3.3.2 EG Microstructure Evolution Under Reducing Condition ---------- 61

3.3.2.1 Pore Size Distribution ----------61

3.3.2.2 Bulk Density and Apparent Porosity ----------64

3.3.3 EG Microstructure Evolution in Pressed Samples

Under Reducing Conditions ----------67

3.3.4 The Influence of the Binder ----------74

3.4 EXPERIMENTAL PROCEDURES TO PRODUCE COATED GRAPHITE --75

3.5 EXPERIMENTAL PROCEDURE TO PRODUCE GRANULATED GRAPHITE ----------78

CHAPTER 4 OXIDATION STUDY ON MgO-MA-C MATERIAL SYSTEM -----79

4.1 INTRODUCTION----------79

4.2 ALUMINIUM AS A STRAIGHT ANTIOXIDANT ----------80

4.2.1 Experimental Procedures ----------81

4.2.1.1 Raw Materials ----------81

4.2.1.2 Methodology ----------82

4.2.1.3 Coating Processes----------82

4.2.1.4 Evaluation of Reactivity of Al or Coated Al in Basic Solutions-------84

4.2.2 Results and Discussion ----------85

4.2.2.1 Influence of Al Size on its Reactivity in Basic Aqueous Medium ----86

4.2.2.2 Influence of Solution on Reactivity of Metallic Aluminium ----------88

4.2.2.3 Influence of Coating Process on Reactivity of

Metallic Aluminium in Basic Medium ----------90

4.2.2.4 Castable Containing Metallic Aluminium ----------92

4.3 EXPERIMENTAL PROCEDURES ----------93

4.3.1 Raw Materials ----------93

4.3.2 Sample Preparation ----------98

4.3.3 Evaluation Methods---------- 100

4.3.4 Oxidation Test Set-ups ---------- 101

4.4 OXIDATION RESISTANCE OF GRAPHITE MATERIALS---------- 107

4.5 OXIDATION RESISTANCE OF PRESSED MATRIX SAMPLES ---------- 110

4.6 OXIDATION RESISTANCE OF MgO-MA-C CASTABLES ---------- 117

4.6.1 Role of Modified Graphite Pellets on Flowability ---------- 117

4.6.2 Role of Modified Graphite Pellets on Mechanical Properties ---------- 119

4.6.3 Oxidation Resistance of MgO-MA-C Castables---------- 120

CHAPTER 5: OXIDATION STUDY ON MgO-M_2S-C MATERIAL SYSTEM - 125

5.1 INTRODUCTION ---------- 125

5.2 EXPERIMENTAL PROCEDURES ---------- 126

5.2.1 Raw Materials ---------- 126

5.2.2 Compositions and Evaluation Methods of MgO-M_2S-C Castables ---------- 130

5.3 FLOWABILITY AND PROPERTIES OF MgO-M_2S-C CASTABLES ------- 132

5.3.1 Influence of Deflocculant on Flowability and Mechanical Property ------- 132

5.3.2 Magnesia Fines on Flow Decay ---------- 135

5.4 CARBON MATERIALS FOR MgO-M_2S-C CASTABLES ---------- 136

5.4.1 Influence of Carbon Source on Flowability ---------- 136

5.4.2 Modified Flake Graphite on Overall Properties ---------- 140

5.4.3 Fracture Behaviour of Graphite containing Castables ---------- 144

5.4.4 Pore Size Distribution of the Castables Using Modified Flake Graphite ----- 146

5.5 OXIDATION RESISTANCE OF MgO-M_2S-C CASTABLES ---------- 148

5.5.1 Influence of Carbon Source on Oxidation Resistance ---------- 148

5.5.2 Introduction of Antioxidants into Extruded Graphite Pellets ---------- 150

5.5.3 Performance of $(EG\text{-}A.O.)_{MS}$ Pellets in MgO-M_2S-C Castables ---------- 151

5.4.4 Effects of Antioxidants in MgO-M_2S-C (4) Castables ---------- 153

CHAPTER 6: INTERPRETATION AND DISCUSSION OF THE RESULTS--- 158

6.1 ROLE OF CARBON SOURCES ---------- 159

6.1.1 Flake Graphite over Other Carbon Sources in Castables ---------- 159

6.1.2 Improvements on Properties of Castables Using Modified Graphite---------- 161

6.1.3 Characteristics of $(EG\text{-}A.O.)_{MA}$ and $(EG\text{-}A.O.)_{MS}$ Pellets---------- 164

6.1.4 Combination of Different Carbon Sources in Castables ---------- 165

6.2 ROLE OF ANTIOXIDANTS---------- 166

6.2.1 Mg (g) Vapor and Gaseous Phases by Antioxidants---------- 169

6.2.2 Pore Size Evolution---------- 176

6.2.3 Distribution and Combination of Antioxidants ---------- 178

6.2.3.1 Antioxidants in Spinel-bonded Material System---------- 179

6.2.3.2 Antioxidants in Forsterite-bonded Material System---------- 182

6.2.4 Complementary Tests on Secondary Carbon Formation ---------- 184

6.3 PROMISING PROPERTIES OF THE CASTABLES---------- 204

CHAPTER 7 CONCLUSIONS AND RECOMMENDATIONS---------- 205

7.1 CONCLUSIONS---------- 205

7.1.1 Justifications Derived From Basic Knowledge---------- 209

7.1.2 Contributions To Be Underlined ----------213

7.1.3 Innovation Experimental Methods Used ----------216

7.2 RECOMMENDATIONS----------217

REFERENCES---------- 219

APPENDIX 1 ---------- 237

LIST OF TABLES

Table 2.1 Typical accepted chemical and physical characteristics of graphite --------- 15

Table 2.2 Properties of MgO-C castable ---------- 35

Table 2.3 Conditions and characteristics of experimental set-ups for oxidation resistance measurement ---------- 45

Table 3.1 Raw materials for modified graphite pellets ---------- 50

Table 3.2 Composition design of extruded graphite pellets ---------- 56

Table 3.3 Compositions of the matrixes ---------- 67

Table 3.4 Composition of granulated graphite (GG) ---------- 78

Table 4.1 Raw materials for coated aluminium experiments ---------- 81

Table 4.2 Samples and designed solutions for the reactivity measurement ---------- 86

Table 4.3 Effect of coated aluminium in MgO-MA-CG castables ---------- 92

Table 4.4 Magnesia materials for MgO-MA-C castables ---------- 94

Table 4.5 Chemical compositions of alumina ultra-fines ---------- 95

Table 4.6 Chemical analysis of silica fume 971U ---------- 97

Table 4.7 Deflocculants for MgO-MA-C castables ---------- 98

Table 4.8 Compositions of the matrixes with different antioxidants ---------- 99

Table 4.9 Compositions of MgO-MA-C castables ---------- 100

Table 4.10 Heating conditions for different oxidation Set-ups A, B, C and D --------- 107

Table 4.11 Antioxidant aluminium in MgO-MA-CG castables ---------- 123

Table 5.1 Magnesia materials for MgO- M_2S -C castables ---------- 128

Table 5.2 Carbon sources for MgO-M_2S-C castables ---------- 129

Table 5.3 List of deflocculants for MgO-M_2S-C castables ---------- 129

Table 5.4 Compositions of MgO-M_2S-C castables ---------- 131

Table 5.5 Quantities of antioxidants in MgO-M_2S-C castables ---------- 131

Table 5.6 Quantities of deflocculants used in MgO-M_2S-C castables ---------- 133

Table 5.7 Properties of MgO-M_2S-C castables (3) with different carbon sources ---- 140

Table 5.8 Properties of modified graphite-containing MgO-M_2S-C castables --------- 142

Table 5.9 Influence of graphite Materials on fracture behaviour of MgO-M_2S-C castables measured by wedge splitting test ---------- 144

Table 5.10 Influence of antioxidants on properties of MgO-M_2S-C (4) castables --- 154

Table 5.11 X-ray diffraction results ---------- 156

Table 6.1 Compositions of the samples for secondary carbon formation (group1)---- 185

Table 6.2 Compositions of the samples for secondary carbon formation (group2)---- 185

Table 6.3 Slag composition ---------- 197

Table 6.4 Elements detected from the edge to the center of the sample MgO-Si after slag test at 1550°C×1h ---------- 202

LIST OF FIGURES

Figure 2.1 Crystallographic structure of graphite ---------- 16

Figure 2.2 Schematic of oxidation mechanisms operative during the oxidation of graphite flake ---------- 19

Figure 2.3 Relationship between partial pressures of CO, CO_2 and O_2 gas and temperatures in presence of carbon at total pressure of 1 atm ---------- 21

Figure 2.4 Relationships between temperature and standard free energy of the reaction of common antioxidants with oxygen ---------- 26

Figure 2.5 Schematic evolution of Al and Al-compounds in the presence of C(s), CO(g) and N_2(g) ---------- 28

Figure 2.6 Stability fields of Al-compounds in MgO-C-Al refractories, under a thermal gradient from 1650°C to 950°C, in a brick width's of 1400mm --- 28

Figure 2.7 Schematic representation of a) active oxidation, b) active-passive transition, c) passive oxidation ---------- 29

Figure 2.8 Influence of carbon sources on water addition of MgO-C castables ------- 34

Figure 2.9 Conventional box furnace ---------- 40

Figure 2.10 Rotating bottom furnace ---------- 40

Figure 2.11 Thermal gradient furnace ---------- 41

Figure 2.12 Vacuum controlled furnace ---------- 41

Figure 2.13 Tubular furnace ---------- 41

Figure 2.14 Horizontal furnace ---------- 42

Figure 2.15 Thermo-balance method ---------- 42

Figure 2.16 Rotary furnace ---------- 43

Figure 3.1 Cathodoluminescence microscopy set-up ---------- 52

Figure 3.2 Schematic view of PoreSizer 9320 system ---------- 52

Figure 3.3 Morphology of extruded graphite EG-0 and EG-AO (SEM photo) --------- 58

Figure 3.4 Behaviour of a water drop on the surface of pressed flake graphite (FG), extruded graphite (EG) and extruded graphite treated by wetting agent (EG-WA) ---------- 60

Figure 3.5a Median pore diameter (μm) of $(EG\text{-}A.O.)_{MA}$ pellets after firing at 1400°C×3h, embedded in coke ---------- 62

Figure 3.5b Cumulative intrusion (%) vs. pore diameter (μm) in $(EG\text{-}A.O.)_{MA}$ pellets 62

Figure 3.6a Cumulative intrusion (%) vs. pore diameter (μm) in $(EG\text{-}A.O.)_{MS}$ pellets 63

Figure 3.6b Median pore diameter (μm) of $(EG\text{-}A.O.)_{MS}$ pellets after firing at 1400°C×3h, embedded in coke ---------- 64

Figure 3.7a Density of extruded graphite $(EG\text{-}A.O.)_{MA}$ pellets ---------- 65

Figure 3.7b Apparent porosity of extruded graphite $(EG\text{-}A.O.)_{MA}$ pellets ---------- 65

Figure 3.8a Density of extruded graphite $(EG\text{-}A.O.)_{MS}$ pellets ---------- 66

Figure 3.8b Apparent porosity of extruded graphite $(EG\text{-}A.O.)_{MS}$ pellets ---------- 66

Figure 3.9 Distribution of graphite flakes inside (EG-0) and (EG-MAOBC) pellets -- 68

Figure 3.10 New compounds formation in $(EG\text{-}A.O.)_{MA}$ in a matrix of MgO without fine carbon (/M) and with carbon (/MC) (CLM observations: spinel-green, MgO-blue or purple, graphite-black)---------- 70

Figure 3.11 Confirmation of MA and M_2S formations in EG by SEM/EDS ---------- 72

Figure 3.12 Effects of incorporating antioxidants and oxides into EG pellets or matrix on spinel formation (green color identified as MA spinel by SEM/EDS) ------ 73

Figure 3.13 Oxidation behaviour of EG-MAOBC and EG-MAOBC$_S$ pellets -------- 74

Figure 3.14 Morphology of coated graphite CG_L ---------- 76

Figure 3.15 Morphology of coated graphite CG ---------- 77

Figure 3.16 Behaviour of a water drop on the surface of pressed flake graphite and coated graphite: a comparison ---------- 77

Figure 4.1 Photography of coated aluminum A101 (AlP101) ---------- 83

Figure 4.2 Set-up for measuring temperature changes of the mixtures of metallic antioxidant emmersed in basic solutions or castables ---------- 85

Figure 4.3 Influence of aluminium size on its reactivity in a basic solution (S1)------ 87

Figure 4.4 Reactivity of metallic A120 in different solutions (S1-S6) ---------- 88

Figure 4.5 Role of coated Al on decreasing the reactivity of metallic aluminum In basic solution (S1) ---------- 89

Figure 4.6 Reactivity of AlR, AlM and AlP in basic solution (S1) ---------- 90

Figure 4.7 Influence of selected pitch and coating process on reactivity of coated Al in basic solution (S1) ---------- 91

Figure 4.8 Main components of MgO-MA-C castables---------- 93

Figure 4.9 Particle size distribution of magnesia fine---------- 95

Figure 4.10 Particle size distributions of alumina fines---------- 96

Figure 4.11 Particle size distribution of reactive alumina, Ap100 ---------- 97

Figure 4.12 Thermobalance with mass spectrometer: Set-up A ---------- 103

Figure 4.13 Unidirectional oxidation in muffle furnace: Set-up B ---------- 104

Figure 4.14 Unidirectional oxidation in tubular furnace: Set-up C ---------- 105

Figure 4.15 Oxidation in bottom-load furnace: Set-up D---------- 106

Figure 4.16 TGA oxidation curves for flake graphite FG and modified graphite (EG, CG, GG) at a heating rate of 5°C/min up to 1350°C (Set-up A) --------- 108

Figure 4.17 Oxidation resistance of $(EG\text{-}A.O.)_{MA}$ by CO_2 gas evolution (Set-up A) 109

Figure 4.18 Influence of antioxidants on oxidation resistance of the matrixes (Unidirectional oxidation at 1400°C with air flow 500 ml/m in Set-up C) -- 110

Figure 4.19 Microscopy observations on sample MC0 (OM/CLM) (After unidirectional oxidation test at 1400°C×3h in Set-up C)---------- 111

Figure 4.20 Microscopy observations on sample MCA2 (OM/CLM) (After unidirectional oxidation test at 1400°C×3h in Set-up C)---------- 112

Figure 4.21 Microscopy observation on sample MCA1B1 (OM/CLM) (After unidirectional oxidation test at 1400°C×3h in Set-up C)---------- 113

Figure 4.22 Influence of antioxidants on mechanical properties and volume change of the matrixes (MC0, MCA1, MCA2 and MCA2B1) ---------- 114

Figure 4.23 Influence of antioxidants on physical properties of the matrixes (MC0, MCA1, MCA2 and MCA2B1) ---------- 115

Figure 4.24a Incremental intrusion vs. pore size by antioxidants in matrix ---------- 116

Figure 4.24b Cumulative intrusion vs. pore size by antioxidants in matrix ---------- 116

Figure 4.24c Influence of antioxidants on median pore diameter of the matrix------- 117

Figure 4.25 Influences of graphitic materials (FG, EG, CG, GG) on flowability of MgO-MA-C castables ---------- 118

Figure 4.26 Influence of graphitic materials on mechanical property of MgO-MA-C castables ---------- 120

Figure 4.27 Influence of graphitic materials (FG, EG, CG, GG) on oxidation resistance of MgO-MA-C castables after firing at 1400°C×3h in set-up B---- 121

Figure 4.28 Influence of antioxidants on oxidation resistance of MgO-MA-EG Castables after firing at 1200°C and 1400°C×3h in Set-up B---------- 122

Figure 4.29 Oxidation resistance of MgO-MA-CG castables (Set-up D) ---------- 124

Figure 5.1 Raw materials and their role in MgO-M_2S-C castables---------- 126

Figure 5.2 Particle size distributions of magnesia fines ---------- 127

Figure 5.3 Influence of deflocculants on flowability of MgO-M_2S-C (1) castables 134

Figure 5.4 Influence of deflocculants on CMOR of MgO-M_2S-C (1) castables ----- 134

Figure 5.5 Influence of magnesia fines on flow decay of MgO-M_2S-C (2) castables 136

Figure 5.6 Influence of different carbon sources on flowability of MgO-M_2S-C (3) castables ---------- 137

Figure 5.7 Influence of flake and modified graphites on flowability of MgO-M_2S-C (3) castables ---------- 138

Figure 5.8 Influence of fine flake graphite on flowability of MgO-M_2S-C (3) castables ---------- 139

Figure 5.9 Influence of fine flake graphite on CMOR values of
MgO-M_2S-C (3) castables (Graphite 5%) ---------- 139
Figure 5.10a CMOR (110°C) vs. carbon sources in MgO-M_2S-C castables -------- 143
Figure 5.10b CMOR (1100/1500°C) vs. carbon sources in MgO-M_2S-C castables -- 143
Figure 5.11 Wedge-splitting tests on MgO-M_2S-C (3) castables---------- 145
Figure 5.12 Pore size distribution of different graphites in
MgO-M_2S-C (3) castables ---------- 147
Figure 5.13 Median pore diameter vs. different graphites in
MgO-M_2S-C (3) castables ---------- 148
Figure 5.14 Oxidation of different carbon sources in MgO-M_2S-C (3) castables
(Oxidation Set-up B, sample 50×50×50 mm) ---------- 149
Figure 5.15 Oxidation behaviour of extruded graphite pellets (EG-A.O.)$_{MS}$
by evaluating relative intensity of CO_2 gas vs. Temperature ---------- 151
Figure 5.16 Oxidation of (EG-A.O.)$_{MS}$ pellets in MgO-M_2S-C (3) castables
(Oxidation set-up D, sample 50×50×50 mm) ---------- 152
Figure 5.17 Influence of antioxidants on oxidation resistance of MgO-M_2S-C (4)
castables (Unidirectional oxidation, Set-up B) ---------- 154
Figure 5.18 Improvement of antioxidants on mechanical property (CCS values) of
MgO-M_2S-C (4) castables ---------- 156
Figure 6.1 Possible courses of reactions in M-C-Al-N-O system ---------- 167
Figure 6.2 Feasible reactions in M-C-Si-O-N system---------- 169
Figure 6.3 Influence of antioxidant Al vs. temperature on gaseous

phases formation in M-C-Al-CO system (by FACT) ---------- 170

Figure 6.4 Influence of antioxidant Si vs. temperature on gaseous phases formation in M-C-Si-CO system (by FACT) ---------- 171

Figure 6.5 Possible courses of reactions within a MgO-C material ---------- 172

Figure 6.6 Magnesia whiskers formed during the oxidation test from MgO-M_2S-C castables, fired at 1400°C×3h with air flow 1000ml/min ---------- 173

Figure 6.7 Magnesia whiskers confirmed by SEM/EDS ---------- 174

Figure 6.8 MgO dense layer formation in cylindrical samples of EG-AB/MC, EG-AM/MC and EG-SB/MC (after unidirectional oxidation at 1400°C×3h) ----- 175

Figure 6.9 Experimental set-up for secondary carbon formation ---------- 186

Figure 6.10 Secondary carbon formation in samples MgO-Al and MgO-Si after firing at 1050°C, 1250°C and 1500°C for 5h in coke ---------- 187

Figure 6.11a New compounds formation in sample MgO-Al after firing at 1550°C for 5 hours in coke ---------- 188

Figure 6.11b New compounds formation in sample MgO-Al after firing at 1500°C for 5 hours in coke ---------- 188

Figure 6.12 X-ray diffraction on magnesia with or without aluminium ---------- 189

Figure 6.13 X-ray diffraction on magnesia with or without silicon ---------- 190

Figure 6.14a Microstructure and new compounds formation in sample MgO-Al after firing at 1050°C and 1250°C for 5 hours in coke (OM/CLM) ---------- 191

Figure 6.14b Microstructure and new compounds formation in sample MgO-Al after firing at 1550°C for 5 hours in coke (OM/CLM) ---------- 192

Figure 6.15 Thermodynamic calculation on secondary carbon formation and various gaseous phases in MgO-Al-CO system (by FACT) ---------- 193

Figure 6.16 Microstructure and new compounds formation in sample MgO-Si after firing at 1050°C, 1250°C and 1550°C for 5 hours in coke (OM/CLM) 195

Figure 6.17 Thermodynamic calculation on secondary carbon formation and various gaseous phases in MgO-Si-CO system (by FACT) ---------- 196

Figure 6.18 Set-up for static slag test---------- 198

Figure 6.19a Slag test on sample with pure magnesia (CLM) ---------- 199

Figure 6.19b Slag totally penetrated into the sample containing only magnesia after slag test at 1550°C×1h in coke (SEM)---------- 199

Figure 6.20 Slag test on sample MgO-Al at 1550°C×1h in coke---------- 200

Figure 6.21a OM/CLM observations on sample MgO-Si after slag test at 1550°C×1h in coke ----------200

Figure 6.21b Penetration layers of sample MgO-Si after slag test at 1550°C×1h in coke (SEM/CLM) ---------- 201

Figure 6.21c Penetration layers showing different textures (area 1-5) on sample MgO-Si by SEM ---------- 201

Figure 6.21d Details on non-penetrated area 5 and spinel layer in sample MgO-Si after slag test at 1550°C×1h in coke (CLM)---------- 202

Figure A1 Schematic view of the wedge-splitting test set-up ---------- 237

Figure A2 The specimen's shape and dimensions for WST ---------- 238

LIST OF SYMBOLS AND NOMENCLATURE

A.P.	Apparent Porosity
A	Aluminium Al
AG	Amorphous graphite
AlM	Molasses-coated aluminium
AlP	Pitch-coated aluminium
AlR	Resin-coated aluminium
AM	Metallic alloy AlMg
AO	Alumina Al_2O_3
B	Boron carbide B_4C
B.D.	Bulk density
CB	Carbon black
CCS	Cold crush strength
CG	Coated graphite
CLM	CathodoLuminescence Microscopy
CMOR	Cold modulus of rupture
EDS	Energy disperssive X-ray spectroscopy
EG	Extruded graphite
EG-A.O.	Extruded pellets with antioxidant and/or oxide fillers
EG-MAOBC$_S$	EG-A.O. pellets with colloidal silica as binder
(EG-A.O.)$_{MA}$	Extruded pellets with in-situ spinel formation

$(EG\text{-}A.O.)_{MS}$	Extruded pellets with in-situ forsterite formation
FG	Flake Graphite
FGf	Flake graphite fine
M	MgO
M_2S	Forsterite
MA	Spinel
OM	Optical microscopy observation
PLC	Permanent linear change
S	Metallic silicon Si
SC	Silicon carbide SiC
SEM	Scanning Electron Microscopy
SO	Silica fume SiO_2
WA	Wetting Agent
WST	Wedge splitting test

CHAPTER 1 INTRODUCTION

Castable refractories have been used more and more intensively in steelmaking for at least two decades, since they require a shorter manufacturing cycle, less energy consumption and less skilled manpower for installation, and are even amenable to automatic installation. The physical, thermo-mechanical and thermo-chemical properties of castable refractories have improved significantly by selecting the right raw materials, binders, bonding systems and additives [1-3]. The development of castable refractories has been conducted step by step firstly on alumina-based systems and more recently on magnesia-based systems. Currently, carbon-containing castables are contemplated to meet the demands from the steelmaking industry [4-7].

This work has been initiated with the perspective of developing carbon containing castables suitable for steel ladle lining, which is one of the biggest item of consumption of refractory in steelmaking, specific consumption being still high as 3.0 kg/ton in BOF and 2.5 kg/ton in EAF for the best shop's practice.

In ladle lining today, alumina-spinel and alumina-magnesia castables [8-12] have been well accepted in the barrel and the bottom, but not act as suitable lining for the slag line zone due to their inferior corrosion resistance to basic slag. Magnesia-based castables [13-15] have superior corrosion resistance to basic slag, and become prospective candidates for slag line zones. However, they exhibit a low slag penetration resistance.

Therefore the main challenges today is to find proper castable material for the slag line of ladles. Is there any solution to improve slag penetration resistance of magnesia-based castables?

Looking back on application of refractories in steelmaking industry, carbon containing bricks have been applied to steelmaking industry since the 1970s. They perform tremendously well in many applications such as basic oxygen furnaces, electric arc furnaces, varieties of vessels and ladles for secondary refining treatments, as compared to bricks without carbon. Magnesia-carbon bricks have been dominant in slag line of ladles for at least a decade. They have superior slag penetration resistance and excellent thermal shock resistance because of the non-wetting of carbon with slag, good thermal conductivity, low thermal expansion and good toughness [16-17]. Obviously, carbon (graphite) has played a determinant role. The tentative answer to the previous question brings out the concept of introducing carbon into castables. However, it is more complicated to insert carbon into castables than in bricks, especially when using graphite [18-19].

Natural flake graphite exhibits the best performance in bricks on account of its high crystallite size, purity, and oxidation resistance and corrosion resistance as compared to other carbon source. However, it becomes the worst situation to insert it into castables, because of its non-wetting and anisotropic properties. Its poor dispersibility leads to higher water demand and higher porosity of the castable, lack of bonding with oxides

and as a consequence high oxidation rate at elevated temperatures. All of the above factors severely limit the benefits expected from flake graphite. The introduction of carbon into castable still faces a challenge to be met. Precursory works will be described in chapter 2.

Oxidation of carbon is a major drawback for oxide-carbon composite refractories [16, 20]. The advantages of using carbon-bonded refractories are based on the presence of carbon, which facilitates excellent thermal shock resistance and slag penetration resistance. When bonding carbon and graphite are oxidized, the porosity of the material increases and this facilitates more penetration by aggressive slag. At this point, any carbon, either flake graphite or other carbon sources, will be subjected to oxidation. Generally castables are inherently more porous than bricks, around 18% of porosity for a carbon containing castable as opposed to 12% or less porosity for a carbon-bonded brick after firing. Therefore the oxidation will happen more readily in a castable than in a pressed brick. Protecting carbon from oxidation becomes a more important issue for carbon containing castables.

A common practice of protecting carbon from oxidation in carbon containing bricks is to add various kinds of antioxidants: metallic additives or metal alloys, and non-metallic additives, such as carbides, borides and nitrides [16, 21]. Carbon-bonded bricks with improved oxidation resistance using antioxidants have been reported in many previous works, but several antioxidants such as metallic additives used in MgO-C bricks cannot

be used in carbon containing castables. The presence of water and water vapour during the drying out do constitute a real danger when metallic antioxidant additions reduce water and form hydrogen.

Good commercial carbon containing castable mixes are still not available on the market because the above mentioned technical problems need to be solved. Oxidation and corrosion resistance of MgO-C castables is still not as good as those of MgO-C bricks due to the higher water addition leading to higher porosity and lower strength.

Two important factors regarding the oxidation of basic carbon containing castables are the nature of the carbon source and the selection of the antioxidants. The difficulties of inserting graphite into castables, the limitation of using antioxidant and the minimization of the porosity of the material stand as the challenges to be tackled.

As previously mentioned magnesia-based castables offer good dissolution corrosion resistance to basic steelmaking slag's attack and hence has a good potential to be used in the slag line. Therefore, introducing graphite into such castables and protecting it from oxidation have constituted the principal goals of this work.

The objectives of this thesis have been set, as follows:

(1) To modify flake graphite in order to obtain an appropriate hydrophilicity, less segregation and higher oxidation resistance of the castable.

(2) To make magnesia-based graphite containing castables having good flowability and promising properties.

(3) To select effective antioxidants and optimize its addition, combination and distribution and thus to restrict oxidation of graphite in castables at elevated temperature.

(4) To uncover the roles of graphite and antioxidants additives in magnesia-based graphite containing castables and to tackle mechanism for oxidation resistance at high temperatures.

This thesis is essentially set on the study of oxidation behaviour of magnesia-based carbon and graphite containing castables.

This thesis has been divided into seven chapters as follows:

In chapter 2 a short literature review on current castable refractories and carbon containing refractories in steelmaking has been provided in order to justify the selected material systems and the merits of the program. It covers a description of the different carbons, their classification and structural characteristics. The background for carbon containing castables as well as the difficulties to be overcome is provided. Carbon oxidation and methodology of protecting carbon from oxidation are highlighted. Furthermore, a review on the methods of measuring oxidation resistance is presented.

In chapter 3, the elaboration and the characterization of modified flake graphite by extruding, coating and granulating methods are documented. The work has been focused on the improvement of agglomeration of flake graphite by incorporating antioxidant additives into the pellets for two magnesia-based castables: the spinel-bonded system and the forsterite-bonded system. Overall experimental procedures, composition design and modification processes are described. The morphology and new compounds formation of the pellets are evaluated by microscopic observations through optical microscopy (OM), scanning electron microscopy (SEM) and cathodoluminescence microscopy (CLM). The density and the pore size distribution of the EG pellets are measured by mercury intrusion method.

The oxidation study on MgO-MA-C material system is presented in chapter 4. The influence of flake graphite and three modified graphites on flowability, mechanical properties and oxidation resistance of the castables is presented. It reveals that the mode of inserting flake graphite plays an important role in optimizing overall properties of the castable. Extruded graphite and coated graphite perform better than straight addition of flake graphite in terms of flowability, mechanical property and oxidation resistance. To study the oxidation behaviour of the castables containing metallic antioxidant aluminium in castable, the reactivities of metallic aluminium and coated aluminium in water-based solutions are documented. Furthermore, the influences of antioxidants on oxidation resistance, mechanical and physical properties as well as pore size distribution of the material are discussed.

The oxidation study on MgO-M_2S-C system is documented in chapter 5. The work primarily focuses on improving flowability with minimum water addition since it greatly influences the overall properties of the castables. The effects of five different deflocculants and their combinations are described and the appropriate combination of deflocculants has been found. The influences of six different carbon sources and three modified graphites on flowability, physical and mechanical properties, pore size distribution as well as oxidation resistances are presented. It shows that carbon source plays a decisive role in minimizing water addition and varying the overall properties of the castles. The modified graphites do effectively improve the oxidation resistance. The optimization of antioxidants with regards to addition, type and combination is described both in extruded graphite pellets and in castables. The effects of antioxidants on carbon protection and strength improvement are discussed along with the results from X-ray diffraction analysis, oxidation tests and crushing strength measurements.

In chapter 6, the interpretation of the experimental results and comprehensive discussions are being addressed. The work focuses on the role of carbon materials and antioxidants. The role of carbon material is discussed in terms of its agglomeration and packaging composition. The role of antioxidants is addressed based upon their influences on pore size distribution, magnesia vapor formation, new compounds formation and secondary carbon formation. Each factor contributes to the improvement of the oxidation resistance.

Finally, the conclusions and the recommendations are enunciated in chapter 7.

It will be shown that it is impossible to totally protect carbon from oxidation. As temperature increases, carbon becomes too reactive and reduces its solid oxide environment and any other oxide intrusion, gas, liquid or slag. However it will be shown that it is possible to optimize the system by the proper: 1) selection of the adequate carbon source, 2) mode of incorporating graphite, 3) use of the antioxidant in an appropriate proportion in both aggregates and matrix fractions, 4) adjustment of the water addition with the good combination of deflucculants and oxidic ultra fines addition, for cement-free castables, the only categories of castables considered in this thesis.

CHAPTER 2 LITERATURE REVIEW

2.1 INTRODUCTION

Carbon and graphite containing refractories have been known for over 200 years. It was used primarily in crucible formulations. Ure [22] referred in his dictionary of arts and manufacturing in 1843 to graphite as being used to make crucibles and portable furnaces and described the crucible as refractory which stands strong heat, does not react with materials melted in it and is capable of bearing considerable change of temperature without cracking. Percy [23] in 1861 reported similar information about graphite containing crucible and stated that the crucible should resist the corrosive medium from the melted lead oxide and the ashes of the fuel. Therefore, the concept of adding graphite into refractory was recognized as offering toughness, thermal shock resistance and corrosion resistance for over 160 years ago.

Carbon-containing brick [24], which appeared around 1960 on the market, were fired magnesia bricks with tar impregnation, later with pitch impregnation. At the same time tar-bonded and later pitch bonded bricks were used. From the mid-sixties on, carbon black additives were used. At the beginning of the seventies, magnesia carbon bricks bonded with synthetic resin and containing graphite appeared on the market. Carbon bonded bricks have been taken for granted in steelmaking since 1970s. From that time, the use of refractory in which carbon and graphite is a significant part of the formulation

has increased dramatically. Carbon-bonded bricks, for example, MgO-C, MgO-CaO-C, Al_2O_3-C, Al_2O_3-ZrO_2-C and Al_2O_3-MgO-C refractories, have been developed rapidly and are now dominant refractories in various applications of the steel-making processes, such as basic oxygen furnaces, electric arc furnaces and ladles for secondary refining treatments [25-28]. Those refractories exhibit superior slag penetration resistance and excellent thermal shock resistance.

Oxidation of carbon, however, is a major drawback for oxide-carbon composite refractories. Obviously, the advantages of using carbon-bonded refractories are based on the presence of carbon. When bonding carbon and graphite are oxidized and disappear, the porosity increases and this results in more penetration by aggressive slag. Therefore, to avoid carbon oxidation, protection of carbon-containing refractories has been a major concern and attracted considerable attention [16].

In the mid 1970s, antioxidants were added into carbon containing refractories to improve oxidation resistance [24]. A variety of antioxidants have been used, such as metallic additives or metallic alloys, and non-metallic additives, like carbides, borides and nitrides. The oxidation resistances of carbon-bonded bricks have thus been improved.

Castable refractories are mixtures of aggregates, fines, binders and additives. They offer advantages over refractory bricks since they constitute joint-free installation, save energy and labor costs, offer environmental and safety advantages over bricklaying [29-

30]. The technical evolution in castable refractories has led to significant improvements on high temperature, mechanical and corrosion resistance of these materials through the use of new binder systems, selection of the raw materials and additives and development of installation methods. The use of castable linings instead of bricks has spread out in many applications over the last thirty years, in particular in steelmaking for at least two decades [31-33].

The focus here will be on steel ladle linings, which represent the biggest items in the specific consumption of refractories in steelmaking and castable refractories for such an application. Castable refractories have been progressing step by step first on alumina-based systems and more recently on magnesia-based systems to meet the increasing needs in the steel-making processes. It has been well accepted that alumina spinel castables and alumina magnesia castables perform well in barrel and bottom of a ladle, but not in slag line because of their low resistance to basic corrosive slag. So far MgO-C brick is still dominant in slag line for ladles, and bricks are still used predominantly [7], at least in North America, for the entire ladle linings.

The development of magnesia based castable is a decisive step in the evolution of the castable refractories for the demand of high resistance to basic corrosive slag [6]. More efforts and attentions are to be paid on the proper choice of the binder and bonding systems [13,34-36] as well as resolving the magnesia hydration problem [37-38], which influences greatly on the workability, strength development and thermal volume stability

[40-42] of the castables compared with alumina-based castables. Magnesia-based castables possess high refractoriness in contact with basic slag and have superior dissolution corrosion resistance and therefore become prospective candidates for the slag line zone in a ladle. The main drawback of this system is its poor penetration resistance, which leads to structural spalling, which is the main wear mechanism in steelmaking ladle's application [7,43]. One effective solution to reduce the penetration of slag is to add carbon into such castables following the same concept used in carbon-bonded brick [7,44]

As reviewed by Rigaud [7], the use of monolithics in steelmaking ladles will be received with much less resistance, once a solution to avoid using magnesia-carbon bricks in slag line will be found. Carbon containing castable holds a big potential to be used in slag line, inspite of a series of technical problems caused by introduction of carbon and the limitation of using some metallic antioxidant.

2.2 CHARACTERISTICS OF CARBON MATERIALS AND NATURAL FLAKE GRAPHITE

Carbon or graphite plays a decisive role in the carbon-containing material. This is because carbons have unique properties over oxide materials.

There are at least two types of carbon, with different nature and reactivity, used in carbon-bonded refractories. One is graphite with different purity, size, crystallization and structure, and the other is residual carbon, which is more reactive, also called secondary carbon, resulting from the pyrolysis of tar, pitch or resin.

Secondary carbon reacts with oxygen, starting around 250-400°C, while carbon like coke, carbon black and amorphous carbon start oxidizing around 400-600°C; natural graphite is the least reactive carbon source, and start to react in air at 600-650°C [21]. Furthermore, natural flake graphite possesses high oxidation resistance, good mechanical strength, high thermal conductivity and low thermal expansion.

2.2.1 Natural and Synthetic Graphite [29, 45-48]

There are two general classifications of graphite: natural and synthetic graphite. Natural graphites are commonly described in three generic terms: amorphous, flake and crystalline. The synthetic graphites are broken down into artificial and synthetic flake.

Amorphous graphite is generally the least graphitic of the natural graphite. However, the term "amorphous" is a misnomer since this material is truly crystalline. Amorphous graphite is a massive form of graphite with a microcrystalline structure. Amorphous graphite occurs in areas similar to coal deposits and carbon content varies between 75-

90% with graphitic content of 20-50%. It is primarily found in Mexico, Korea, China and Austria.

Natural flake graphite is easily identified with its flaky crystalline structure compared to amorphous graphite. Natural flake graphite has a graphitization of around 99 % with carbon content reaching 90-98%. Flake graphite is found in many localities throughout the world. Currently U.S.A. supplies are imported primarily from China, Canada, Brazil, Madagascar, Mozambique and Zimbabwe. The quality of flake graphite is generally evaluated by its flake size, impurity and fixed carbon content.

High crystalline natural graphite is quite unique, with carbon content over 96% and typically shows needle-like morphology and exhibits better properties than those of extremely well graphitized synthetic graphite. Sri Lanka is the only area known to produce commercially viable quantities although it is found in a number of other locations.

Synthetic graphites are produced from calcined petroleum coke heat treated to over 2800°C, mainly to process graphite electrodes. These materials are 85-95% graphitized with carbon content of 98-99.5%, respectively.

Considering the cost and characteristics of graphite, natural flake graphite is the preferred source to use in carbon containing refractories. Typical technical data on different graphites are listed in Table 2.1.

Table 2.1 Typical accepted chemical and physical characteristics of graphite [29]

Natural graphite	Amorphous	Flake	Crystalline
Carbon, %	81.0	90-96	96.7+
Sulfur, %	0.10	0.10	0.70
True density, g/cm^3	2.31	2.26	2.26-2.29
Graphite content, %	28	90-96	97
Morphology	Granular	Flaky	Plate, needle
Synthetic graphite	Type I	Type II	Flake
Carbon, %	99.9	99.0	97.0
Sulfur, %	0.01	0.01	0.07
True density, g/cm^3	2.25	2.24	2.24
Graphite content, %	99.0	93.0	95.0
Morphology	Granular	Granular	Flaky

2.2.2 Characteristics of Graphite

1) Crystalline structure

Cooper [47] reported a detailed study on the graphite-nature's unique raw material. Carbon atoms are in a planar hexagonal ring array bonded at 120°C to each other, in the sp^2 state. Two dimensionally ordered sheets of rings, known as layers, are stacked one

on top of the other parallel with the "C" crystallographic axis, as shown in Figure 2.1. In simplistic terms there is no free bond out of the plane and as a consequence there is no propensity for it to react with any other material. It results in a low surface energy and thus it is not readily wet. The surface energy figures of 0.04-0.15 J/m^2 for basal plane and 1-4 J/m^2 for the edge. As a comparison, for oxide refractory, the surface energy might be 0.5-0.7J/m^2. It clearly shows the edge atoms are more reactive than those in plane. In the crystal, the layers are stacked up and only bonded by Vander Waals forces and there is no chemical bond.

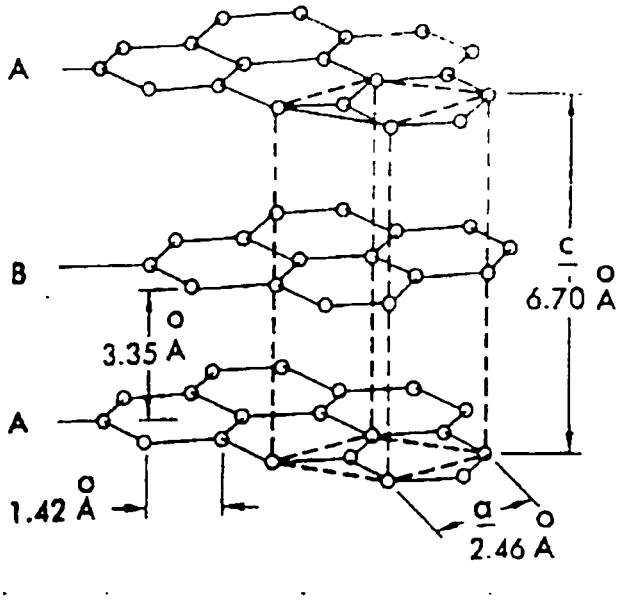

Figure 2.1 Crystallographic structure of graphite [47]

2) High thermal stability.

The bond strength within graphite is high, and the atom movement is slow. Graphite will not melt, and even under 100 atmospheres of argon its melting point is around 3750°C.

3) Anisotropy property.

The bond in the layer plane of graphite is very strong and the bond between layers is weak. The flake is about 60 or more times larger in "diameter" than that in thickness. The anisotropy can be affected by mix, compress, relative size of the graphite and the constituents of the body in refractory. The plane structure results in anisotropic properties, e.g., thermal expansion is much bigger in the direction of perpendicular to plane than that parallel to the planes. The thermal conductivity parallel to the planes is higher than that perpendicular to the planes.

4) Volume texture.

Graphite containing refractory contains generally 5-30% weight percentage of graphite in a formulation depending on the property required. At low level of addition, it is possible to affect a significant improvement in corrosion resistance, but to improve physical properties such as thermal shock resistance and thermal conductivity; the higher levels of addition are needed. Based upon the purity, the specific gravity of graphite is 2.26-2.3 g/cm^3; lower than that of refractory grains, such as magnesia, doloma and alumina, with bulk densities 3.4, 3.2 and 3.8 g/cm^3 respectively. Therefore, it is vital to consider the texture influence of graphite on a volume basis if high amount of graphite used in a formulation of graphite containing refractories.

5) Low thermal expansion.

Upon heating, there is no contribution from the graphite to the thermal expansion of the composite body. Thus when graphite is used to a material the thermal expansion of the material decreases with increasing graphite level.

6) High thermal conductivity.

Observation on compacted natural graphites give results in the direction of the layer plane in the region of 100-300 W/mK, and normal to the layer plane of 10-20 W/mK. The anisotropy was in the range of 10:1 to 35:1, the higher figure driving from coarser graphite. Since the conductivity of a typical fired oxide refractories will be only a few W/mK, it is important to understand that these levels of conductivity of graphite, tens of W/mK, can not be achieved from other oxide materials.

7) High thermal shock resistance.

The thermal shock resistance of racked refractory is well described by Hasselman's equation as $R_{st}=(\gamma/E\alpha^2)^{1/2}$ where γ is work of fracture, α is thermal expansion and E is Young's modulus. Generally, addition of graphite to a refractory increases the work of fracture, lowers the thermal expansion and modulus of elasticity. Thus the thermal shock resistance of graphite containing refractory is increased comparing to that of refractory without graphite. In order to take account of thermal conductivity which will influence the level of stress generated in thermal shock through determining the thermal gradient within the body, it goes further to define Rst' as Rst·k, where k is thermal conductivity. Obviously, thermal shock resistance is further enhanced as graphite levels increase.

8) High corrosion resistance.

Graphite containing refractory exhibits superior corrosion resistance to flux and slag attack because being non-wetted graphite shows no propensity to dissolve in oxide or halide melts and is insoluble in the common non-ferrous metals.

9) Oxidation above 400-500°C.

It is the weakness of graphite refractories and one, which needs techniques to be adopted to prevent or reduce oxidation. In a perfect crystal it is believed that oxidation takes place only at the flake edge. In real practice, however, some attacks do happen through the layer plane via points of imperfections, as illustrated in Figure 2.2.

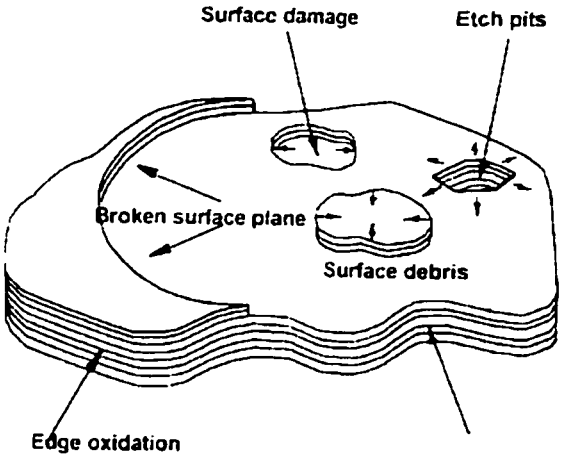

Figure 2.2 Schematic of oxidation mechanisms operative during the oxidation of graphite flake [47]

2.3 OXIDATION OF CARBON IN REFRACTORIES

Carbon is very sensitive to oxidation. There are three types of carbon oxidation reaction in carbon-containing refractories in presence of air and slag [21]: 1) reaction with O_2 gas in the atmosphere, 2) reaction with solid or liquid oxide or gaseous sub-oxide within the refractories itself, 3) reaction with iron oxide and easily reducible oxides in slag. The first type of reaction is called direct oxidation. The second and the third types of reaction are called indirect oxidation. In most cases, oxidation refers to direct oxidation.

From a practical point of view in the temperature range of 400-1400°C and P_{O2} over 10^{-4} atmosphere, direct oxidation is dominant and represents a major concern. At temperature over 1400 °C, indirect oxidation becomes noticeable, being predominant in many cases at 1600°C and above. Most of the efforts of preventing carbon from oxidation are made to avoid direct oxidation of carbon.

When carbon-bonded refractories serve at practical temperature, the carbon near the surface of the refractories will react with O_2 to form CO and CO_2 gas [49], as shown in Figure 2.3. This figure shows the change of partial pressure of CO (g), CO_2 (g) and O_2 (g) under coexistence of carbon at total pressure of 1atm. With increased temperatures, P_{CO} increases, and CO (g) becomes dominant after temperature higher than 900°C.

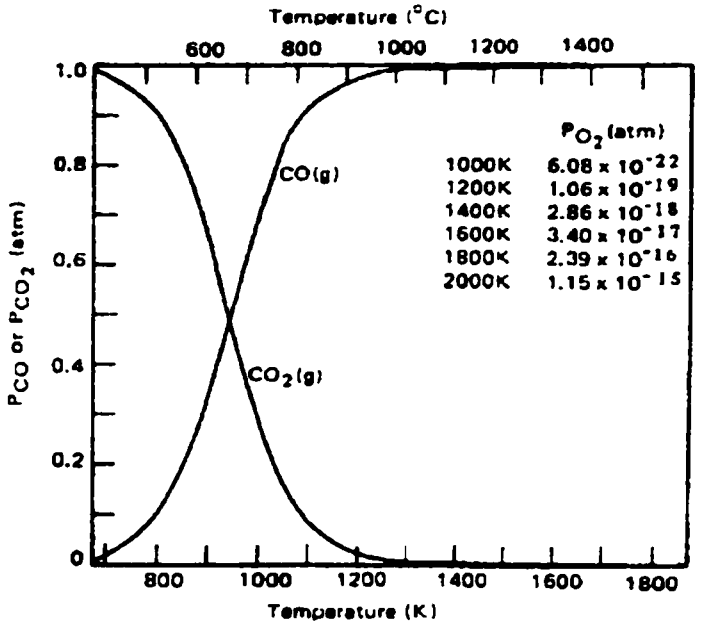

Figure 2.3 Relationship of partial pressures of CO, CO_2 and O_2 gas with Temperatures in presence of carbon at total pressure of 1atm [49]

Kinetic approaches were studied mainly only on simplified reaction systems. Surface reaction rates are known to be dependent on a variety of factors, such as chemical composition, density, porosity and presence of surface defects, crystallinity and crystallographic orientation. Studies on gas phase diffusion-limited oxidation kinetics have generally focused on gas diffusion through continuous pores or cracks or pore or crack sealing by a condensed matrix-oxidation reaction product. For more complex system, with antioxidant additives, kinetic studies are to be completed.

Except for easily oxidized carbon, carbon-bonded refractory also contains oxides and pores. Such heterogeneous reactions, involving a porous solid and a gas, generally include several steps [50]: 1) *mass transport* of O_2 to the surface of the porous solid, 2) *diffusion* of the O_2 within the pores of decarbonized layer, 3) *chemical reaction* of graphite with oxygen on the solid surface, 4) *diffusion* of the gaseous product through the porous solid, 5) *mass transfer* of the gaseous product into the bulk gas steam.

At low temperatures, where the intrinsic reactivity of the solid is low, a molecule of gaseous reactant entering the porous solid has a high probability of diffusing deeply into the porous body before finally reacting with the pore surface. The concentration of gaseous reactant is essentially uniform throughout the porous solid and equal to that in the bulk gas stream. The overall rate is controlled by the gas-solid chemical reaction that takes place with the gaseous reactant concentration at the level in the bulk gas stream. This is the early stage of oxidation, no clear decarbonized layer has formed yet [51].

At intermediate temperatures, where the intrinsic solid reactivity is greater, the probability of a gaseous reactant molecule penetrating deeply into solid is small. Most of the reactions occur in the zone near the external surface of the solid. Diffusion within pores limits the overall rate of the reaction but does not control it because both chemical reaction and pore diffusion exert an influence on the progress of reaction. Under such condition, decarbonized layer do form.

At even higher temperatures, the intrinsic solid reactivity will be so high that the gaseous reactant molecules will react with the solid as soon as they have crossed the boundary layer enveloping the solid. The concentration of the gaseous reactant at the external surface of the solid is near zero and the progress of reaction controlled by external mass transfer.

Many factors govern oxidation of carbon, such as internal factors like carbon material, its amount, purity, type, size and structure as well as porosity and external factors like atmosphere and temperature.

Regarding to the nature of carbon material, based on the study of both oxidation and corrosion resistance of MgO-C bricks with 4 different types of flake graphites, Li and Rigaud [52] indicated that the use of high-purity graphite or graphite with large flake size retards carbon oxidation in an oxidizing atmosphere. Corrosion resistance is a pre-conditioned by the oxidation process. As carbon phase is oxidized, the impurity phase of the flake graphite left in the decarbonized layer promotes refractory wear by the slag. Cooper [53] substantiated the role of flake graphite on the performance of alumina-based and zirconia based refractories. Sakaguchi et al [54] concluded that the use of fine graphite results in the dense brick texture, which retards chemical reactions and thus improves oxidation, abrasion and corrosion resistance. Yamaguchi and Zhang [55] compared the oxidation behaviours of various kinds of carbon and claimed that during

heating, Al_2O_3 accelerates the oxidation of graphite, and TiO_2, ZrO_2 and MnO inhibit the oxidation of graphite.

2.4 METHODOLOGY OF PROTECTING CARBON FROM OXIDATION

2.4.1 Carbon Protection

At temperature above 1400°C, indirect oxidation of carbon assumes a leading role in the carbon-containing refractory [21]. Graphite reacts with solid or liquid oxides or gaseous sub-oxides, which are present in the system. It is known that the depth of oxidation decreases for the bricks with higher magnesia content. This is attributed to the formation of the MgO dense zone resulting from the reduction of MgO in the brick in contact with carbon, followed by subsequent re-oxidation near the hot face, where, $MgO(s) + C \rightarrow Mg(g) + CO$ and $2Mg(g) + O_2 \rightarrow 2MgO(s)$, where, the secondary periclase bridges the grains and act as a protective barrier to facilitate protection of carbon from oxidation. In addition, in most cases during practical uses at a higher temperature (1600°C), refractories are exposed to either slag or liquid metal, at very low P_{O2} condition. The outside zone of the material is positively sealed from the inside, which decreases oxygen diffusion inwards.

At temperature below 1400 °C, however, carbon direct oxidation is dominant. A common practice on carbon protection is to incorporate antioxidant into refractory composition.

From laboratory work to field application of carbon-bonded refractories, many R&D have been carried out on using antioxidants to prevent carbon from oxidation in carbon-bonded bricks. The reports on antioxidants in castables are still limited. Such materials on drying liberate water vapor, which will react with the antioxidants, generating eventually hydrogen and this constitutes a potential hazard, to be documented in this thesis.

For an arbitrary reaction $M(s) + O_2 = MO_2(s)$, at equilibrium conditions, $\Delta G^o = -RT\ln 1/P_{O2}$. Figure 2.4 shows the relationship between the temperature and the standard free energy change of the reaction of different metals with oxygen. As can be seen under working temperature up to T = 1600°C, antioxidants have a greater affinity for oxygen than carbon. This is why, at first glance, antioxidant can protect carbon from oxidation.

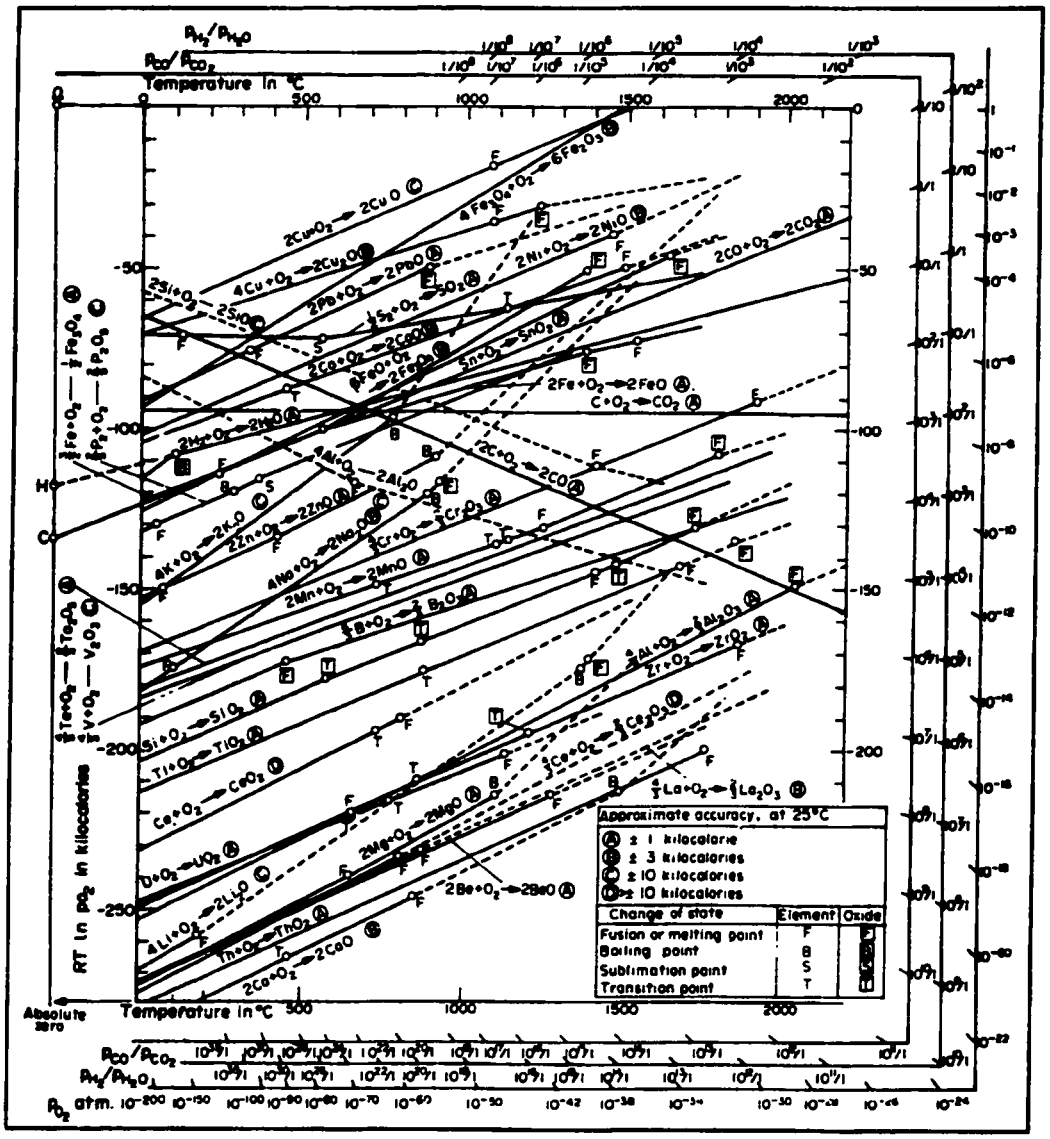

Figure 2.4 Relationships between temperature and standard free energy of the reaction of common antioxidants and oxygen [39].

Consequently, O_2 (g) will be very low, N_2 (g) will remain and CO (g) and MgO(s) will be the major sources of oxygen in the system MgO-C refractories with antioxidants [21]. Five typical reactions for antioxidant (A.O.) may occur as below.

A.O. + C (s) → Carbide (s); Carbide (s) + CO (g) → Oxide + C (2.1)

A.O. + CO (g) → Oxide (s, l, or g) + C (s) (2.2)

A.O. + MgO (s) → Mg (g) + Oxide; Mg (g) + CO (g) → MgO (s) +C (2.3)

A.O. + N_2 (g) → Nitride (s,l); Nitride (s,l) +CO (g) → Oxide (s,l) + C (s) +1/2 N_2 (g) (2.4)

A.O. + Oxides* → Sub-oxides (g); Sub-oxides + CO (g) → Oxide + C (2.5)

Accordingly, many competing reactions take place in the porous refractory containing graphite and metallic antioxidants. The nitride, carbide and complex oxide products may partially fill in the internal porosity, contributing significantly to the bonding of the major constituents and altering hot strength and other properties.

From the reaction (2.1) to (2.5), the effect of pore blocker can be obtained in the case of formation of solid oxides, which causes a net gain in volume, reduces the porosity and increases the mechanical strength. When the oxide formed is liquid, it can block pores and prevent inward diffusion of oxygen. It should be noticed that this might lead to a reduction of slag resistance and of strength at high temperatures. As can be seen, in each case, carbon can be recreated from CO reduction, and thereby better carbon protection is achieved. The predominant reaction products may change with temperature, atmosphere and pressure variations.

2.4.2 Typical Antioxidants

Metallic antioxidants, such as aluminium, silicon and magnesium, are commonly used in carbon-bonded refractories, metallic aluminium powder being the most common of all. The changes of aluminium and aluminium-compounds under coexisting C (s), CO (g) and N_2 (g) during the heating process are illustrated in Figures 2.5 and 2.6 respectively.

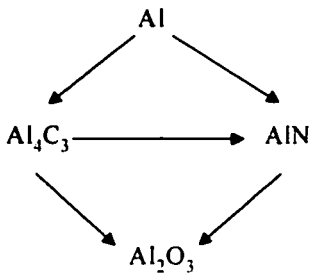

Figure 2.5 Schematic evolution of Al and Al-compounds in the presence of C (s), CO (g) and N_2 (g) [56]

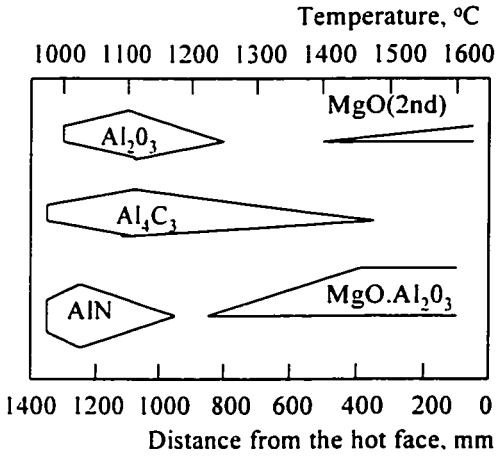

Figure 2.6 Stability fields of Al-compounds in MgO-C-Al refractories, under a thermal gradient from 1650 to 950°C, in a brick width's of 1400mm [56]

The reaction products, like Al_4C_3, AlN, Al_2O_3 and $MgAl_2O_4$ [56-61], lead to a volume expansion and closure of pores, which prohibit the diffusion inward of oxygen. Furthermore, the AlN whiskers, the Al_4C_3 crystals and the high melting point spinel which form contribute to the increase in high-temperature strength. It is clear that to add an optimum amount, type and size of aluminium need to be taken into account. Too

much aluminium will affect overall porosity and reduce corrosion resistance and strength.

Silicon powder has been used successfully to improve oxidation resistance in carbon-containing bricks [59-63]. The oxidation of silicon and the intermediate products, such as SiC and Si_3N_4, can result in the formation of a passive protective films of SiO_2, which causes weight gain, or can occur actively resulting in SiO (g) or CO (g) or N_2 (g) and weight loss, as shown schematically in Figure 2.7. In active oxidation, oxygen arriving at Si surface is totally consumed to form SiO (g), which diffuses away from the reaction site at about the same rate as oxygen diffuses to the site. The reaction can continue at a steady state. Whereas, in passive oxidation, a stable SiO_2 film is present and further oxidation is only possible by oxygen diffusion through this film. Passive oxidation is almost always preferred to offer protection in service.

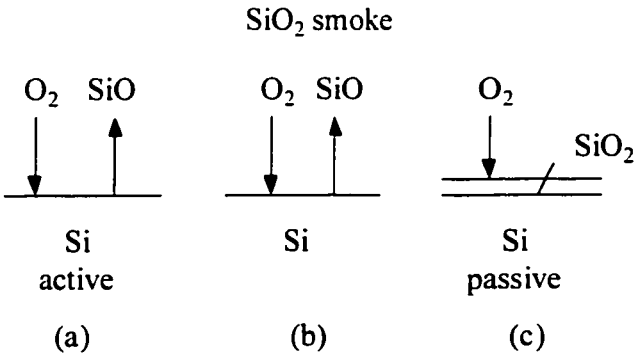

Figure 2.7 Schematic representation of a) active oxidation, b) active-passive transition, c) passive oxidation [63]

For the magnesia-carbon brick with Mg metal as antioxidant, since Mg metal boils at approximately 1100°C, it vaporizes and oxidizes near the brick's hot face, forming a dense MgO layer. This effectively seals pores on the hot face of the brick, preventing carbon oxidation [64]. The potential danger of handling such a pyrophoric powder in industry as well as its cost and availability has prompted the use of Mg-Al alloys instead. Alloys, such as Mg-Al, Al-Si and Ca-Si-Mg, have been tested in MgO-C bricks [61,21]. With Al-Mg alloys not only oxidation resistance but also strength are improved beyond the values reached by using Al or Mg alone. The same observations were made for Al-Si alloys. Al-Mg alloys plus zircon and SiC have also been tried with some success to enhance thermal stress cracking resistance. Some commercial products are available using M_1+ M_2 or M_1-M_2 alloys, and the possible combinations are being extended. One of the concerns on using these additives is to control the amount of addition needed in order not to compromise with the slag corrosion resistance of the refractories.

In the group of non-metallic antioxidants, boron-containing compounds have been wildly adopted. Many different sources of boron-bearing compounds [16,65-70,73], such as B, B_4C, B_2O_3, CaB_6, ZrB_2, $Mg_3B_2O_6$, $Ca_3B_2O_6$, have been used in carbon-bonded refractories. T. R. Lipinski, et al [65-67] explained that the reason to use boron type of antioxidant is linked to the fact that the intermediate products of the reactions are mostly liquid phases, which have a more global effect in blocking the pores of the bricks. Also

the gases formed [Mg (g) and B_2O_2 (g)] react toward oxygen and reduce oxygen partial pressure in pores of the material.

Considering antioxidant packages, the work is mainly focused on improving hot modulus of rupture of the material. Boron-based antioxidants are very efficient agents to protect carbon from oxidation. It leads to the formation of a liquid phase, blocking pores and effectively protects carbon from oxidation in carbon-containing refractories. As a consequence, however, it affects negatively the hot strength and corrosion resistance of the refractories, and thereby limits its usefulness to very specific cases. Using a package of several antioxidants was proven to overcome the shortage and to extent the effect of each antioxidant.

MgO-C refractories with high values of hot modulus of rupture (HMOR) have been achieved using antioxidant packages of boron-containing compounds and Al or Al alloys simultaneously. Hayashi et al. [70] investigated the effect of the simultaneous addition of Al+B_2O_3-MgO or Al+B_2O_3-CaO in the mixes containing 30% graphite. The HMOR at 1400°C is higher than that of samples containing only Al or boron compounds. $MgAl_2O_4$ is being formed at about 1000 °C when Al and boron compounds are added simultaneously. Similar results using Al+SiB or Al+BN with 16% graphite regarding the HMOR at 1400°C and 1500 °C were also reported by Palco et al [71]. Hirai et al [72] worked on the effect of additives on the formation of $MgAl_2O_4$ from MgO and Al_2O_3 and reported that the addition of CaB_4O_7 *and* B_2O_3 accelerates the formation of

$MgAl_2O_4$. Klaus et al. [77] reported aluminium is more effective because it promotes the formation of Mg vapor in the brick and permits reaction with slag to produce a protective layer.

As an example of using experimental synthetic antioxidant, the behaviour and effect of synthetic antioxidants $Al_8B_4C_7$ or Al_4SiC_4 were reported by Yamaguchi et al. [78-79]. The hydration resistance of Al_2O_3-C refractory was greatly improved and from high to low in the order of Al_4SiC_4, Al+Si to Al; the oxidation resistance, in the order of Al, Al_4SiC_4 to Si. The open pores decreased with addition of Al_4SiC_4, Al or Si. $Al_8B_4C_7$ and Al_4SiC_4 react with CO (g) to form Al_2O_3-B_2O_3 and Al_2O_3-SiO_2 protective layers respectively on the surface of the refractories, thus inhibiting carbon oxidation.

2.5 CURRENT STATUS OF CARBON-CONTAINING CASTABLES

Many commercial tentatives have been made to use castable refractories instead of shape refractories in steel ladles, to cope with the decreasing number of bricklayers and to reduce the unit consumption of refractories. With the metallurgical changes, which happened in the steelmaking process, especially the introduction of secondary refining technology in ladles, the requirement on any castable refractory are very stringent. Although alumina based castables, such as alumina spinel castable or alumina magnesia castable have been accepted to apply to ladle barrel and bottom under severe conditions, they are not acceptable as slag line refractories where more basic corrosive slag is used.

Some newly developed magnesia-based castables like magnesia spinel-bonded castable and magnesia forsterite-bonded castable have demonstrated strong corrosion resistance. The main drawback of those magnesia-based castables, however, is their poor penetration resistance. To increase penetration resistance, adding carbon into castable is obvious approach since it works so well for carbon-bonded bricks.

However, carbon containing castable faces many technical restrictions. The introduction of flake graphite into refractory is highly desirable with respect to its corrosion and thermal shock resistance, but the poor water dispersibility of flake graphite causes high demand of water addition and thus high porosity of the castable, which limits the benefit expected from flake graphite as compare to other carbon sources.

2.5.1 Carbon Material in Castables

Considering the dispersion and wetting problems of carbon material, carbon sources such as pitch, coke and carbon black, without any graphitic materials, have been used at first to minimize the problem of high water demand and thus minimize the porosity of the castable.

Teranishi et al [80] reported the influence of carbon source on flowability of castable. The results showed that water content of the MgO-C castable with 5% carbon can reach

over 18% with flake graphite, over 9% with amorphous graphite and 6% with pitch and carbon black, as shown in Figure 2.8.

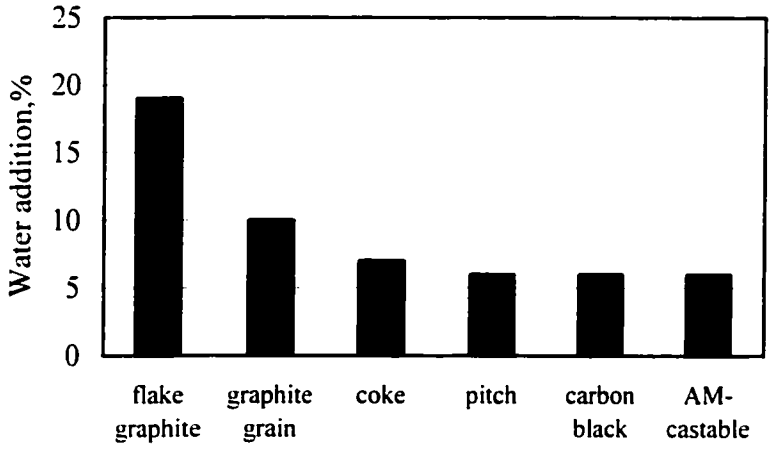

Figure 2.8 Influences of carbon sources on water addition of MgO-C castable [80]

It indicates, obviously, that these high values of water content from graphite addition implied their unsuitability for realizing a dense structure. Pitch and carbon black were effective for reducing water since they demanded as little water as the Al_2O_3-MgO castable. Therefore, to avoid cracking after drying, a combination of pitch and carbon was selected in MgO-C castable, which was then used for the repair of the slag line of a LF ladle. The properties of this magnesia-carbon castable are listed in Table 2.2. The encouraging result from practical application represented that the durability of the slag line was more than twice that obtained by the conventional Al_2O_3-MgO castable.

Table 2.2 Properties of MgO-C castable [80]

Chemical composition, %	MgO	90
	C	5
Apparent porosity, %	110°C-24h	15.3
	1500°C-3h	18.2
Bulk density, %	110°C-24h	2.71
	1500°C-3h	2.65
Crushing strength, MPa	110°C-24h	28.3
	1500°C-3h	25.4
Linear change, %	1500°C-3h	0.64

Reports on plant trials of MgO-C castables are so far still limited so far. MgO-SiO_2–C castable [81], which contained 85% MgO grains, 7% SiO_2 and 7% carbon, was reported to achieve excellent strength over a temperature range of 20 to 1600°C. The slag corrosion resistance is comparable to resin-bonded magnesia-graphite brick for ladle slag line.

These results are encouraging to pursue the study of carbon containing castable. It also indicates that graphite performs the best in carbon-bonded bricks, but the worst if flake graphite is directly added into castable. Therefore, in order to take full advantages of graphite, new ways of inserting graphite have to be found.

2.5.2 Graphite in Castables

For incorporating graphite into castable, some new approaches on surface modification of the flake graphite are carried out to minimize the problem caused by graphite on high water demand. So far, solutions in modifying hydrophilic properties of flake graphite include:

1) Surface coating of graphite by Al_2O_3, TiO_2, ZrO_2-Al_2O_3, SiC [18-19,82-85]

Surface coating is based on the principle that most of oxides and carbides have better water dispersibility and wettability than flake graphite. Therefore, to coat hydrophilic agents on the surface of flake graphite is expected to improve dispersibility of graphite.

Yoshimatsu et al [84] investigated the Al_2O_3 coating on the surface of flake graphite. A chelate compound of alumina ($(Al(OC_3H_7)2(C_6H_9O_3))$) was coated on the flake graphite surface by firstly mixing it in a high speed machine and then the mixture was heated at 500°C for two hours in air. The wettability was evaluated by measuring the volume of sediment, packaging density of sediment and fraction of floating graphite in water. The result shows that wettability was improved but no further reports were found documenting its use in castable.

Yu et al (1996) [82-85] studied TiO_2-coated flake graphite by similar method as mentioned above. The flow value of coated flake graphite is 154mm, with TiO_2 coating,

whereas the flow value of untreated flake graphite is only 118mm. It is also confirmed that TiO_2 coating improves the oxidation resistance of coated graphite, but lack of further information on its use in castable.

To improve oxidation resistance of flake graphite, Li et al (1998) [83] worked with a ZrO_2-Al_2O_3 composite powder, which was synthesized and then coated on the surface of graphite (purity 98%, particle size <150μm), by heating a mixture at 1100°C for four hours in an inert atmosphere of nitrogen or argon. The oxidation temperature of the coated graphite was improved as compared to uncoated graphite. There are no further report on the hydrophilic properties of ZrO_2-Al_2O_3 coated graphite.

Sakamoto et al (1995) [18,81] made SiC-coated graphite by a high-speed impact method. SiC particle (5 μm) can stick on the surface of the graphite (100-150μm) by employed impact force, compress force and friction force during the mixing. Scanning electron microscopy observations show that very fine SiC powders cover the surface of graphite and the shape of the graphite becomes spherical. The improvement of SiC coated graphite on dispersibility was confirmed by Zeta-potential measurement on the slurry and flowability measurement on Al_2O_3-SiC-C castables. This method produces coated graphite at a low cost, but coating can be removed during abrasion mixing because only physical binding between SiC and graphite.

2) Hydrophilic treatment by surface active agents

Kawasaki et al (1989) [19] used two active agents to form one layer of water-soluble polymer (cationic cellulose) and a deposition of a second layer of sodium silicate to obtain graphite with better hydrophilic property. Isomura et al (1998) [86] reported Al_2O_3-spinel-C castable was developed by using self-developed dispersant. The hydrophilic property of the castable was improved by using this special dispersant, which has a higher effect on improving hydrophilic property compared to conventional dispersants such as polycarboxylic acid and polyacrylic acid. The hydrophilic property was improved on amorphous graphite, artificial graphite and spherical graphite with size of D_{50} between 20-100 mesh, but not on flake graphite.

3) Agglomeration of graphite by extruding

Zhou and Rigaud [87] made micropellets of graphite by extruding method and used them in Al_2O_3-SiC-C castable. The results show a net advantages of using micropellets of graphite over flake graphite on flowability, mechanical property and corrosion resistance. Early in this thesis work, He et al [88] also used micropellets of graphite in MgO-C castable and confirmed the improvements in terms of flowability, mechanical property and oxidation resistance, as compared to the case of directly using flake graphite.

2.5.3 Antioxidants in Castables

To eliminate water reaction problem, some investigations have been made on coated metal or metallic alloy. Goda (1996) [89] reported that surface-treated Al-Si alloy powder with a protective surface layer obtained by atomization of the alloy Al-Si powders in an aluminum phosphate solution, could be used in a MgO-C castable. Ouchi (1998) [90] used coated metal Al, treated in an aluminum phosphate solution, in joint packing material. Other work was made to coat aluminum alloys in a trivalent chromium solution (Delaunois, 1997 and Pearlstein, 1994) [91]. No specific results have been published since from those authors.

2.6 REVIEW OF METHODS MEASURING OXIDATION RESISTANCE

The oxidation of carbon-bonded refractories includes gas oxidation by O_2 gas, solid oxidation by internal reactions with oxides, such as with MgO in MgO-C bricks, and liquid oxidation by FeO or MnO etc. in slag. Common oxidation resistance of carbon refers to the reaction with O_2 gas.

2.6.1 Existing Methods

So far there are several different experimental setups as illustrated in Figures 2.9-2.16 [92-97] to evaluate oxidation resistance of carbon-bonded refractories. Measuring the

weight change, the thickness or area of the decarbonized zone, the loss of strength, the volume of CO gas released and observing the change of microstructure all have been taken into account.

Weight change is commonly used to evaluate oxidation resistance of carbon material. Weight of sample is measured and calculated either discontinuously after firing sample for different time intervals or continuously by using a thermo balance. The limitation of this method is that it is difficult to distinguish if the contributions come from the weight losses or weight gains, which occur simultaneously. Generally, evaluating weight change is better for simple system.

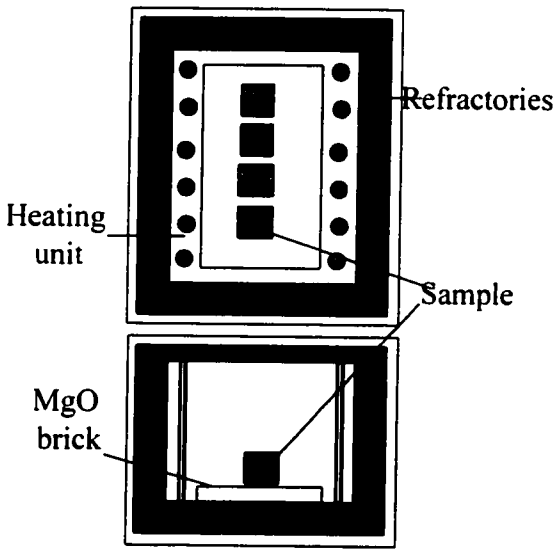

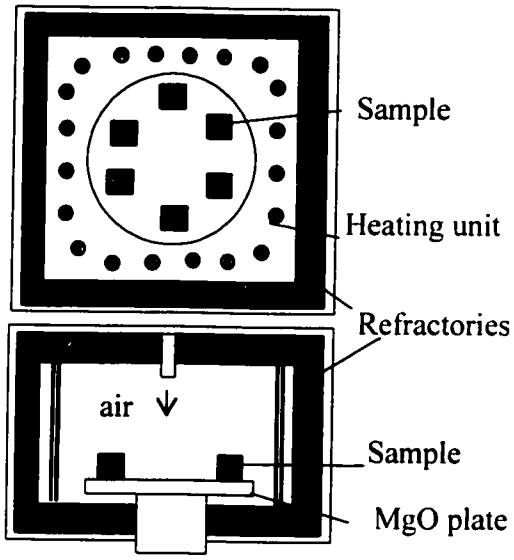

Figure 2.9 Conventional box furnace [92] Figure 2.10 Rotating bottom furnace [92]

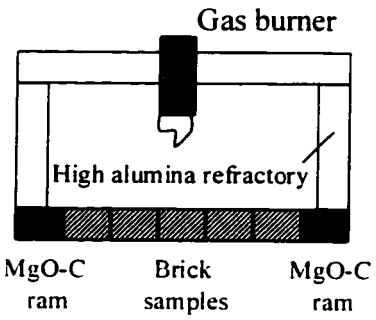

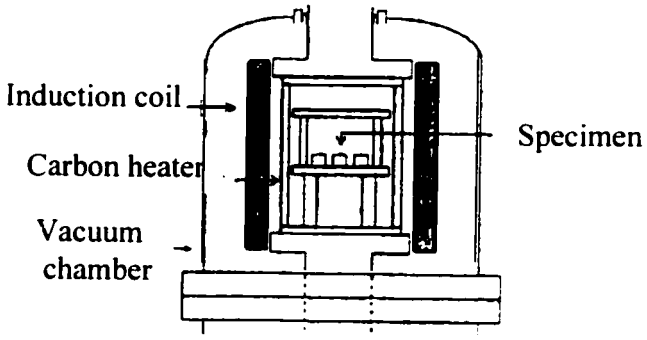

Figure 2.11 Thermal gradient furnace [93] Figure 2.12 Vacuum controlled furnace [94]

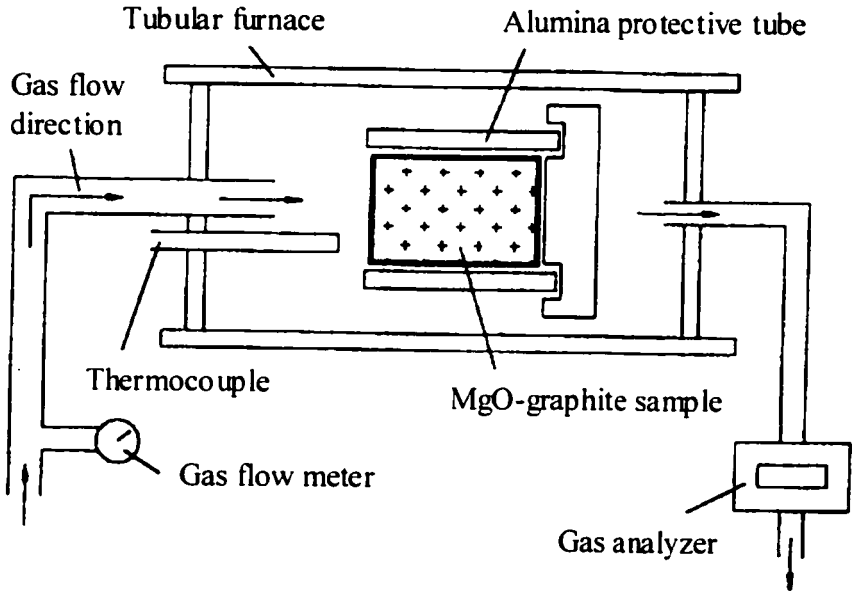

Figure 2.13 Tubular furnace [95]

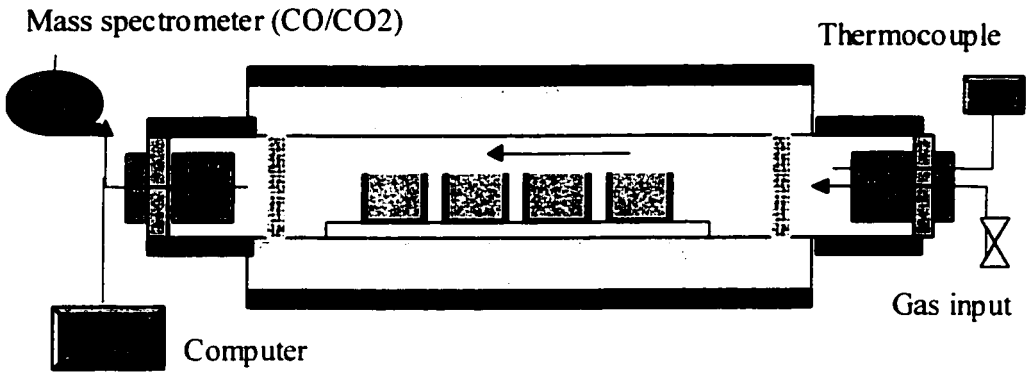

Figure 2.14 Horizontal furnace [96]

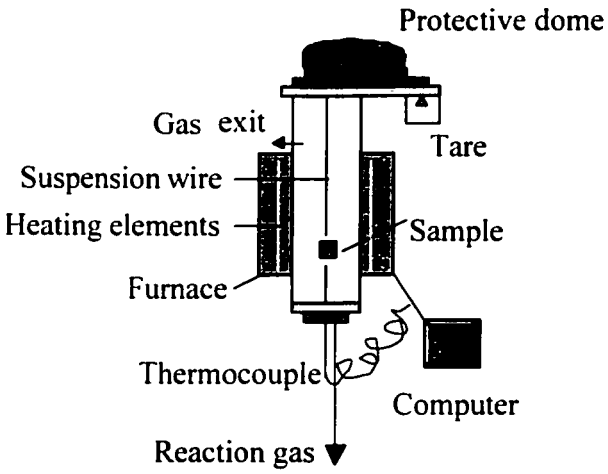

Figure 2.15 Thermo-balance method [95]

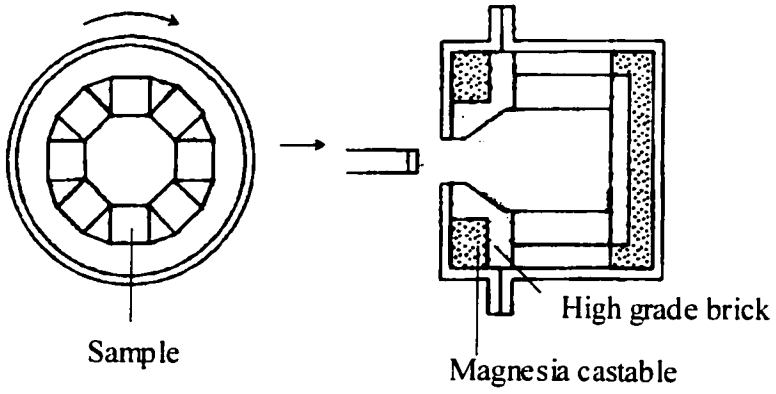

Figure 2.16 Rotary furnace [97]

The measurement of the thickness of an oxidized layer or the oxidized area of a cylindrical or a square sample is the most common way to report oxidation behaviour. The section of sample illustrates directly the overall difference between the oxidized and non-oxidized area. It is very efficient for the purpose of comparison, but may be misleading because of unclearly defined edges between oxidized and non-oxidized layers when the situation is more complicated. When the samples are in a thermal gradient, from hot to cold face, according to Lipinski [65], there are at least three zones to be evaluated, depending on the extrinsic conditions imposed. In the hottest zone, also called the decarbonized region, there is no graphite is left. In the intermediate zone, some carbon may still be present and then it is an undecarbonized zone. Because of different condition in different zones, antioxidants may favor different reactions, and thereby lead to different results of oxidation resistance.

different condition in different zones, antioxidants may favor different reactions, and thereby lead to different results of oxidation resistance.

The volume of CO released can be measured in certain experimental setups. It directly indicates the oxidation of carbon in a material. In addition, indirectly, the loss of the strength is also sometime taken into account for the evaluation of the oxidation behaviour. Accordingly, microscopic observation, X-ray diffraction analysis and physical property are used to confirm the changes of microstructures of the materials and explain how the oxidation resistance is improved. In Table 2.3 are summarizes the conditions and characteristics of the different experimental set-ups.

2.6.2 Comparison of Test Conditions and Outcomes

The test conditions very a lot, whether static or dynamic methods are applied. In the static situation, various heating, duration and cooling conditions are used. Samples can be fired from room temperature to design temperature, held for some time and cooled down, or samples can be put into a furnace at a fixed temperature, and removed after heating for fixed time. When heating samples in an electric furnace, test conditions, as shown in Figures 2.9-2.12, should be carefully considered including the number of samples, the space between samples, the distribution and the dimension of the samples, and the air flow and convection characteristics in the chamber.

Table 2.3 Conditions and characteristics of experimental set-ups for oxidation resistance measurement [92-97]

Device	Convention box furnace	Rotating bottom furnace	Thermal gradient furnace	Vacuum controlled furnace	Horizontal tube furnace	Tubular furnace	Rotary furnace	Thermo-balance
Sample	Cubic Cylinder Bar	Cubic Cylinder Bar	Brick size	Cubic Cylinder Bar	Cubic Cylinder Bar	Cylinder	Bar	Powder Piece Pellet
Number of sample	several	several	6	several	several	1	6 / 8	1
Thermal gradient	no	no	yes	no	no	yes / no	yes	no
Vaccum condition	no	no	no	yes	no	no	no	no
Unidirectional oxidation	yes / no	yes / no	yes	yes / no	yes / no	yes	yes	no
Continuity	no	no	no	no		yes	no	yes
Environment								
Free convection	yes	yes	no	yes	yes	yes	no	yes
Forced convection	no	no	yes	no	no	yes	yes	yes
Choice of gases	no	no	no	yes	yes	yes	no	yes
Static (S) / dynamic (D)	S	D	S	S	S	S	D	S
Evaluation								
Weight change	yes	yes	yes	yes	yes	yes	no	yes
Depth of decarbonized zone	yes	yes	yes	yes	yes	yes	yes	no
Area of decarbonized zone	yes	yes	yes	yes	yes	yes	yes	no
Loss of strength	yes	yes	yes	yes	yes	yes	no	no
Vol% of CO gas released	no	no	no	no	yes	yes	no	yes
Change of microstructure	yes	yes	yes	yes	yes	yes	yes	yes

For horizontal tube furnace (Figure 2.14) and tubular furnace (Figure 2.13), not only unidirectional oxidation (with protected crucible design), temperature and atmosphere can be easily monitored, but also a gas analyzer can be used to record amounts of CO_2 gas formed from the oxidation of carbon (also Figure 2.14). The limitation with tubular furnace is on the number of the samples which can be tested in each run.

For dynamic measurement of oxidation, a rotary furnace (Figure 2.16) is used to oxidize the sample with heating from one side only. Commonly six or eight samples can be fired from room temperature to a design temperature, held for certain time and cooled down, with 2 to 4 rpm rotation during the test. The advantages of this setup are that both unidirectional oxidation and temperature gradient can be exerted. It seems to be meaningful in terms of simulating service condition. The disadvantages of this setup are the difficulty in controlling atmosphere and the repeatability of test runs. Another dynamic measurement is in a box furnace with a bottom-turning table (Figure 2.10). All samples are uniformly heated and good repeatability is obtained compared to a the box furnace without bottom rotation.

Measurements can be performed continuously from thermo-balance (Figure 2.15), tubular furnace setups (Figure 2.14) or horizontal tube furnace (Figure 2.13). In thermo-balance setup, the samples can be easily performed at an isothermal condition at a given temperature or a non-isothermal test at a given heating rate in selected a atmosphere to

measure weight loss. The limitation of this method is that only small-sized sample for each run is feasible and the rate of gas flow is limited at a low level.

As can be seen, each experimental setup has its own characteristics and limits. Many factors have to be considered in order to evaluate oxidation resistance. Generally, the most important external factors are temperature, atmosphere and pressure; the most intrinsic factors are nature of carbon material, antioxidant, porosity, pore size and microstructure of the materials. For carbon containing refractories, it must be recalled that the porosity can change greatly with thermal cycling, from 3-5% on as received condition to 30-50% after total removal of carbon. As so many factors affect oxidation resistance, in most cases, one test method is not enough to evaluate oxidation resistance satisfactorily. For comparative purpose, relative value of measurement is better than absolute value.

CHAPTER 3 PACKAGING FLAKE GRAPHITE

3.1 INTRODUCTION

To select a suitable carbon source and protect it from oxidation are important factors for developing carbon-containing castables. Graphite is highly desirable with respect to its high corrosion and thermal shock resistance as well as high oxidation resistance than other carbon sources. Its usefulness has been clearly demonstrated in resin-bonded magnesia carbon bricks. However, the poor water dispersibility of graphite flakes causes higher demand of water addition and more porous structure of the castables compared to the mixtures without any carbon. This drawback limits the benefits expected from graphite in developing graphite-containing castables. Therefore, in the early stages, the developments of carbon-containing castables were limited to the use of petroleum coke, pitch, carbon black and amorphous graphite as carbon source, which provide the acceptable flowability of the castables, compared with straight addition of graphite flakes, as reviewed in chapter 2.

Inferior oxidation resistance of those kinds of carbon sources as compared to flake graphite results in a higher wear rate of the materials due to the loss of carbon. In order to develop superior quality of carbon-containing castables, approaches to incorporate graphite flakes into castables induced the present efforts, on how to package and/or modify the graphite flakes and how to make its use acceptable in castables. This is

described in this chapter. The research efforts are mainly concentrated on two parts: 1) on improving hydrophilic property of flake graphite and reducing segregation during mixing, and therefore contributing to good flowability and physical properties, 2) on increasing the oxidation resistance of the modified graphite materials.

In this chapter, three different modified graphite pellets, named as extruded graphite (denoted as EG), coated graphite (denoted as CG) and granulated graphite (denoted as GG) are produced and studied in terms of their composition design, morphology and hydrophilic property. The extruding, coating and granulating processes are described with a greater emphasis on EG pellets. The improvements on upgrading EG pellets by incorporating antioxidants and oxides are highlighted.

3.2 EXPERIMENTAL PROCEDURE TO PRODUCE EXTRUDED GRAPHITE

3.2.1 Experimental Plan

The aims of the research were: 1) to reduce the specific surface area of graphite by agglomerating or packaging graphite flakes together, 2) to optimize the pellets in terms of density and pore size by incorporating some additives, 3) to protect graphite from oxidation by using suitable antioxidants and oxides inside the pellets.

3.2.2 Raw Materials

The raw materials used to produce modified graphite pellets, either EG, CG or GG, include natural graphite flakes, carbon black, pitch, antioxidants, oxides, liquid binders and wetting agent, are listed in Table 3.1.

Table 3.1 Raw materials for modified graphite pellets

Code	Material	Specification	Brand and Manufacture
1	Flakes graphite	Fixed C ≥ 97.0%, < 75 μm	*Stratmin 200* Stratmin Graphite Co., Canada
2	Carbon	Fixed C ≥ 97.7%, 5.0 μm	Maluka CCM Osaka Kasei, Japan
3	Pitch	Fixed C ≥ 60.0%, <1.0 mm	Pellet pitch Zhenjiang Jiaohua, China
4	Al	Al ≥ 99.0%, < 75μm	*Al-101* Reade Manufacturing Co., USA
5	AlMg	< 75 μm	Reade Manufacturing Co., USA
6	Si	Si ≥ 99.0%, < 10 μm	*J-99* Elkem ASA Materials
7	SiC	97.7 % < 75 μm	Exolon-ESK Co., USA
8	B_4C	B_4C >90.0%, B_2O_3 < 7.0%, < 45 μm	*Tetrabor* ESK GmbH, Germany
9	MgO	≥ 98.0%	LUD 98 Marelan Plant, Resco Products Co.
10	Al_2O_3	Al_2O_3 ≥ 99.0 % <1.0 μm	A-1000SGD Alcoa, USA
11	Al_2O_3	Al_2O_3 ≥ 99.0 %	A-16<1.2 μm, T64 <45 μm Alcoa, USA
12	SiO_2	≥ 98.0 % < 1.0 μm	971 U Elkem Materials, Norway
13	Molasses	100%	*Grandma*, Grandma Food Products Co., Canada
14	Colloidal Silica	Silica	Aldrich Chemical Co., Inc.
15	Wetting agent	Glydol	Zschimmer & Schwarz, GmbH Co.

For improving the quality of the extruded graphite pellets, selected antioxidants were either aluminium (Al) and silicon (Si), or aluminium-magnesium alloy (AlMg), a boron bearing powder -- boron carbide (B_4C) as well as oxide additives, i.e., magnesia (MgO), alumina (Al_2O_3) and silica (SiO_2). The antioxidants and oxides were incorporated into extruded graphite pellets to increase their density, favor a better distribution of flake graphite during mixing, improve their microstructure and oxidation resistance. Two liquid binders, i.e., molasses (denoted as M) and colloidal silica (denoted as S) were used and compared, but the essential of the work in this thesis has been done with molasses.

3.2.3 Characterization Tools

3.2.3.1 Microscopy Observations

Microstructure studies were carried out by optical microscopy (OM, Nikon Eclipse), scanning electron microscopy coupled with energy depressive X-ray spectroscopy (SEM/EDS, IEOL JSM-840), as well as cathodoluminescence microscopy (CLM, luminoscopy ELM-3RX, see Figure 3.1). Microscopic observations were performed on the original modified graphite pellets and the compressed cylindrical samples containing extruded graphite pellets and matrix constituents of MgO-C-antioxidants castables. The cylindrical samples were prepared by compressing the mixture of magnesia-based matrix with modified graphite into a diameter of 25mm and a height of 25mm at a

pressure of 70MPa. Then the cylindrical samples were fired under unidirectional oxidation condition at 1400°C×3h. After cooling down, the samples were cut in cross section and prepared for microstructure examination.

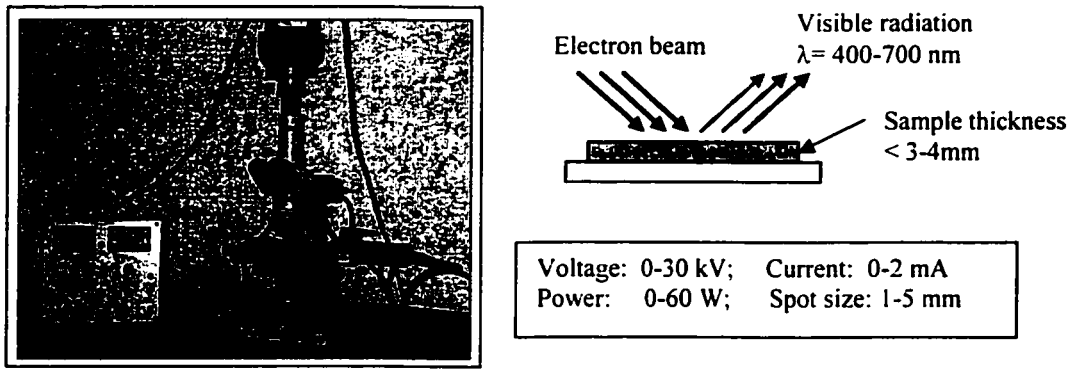

Figure 3.1 Cathodoluminescence microscopy set-up

3.2.3.2 Pore Size Distribution

Both total porosity and pore size distribution are important factors influencing oxidation resistance and corrosion resistance. The pore size distribution of extruded graphite pellets were measured by mercury porosimeter. Extruded graphite pellets with a diameter of ∅1.0mm were fired at 1400°C×3h in coke before performing the measurements.

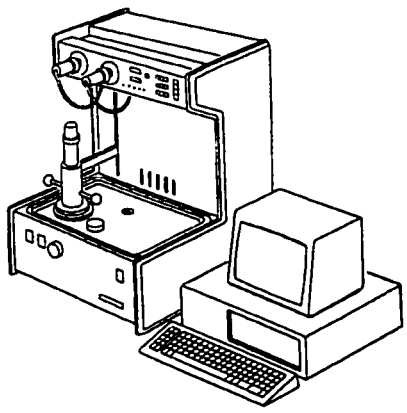

Figure 3.2 PoreSizer 9320 system [99]

The PoreSizer 9320 was used to measure pore size distribution and density of the extruded pellets. It is a 30,000 psia (207 MPa) mercury porosimeter covering the pore diameter range from approximately 360 to 0.006μm, as shown in Figure 3.2. The unit has two built-in low-pressure ports and one high-pressure chamber. Low pressure measurement covers pressures from 0 to 30 psia (0.207MPa), and pore diameters from 360 to 6μm. High-pressure range covers from 0 to 30,000 psia (207MPa), and pore diameter from 6 to 0.006μm.

Mercury porosimetry is based on the capillary law governing liquid penetration into small pores. From this law, in the case of a non wetting liquid like mercury and cylindrical pores, the pore diameter intruded by mercury at each pressure is calculated using the Washburn's equation [99]:

$$D = \frac{-4\gamma\cos\theta}{P} \qquad (3.1)$$

Where, D = the pore diameter; γ = the surface tension of Hg

θ = the contact angle of Hg on carbon ceramics

P = the applied pressure

The surface tension of mercury varies with purity, and its accepted value γ is 485 dynes/cm. The contact angle between mercury and solid containing the pores varied with solid composition. For carbon-containing materials, contact angle of 150° has been selected for the calculation

3.2.3.3 Bulk Density Measurement of Extruded Graphite Pellets

Bulk density of extruded graphite pellets was measured by mercury intrusion method. All samples were treated at 1400°C for 3 hours in coke before the measurement were taken.

3.2.3.4 Wettability of Graphite Material

Samples were prepared by compressing the graphitic material, FG, EG or CG, into ∅25mm×5mm tablets at a pressure of 70MPa. One drop of water using a clean plastic dropper was put on the surface of each type of tablets. Then a photo of water on the surface of the tablet was taken. The wettability of the graphite was evaluated by wetting angle measured using image analysis software "Image-Pro Plus".

3.2.4 The Extruding Process

The parameters considered to improve the characteristics of EG were based upon the observations of 1) the distribution of graphite flakes inside pellets, 2) the pore size distribution, 3) the densification, 4) the microstructure change, 5) the hydrophilic property, 6) the oxidation resistance of the pellets.

3.2.4.1 The Composition Design

Extruded graphite pellets were designed to fit with the type of castables to be made. For spinel bonded MgO-MA-C castables, EG pellets were formed by incorporating antioxidants Al, AlMg and B_4C as well as oxides MgO and Al_2O_3 (denoted as (EG-A.O.)$_{MA}$). For forsterite bonded MgO-M_2S-C castables, EG pellets were formed by adding antioxidants Si, SiC, B_4C and oxides MgO and SiO_2 (denoted as (EG-A.O.)$_{MS}$).

Five antioxidants, three oxides and their combinations, as well as two different binders were explored in order to improve the quality of the EG pellets. EG pellets with 100% FG, without any additive are denoted as EG-0. The other EG pellets contain 80% FG with 20% additives containing antioxidants with or without oxide fillers. In total 15 different kinds of extruded graphite pellets were produced as shown in Table 3.2. It is noted that both EG-MAOBC and EG-MAOBC$_S$ contained 4% of fine carbon black. The binder in EG-MAOBC$_S$ is colloidal silica instead of molasses.

3.2.4.2 The Extrusion Process

1) Mixing

All ingredients are introduced into the Hobart N50 mixer, then dry mixed for 2 minutes. Based on the composition of the extruded graphite, with or without additive, the addition of 30-34 wt.% of binder is made. The binder is prepared by diluting pure molasses with

6% water. Mixing in the Hobart is continued for 5 minutes, until the wet mixture reaches a desired plasticity. Generally, the wet mixture needs to be used up within one hour.

Table 3.2 Composition design of extruded graphite pellets

Code	FG	Al	AlMg	B_4C	Si	SiC	MgO	Al_2O_3	SiO_2	CB	C
EG-0	100										95
EG-B	95			5							90
EG-A	80	20									76
EG-AM	80		20								76
EG-AB	80	15		5							76
EG-ABM	80	6		4			10				76
EG-AO	80							20			76
EG-AOB	80			5				15			76
EG-MAOBC	46			5			30	15		4	48
EG-MAOBCs	46			5			30	15		4	48
EG-S	80				20						76
EG-SC	80					20					76
EG-SB	80			5	15						76
EG-SCB	80			5		15					76
EG-SOB	80			5					15		76

2) Extruding

There are different plate-models with different diameters for controlling the diameter of the pellets. In order to study the distribution of graphite flakes and microstructure change of the pellets, three diameters of Ø3.0mm, Ø1.0mm and Ø0.5mm were selected

in this work. After setting up a selected plate-model, the wet mix is fed continuously to the belly of the extruder. The flowing green material is pushed through the plate forming noodle-like extruded strings falling into a glass or steel container.

3) Curing and Drying

The green extruded material is kept at ambient temperature for over 6 hours, then heated in a drier at a rate of 1°C/min up to 200°C, and kept for over 16 hours to remove the volatile. The drier used is a Cole-Palmer Oven.

4) Crushing

After drying, the noodle-shaped material is crushed to 2-5mm in length, using a vibrating-crushing and sieving method. The length of the extruded pellets is controlled through adjusting the vibrating time.

The different extruded graphite pellets were obtained and divided into three groups: 1) (EG-0), without any additives inside of the pellets. 2) $(EG\text{-}A.O.)_{MA}$, with additives such as Al, AlMg, B_4C, MgO and Al_2O_3 as well as their combination. 3) $(EG\text{-}A.O.)_{MS}$, with additives such as Si, SiC, MgO and SiO_2 as well as their combination. A special study on the influence of the binder was performed on $EG\text{-}MAOBC_S$ pellets. For all other $(EG\text{-}A.O.)_{MA}$ and $(EG\text{-}A.O.)_{MS}$ pellets, molasses was used as a binder.

3.3 CHARACTERISTICS OF EXTRUDED GRAPHITE PELLETS

The morphology of extruded graphite pellets as observed in SEM is shown in Figure 3.3.

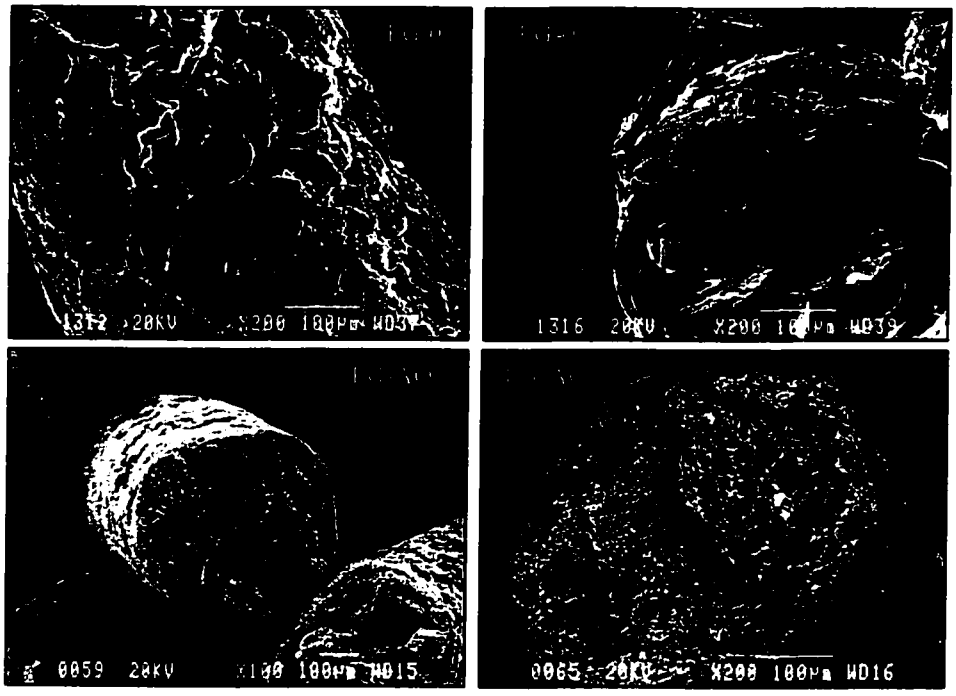

Figure 3.3 Morphology of extruded graphite pellets EG-0 and EG-AO (SEM photo)

It can be seen that graphite flakes are well agglomerated together and clearly visible within each extruded graphite pellet, where the same size of graphite flakes was used in EG-0 and EG-AO. After incorporating antioxidant and/or oxide into the pellets (here, EG-AO), a denser structure was obtained. The surfaces of flake graphite in EG-AO pellets are not only coated with binder, but also partially coated with refractory oxide.

Three sets of results are being performed to characterize those 15 different EG-A.O. pellets. The wettability measurement is explained in section 3.2.3.4. Then pore size distribution measurement on individual pellets fired up to 1400°C for 3 hours under reducing conditions is described in section 3.2.3.2. Finally, microscopy observations (section 3.2.3.1) on pressed samples, containing EG-A.O. pellets and various matrix fractions to be used in the castable, are illustrated, in MgO-MA-C and MgO-M_2S-C systems. The pressed samples have also been fired at 1400°C for 3 hours, under reducing conditions.

3.3.1 Hydrophilic Behaviour of EG Pellets

The results of wettability measurements on flake graphite and extruded graphite pellets are shown in Figure 3.4. The pictures clearly illustrate that extruded graphite pellets have smaller wetting angle (49°-34°) and better wettability than that of flake graphite (wetting angle 76°) due to the modification of graphite flakes. The improvement of the hydrophilic property of extruded graphite as well as the agglomeration of the flake graphite in EG pellets will contribute to a lower water addition and a better flowability of the castable.

In order to further improve hydrophilic property of EG pellets, hydrophilic treatment was performed on EG pellets using the solution containing wetting agent glydol. EG pellets were firstly immersed into the solution for over 8 hours at room temperature and

then were removed from the solution and dried, named as EG-WA pellets. After drying, the EG-WA pellets were compressed into a tablet as described in section 3.2.3.4. The wettability was compared in Figure 3.4. It shows that the hydrophilic treatment is efficient to improve wettability of the pellets. In this work, EG pellets were directly used in castables, where the wetting agent was added into the water, which is used for casting.

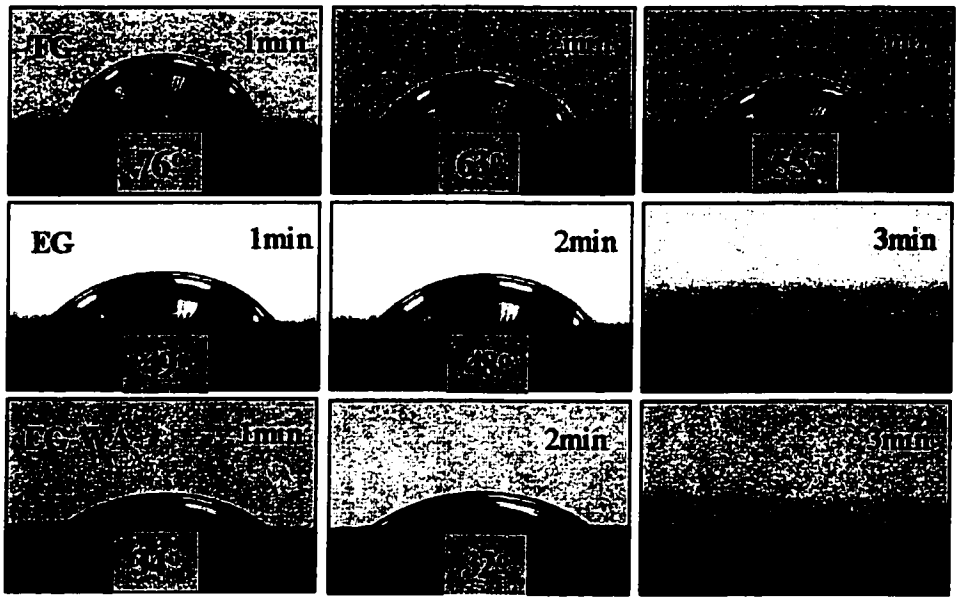

Figure 3.4 Behaviour of a water drop on the surface of pressed flake graphite (FG), extruded graphite (EG) and extruded graphite treated by wetting agent (EG-WA)

3.3.2 EG Microstructure Evolution Under Reducing Condition

In order to understand the behaviour of the pellets, it was decided to follow their microscopic structure, after firing under reducing conditions: the pore size distribution, the bulk density and the apparent porosity were determined, after each heat treatment.

3.3.2.1 Pore Size Distribution

The pore size distributions of EG-A.O. pellets were measured by mercury intrusion method, as described in 3.2.3.2. The results are illustrated in Figure 3.5 for $(EG\text{-}A.O.)_{MA}$ and Figure 3.6 for $(EG\text{-}A.O.)_{MS}$. The pellets were fired at 1400°C for 3 hours in coke.

For $(EG\text{-}A.O.)_{MA}$ system:

- Incorporating antioxidant and oxide into the pellets effectively reduced the median pore diameter of extruded graphite pellets. The median pore diameter of the pellets change from 8.75μm for EG-0 to 1.13-2.26μm for $(EG\text{-}A.O.)_{MA}$, see Figure 3.5a.
- Comparing pore size distribution with 80% of cumulative volume intrusion, sample EG-0 has pores distributed in the ranges of 20 to 4μm and $(EG\text{-}A.O.)_{MA}$ in the ranges of 20 to 0.2μm, see Figure 3.5b.
- For pore size over 4μm, EG-0 reaches 80% of cumulative intrusion, $(EG\text{-}A.O.)_{MA}$ only have less than 20% of cumulative intrusion, see Figure 3.5b.

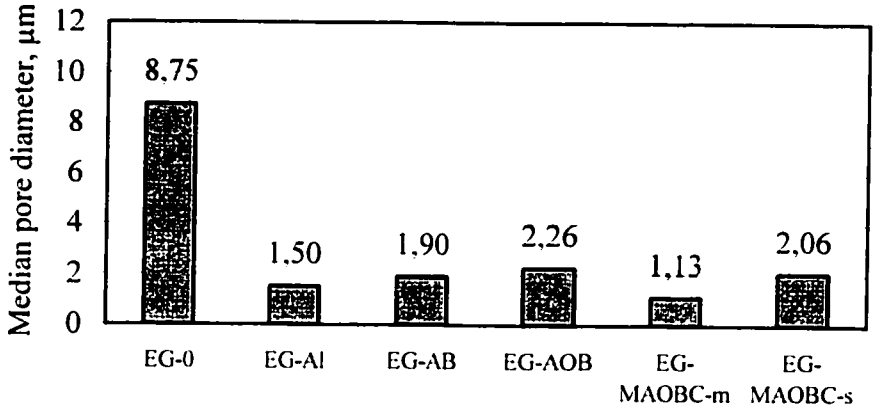

Figure 3.5a Median pore diameter (µm) of $(EG\text{-}A.O.)_{MA}$ pellets after firing at 1400°C×3h. embedded in coke

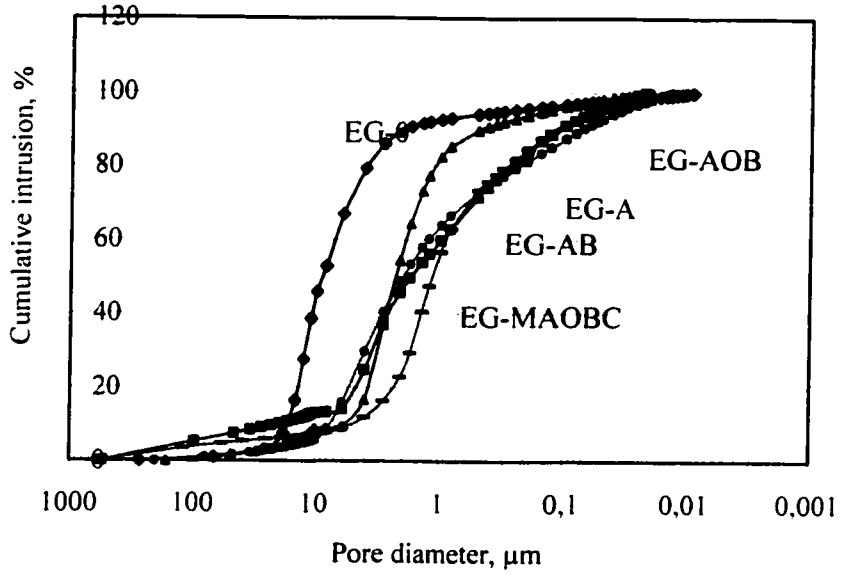

Figure 3.5b Cumulative intrusion (%) vs. pore diameter (µm) in $(EG\text{-}A.O.)_{MA}$ pellets after firing at 1400°C×3h. embedded in coke

For $(EG\text{-}A.O.)_{MS}$ system:

- Comparing pore size distribution with 80 % of cumulative volume intrusion, sample EG-0 has pores distributed in the ranges of 20 to 4μm and $(EG\text{-}A.O.)_{MS}$ in the ranges of 20 to 0.50μm (see Figure 3.6a).
- For pore size over 5μm, EG-0 reaches 78% of cumulative intrusion, $(EG\text{-}A.O.)_{MS}$ have less than 50 % of cumulative intrusion (Figure 3.6a).
- Median pore diameter changes from 8.75μm for EG-0 to 4.93 to 0.50μm for $(EG\text{-}A.O.)_{MS}$ (Figure 3.6b).

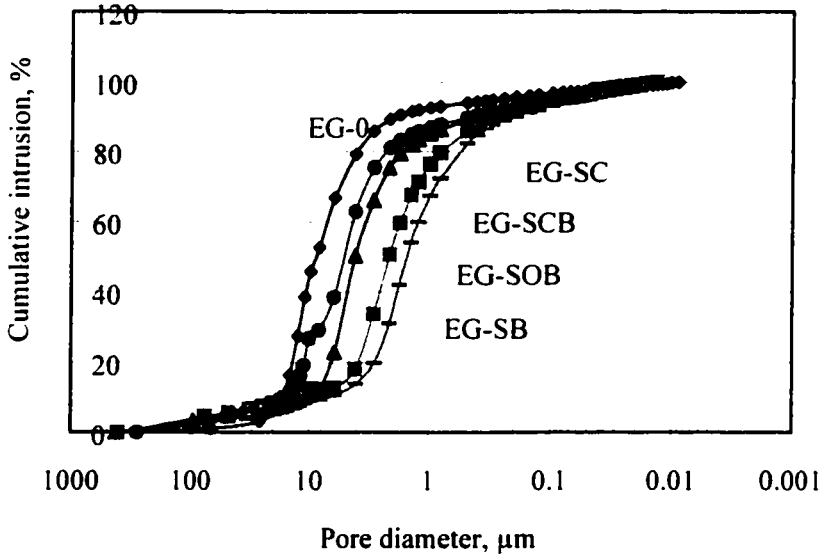

Figure 3.6a Cumulative intrusion (%) vs. pore diameter (μm) in $(EG\text{-}A.O.)_{MS}$ pellets after firing at 1400°C×3h, embedded in coke

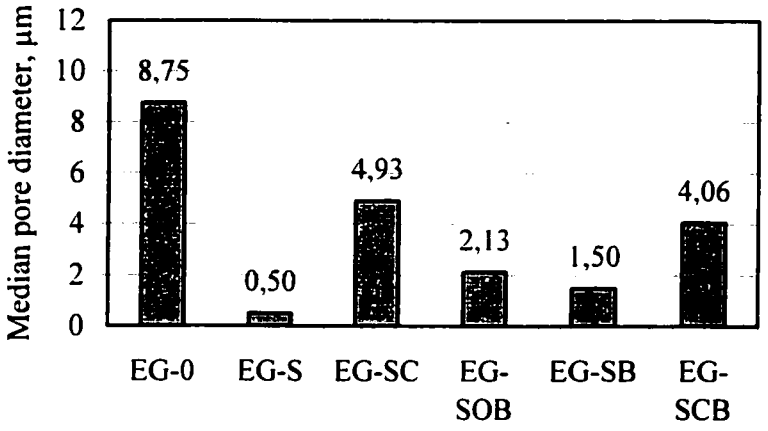

Figure 3.6b Median pore diameter (µm) of $(EG\text{-}A.O.)_{MS}$ pellets after firing at 1400°C×3h, embedded in coke

It can be seen that incorporating antioxidants and oxides into the pellets effectively reduces pore size and prevents the formation of big pores of the pellets. The pore sizes are shifted to the smaller pore range of 20 to 0.2 µm. This positive change of the texture should and will contribute to a higher oxidation resistance, as it will be seen in the next two chapters.

3.3.2.2 Bulk Density and Apparent Porosity

The bulk density and apparent porosity of extruded graphite pellets were determined from mercury intrusion measurements. The results are shown in Figures 3.7 and 3.8.

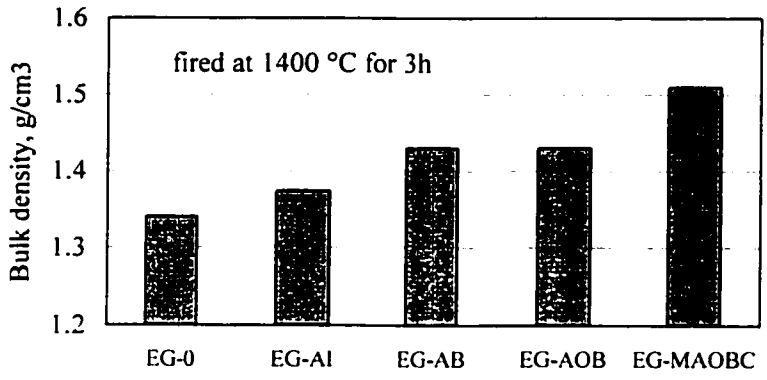

Figure 3.7a Density of extruded graphite $(EG\text{-}A.O.)_{MA}$ pellets

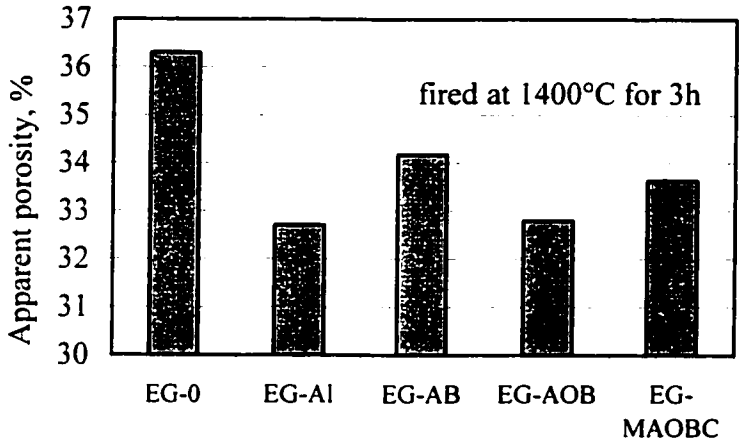

Figure 3.7b Apparent porosity of extruded graphite $(EG\text{-}A.O.)_{MA}$ pellets

The influences of metallic additions and oxide fillers are clearly shown in Figures 3.7a and 3.7b, taking as a reference of the EG-0 pellets without any addition. The density of $(EG\text{-}A.O.)_{MA}$ pellets increases from 1.34g/cm^3 to 1.52g/cm^3, while in the $(EG\text{-}A.O.)_{MS}$

pellets the increase is only from 1.34g/cm^3 to 1.36g/cm^3. No special attention was given to try to explain this difference in behaviour, but this should be something to consider, as this thesis work will be pursued. The important factor is that all extruded graphite pellets with addition of antioxidant and oxides have smaller pores as compared to that of EG-0 pellets.

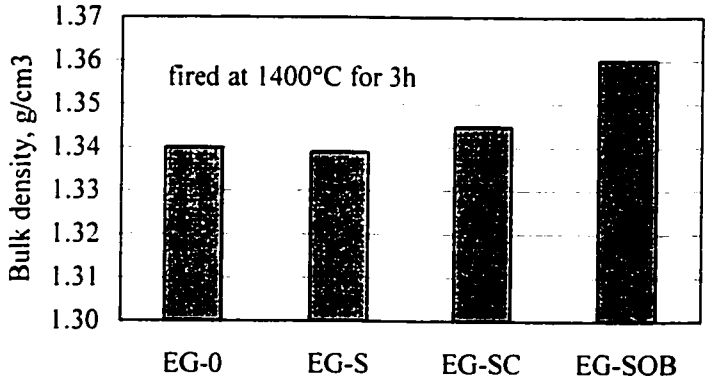

Figure 3.8a Density of extruded graphite (EG-A.O.)$_{MS}$ pellets

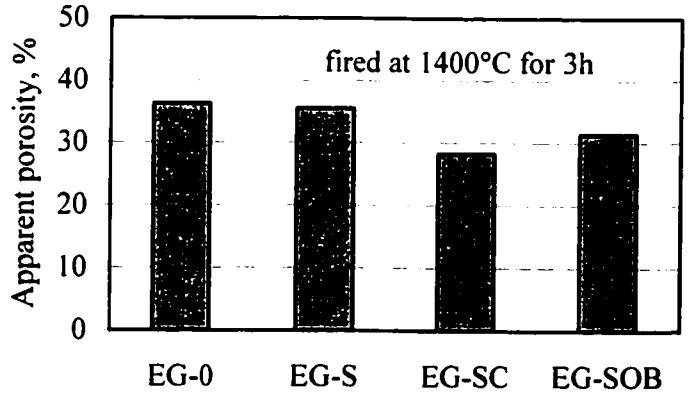

Figure 3.8b Apparent porosity of extruded graphite (EG-A.O.)$_{MS}$ pellets

3.3.3 EG Microstructure Evolution in Pressed Samples, Under Reducing Conditions

The pellets were mixed with a magnesia-based matrix. The mixture was compressed into a Ø25×25mm cylinder at a pressure of 70MPa and then fired at 1400°C for 3 hours in coke for microscopy observation. The compositions of the matrixes were based on the basic carbon-containing castable systems, as given in Table 3.3. The reason of doing this is that antioxidant, refractory oxide, graphite and fine carbon may stimulate some reactions within the system and form new solids, gaseous phases or liquid phases which possibly influence the texture of the pellets. New compounds formation inside of extruded graphite pellets can be in-situ formation from the designed composition itself, and also can be influenced by matrix composition, when antioxidant and carbon are used. The matrix includes magnesia fine with or without fine carbon or antioxidant. The microscopy observations on new compound formations were investigated by OM, CLM and SEM methods on (EG-0), $(EG\text{-}A.O.)_{MA}$ and $(EG\text{-}A.O.)_{MS}$ pellets.

Table 3.3 Compositions of the matrixes (wt.%)

Matrix code	MgO	AlP	Si	Al_2O_3	SiO_2	B_4C	CB
M	100						
MC	85						15
MABC	75	10				2.5	15
MAOBC	60			25		2.5	15
MSBC	75		10			2.5	15
MSOBC	60				25	2.5	15

The distribution of graphite flakes in extruded graphite pellet, with or without additives, was first observed by optical microscopy (OM) and cathodoluminescence microscopy (CLM), as shown in Figure 3.9.

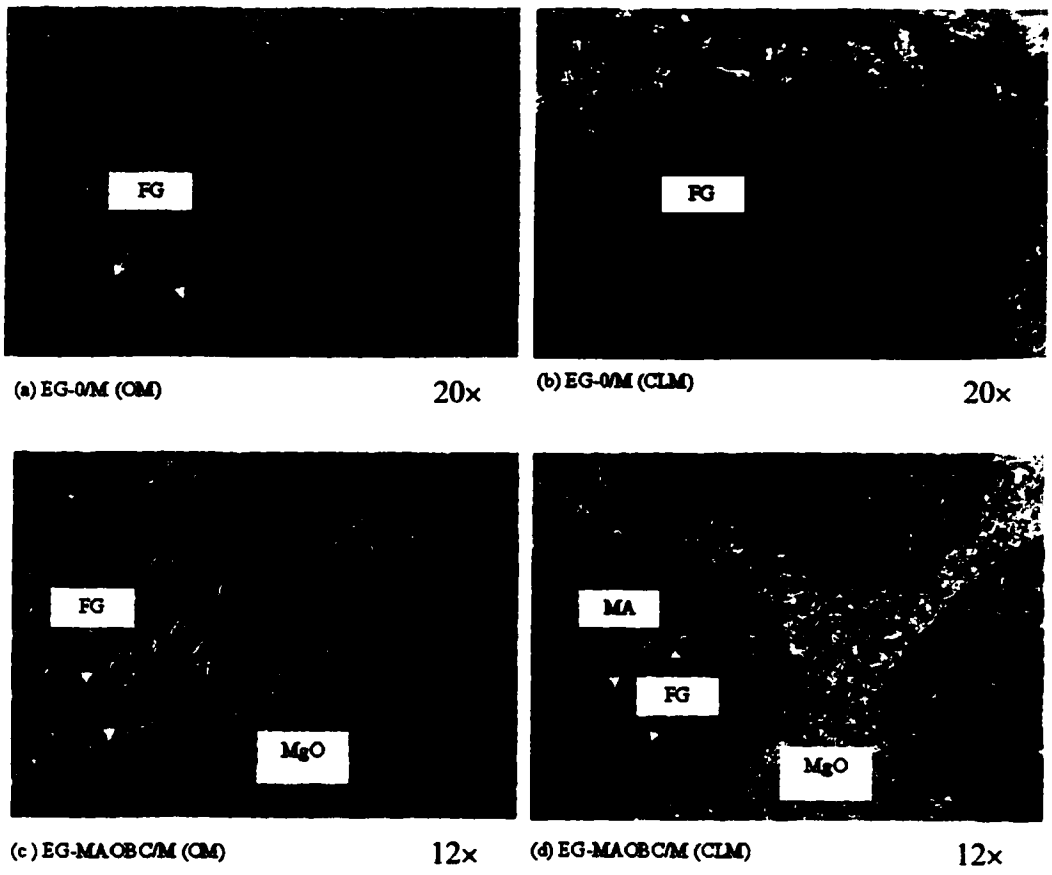

Figure 3.9 Distribution of graphite flakes inside (EG-0) and (EG-MAOBC) pellets (the pellets mixed with magnesia fine and pressed into cylindrical sample, and fired at 1400°C×3h: FG is flake graphite and MA is $MgAl_2O_4$ spinel)

After firing at 1400°C for 3 hours, the formation of the spinel, $MgAl_2O_4$, was observed in extruded pellets. The spinel, $MgAl_2O_4$, crystals with a characteristic regular, 'faceted' morphology, were identified by X-ray microanalysis (EDS) in SEM. The distinctive green coloring of spinel areas in CLM images facilitated analysis of spinel distribution in various types of extruded pellets. The influence of additives and its combination on new compounds formation inside the extruded graphite pellets is further illustrated in Figures 3.10-12. In Figure 3.10, the spinel formation inside EG pellet is strongly influenced by the type of additives (Al→A, AlMg→AM, B_4C→B, MgO→M, Al_2O_3→AO) and by the matrix (MgO→M or MgO+Carbon→MC). Sample EG-A/M (pellets/matrix) shows that MA spinel formed only slightly at the periphery of the pellets, when aluminium alone is used as additive in pellets. In the case of the combination of aluminium and boron carbide in pellets (sample EG-AB/M), more spinel is formed inside of the pellets, since boron carbide promotes spinel formation. In sample EG-AMB/M, which contains magnesia, aluminium and boron carbide, even more in-situ spinel in the pellets is formed. When aluminium is replaced by fine alumina, more spinel is found inside of the pellets, see sample EG-MAOBC/M. The alumina used in this case was ultra-fine alumina, much finer than the aluminium particles, hence more susceptible to react with magnesia fine to form spinel.

The sample with aluminium-magnesium alloy (AM) presents more spinel formation than that sample with only aluminium additives since AM is more effective being a source of magnesia. The comparison of sample EG-AB/MC with sample EG-AB/M suggests that

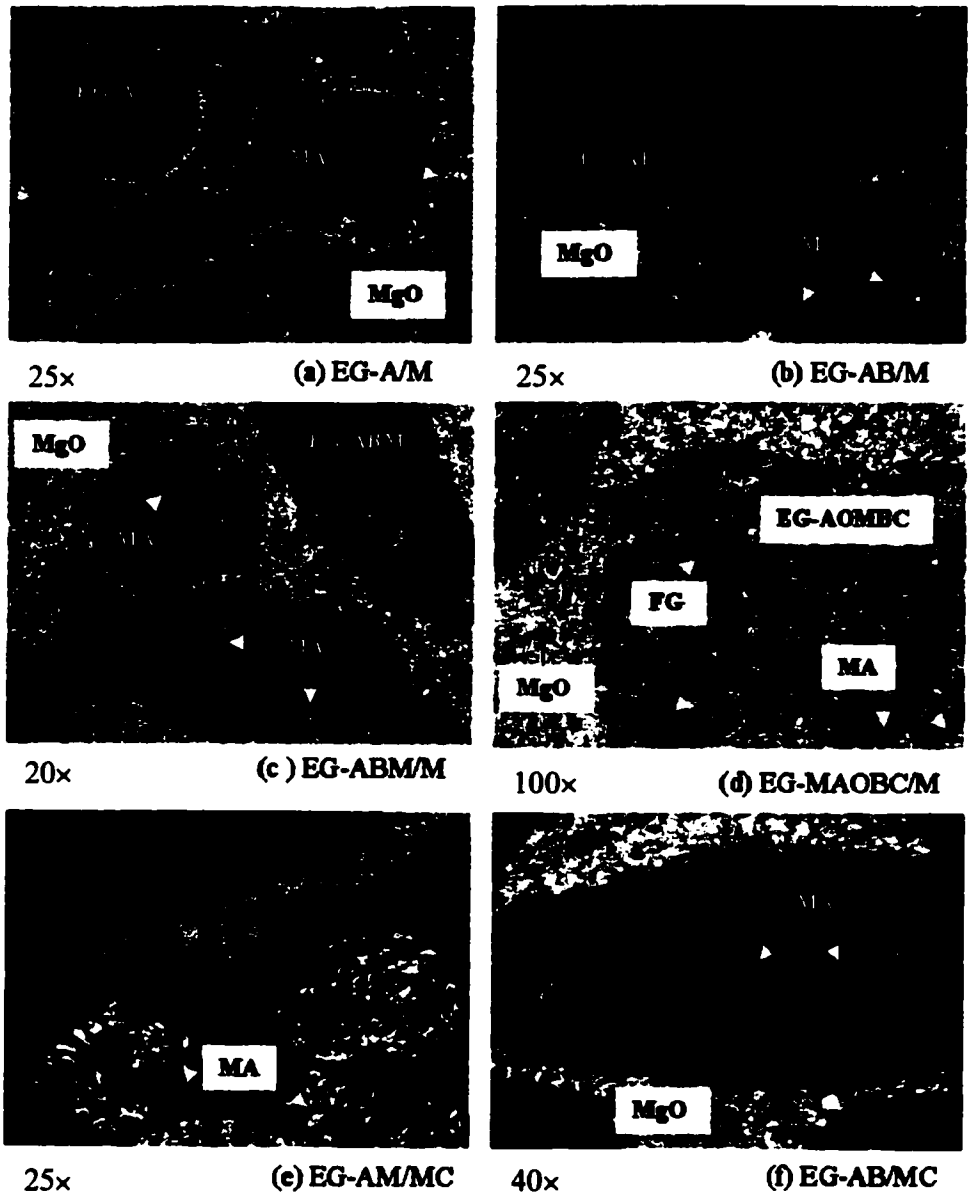

Figure 3.10 New compounds formation in $(EG\text{-}A.O.)_{MA}$ in a matrix of magnesia without fine carbon (/M) and with fine carbon (/MC)

(CLM observation: spinel-green, MgO-blue or purple, graphite-black)

the addition of fine carbon in matrix stimulates MA formation through magnesium vapor in the system. Indeed, spinel crystals were observed in the pellets, which did not contain MgO at all, eg. In samples EG-AOB/MABC and EG-SB/MSBC, see Figure 3.11. Apparently, during the firing, Mg vapor was formed in the system, and penetrated into the relatively porous pellets and reacted with Al_2O_3 in pellets to form spinel.

Although all EG pellets were imbedded in coke, during the thermal treatment, the temperature and the local partial pressure of oxygen were high enough to readily favour the reactions of spinel formation. Figures 3.11 and 3.12 serve to illustrate further evidence in even more complex systems, for such samples as EG-AB/MABC, EG-SB/MSBC and EG-AOB/MABC pressed samples. The influence of both the EG pellets content and the matrix composition is clearly demonstrated.

More spinel is formed inside EG-AOB and EG-AB pellets when antioxidant aluminium, boron carbide and fine carbon are added into the matrix. This addition of antioxidant and fine carbon into the matrix seems to promote magnesium vapor Mg (g) formation in the system. This Mg (g) vapour diffuses into the pellets and acts as fine magnesia reactant to form spinel, and therefore promote more spinel formation inside of the EG pellets. With silicon and boron carbide additives in the pellets, the formation of forsterite (M_2S) phase was observed both in pellets and in the matrix of the sample EG-SB/MSBC, which would also involve the effect of Mg (g) vapour.

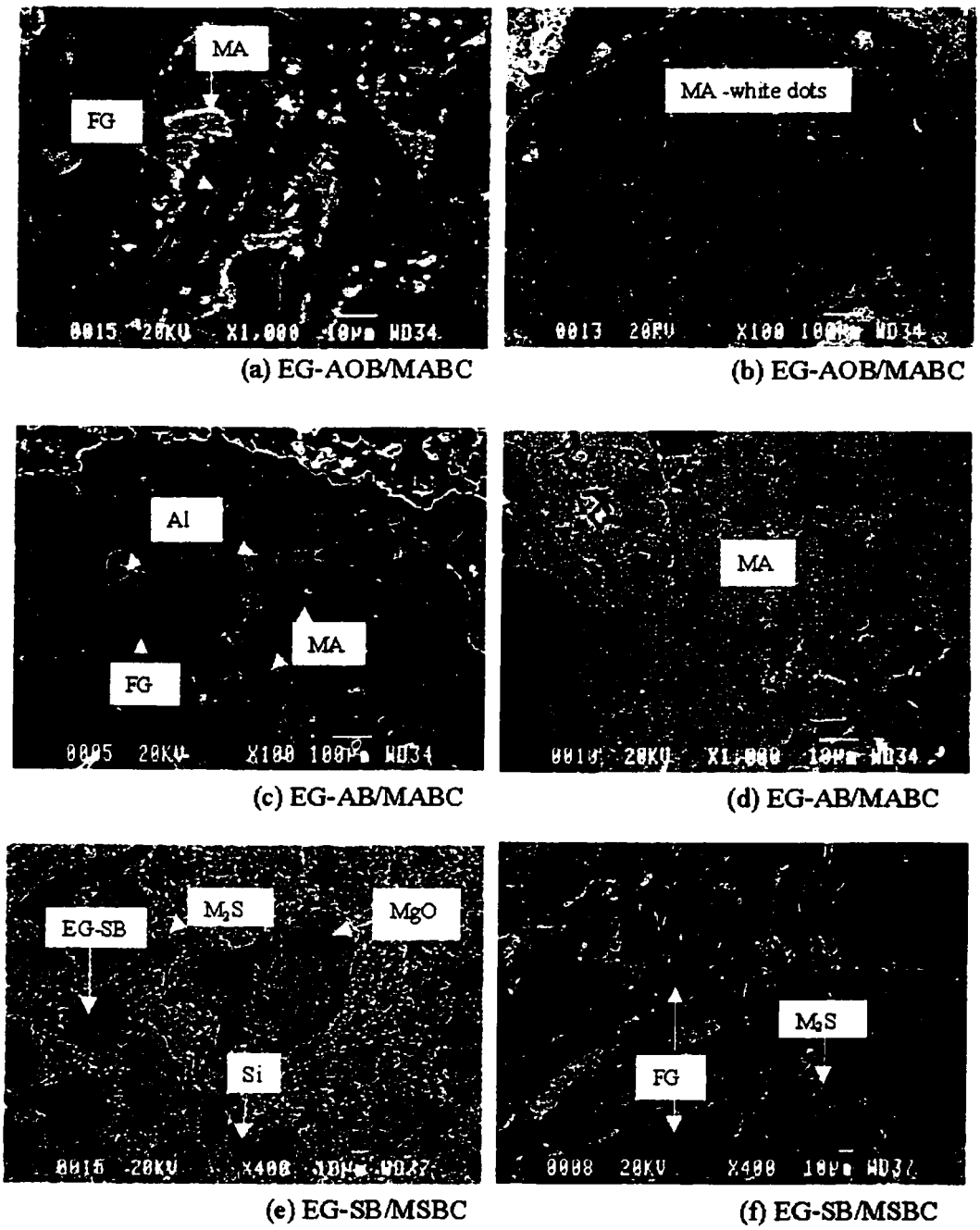

(a) EG-AOB/MABC (b) EG-AOB/MABC

(c) EG-AB/MABC (d) EG-AB/MABC

(e) EG-SB/MSBC (f) EG-SB/MSBC

Figure 3.11 Confirmation of MA and M_2S formations in EG by SEM/EDS

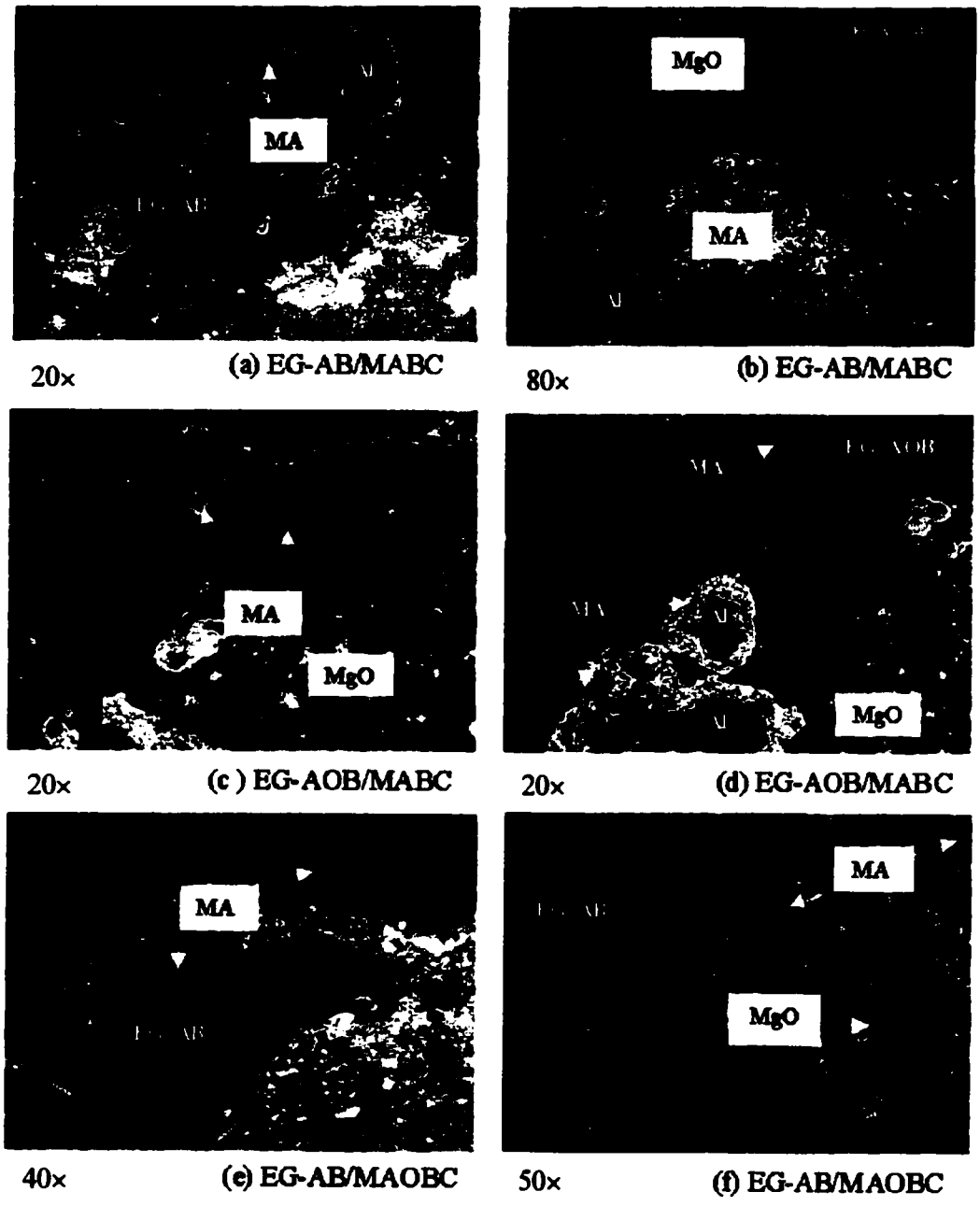

Figure 3.12 Effects of incorporating antioxidants and oxides into EG pellets or matrix on spinel formation (green color identified as MA spinel by SEM/EDS)

3.3.4 The Influence of the Binder

Other effort was made to assess the role of molasses, replaced by liquid colloidal silica during the extrusion process, and compared in sample EG-MAOBC. The microstructures of the pellets are similar in terms of graphite flake distribution and compounds formation. The behaviour of EG-MAOBC$_S$ pellets was directly measured by CO_2 gas intensity evolution to evaluate its oxidation resistanc, in comparison with EG-MAOBC pellets. The oxidation resistance of EG-MAOBC$_S$ pellets is close to that of EG-MAOBC pellets regarding to their oxidation temperature and relative intensity of CO_2 gas evaluation, as given in Figure 3.13.

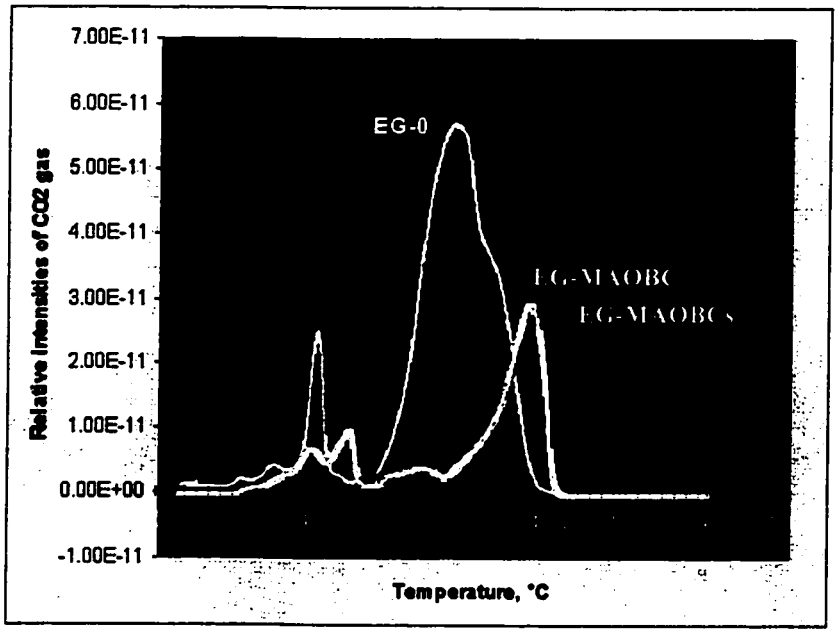

Figure 3.13 Oxidation behaviour of EG-MAOBC and EG-MAOBC$_S$ pellets

There is a small oxidation peak for EG-MAOBC$_S$ because fine carbon CB was used. There are two small peaks for EG-MAOBC since binder M and fine carbon CB were used in the pellets. The bulk densities of EG-MAOBC and EG-MAOBC$_S$ are 1.51g/cm^3 and 1.43g/cm^3, respectively. The median pore sizes of EG-MAOBC and EG-MAOBC$_S$ are 1.13 and 2.06μm, respectively. Considering all the aspects, the nature of the binder, the advantage and disadvantage of two binders, molasse was selected for the rest of the extruded graphite pellets.

3.4 EXPERIMENTAL PROCEDURE TO PRODUCE COATED GRAPHITE

In this research work, pitch was selected produce pitch-coated graphite because pitch has not only good fluidity, when heated, but also can act as second source of carbon to increase carbon input in the material.

Two distinct processes have been used, called process A and B:

Process A: Mix flake graphite (70%) and pellet pitch (30%) together with 5% water addition, with or without antioxidant addition (15% A.O. replace FG). Compress the mix into a bar with a cross section of 200×50mm at a pressure of 70MPa. Dry the compressed bars at heating rate of 2°C/min up to 180°C and keep holding time over 12 hours. Crush the bars into grains with size less than 1.0mm. The pitch-coated graphite was made in the laboratory, and denoted as CG$_L$.

Process B: Mix flakes graphite (70%) and pitch (30%) together, with or without addition of antioxidant (3%). Heat and stir the mixture at designed heating condition. Granulate the mix into grains with a size less than 1.0mm, with or without hydrophilic treatment. Pitch-coated graphite for process B is commercially available, from Osaka, Japan, denoted as CG.

The morphology of pitch-coated graphite is given in Figures 3.14 and 3.15. The photos show that CG from industrial scale provides better coating quality due to better-equipped fabrication devices and procedures are used. The shapes of the graphite flakes are more clearly identified than that of CG_L.

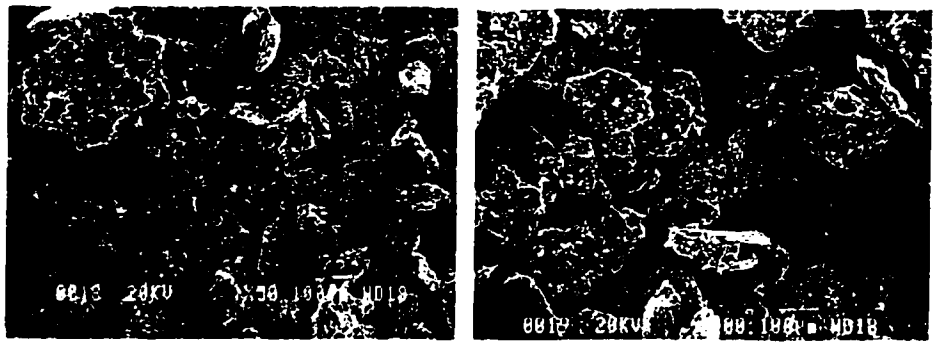

Figure 3.14 Morphology of CG_L

Figure 3.15 Morphology of the CG

By measuring the wetting angle of a water drop on the surface of pressed CG sample, the hydrophilic property of CG is improved as compared to that of FG since the wetting angle decreased from 76° for FG to 48° for CG, as shown in Figure 3.16.

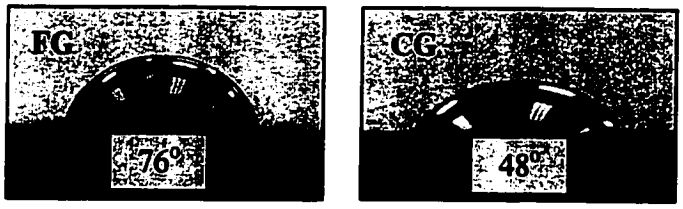

Figure 3.16 Behaviour of a water drop on the surface of pressed flake graphite and coated graphite: a comparison

3.5 EXPERIMENTAL PROCEDURE TO PRODUCE GRANULATED GRAPHITE

The granulating process was briefly explored, using phenolic resin as a mixing binder to agglomerate flake graphite together and then crush or granulate the product. The raw materials and the composition of the granulated graphite (denoted as GG) are listed in Table 3.4. The process description is as follows:

Mix alumina (65%) and flake graphite (35%) together, with or without antioxidant Al or Si (3%). Wet blends the mixture with liquid resin (7.0%) adjusting viscosity for 5 minutes. Compress the wet-mix into 200×50×50mm bars at a pressure of 70MPa. Heat the bars at 180°C for 24 hours. The bulk density of the GG is 2.4g/cm^3, and the cold modulus of rupture of the bar is 16.4MPa. Finally, crush the bars into grains with a size less than 1.0mm.

Table 3.4 Composition of granulated graphite (GG)

Raw materials	Size	Percentage, %		
Tabular alumina	< 1.19 mm	30	28	28
	< 45 μm	25	24	24
A16	< 1.2 μm	10	10	10
Antioxidant				
Al	< 75 μm		3	
Si	< 10 μm			3
Flake graphite	< 75 μm	35	35	35
Phenolic resin	liquid	7	7	7

CHAPTER 4 OXIDATION STUDY ON MgO-MA-C MATERIAL SYSTEM

4.1 INTRODUCTION

This chapter is designated to consign all the results obtained on the oxidation resistance characterization of cement-free, magnesia based, spinel bonded castables, containing graphite, the MgO-MA-C system. The purpose is to illustrate the influence of the modified graphite FG, EG, CG and GG pellets on properties of the castables and various strategies which have been adopted to optimize the oxidation resistance of the castables. Results include datas on flowability, physical and mechanical properties obtained on both pressed samples and cast samples in order to understand the roles of carbon source and antioxidant. Before going into those results, a preliminary study was preformed on the use of aluminium, since the aim of this thesis was not only to focus on selecting the proper carbon but also on improving the oxidation resistance using proper antioxidants. Would it be sufficient to add the proper antioxidant straight in a carbon containing castables to achieve good performances? Answers to this question will be documented first, then the other results will follow in 3 steps: improvements on oxidation resistance in graphite materials, in matrix materials and in MgO-MA-C castables.

4.2 ALUMINIUM AS A STRAIGHT ANTIOXIDANT

The role of antioxidant has been documented in carbon-bonded bricks. However common metallic antioxidant aluminium is difficult to be used in a castable because of the following exothermic reaction in aqueous medium.

$$2\,Al + 6\,H_2O = 2\,Al(OH)_3 + 3\,H_2\uparrow \qquad (4.1)$$

The generated hydrogen gas leads to the deterioration of the castable in terms of physical and mechanical properties, oxidation resistance and corrosion resistance of the castables.

To eliminate the hydration problem, some investigations have been made on coated metallic or metallic alloy powder as reviewed in chapter 2. In this chapter, efforts on using metallic aluminium in basic castables were conducted. It includes an overall experimental design and the study on reactivity of aluminium powder or coated aluminium powder in basic aqueous medium. Furthermore, the coated aluminium was tested in basic castables. The reactivity of aluminium or coated aluminium in different solutions was evaluated by temperature measurements based on the exothermic reaction shown in equation (4.1).

4.2.1 Experimental Procedures

4.2.1.1 Raw Materials

Raw materials are listed in Table 4.1.

Table 4.1 Raw materials for coated aluminium experiments

Type	Grade	Specification	Company
Al	A101	Al 99.7 % 150 - 45μm, 15-25% < 45μm, 78-85%	Alcoa, U.S.A.
	A120	Al 99.7 %, 355 - 45 μm, 62-72% < 45μm, 28-38 %	Alcoa, U.S.A.
	A48	Al 99.0 %, < 355μm	Fisher Scientific Company, U.S.A.
	A28	Al 99.0%, < 850μm	Fisher Scientific Company, U.S.A.
Coating material	P	Pellet Pitch	Jiaohua Plant, Zhenjiang, China
	M	Molasse	Grandma food, Products Co. Canada
	R	Phenolic resin	RL 2300 Borden chemical, U.S.A

4.2.1.2 Methodology

Coating aluminium powder includes selecting coating materials, aluminium powders, coating processes and evaluation methods. Four different aluminium powder and three types of coating materials were used. Two different coating processes were carried out and investigated. The temperature measurement was taken as a measure of the evolution of the on-going reaction when metallic aluminium (denoted as Al) or a coated aluminium is introduced into either a solution or a basic castable.

4.2.1.3 Coating Processes

Pitch-coated aluminium

There are two different coating processes conducted in making pitch-coated aluminium, as described in the following.

Coating process I, Mix Al powder (65%) and pellet pitch (35%) together. Place the mixture in a metallic container and then put the container into a dryer. Heat the mixture at a heating rate of 5°C/min to 180°C and keep the mixture at 180°C for over 12 hours. After cooling down, crush the mixture into grain size less than 1.0mm. The pitch-coated Al powder was obtained, denoted as AlP-I.

Coating process II, Mix Al powder (65%) and pellet pitch (35%) together. Put the mixture into a metallic container. Stir the mixture while heating it up to a temperature of 200°C, and continue to stir the mixture at the temperature of 200°C for over ten minutes. After the surface of the metal powder is well covered by melted pitch, let the mix cool down naturally. Crush the mixture into particle size less than 1.0mm. The pitch-coated aluminium was obtained, denoted as AlP, as shown in Figure 4.1.

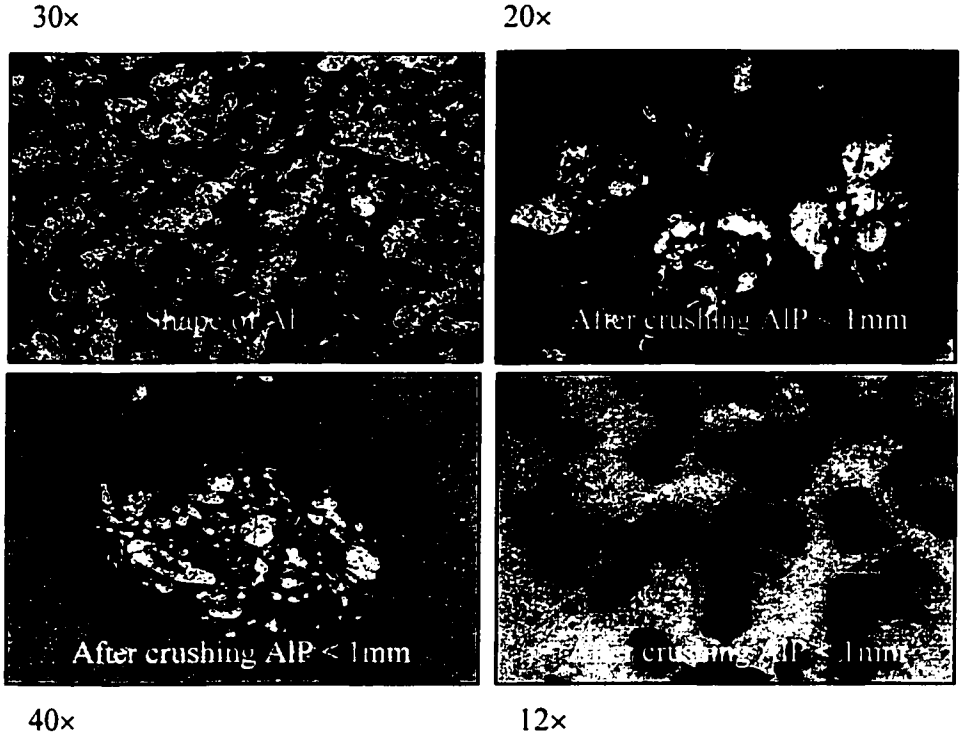

Figure 4.1 Photography of coated aluminium A101 (AlP101)

Figure 4.1 shows the photography of the shape of fine aluminium powder A101 (<45μm) and coated aluminium AlP101 (<1mm). The pictures illustrate that aluminium particles are well coated by melted pitch, which has a proper melting point and good

flowability at the given heating condition. The good coatability of particles less than 0.3mm is further verified by microscopy observations.

Molasses-coated aluminium and resin-coated aluminium

In order to obtain an acceptable coated aluminium, other approaches were made by selecting liquid molasses and phenolic resins as the coating materials. Firstly, mix the aluminium powder (84%) with a liquid molasses (16%) or a liquid resin (16%) for 5 minutes at room temperature. Place the mixture in a metallic container, and then put the container into a dryer. Heat the mixture at a heating rate of 5°C/min to 180°C and hold the temperature of 180°C for over 12 hours. The aluminium powder was well covered and bonded together by the coating material. After cooling down, the mixture was crushed into particle size less than 1.0mm. The coated Al by molasses or resin so obtained is named as AlM and AlR, respectively.

4.2.1.4 Evaluation of Reactivity of Al or Coated Al in Basic Solutions

Two methods can be used to evaluate the reactivity of Al and coated Al powders in basic solutions. Based on the reaction given in equation (4.1), the quantitative measurements can be carried out through collecting hydrogen gas created during the reaction, or by recording temperature change during the exothermic reaction. In this work, a new set-up was established in the laboratory, in which the temperature was recorded continuously during the experiment, as illustrated in Figure 4.2.

Considering the variety of the castable medium, seven solutions were designed in which the matrix, the binder and the additive were considered. The samples include the original aluminium powders with different types and sizes, the coated aluminium powders with different coating materials and coating processes, as listed in Table 4.2.

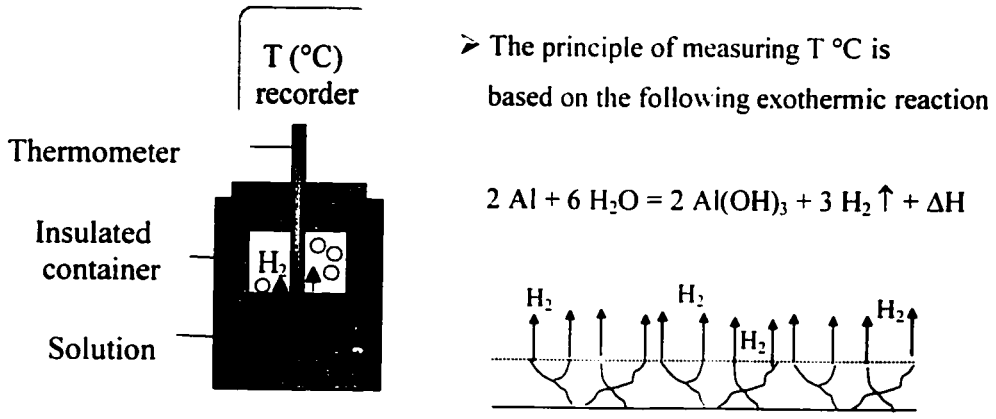

Figure 4.2 Set-up for measuring temperature change of the mixture of metallic antioxidant emerged in different basic solutions or castables

4.2.2 RESULTS AND DISCUSSION

Based on the measurements on groups I to VII, as listed in Table 4.2, the reactivity of Al and coated Al in different solutions are illustrated in Figures 4.3-4.7.

4.2.2.1 Influence of Aluminium Size on its Reactivity in Basic Aqueous Medium

There are many different factors influencing the reactivity of metallic Al powder in a given solution. Figure 4.3 illustrates the size influence on the reactivity of aluminium in a basic aqueous medium (S1), which is the most common medium related to the basic castable.

Table 4.2 Samples and designed solutions for the reactivity measurement

Group	Type	Brand	Solution
I	Metal Al	A101, A120 A48, A20	S1: MgO (45g) + water (25ml)
II	Metal Al	A120	*S1-S6 ($MgO+Al_2O_3$) 45g + water (25ml)
III	Metal Al	A101	S7: water (25ml)
IV	Coated Al : A101	AlP, AlM, AlR	S1: MgO + water
V	Coated Al: A120	AlP-I, AlP	S1: MgO + water
VI	Al or Coated Al	A101, AlP101 **AlP_{J30}	S1: MgO + water
VII	Coated Al	AlP120	MgO-C castable

* S1-S6	S1	S2	S3	S4	S5	S6
Code	M25	M20A5	M15A10	M10A15	M5A20	A25
MgO, %	100	80	60	40	20	0
Al_2O_3, %	0	20	40	60	80	100

* Properties of fine MgO (Mf) and fine Al_2O_3 (A-1000SGD) are introduced in Chapter 5.

** AlP_{J30}: from commercial product, Osaka, Japan

In Figure 4.3, the finest powder of A101, with the particle size of 78-85% minus 45μm, reaches the highest reaction temperature after a reaction time of 3-4 hours. Metal A120, with the particle size 28-38% minus 45μm, coarser than that of A101, presents a slight lower maximum reaction temperature and a delayed reaction time, in which the highest temperature occurs after the reaction time of 9-10 hours. Metal A48 and A28 show a much lower maximum reaction temperature and a delayed reaction time since the particle size is much coarser than that of A101 and A120. Therefore, the reaction of metallic Al in a basic solution is strongly influenced by the size of the reactant aluminium, as derived from Figure 4.3. The finer the metal powder, the higher the reactivity is. It is a surface area effect.

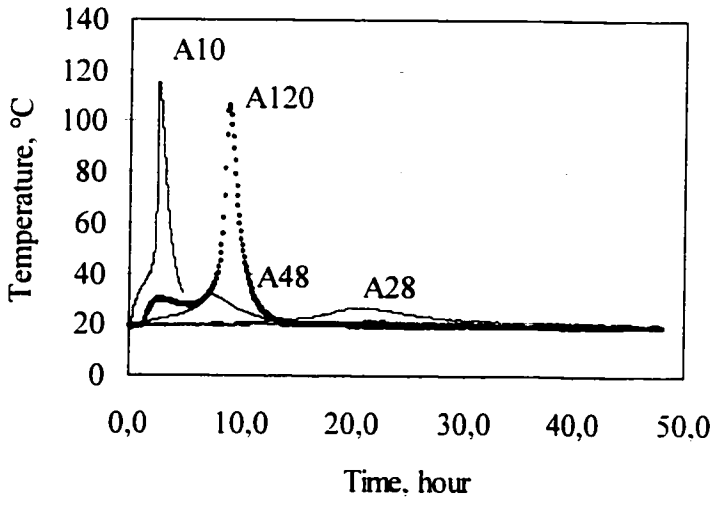

Figure 4.3 Influence of aluminium size on its reactivity in a basic solution (S1)

Considering the different compositions and possible binders used in the basic castables the reactivity of the metallic aluminium A120 in different groups of solutions was measured in order to understand the reaction degree of the metallic aluminium powder in different combination of the materials, as presented in Figure 4.4.

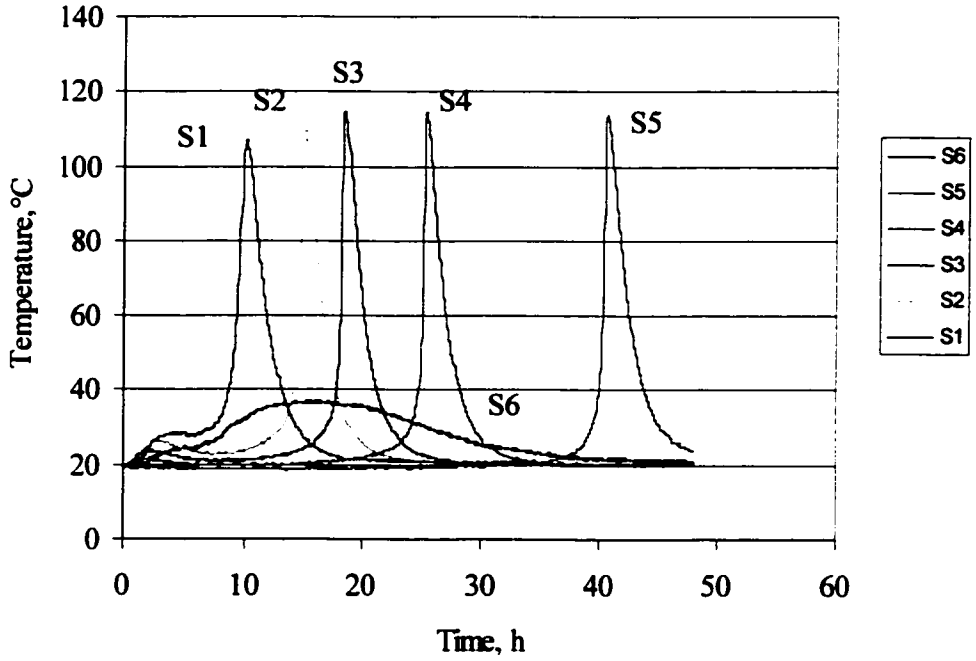

$MgO/Al_2O_3 = 25 / 0 \sim 0 / 25$ (S1–S6)

Figure 4.4 Reactivity of metallic A120 in different solutions (S1-S6)

From a magnesia-based solution (S1, in Figure 4.4) to a solution with reduced amount of magnesia (S1 to S5), the reaction time at the maximum reaction temperature is greatly

delayed from 10 hours for sample M25 (S1) to 40 hours for sample M5A20 (S5). The reaction of the sample containing magnesia reaches similar maximum reaction temperature. The comparison between sample M25 and A25 illustrates that the reaction degree and the reaction rate of Al powder in an alumina-based solution (S6) are much smaller and slower than that of the solution containing magnesia.

As a comparison, the reactivity of Al or coated Al in basic solution S1 is also superimposed in Figure 4.5. It further indicates that the reaction degree of metallic aluminium in a basic medium is very strong and coated Al can effectively eliminates this reaction

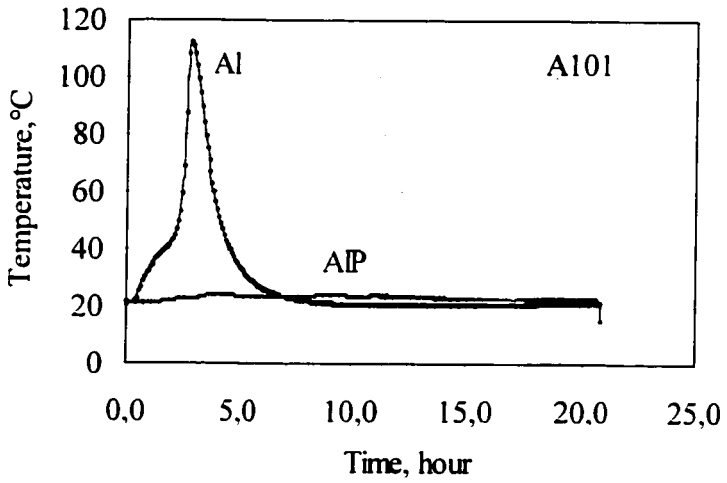

Figure 4.5 Role of coated aluminum on decreasing the reaction of metallic aluminium in basic solution S1

Since the basic medium is absolutely dominant in basic castable, how to decrease this reaction becomes an important factor to be studied. The reactivity of aluminium in a

basic medium must be controlled in order to be able to use metallic antioxidant in castables and to study its influence on oxidation resistance of basic carbon-containing castables.

4.2.2.3 Influence of Coating Process on Reactivity of Metallic aluminium in Basic Medium

As described earlier, three different coating materials were selected to coat metallic aluminium powder. Figure 4.6 compares the reactivity of coated aluminium powder in the basic solution (S1) by using three different types of coating materials.

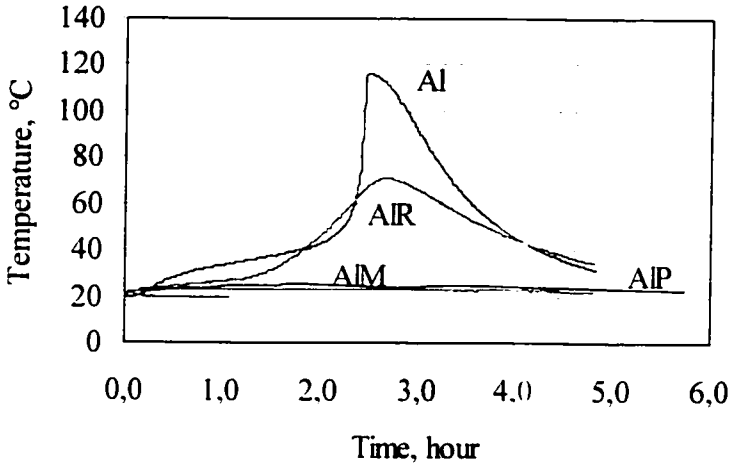

Figure 4.6 Reactivity of AlR, AlM and AlP in basic solution (S1)

Figure 4.6 illustrates that the pitch-coated aluminium (AlP) and molasses-coated aluminium (AlM) are better than resin-coated Al (AlR).

Reactivity of coated metallic aluminium by coating process I or II is compared in Figure 4.7. It reveals that the quality of the coating is varied by different coating process, see sample A48-P (I) and A120-P (II) in Figure 4.7. Finer powder of A120 coated by coating process II performs better than that of the coated powder A48 made by coating process I. The difference between the two processes indicates the efficiency of blending and the stirring time during the pitch melting process.

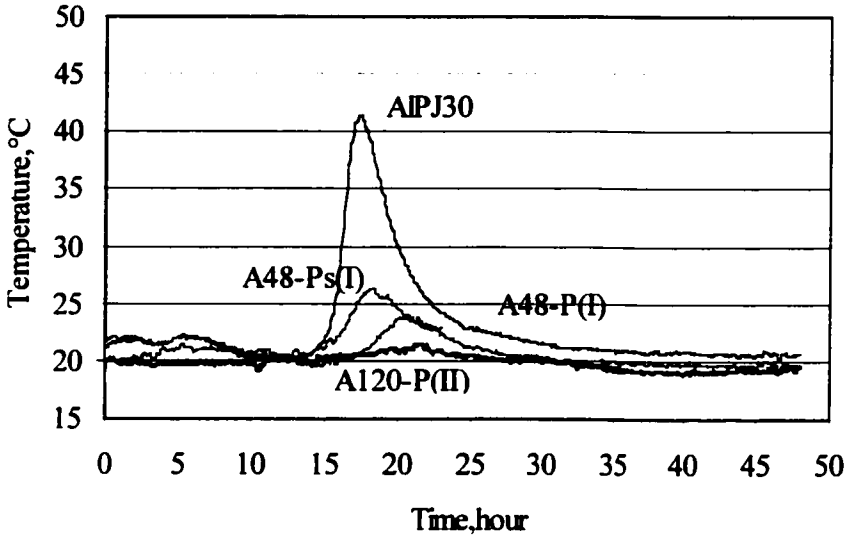

Figure 4.7 Influence of selected pitch and coating process

on reactivity of coated Al in basic solution (S1)

Moreover, different pitch and process may lead to different coating quality and result in different reactivity of the coated aluminium in the basic medium, see lines A48-Ps (I),

A48-P (I). Other coated aluminium source (AlP_{J30}) was shown in Figure 4.7, as seen line AlPJ30. By carefully selecting the proper pitch, with a reasonable melting point and a good flowability under given heating condition, the quality of the coating can be verified.

4.2.2.4 Castable Containing Metallic Aluminium

In order to examine the effect of coated aluminium in a basic castable, the reactivity of the coated aluminium, with an addition up to 4% in MgO-MA-CG castables, was tested by measuring the temperature changes of the MgO-based castables. The initial results prove that coated fine aluminium powder suppresses the generation of hydrogen gas, and can be possibly used in MgO-C castable. see Tables 4.3.

Table 4.3 Effect of coated aluminium in MgO-MA-CG castables

Al, wt.%	0.2	1.0		
Coated Al, wt.%			2	4
Carbon content, wt.%	6	6	6	6
After casting, H_2 gas	No evidence	large	No evidence	No evidence
Temperature, °C	24	69	29	33
Appearance of sample	OK 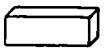	enlarged 	OK 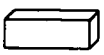	OK 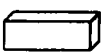

4.3 EXPERIMENTAL PROCEDURES

4.3.1 Raw Materials

There are six groups of materials to consider in MgO-MA-C castables, as illustrated in Figure 4.8: aggregates, oxide fines, binder and bonding systems, carbon materials, antioxidants and other additives.

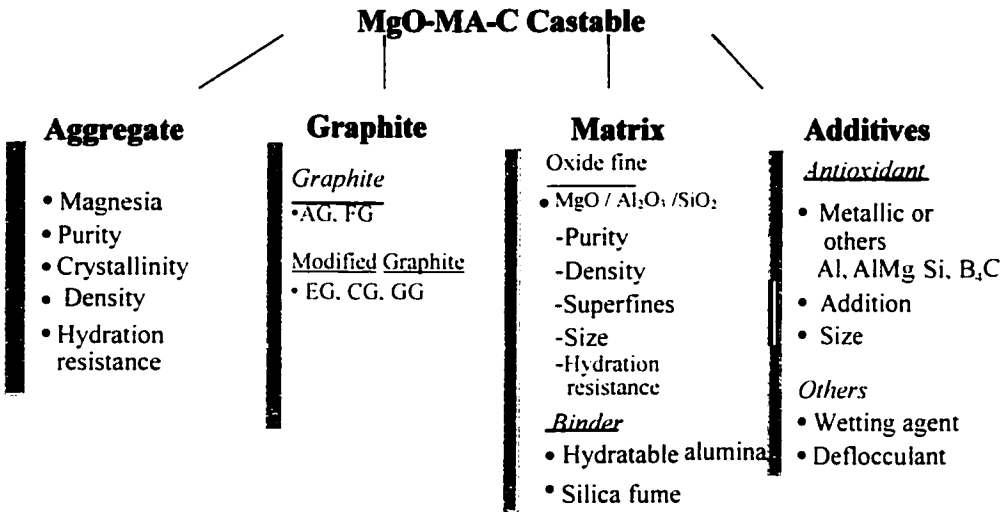

Figure 4.8 Main components of MgO-MA-C castable

The raw materials are: 1) magnesia aggregate, 2) magnesia and alumina fines, 3) graphitic materials: natural flake graphite and EG, CG and GG pellets, 4) binders: hydratable alumina and silica fume, 5) antioxidants: metallic aluminium, metal alloy AlMg, silicon and boron carbide, 6) other additives: deflocculants and wetting agent.

Magnesia

Sintered magnesia from Israel (CF 99) was used as magnesia aggregate, which is a high purity magnesia with a crystal size of 70 to 90μm. Four size fractions of magnesia, 6.7-3.35mm, 3.35-1.18mm, 1.18-0.3mm and <0.3mm were applied. Ball-mill fine magnesia from Ludington grains was selected and its property as well as particle size distribution are given in Table 4.4 and illustrated in Figure 4.9, respectively.

Table 4.4 Magnesia materials for MgO-MA-C castables

Magnesia	Aggregate CF 99	Fine powder LUD 97A
Code	MgO	Mf
Chemical composition, %		
MgO	99.30	96.40
Al_2O_3	0.03	<0.10
SiO_2	0.03	0.31
CaO	0.63	1.84
Fe_2O_3	0.04	0.39
BSG, g/cm^3	3.44	3.38
Source	DSP	Ludington

Alumina

Tubular Alumina, T64, Al_2O_3>99.0%, with size of <45μm from Alcoa Industrial Chemicals, was selected as alumina fine. It is a sintered alumina with α-Al_2O_3 tubular-shaped crystals with a median range of 40 to 200μm. It has excellent thermal volume

stability and thermal shock characteristics due to its large crystals with closed spherical pores entrapped upon recrystallization during rapid sintering.

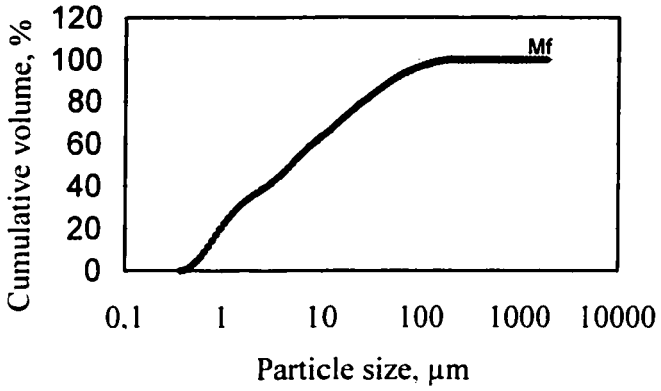

Figure 4.9 Particle size distribution of magnesia fine

Calcined alumina A12 and A1000SGD were selected as ultra-fines (<10μm). Dispersible A-1000SGD, a calcined alumina, is a superfine material with nominal particle size of <1.0μm, to be used to reduce the water demand, by filling sub-micron holes in a manner similar to that of silica fume in refractory mixes designed for maximum packing. The particle size distribution and chemical composition of A12 and A1000SGD are shown in Table 4.5 and Figure 4.10.

Table 4.5 Chemical composition of alumina ultra-fines

	Al_2O_3	Na_2O	SiO_2	Fe_2O_3	CaO	MgO	B_2O_3	Density g/cm^3
A12	99.8	0.18	0.02	0.01	0.02	<0.002	0.3	3.79
A1000SGD	99.8	0.06	0.03	0.02	0.02	0.03	<0.003	3.89

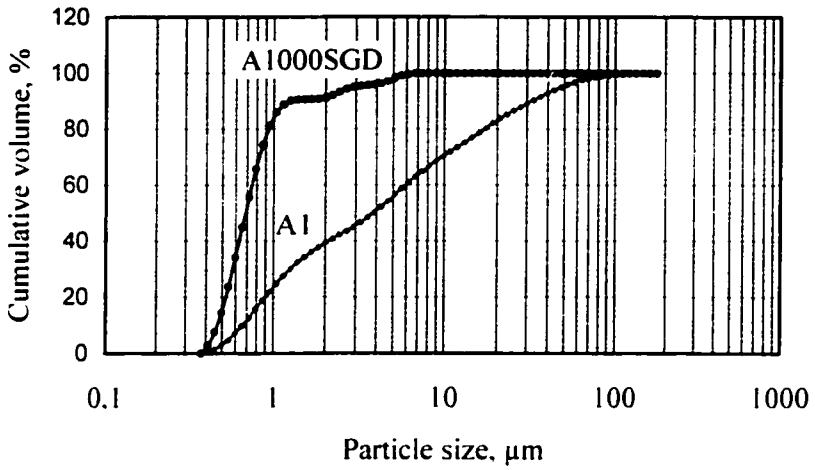

Figure 4.10 Particle size distributions of alumina fines

Carbon sources

The four graphite materials described earlier as FG, EG, CG and GG were used in MgO-MA-C castables. The properties of the graphite materials have been discussed in chapter 3.

Hydratable alumina

Hydratable alumina (H-Al_2O_3) is an hydraulically setting reactive alumina designed for use as a binder in refractory compositions. Since it contains no calcium-based compounds (CaO <0.1%) to avoid the formation of low melting glassy CaO-containing phases in refractory mix, high resistance to slag and molten metal attack can be expected. Hydratable alumina particles are basically amorphous and very fine with a

surface area of more than $20m^2/g$. It develops strength through hydration. Alphabond 100 from Alcoa (denoted as Ap100) was used in this work. The particle size distribution of hydratable alumina is shown in Figure 4.11.

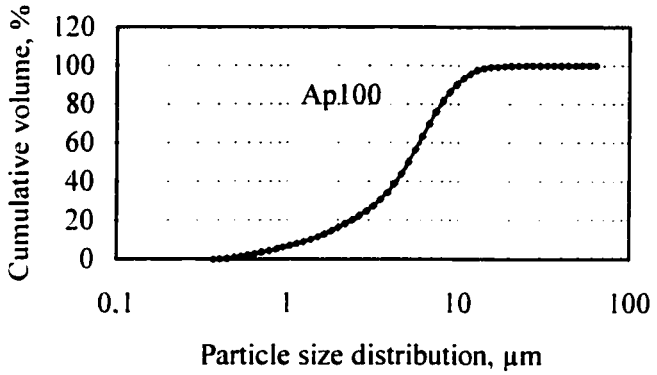

Figure 4.11 Particle size distributions of hydratable alumina, Ap100

Silica fume

Silica fume is amorphous, made of very fine spherical shape particles, with very high specific surface area ($>20m^2/g$). As a binder, silica fume 971U from Elkem Materials, Norway, was used. Table 4.6 provides its chemical analysis.

Table 4.6 Chemical analysis of silica fume 971U (%)

SiO_2	Fe_2O_3	CaO	MgO	K_2O	Na_2O	C	L.O.I. at 975°C
98.2	0.05	0.13	0.15	0.31	0.08	0.50	0.50

Deflocculants

In order to reduce water addition and obtain good flowability, three different deflocculants were used in MgO-MA-C castables, as listed in Table 4.7.

Table 4.7 Deflocculants for MgO-MA-C castables

Chemical name	Denotation
Sodium hexametaphosphate	S6P
Galoryl	G
Monosodiumcitrate	ACM

Antioxidants:

Antioxidants metallic aluminium Al and silicon Si, metallic alloy aluminium-magnesium AlMg and boron carbide B_4C were used in MgO-MA-C material system to prevent carbon from oxidation. Typical properties of antioxidants were listed in Table 3.1.

Wetting agent:

Glydol was used as a wetting agent in this work.

4.3.2 Samples Preparation

As previously announced, two different sets of samples are considered: pressed cylindrical samples of antioxidant in matrix constituents and cast samples from castable mixes, including aggregates, matrix and graphite pellets. The pressed samples were

compressed at a pressure of 70MPa into a cylindrical shape with a diameter of ∅19mm and height of 25mm. The composition of those four distinct cylindrical samples are given in Table 4.8.

Table 4.8 Compositions of the matrixes with different antioxidant (wt.%)

Materials	Code	MC0	MCA1	MCA2	MCA1B1
MgO fine	Mf	60	52	44	44
Flake graphite	FG	40	40	40	40
Metallic aluminium	A101		8	16	8
Boron carbide	B				8

The castable samples were cast according to ASTM C974-87(1998) procedure. The samples were dry mixed for 3min and wet mixed for 3 min after adding water, in an Hobart mixer. Then the samples were cast using a vibration table, which works at 0.40mm of amplitude and 60 Hz of frequency. After casting, the samples were cured in mould at room temperature (20-22°C) for 24 hours. After demoulding, the samples were dried at 110°C for 24 hours. The samples, 160×40×40mm, were made for the determination of bulk density (B.D.), apparent porosity (A.P.), permanent linear change (PLC) and cold modulus of rupture (CMOR). Other sample sizes for oxidation test were considered: samples of 50×50×50mm directly cast and samples of 40×40×50mm cut from cast samples of 40×40×160mm.

The compositions of the castables are listed in Table 4.9. The particle size distribution [100-102] was designed according to Andreasen equation and the coefficient q-value is 0.29.

Table 4.9 Compositions of MgO-MA-C castables (wt.%)

Code	MgO-MA-C	MgO-MA-EG	MgO-MA-CG
MgO	80	80	82
T64+A12	5-10	5-10	-
T64+A1000SDG	-	-	6-10
H-Al_2O_3	3	3	-
SiO_2	1	1	2
Graphite	FG, EG, CG, GG	EG	CG
C	5	5	6
AlP	Al 0.2	Al 0.2	0 / 2 / 4
Si		1/ 2	/ (AlP-2+Si-1)
B_4C	0.5	(1/ 2)	/ (AlP-2+B4C-0.5)
Water, wt.%	5.5-8.5	6.3	5.4
Flow value, mm	>150	>150	160-195

4.3.3 Evaluation Methods [99, 103-106]

Different methods have been used to measure and evaluate the properties of the raw materials, the matrixes and the castables:

Flowability was measured according to ASTM C860-91(1995) method with a flow cone size of ∅(70-100)×70mm. The castable mass was firstly dry mixed for 3min and then wet mixed for 3 min after adding water by using Hobart N50 mixer. Then certain

holding the cone firmly on a Sinex vibrating table (600×600mm). After leveling the surface to the top of the cone, the cone was carefully removed, and then vibrated for 30 seconds at 60Hz frequency and 0.4mm in amplitude. The diameter of the spread mass was measured at 3 impartial corners. The flow value was calculated as the average of 3 measurements.

Particle size distribution of raw material was measured by particle size analyzer (LS200, COULTER). Bulk density (B.D.) and apparent porosity (A.P.) of the material were determined based on ASTM C830-93 method. Mechanical properties (CMOR) were tested according to ASTM C133-97 method. Permanent linear change was measured by ASTM C1407-98. Each value of B.D., A.P., PLC, and CMOR is the average of three parallel samples. Pore size distribution of extruded graphite pellets and cylindrical sample from matrix was measured by mercury porosimeter (PoreSizer 9320). Microscopy observations were performed through OM, CLM and SEM. Complementary chemical and X-ray diffraction analysis were also performed.

4.3.4 Oxidation Test Set-ups

Four different oxidation set-ups were used in this work. Each set-up has its own characteristics. The configuration and characteristics of each set-up are shown in Figures 4.12-4.15. The heating conditions are listed in Table 4.10.

Set-up A: TGA and CO_2 Gas Evolution

TGA and CO_2 gas analysis were carried out on flake graphite, modified graphite and extruded graphite pellets containing different antioxidants. The configuration of the set-up is shown in Figure 4.12, named as Set-up A. The advantages of this set-up include easy controlled atmosphere, a combination of TGA and CO_2 gas analysis. The CO_2 gas evolution gives better oxidation resistance for the sample containing antioxidants since the weight loss is not enough to be taken as a judgement on the oxidation resistance when antioxidant offers weight gain. The disadvantage of this set-up is that only small amount of the sample can be used. The heating conditions are listed in Table 4.10.

In the first group, flake graphite (FG) and modified graphite (EG, CG and GG) were tested for TGA analysis to understand the oxidation behaviour of modified graphite. The sample was compressed into a cylinder with a diameter of 19mm at a pressure of 70MPa to avoid the size difference of each modified graphite material.

In the second group, extruded graphite (EG), with or without antioxidant, were test by TGA and CO_2 mass spectrometer analysis in order to study the oxidation behaviour of flake graphite, extruded graphite as well as the role of antioxidant. The same amount of carbon content was used in each measurement. Original extruded graphite pellets were directly tested.

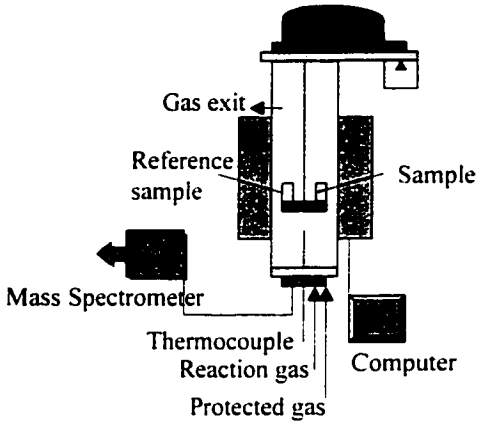

SETARAM: SETSYS 16/18

Test condition:
- up to 1700°C
- atmosphere control
- sample: carbon powder or pellets

Evaluation
- TGA
- CO_2 gas evolution

Figure 4.12 Thermobalance with mass spectrometer: Set-up A

Set-up B: Unidirectional Oxidation in Muffle Furnace

The castable samples (Table 4.9) were tested by unidirectional oxidation test in Set-up B, see Figure 4.13. The heating condition is listed in Table 4.10. The advantage of this set-up is easy to use. The samples are placed in the centre of the furnace to obtain uniform atmosphere and reproducible test results. The depth of decarbonized layer was taken as evaluation on oxidation resistance. Microscopy observations were used to study the role of the antioxidants. No air-flow control can be performed in this set-up.

Castable samples were cast in the mould with dimension of 50×50×50mm. After demoulding, the samples were cured at 110°C for 24 hours. Then the samples were

placed in the centre of an alumina crucible with coke protection. Only the top surface of the sample was exposed to air for unidirectional oxidation. After oxidation test, each sample was cut in cross section for further observation. The decarbonized depth was measured. The average of 3 values from each sample was taken as oxidation evaluation.

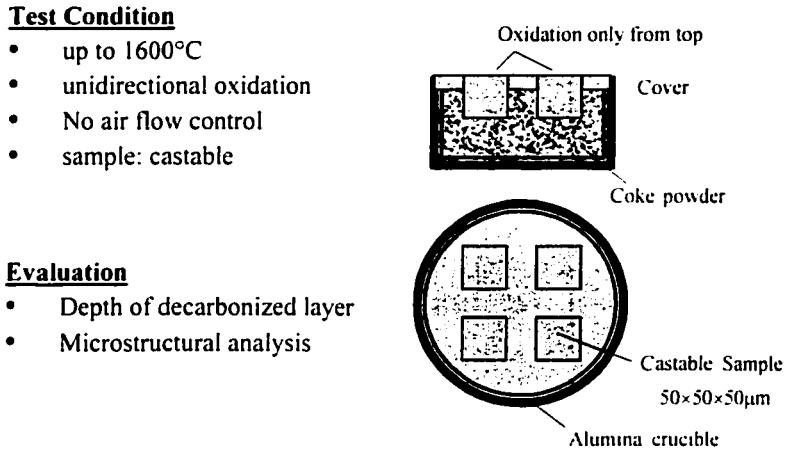

Figure 4.13 Unidirectional oxidation in muffle furnace: Set-up B

Set-up C: Unidirectional Oxidation in Tubular Furnace

Some renovations were done on the tubular furnace to obtain controlled air-flow, uniform distribution of atmosphere and unidirectional oxidation, as shown in Figure 4.14. The heating condition is listed in Table 4.10. Unidirectional oxidation tests with controlled air flow and available microscopy observations on tested samples were achieved. The limitation of this set-up is the size of the sample because of the internal volume of the furnace. Therefore only compressed cylindrical samples from the matrix

were used. In this set-up, the reproducible tests were obtained at air flow equal or over 500ml/min.

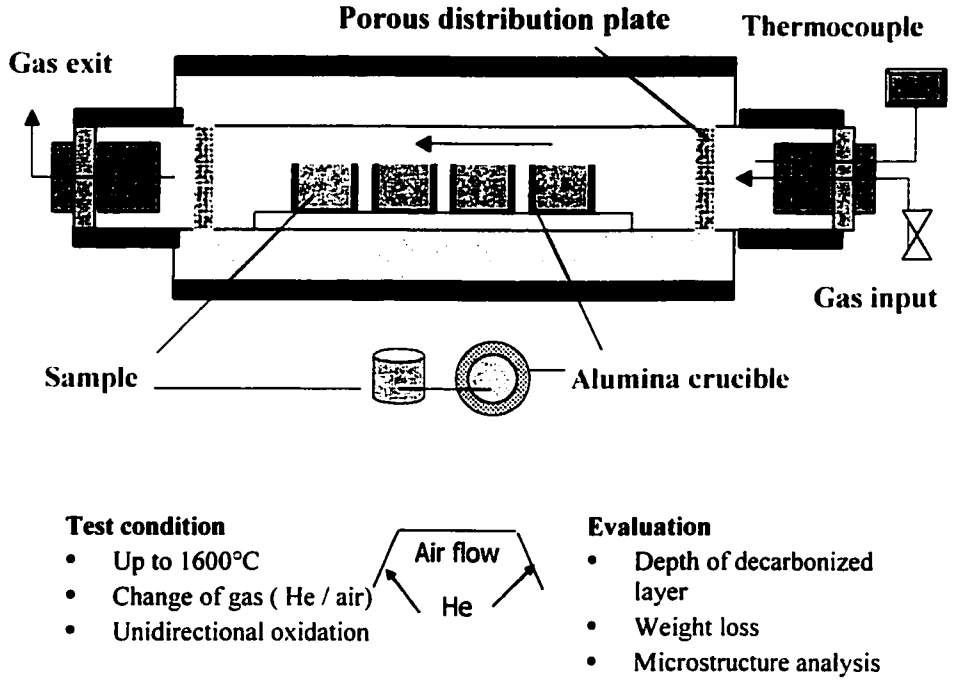

Figure 4.14 Unidirectional oxidation in tubular furnace: Set-up C

The matrix mixtures containing magnesia fine, fine graphite and different antioxidants (Table 4.8) were compressed into cylindrical samples with a diameter of 19mm and height of 25mm at a pressure of 70MPa. The samples were put into alumina crucibles with coke protection. Only the top surfaces of the samples were exposed to air for unidirectional oxidation test, as shown in Figure 4.14. After heat treatment, the samples were cut in cross section. The depth of decarbonized layer was measured. The average of three values of decarbonized depth was taken as the oxidation value.

were cut in cross section. The depth of decarbonized layer was measured. The average of three values of decarbonized depth was taken as the oxidation value.

Set-up D: Oxidation Test in Bottom-Load Furnace

The castable samples were tested in bottom-load furnace (Set-up D), as shown in Figure 4.15. The heating condition is listed in Table 4.10. The advantages of this set-up are its controlled air-flow and atmosphere, measured oxidation area and possible microscopy observations on the sample after the oxidation test.

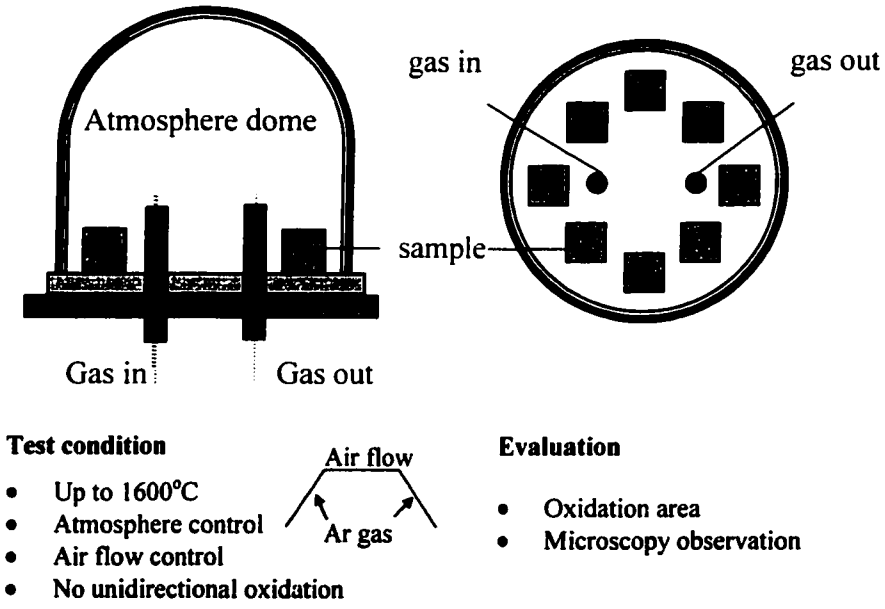

Figure 4.15 Oxidation in bottom-load furnace: Set-up D

Two different sizes of castable samples were prepared for oxidation tests. Sample with the size of 50×50×50mm were cast in the mould and then cured at 110°C for 24 hours.

The sample with the size of 40×40×50mm were cut directly from the cast sample with the size of 40×40×160mm. After oxidation treatment, the samples were cut in cross section, then original area and oxidation areas were measured by using a computer software "Image-Pro Plus". The oxidation index, which was calculated based on oxidation area divided by original area, was taken as the evaluation value. Reproducible test results were obtained at the given conditions.

Table 4.10 Heating conditions for different oxidation Set-ups A,B,C,D

Set-up	Set-up A	Set-up A	Set-up B	Set-up C	Set-up D
Sample	FG,EG CG,GG	EG-0 $(EG\text{-}A.O.)_{MA}$ $(EG\text{-}A.O.)_{MS}$	Castable 5x5x5cm	Matrix+EG matrix+A.O. Ø19×25mm	Castable 5x5x5cm 4x4x5cm
Heating rate, °C/min	5	5	5	5	5
Cooling rate, °C/min	5	5	5	5	5
Holding time, hour	5	1	3	3	3
Oxidation Temperature, °C	T_{room}-1350	T_{room}-1400	T_{room}-1200 T_{room}-1400	1400	1200, 1400
Heating up	air	air	air	He	Ar
Holding time	air	air	air	air	air
Cooling down	air	air	air	He	Ar
Air flow, ml/min	500	500	no	500	1000
Evaluation	TGA	CO_2 gas	decarbonized depth, mm	decarbonized depth, mm	oxidation ratio,%

4.4 OXIDATION RESISTANCE OF GRAPHITE MATERIALS

The oxidation behaviours of four graphitic materials are exhibited through TGA oxidation curves in Figure 4.16. The initial weight loss for extruded graphite pellets is

clearly due to the oxidation of the binder. The final weights of the specimens after 5 hours are a measurement of the ash content, of the order of 3.0%. The noticeable difference of the final weight loss for the granulated graphite is simply due to the addition of alumina. The modified graphite EG and GG show the lower oxidation rate compared with flake graphite FG. Modified graphite CG has lower oxidation resistance because of pitch contained in CG.

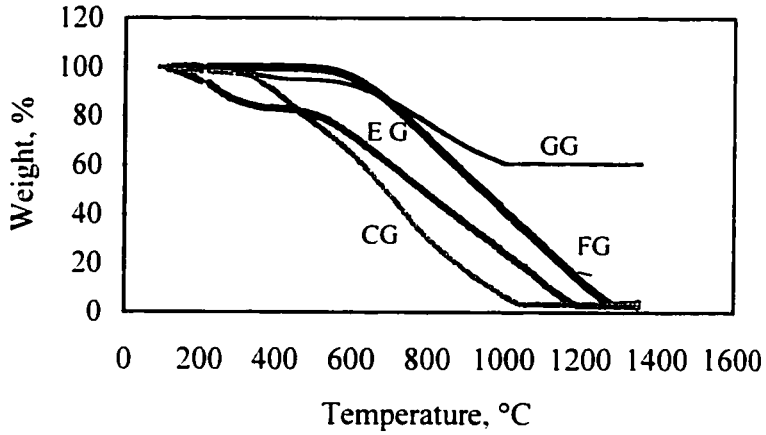

Figure 4.16 TGA oxidation curves for flake graphite FG and modified graphite (EG, CG, GG) at a heating rate of 5°C/min up to 1350°C (Set-up A)

To improve oxidation resistance of extruded graphite pellets for spinel-bonded castables, antioxidants such as metallic Al, metallic alloy AlMg, boron carbide B_4C, oxides MgO and Al_2O_3 were incorporated into extruded graphite pellets. The oxidation resistance of $(EG\text{-}A.O.)_{MA}$ pellets were evaluated by CO_2 gas evolution. The results are shown in Figure 4.17.

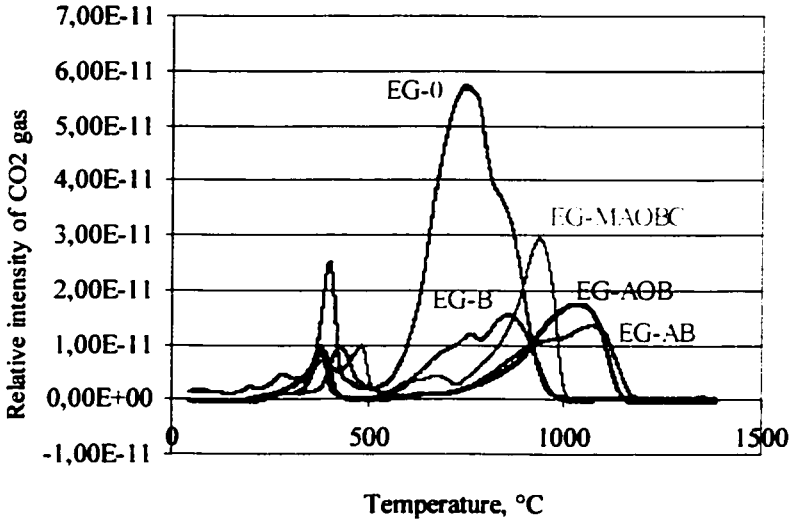

Figure 4.17 Oxidation resistance of $(EG\text{-}A.O.)_{MA}$ by CO_2 gas evolution (Set-up A)

There are two peaks for each sample in Figure 4.17. The first peak is simply due to the oxidation of the binder. The second peak shows the oxidation of extruded graphite. The oxidation resistance of extruded graphite was effectively improved by incorporating antioxidant or oxide into extruded graphite pellets in terms of the starting oxidation temperature and relative intensity of CO_2 gas. The oxidation temperatures of $(EG\text{-}A.O.)_{MA}$ were increased up to 200°C as compared to that of EG-0. Extruded graphite with the combination of aluminium and boron carbide (EG-AB) gives the best result. The sample with the combination of alumina and boron carbide (EG-AOB) shows a similar starting oxidation temperature and slightly higher relative intensity of CO_2 gas as compared to that of (EG-AB). Boron carbide along is also efficient to improve oxidation resistance, but not as good as those of (EG-AB) and (EG-AOB) on starting oxidation

resistance, but not as good as those of (EG-AB) and (EG-AOB) on starting oxidation temperature. Sample (EG-MAOBC) has higher oxidation in terms of CO_2 gas intensity as compared to other antioxidant package because of the 4% fine carbon CB used in the pellets, but still offer higher oxidation resistance than that of (EG-0) due to its denser structure and smaller pore size in the pellets.

4.5 OXIDATION RESISTANCE OF PRESSED MATRIX SAMPLES

The effect of antioxidant was studied in a magnesia-based matrix in order to see its influence on oxidation resistance as well as volume change, mechanical and physical property. The compositions of the samples are listed in Table 4.8. The oxidation resistance is shown in Figure 4.18, where the oxidation depth of MC0 fired at 1400°C for 1 hour was taken as a reference and oxidation index was calculated.

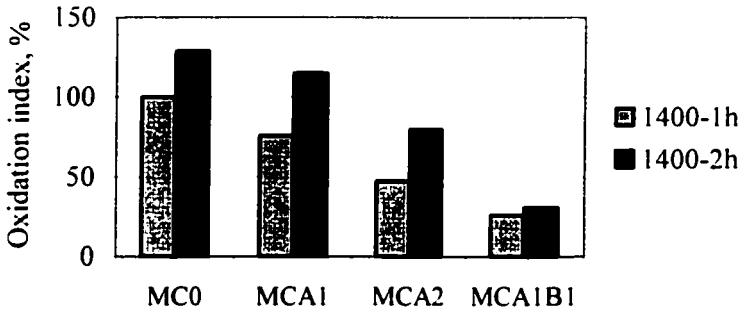

Figure 4.18 Influence of antioxidants on oxidation resistance of the matrixes

(Unidirectional oxidation at 1400°C with air flow 500 ml/m in Set-up C)

Figure 4.8 demonstrates that the oxidation resistance of the matrix was effectively improved by the addition of antioxidant aluminium or its combination with boron carbide. The oxidation resistance was increased when higher amounts of aluminium were used, as compared the sample MCA1 with the sample MCA2. The best oxidation resistance was obtained in the sample with the combination of aluminium and boron carbide (MCA1B1). The oxidation of graphite was increased with time in all samples. After oxidation test at 1400°C in Set-up C, the microscopy observations (OM, CLM, SEM) were conducted on samples MC0, MCA2 and MCA1B1, as illustrated in Figures 4.19-4.21.

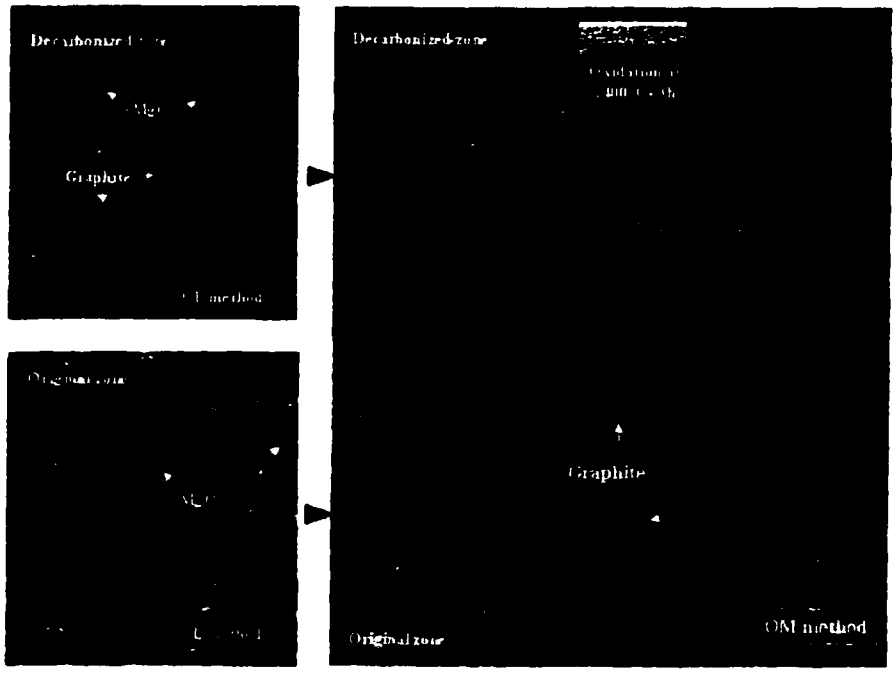

Figure 4.19 Microscopy observations on sample MC0 (OM/CLM)

(After unidirectional oxidation at 1400°C×3h in Set-up C)

In sample without antioxidant (MC0), flake graphite was easily oxidized and left pores in the matrix, see decarbonized layer in OM picture in Figure 4.19. Inside of the sample, graphite flakes were distributed among magnesia particles and blue colour was identified as magnesia in CLM picture.

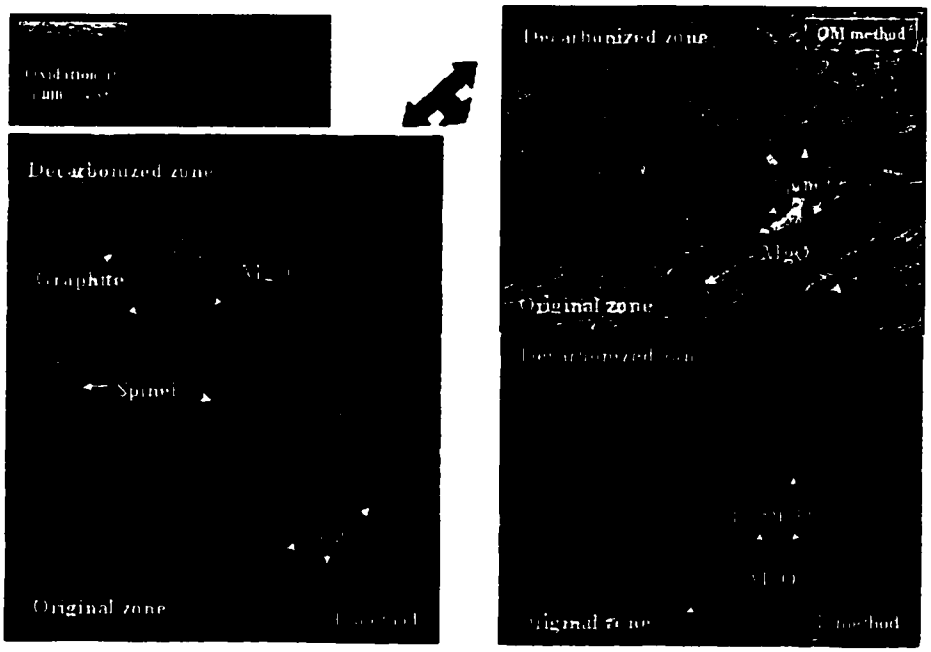

Figure 4.20 Microscopy observation on sample MCA2 (OM/CLM)

(After unidirectional oxidation at 1400°C×3h in Set-up C)

In the case of using aluminium in the material, new compound spinel was formed around aluminium through OM observation as shown in Figure 4.20. More spinel was found in

the zone close to the decarbonised layer, see CLM picture, where green and blue colour were identified as spinel and magnesia, respectively, confirmed by OM and SEM.

In the case of the combination of aluminum and boron carbide (see Figure 4.21), the highest oxidation resistance was obtained in sample MCA1B1 since boron carbide not only leads to low melting compounds formation which blocks pores and reduces oxygen inward diffusion, but also stimulates spinel formation. A dense spinel layer was observed in the zone close to the decarbonized layer. This dense layer is beneficial to improve oxidation resistance.

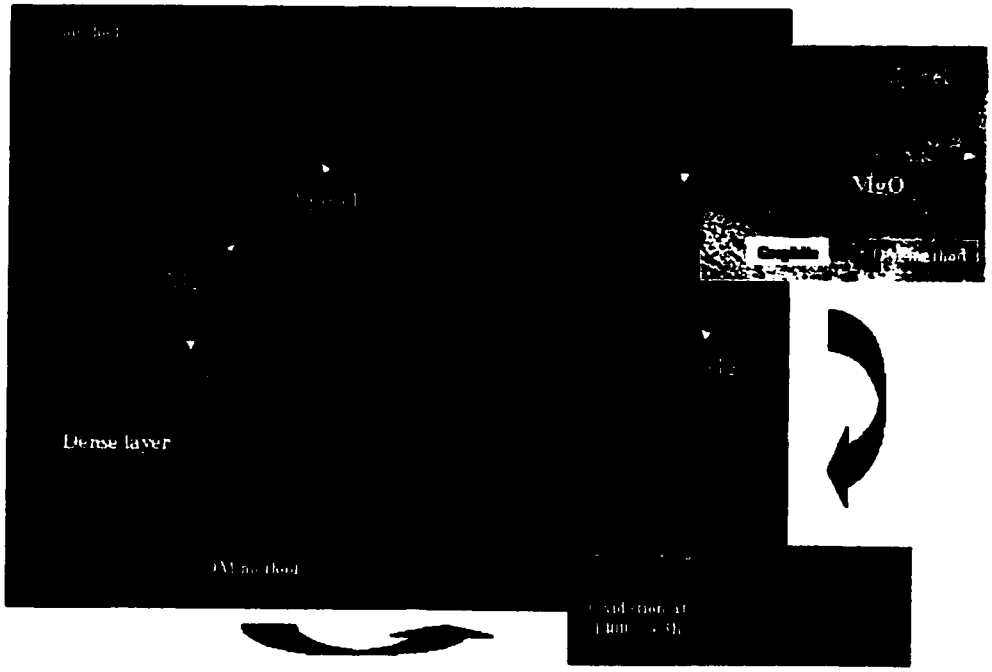

Figure 4.21 Microscopy observations on sample MCA1B1 (OM/CLM)

(After unidirectional oxidation at 1400°C×3h with air flow 500ml/min in Set-up C)

The influences of antioxidants on mechanical property and volume change of the matrix are shown in Figure 4.22. It can be seen that mechanical property increases with addition of the antioxidant at a temperature of 800°C and above. The higher the amount of aluminium, the higher the strength value is. With the same amount of aluminium, the combination of aluminium and boron carbide offers higher strength values than that of sample with only the addition of aluminium. The higher strength values were obtained in the temperature range of 1000-1200°C. Microscopy and X-ray diffraction analysis show that the new compounds, Al_4C_3, Al_2O_3 and spinel, are formed, which contribute to the development of strength. The volumes of the samples with antioxidants start to increase at 1000°C and reach the highest values around 1200°C with formation of spinel. The volume of the sample without antioxidant (MC0) is stable at the different temperatures treatment used.

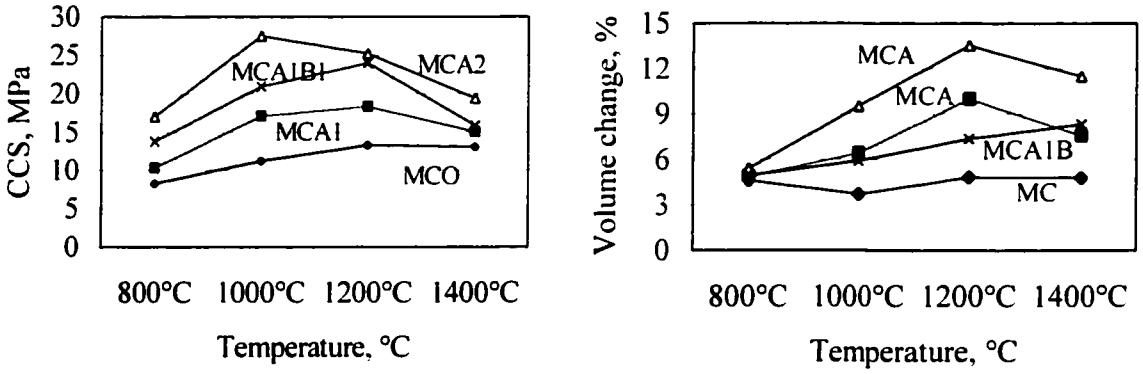

(a) CCS vs. temperature (°C) (b) volume change vs. temperature (°C)

Figure 4.22 Influence of antioxidant on mechanical property and volume change of the matrix (MC0, MCA1, MCA2 and MCA1B1)

The physical properties of the matrixes are given in Figure 4.23. It exhibits that the bulk density of the sample with antioxidant decreases and the apparent porosity increases at the given composition and heating condition. Hence, the influence of antioxidant on mechanical property, volume change and physical property of the material need to be taken into account.

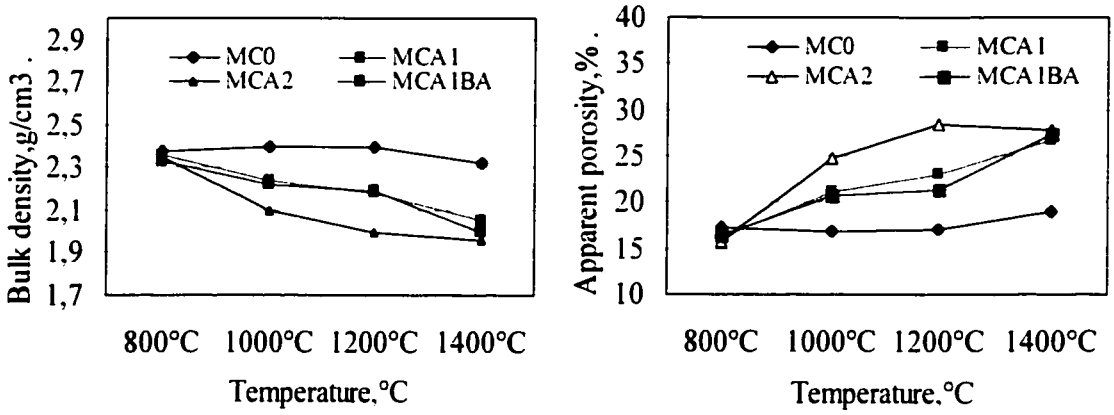

(a) B.D. vs. temperature (°C) (B) A.P. vs. temperature (°C)

Figure 4.23 Influence of antioxidant on physical property of the matrix (MC0, MCA1, MCA2 and MCA1B1)

To understand the microstructure change of the materials with the addition of antioxidants, the pore size of cylindrical samples (MCO, MCA1, MCA2, MCA1B1) were measured by the mercury intrusion method. The results are shown in Figure 4.24. The positive change on pore size distribution of the materials was achieved through incorporating antioxidants into the materials. The test reveals that the pore sizes were

distributed in the range of 7 to 0.03μm for MC0 and 1 to 0.02μm for the samples with antioxidants, see Figure 4.24a.

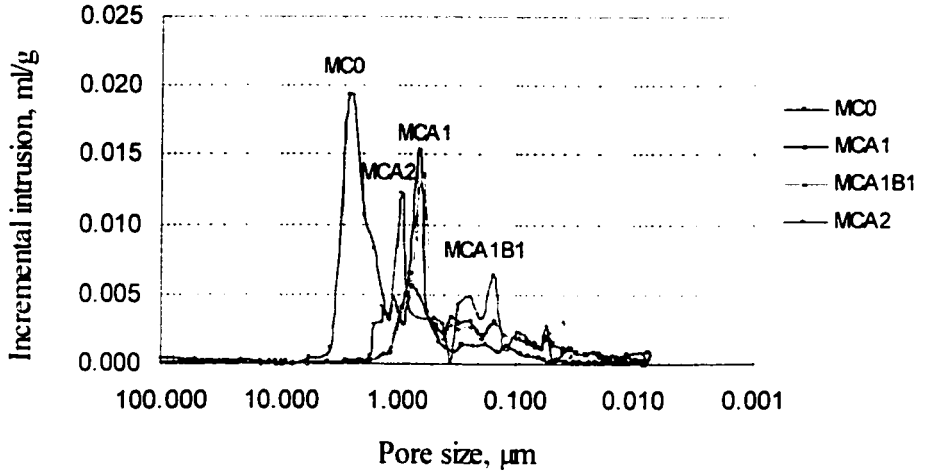

Figure 4.24a Incremental intrusion vs. pore size by antioxidants in matrix

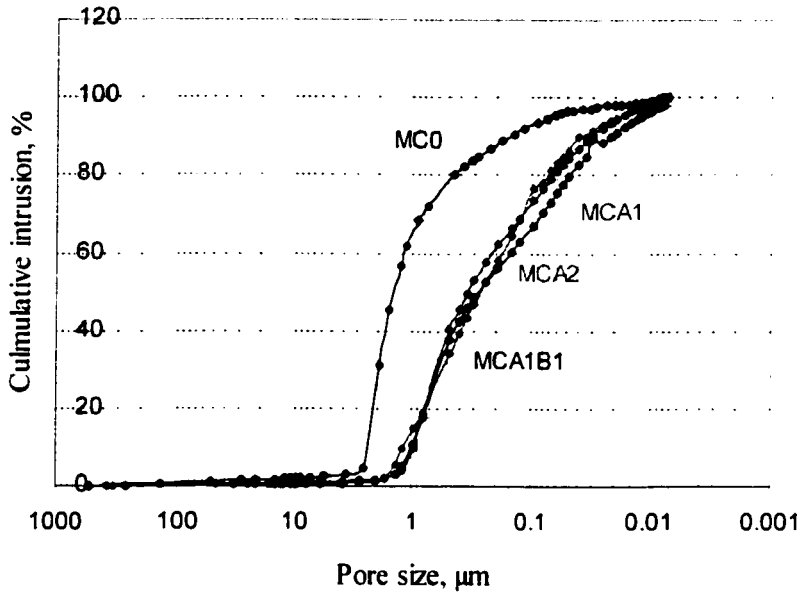

Figure 4.24b Cumulative intrusion vs. pore size by antioxidant in matrix

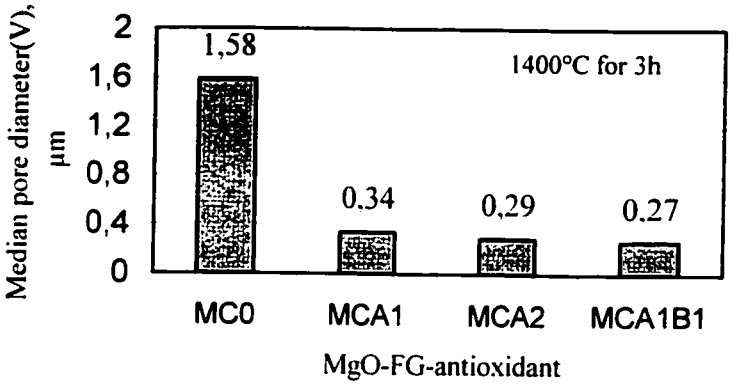

Figure 4.24c Influence of antioxidants on median pore diameter of the matrix

To reach 80% cumulative intrusion value, the pore sizes are in the range of 7-0.5μm for MC0 and 2-0.07μm for the samples with antioxidants, as shown in Figure 4.24b. In Figure 4.24c, the median pore size was decreased from 1.58μm for the sample without antioxidant (MC0) to 0.34μm (MCA1), 0.29μm (MCA2) and 0.27μm (MCA1B1), respectively. The results illustrate that antioxidant effectively reduces the pore size of the materials. This contributes to improving the oxidation resistance and the mechanical property.

4.6 OXIDATION RESISTANCE OF MgO-MA-C CASTABLES

4.6.1 Role of Modified Graphite Pellets on Flowability

A good flowability with minimum water demand is always highly desirable in developing a castable. As reviewed earlier, different carbon sources have a strong

influence on flowability of castables, especially in the case of using flake graphite into castables. The influences of graphitic materials FG, EG, CG, GG on flowability of MgO-MA-C castables are demonstrated in Figure 4.25. The compositions of the castables are given in Table 4.9.

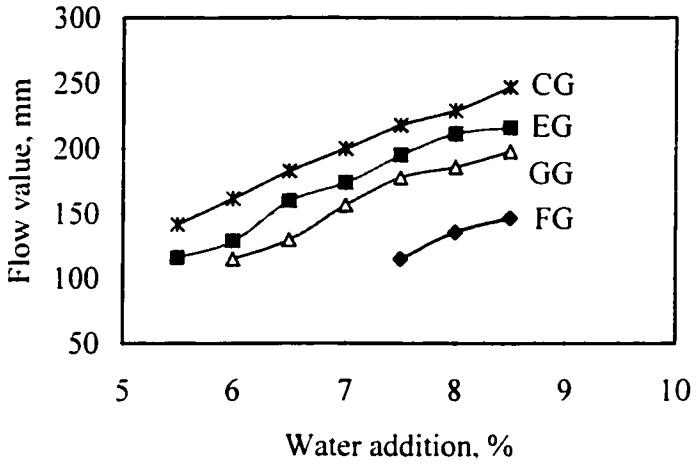

Figure 4.25 Influences of graphitic materials (FG, EG, CG, GG) on flowability of MgO-MA-C castables

To reach a flow value of 150mm or over 150mm, Figure 4.25 clearly reveals that the water addition is 8.5% for flake graphite containing castable, and 7%, 6.3%, 5.7% for GG, EG and CG containing castables, respectively. Incorporating flake graphite directly into castable needs 2% or over 2% more water addition to reach a similar flow value as compared to the cases of using modified graphite materials (EG and CG). GG graphite containing castable also shows a positive improvement on reducing water addition, but not as good as those of EG and CG containing castables. The results show that effective

surface modifications of graphite flakes were achieved by extruding, coating and granulating methods.

4.6.2 Role of Modified Graphite Pellets on Mechanical Properties

The influence of graphitic materials on the mechanical property of MgO-MA-C castables is given in Figure 4.26. Cold modulus of rupture was measured by using 3 points bending conventional method. Values of CMOR increase from 2-4 MPa for FG castable to 3-6MPa for EG and CG castables, depending on the firing temperatures. It corresponds to an increase of 60 to 100% over the flake graphite case taken as the reference material. The improvement of the mechanical property with increased temperature is due to the presence of specific antioxidants Al and B_4C, which refers to the formation of magnesia-borate melt then enhancing the formation and crystallization of magnesia-alumina spinel in MgO-C material.

The increases of CMOR of EG and CG over FG, at each temperature, are directly related to the water additions needed to achieve the same flowability (at 150mm) and hence the inherent open porosity of the castables. In the case of the granulating graphite castable, the results are not as good as expected since the crushed granulated graphite particles result in lower flowability, as compared to CG and EG containing castables.

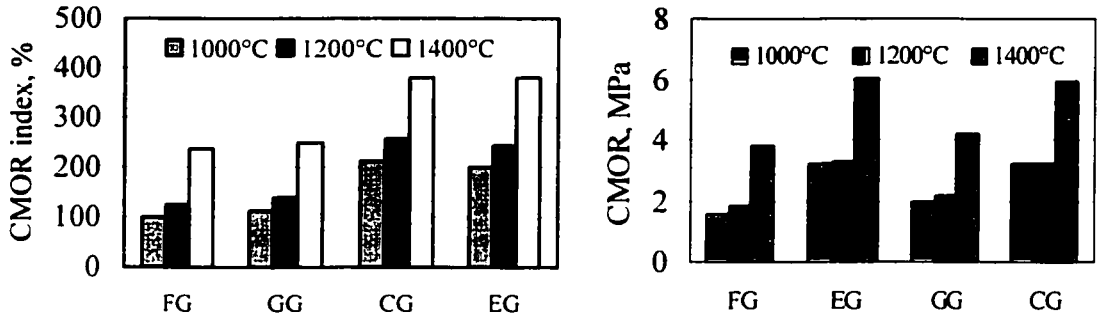

(a) CMOR index vs. graphitic materials (b) CMOR vs. graphitic materials

Figure 4.26 Influence of graphitic materials on mechanical property of MgO-MA-C castables

4.6.3 Oxidation Resistance of MgO-MA-C Castables

The influences of graphitic materials on oxidation resistance of MgO-MA-C castables are shown in Figure 4.27, where the oxidation index is calculated based on oxidation depth and taken FG containing castable as a reference.

The oxidation resistance of EG, CG and GG containing MgO-MA-C castables are effectively increased and higher than that of FG containing MgO-MA-C castable. It reveals that the surface modification of graphite flakes by extruding, coating and granulating methods contributes to sufficiently reducing water addition and improving oxidation resistance as compared to that of directly using flake graphite. The oxidation resistance of GG containing castable is lower than that of EG and CG containing castables but higher than that of FG containing castable. This can be explained that the

flowability of GG containing castable is lower than that of EG or CG containing castables, but higher that that of FG containing castable at the same water addition. This illustrates that the mode of incorporating graphite into castable plays an important role in the oxidation resistance. High water addition leads to high porosity and high oxidation of the material because water transforms to pores upon heating and high porosity and big pores facilitate oxidation of carbon. In addition, the nature of the carbon acts as another important factor affecting the oxidation of the material. CG containing castable has the lowest water addition but still slightly higher oxidation than that of EG containing castable because CG pellets contains 30% pitch, which causes higher oxidation than graphite.

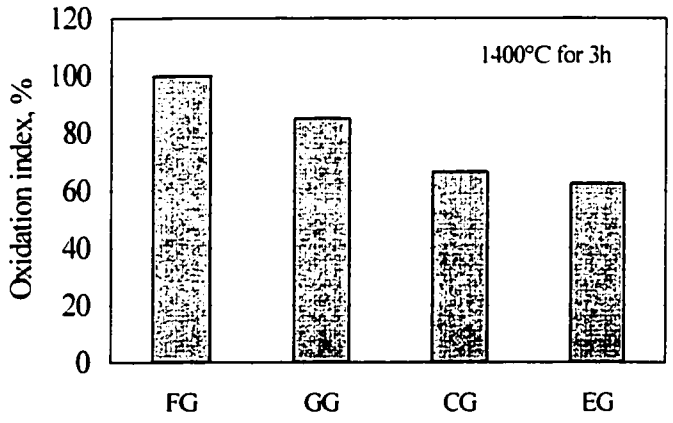

Figure 4.27 Influence of graphitic materials (FG, EG, CG, GG) on oxidation resistance of MgO-MA-C castables after firing at 400°C×3h in Set-up B

Influences of antioxidants silicon and boron carbide on oxidation resistance of MgO-MA-EG castables are shown in Figure 4.28.

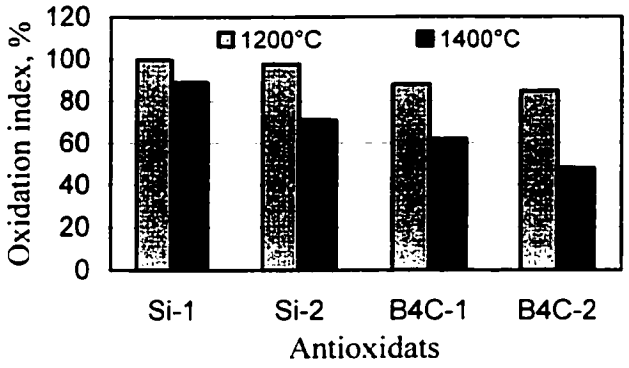

Figure 4.28 Influence of antioxidants on oxidation resistance of MgO-MA-EG castables after firing at 1200°C and 1400°C for 3 hours in Set-up B

The castables contain 3% hydratable alumina and extruded graphite pellets with different antioxidants in the graphite pellets and in the matrix. Each castable contains 5% carbon. A combination of 0.2% Al with either 1% or 2% of silicium or boron carbide was used as antioxidants. As expected from previous results on MgO-C bricks, the antioxidant package Al+B_4C is more efficient than Al+Si in the castables. The microscopy observations show that boron carbide not only stimulates dense spinel layer formation and also promotes a liquid formation, which blocks pores. These positive changes on the microstructure of the material increase the resistance to inward oxygen diffusion and therefore increase the oxidation resistance. Furthermore, the relative protection of graphite from oxidation is greater at 1400°C than that at 1200°C since the antioxidants become more effectively act at higher temperatures.

The influences of antioxidant aluminium on the oxidation resistance of MgO-MA-CG castables were tested in Set-up D, as shown in Figure 4.29. Each sample contains 6% carbon and 4% super fine A1000SDG. No hydratable alumina was used in this group. The addition and the combination of metallic aluminium with either silicon or boron carbide in MgO-MA-CG castables are listed in Tables 4.9 and 4.11.

Table 4.11 Antioxidant aluminium in MgO-MA-CG castables

Code	A0	A2	A4	A2B05	A2S1
AlP	0	2	4	2	2
B_4C				0.5	
Si					1
Water,%	5.2	5.4	5.4	5.4	5.4
Flow value, mm	190	195	160	185	170
B.D.110°C, g/cm^3	2.85	2.77	2.70	2.77	2.76
PLC 1500°C x 3h.%	0.23	0.98	1.27	1.2	0.9

The results indicate that coated aluminium with addition up to 4% can be possibly used in castables. The effect of metallic Al on increasing oxidation resistance of the castables is further confirmed, as shown in Figure 4.29. The oxidation resistance is increased with single aluminium addition or the combination of aluminium and silicon or boron carbide. Concequently, the combination of different antioxidants exhibits higher oxidation resistance than that of using single antioxidant. Better oxidation resistance of the castable is obtained with the sample containing 2% aluminium as well as its combination with 0.5% boron carbide or 1% silicon. It was also found that the higher

addition of metallic aluminium up to 4% did not further improve the oxidation resistance of the castable. This may be caused by undesired expansion, which leads to higher porosity and oxidation.

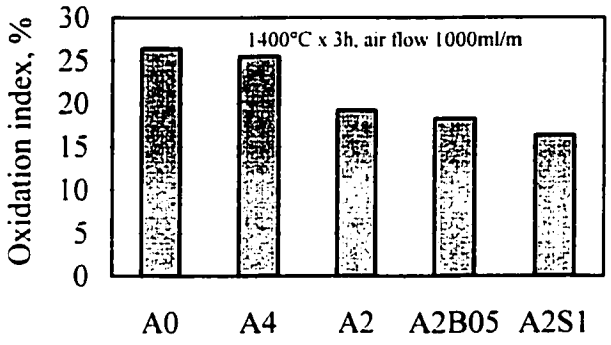

Figure 4.29 Oxidation resistance of MgO-MA-CG castables (Set-up D)

CHAPTER 5 OXIDATION STUDY ON MgO-M_2S-C MATERIAL SYSTEM

5.1 INTRODUCTION

This chapter describes cement-free magnesia-based forsterite-bonded castables containing graphite, the MgO-M_2S-C system. The purpose is to illustrate the influence of FG, EG and CG pellets on properties of the castables as well as the various strategies which have been adopted to increase the oxidation resistance of the castables, with an emphasis on the role of other carbon source, other than modified graphite pellets.

To develop magnesia-based forsterite-bonded carbon-containing castables (MgO-M_2S-C castables), magnesia fine and silica fume were selected to act as the binders and bond-forming agents. The reasons for using silica fume are: 1) to minimize the porosity, i.e., replace some of the water addition, in connection with particle size distributions, 2) to improve the hydration resistance of magnesia and offer essential binding strength, 3) to take part in the forsterite formation.

In this chapter, the influences of different deflocculants, magnesia fines, carbon sources and antioxidants on overall properties of MgO-M_2S-C castables are presented. The properties of 25 different MgO-M_2S-C castables are described, in terms of physical and mechanical properties, pore size distribution and oxidation resistance. Different ways to maximize the oxidation resistance of the products are documented.

5.2 EXPERIMENTAL PROCEDURES

5.2.1 Raw Materials

The selection of raw materials and their roles in magnesia-based forsterite-bond carbon-containing castables are illustrated in Figure 5.1.

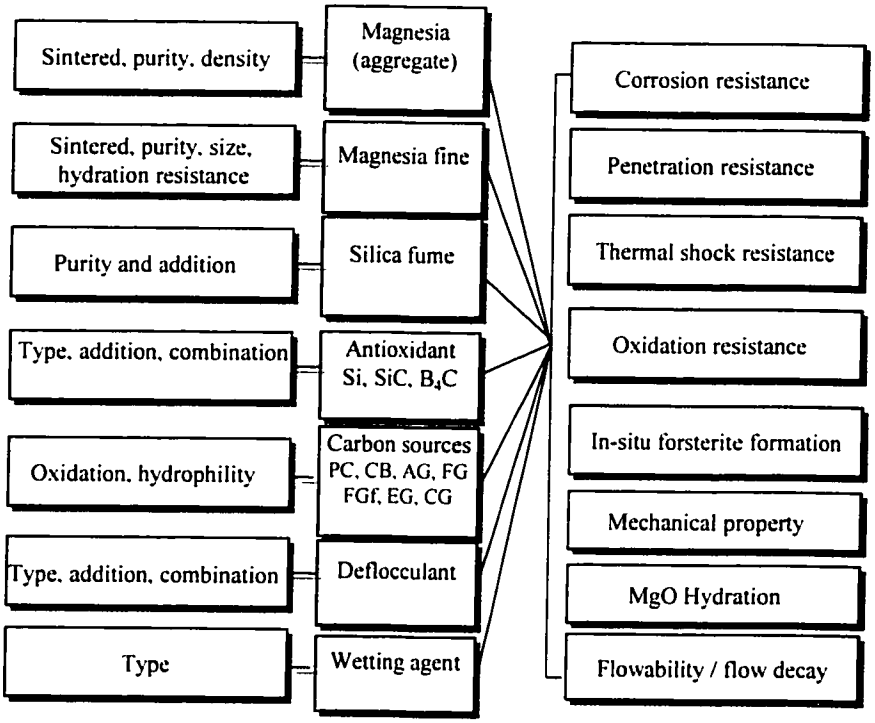

Figure 5.1 Raw materials and their roles in MgO-M_2S-C castables

Development of a magnesia-based carbon-containing castable includes selecting magnesia aggregate and fines, carbon source, binder and bonding systems and

antioxidants as well as some additives, such as deflocculant and wetting agent. The concerns on magnesia aggregate and fine powders were focused on its purity, density, size and hydration resistance. Considering the binder and the bonding systems, oxide fines such as MgO and SiO_2 as well as antioxidants silicon, silicon carbide and boron carbide were selected. Carbon sources, such as pitch-carbon, carbon black, amorphous graphite, flake graphite and modified graphite, were taken into account for their oxidation resistance and hydrophilic property. Some essential additives like deflocculants and wetting agent were determined.

Magnesia fines with different particle size distributions were used. Their properties are listed in Table 5.1 and their particle size distributions are illustrated in Figure 5.2.

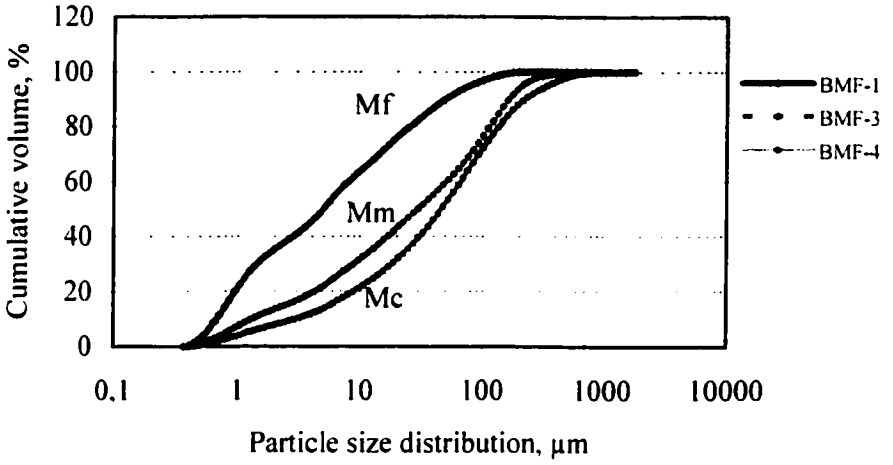

Figure 5.2 Particle size distributions of magnesia fines

Table 5.1 Magnesia materials for MgO-M_2S-C castables

Code	Mc	Mm	Mf
Magnesia	CF99	LUD 98	LUD 97A
Chemical composition, %			
MgO	99.30	98.13	96.40
Al_2O_3	0.03	0.08	< 0.10
SiO_2	0.03	0.66	0.31
CaO	0.63	0.91	1.84
Fe_2O_3	0.04	0.14	0.39
BSG	3.44 g/cm^3	3.34 g/cm^3	3.38 g/cm^3
Source	DSP	Ludington	Ludington

Magnesia aggregate, silica fume and wetting agent are the same as described in section 4.3.1 of chapter 4. Antioxidants metallic silicon, silicon carbide and boron carbide are listed in section 3.2.1 of chapter 3.

In this chapter a broader range of carbon sources has been used. The different carbons are: 1) green pitch-coke, containing 70-80% highly crystallized mesophase type carbon (denoted as PC), from OSAKA KASEI, Japan; 2) carbon black (denoted as CB), from OSAKA KASEI, Japan; 3) amorphous graphite (denoted as AG), from Cummings-Moore Graphite Co., USA; 4) natural flake graphite (FG), from Stratmin Graphite Co., Canada; 5) flake graphite fines (denoted as FGf), from Stratmin Graphite Co., Canada; 6) modified graphite pellets (EG, CG, GG), as described in chapter 3. Some properties of various carbon sources are listed in Table 5.2

Table 5.2 Carbon sources* for MgO-M_2S-C castables

Symbol	PC	CB	AG	FG	FGf
Softening point, °C	>320				
Fixed carbon, %	85	97.7	85.3	97	97
Volatile matter,%	15	2.0			
Ash content, %	<1	0.3	14.7		
Size	<1.0mm	<5μm	<1.0mm	<75μm	<5μm
Status	powder	fine powder	powder	flake	fine powder

* Modified graphite: EG, CG and GG, see Chapter 3

Five different deflocculants were investigated and determined in MgO-M_2S-C castables, as listed in Table 5.3.

Table 5.3 List of deflocculants for MgO-M_2S-C castables

Commercial term	Denotation
Sodium hexametaphosphate	S6P
Galoryl	G
Monosodium citrate	ACM
Darvan 7S	D7S
Sodium dihydrogenecitrate	SD

5.2.2 Compositions and Evaluation Methods of MgO-M_2S-C Castables

In this work, the particle size distribution of the castables was designed and adjusted based on Andreassen equation, where continuous particle size distribution of a mixture offers the best result for castable. The expression of the Andreassen distribution is: $CPFT = [(d/D)^q] \cdot 100$, with CPFT being the cumulative percent finer than; d: the particle size; D: the maximum particle size; q: the distribution coefficient (q-value).

Four fractions of magnesia aggregate were used: 6.7-3.35mm, 3.35-1.18mm, 1.18-0.3mm and <0.3mm. The particle size distribution of the castable was calculated based upon the addition of aggregate and fines, in which the q-value is 0.29.

Four groups of magnesia-based forsterite-bonded carbon-containing castables were investigated in this chapter, to study the role of deflocculants, magnesia fines, carbon sources and antioxidants. The compositions of MgO-M_2S-C castables are listed in Tables 5.4 and 5.5.

Concerning the preparation of castable samples and the evaluation methods on flowability, bulk density (B.D.), apparent porosity (A.P.), mechanical property CMOR and CCS, permanent liner change (PLC) as well as oxidation resistance, same procedures were employed, as described in chapter 4. One newly involved evaluation

method is the Wedge splitting test (WST), which is used to measure the work of fracture of the material and to evaluate their fracture's behaviour and thermal shock parameters. The experimental method is described in Appendix 1.

Table 5.4 Compositions of MgO-M_2S-C castables (wt.%)

Code	MgO-M_2S-C(1)	MgO-M_2S-C(2)	MgO-M_2S-C(3)
MgO	> 89	> 87	> 87
MgO fine	Mf	Mc, Mm, Mf	Mf / Mf+Mc
SiO_2	3	3	1, 2, 3
Non-graphite carbon	-	-	PC, CB
Graphite	AG	AG	AG, FG, FGf, EG, CG $(EG\text{-}A.O.)_{MS}$
Carbon content	6	6	6
Antioxidant	-	2 (Si)	2 (Si)
Factors studied	deflocculant	magnesia fine	carbon source
Parameters	Flowability, CMOR	Flow decay	Flowability, B.D., A.P. PLC,CMOR, pore size, Oxidation resistance

Table 5.5 Quantities of antioxidants in MgO-M_2S-C castables (4) (wt.%)

Code	SO3 / SO5	S2	S4	S6	SC2	SC4	SC6	S2SC2	S2SC2*	S2B
MgO+Mf	>87	>87	>85	>83	>87	>85	>83	>85	>87	>86
SiO_2	3 / 5	2	2	2	2	2	2	2	1	2
Graphite	AG	AG	AG	AG	AG	AG	AG	AG	AG	AG
Carbon	6	6	6	6	6	6	6	6	6	6
Si	0	2	4	6				2	2	2
SiC					2	4	6	2	2	
B_4C										0.5

5.3 FLOWABILITY AND PROPERTIES OF MgO-M_2S-C CASTABLES

To reach a good flowability with a minimum water addition is one of the most important property of a castable. The amount of water used in a castable mix has a significant influence on overall properties of a castable since the water transforms to porosity upon heating. Many factors, such as the nature of the raw materials, the particle size distribution, the type of a binder, oxide fine, deflocculant, setting adjusting agent, carbon source and wetting agent, influence the flowability of a castable. After the material system being selected and the particle size distribution being designed, the more important factors in improving the flowability of a castable are the nature of the oxide fines, deflocculants and carbon sources.

5.3.1 Influence of Deflocculant on Flowability and Mechanical Property

Among the factors influencing flowability, the effect of deflocculant can be significant. Based on the nature of the raw materials used in a castable, appropriate deflocculant as well as its combinations need to be detremined. Table 5.6 lists the deflocculants and their combinations used in MgO-M_2S-C (1) castables (see Table 5.4), in which amorphous graphite was used and the carbon content was fixed at 6%. The symbol '>' in Table 5.6 refers to an addition of 0.05%.

Table 5.6 Quantities of deflocculants used in MgO-M_2S-C (1) castables

Deflocculant	D1	D2	D3	D4	D5	D6	D7	D8	D9	D10
S6P	>	>	>	>>>	>>>			>>>	>>	>
G	>	>>	>>>		>	>>	>>	>>	>	>>
D7S						>>				
SD							>>		>	>
ACM			>							

Figures 5.3 and 5.4 illustrate the influences of deflocculants on flowability and mechanical properties of MgO-M_2S-C (1) castables. It indicates that different deflocculants, either single or in combination, strongly influence the flowability and the mechanical properties of a castable. With deflocculant package D1 to D10 in MgO-M_2S-C castables, the water addition changes from 6% to 8% in order to reach an acceptable flow value (>150mm). Modulus of rupture, CMOR, after drying at 110°C for 24 hours, varies from 3 to 12MPa.

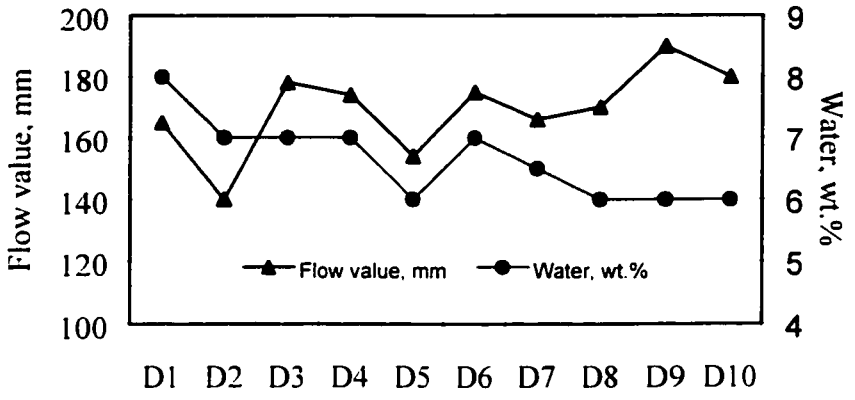

Figure 5.3 Influence of deflocculants on flowability of MgO-M_2S-C (1) castables

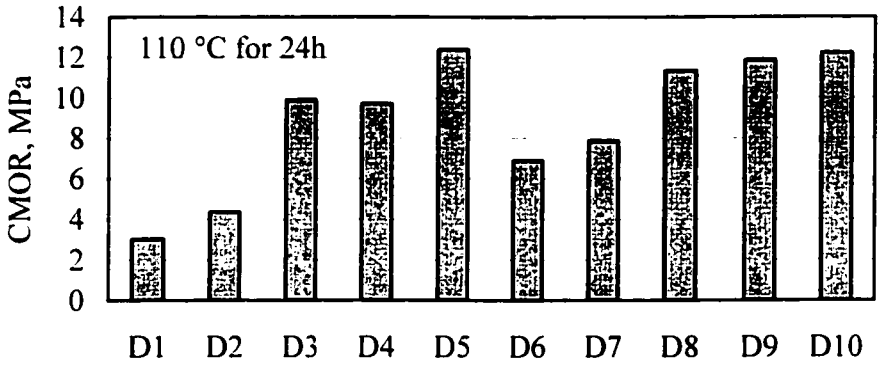

Figure 5.4 Influence of deflocculants on CMOR of MgO-M_2S-C (1) castables

The addition of galoryl alone is not sufficient to reduce water addition. The combination of galoryl (G) with sodium hexametaphosphate (S6P) or Darvan 7S (D7S) or sodium dihydrogenecitrate (SD) performed well. Deflocculant S6P is more efficient than D7S and SD in reducing water addition and improving mechanical properties. The

deflocculant packages D5 and D8 to D10 reach flow value over 150mm at water addition of 6% and offer higher strength values. Samples without SD or ACM show faster setting. Considering flowability, mechanical properties and setting time, the deflocculant package D9 provided better results over other deflocculant packages and was chosen exclusively for the remaining part of this thesis.

5.3.2 Magnesia Fines on Flow Decay

For magnesia-based castable containing over 70% MgO, its workability, regarding to flow value, flow decay and setting time, remains a difficult aspect to overcome. Flow decay refers to that the flowability decreases with the increase of the time. Several factors, such as the nature of the raw material and the nature of the additives, influence flow decay. In this thesis, the nature of magnesia fine was a dominant factor. In Table 5.4 are listed different magnesia fines in MgO-M_2S-C (2) castables for the study of flow decay. The results on flow decay of MgO-M_2S-C (2) castables are illustrated in Figure 5.5, which exhibits that the size of magnesia fine has a strong impact on flow decay. The finer the magnesia, the faster the flow decay is. Therefore, the combinations of different magnesia fines, together with different kinds of deflocculants, are required for an acceptable workability of a basic castable.

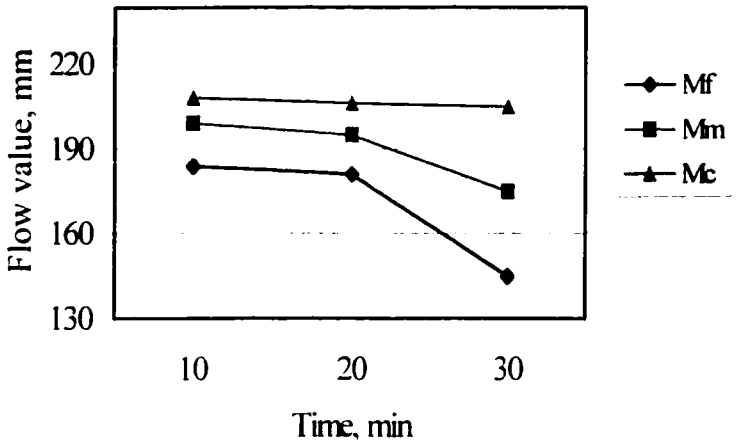

Figure 5.5 Influence of magnesia fines on flow decay of MgO-M_2S-C (2) castables

5.4 CARBON MATERIAL FOR MgO-M_2S-C CASTABLES

5.4.1 Influence of Carbon Source on Flowability

The influences of carbon sources on flowability of MgO-M_2S-C (3) castables are demonstrated in Figures 5.6-5.9. The results reveal that around 2% or over 2% more water is needed for flake graphite containing castable to reach an acceptable flow value over 150mm as compared with other carbon sources such as pitch-carbon, carbon black and amorphous graphite (Figure 5.6). With 6% water addition, PC, CB and AG containing castables reach flow value over 200mm. For directly using flake graphite into MgO-M_2S-C castables, water addition up to 8% is required to reach a flow value around 180mm. Therefore, to decrease water addition and obtain a dense structure of the castable, new way of adding flake graphite into castables must be considered.

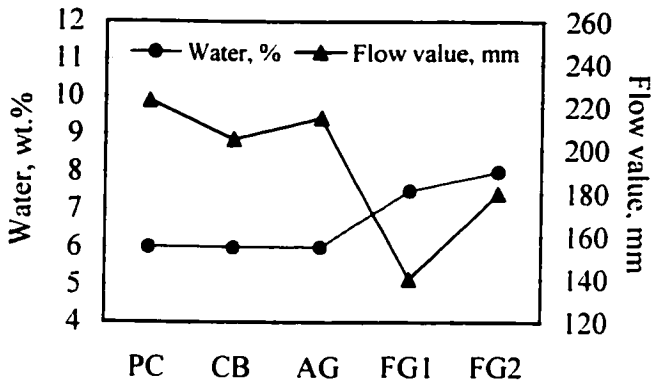

Figure 5.6 Influence of different carbon sources on flowability of MgO-M_2S-C castables

The advantages of using different modified flake graphite, EG, CG and GG pellets, have been documented in the previous chapter and are not presented here, see section 4.6.1. In the continuation of the work in the MgO-M_2S-C system, the combinations of packaging graphite pellets and fine carbon in the matrix of the castables were studied and evaluated, as seen in Figure 5.7. It shows that the flowability of the castables containing EG or CG pellets in combination with fine carbon CB demonstrates very good results over the castable containing FG, regarding to water addition and flow value.

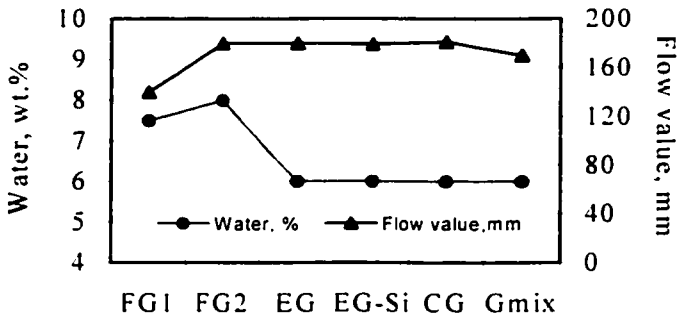

Figure 5.7 Influence of flake and modified graphites on flowability of MgO-M_2S-C (3) castables

As a result, fine carbon CB 1% can be used in combination with modified graphite in castables. Then, additional fine graphite was further studied in Gmix castable, where a combination of EG 4%, CG 1% and FGf 1% acts as carbon input. As a first measurement of incorporating fine graphite into castable, the influence of fine flake graphite on flowability and mechanical property was tested, as shown in Figure 5.8. To reach acceptable flow value of over 150mm, It represents that water addition increases from 6% to 8% when fine flake graphite was increased from 1% to 3% in MgO-M_2S-C castables. Obviously, the increase of water decreases the mechanical property of the castables, as shown in Figure 5.9. Therefore the type and the amount of fine flake graphite needs to be carefully controlled. The influence of fine carbon on the overall property of a castable will be discussed in the next section.

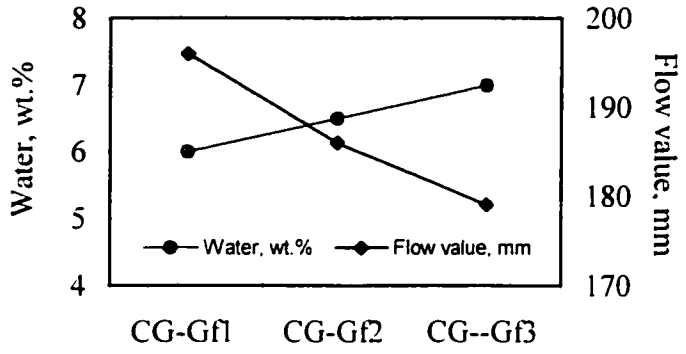

Figure 5.8 Influence of fine flake graphite on flowability of MgO-M_2S-C (3) castables

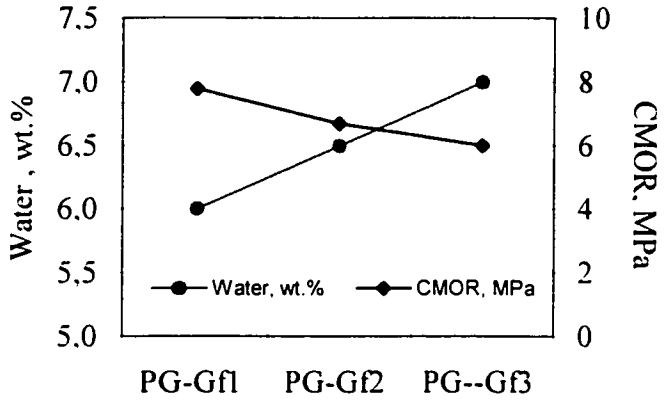

Figure 5.9 Influence of fine flake graphite on CMOR values

of MgO-M_2S-C (3) castables (Graphite 5%)

5.4.2 Modified Flake Graphite on Overall Properties

Table 5.7 lists the properties of MgO-M_2S-C (3) castables with carbon sources such as non-graphite carbons and graphitic materials. The castables contain over 87% magnesia, together with silica fume and antioxidant silicon for forsterite bond. Each sample contains 1% fine carbon (CB) with size of 5μm and the total carbon content of the castables is 6%. Magnesia fine (Mf) was used in each castable.

Table 5.7 Properties of MgO-M_2S-C (3) castables with different carbon sources

Carbon source	PC	CB	AG	FG1	FG2
Water, %	6	6	6	7.5	8
Flow value, mm	223	180	215	177	190
B.D., g/cm^3					
110°C × 24h	2.71	2.81	2.78	2.66	2.67
1100°C × 3h	2.68	2.77	2.76	2.65	2.62
1500°C × 3h	2.67	2.80	2.83	2.69	2.68
A.P., %					
110°C × 24h	11.15	9.60	11.70	12.69	13.27
1100°C × 3h	18.32	16.45	15.86	19.49	19.98
1500°C × 3h	19.09	15.93	14.66	19.33	19.80
CMOR, MPa					
110°C × 24h	9.88	12.36	10.54	9.51	8.41
1100°C × 3h	6.23	8.38	4.79	5.56	4.90
1500°C × 3h	5.19	11.13	5.90	6.71	6.75
PLC, %					
1100°C × 3h	-0.13	-0.08	-0.04	-0.28	-0.14
1500°C × 3h	0.04	0.09	0.33	-0.36	-0.31

As described earlier, the carbon source greatly influences flowability of carbon containing castables. Furthermore, it affects physical properties, mechanical properties and oxidation resistance of the castables. Table 5.7 indicates that the direct introduction of flake graphite results in a high water demand, low bulk density, high apparent porosity and low mechanical properties. Carbons with high volatile content, such as PC and AG containing castables, decrease CMOR of the castables at higher temperatures. CB containing castable demonstrates good overall properties in this group of carbon containing castables

The physical and the mechanical properties of MgO-M_2S-C castables with the addition of modified graphite (EG, EG-Si, CG, Gmix) are listed in Table 5.8 and Figure 5.10. Each sample contains 1% fine carbon CB with a total carbon content of 6%. Gmix is a combination of EG 4%, CG 1%, CB1% and FGf 1%. The results show that good properties of green body of carbon containing castables were obtained for all the samples in terms of flowability over 170mm and CMOR over 8MPa after drying at 110°C for 24 hours. Modified graphite represents a very positive advantage over straight addition of flake graphite concerning physical and mechanical properties. The properties of the castable containing carbon black (CB) and modified graphite EG, EG-Si and CG are superior to that of pitch-carbon, flake graphite and amorphous graphite containing castables, especially at higher temperature. The sample containing Gmix obtains good flowability at a water addition of 6% and good mechanical and physical properties after drying the green body. However, fine graphite (FGf) decreases bulk density and

mechanical properties after heat treatment at temperatures of 1000°C and 1500°C. This may be explained that the fine graphite, here with size of minus 5μm, plus 1% CB, too much fine carbon, prevents the sintering and the development of strength of the material.

Table 5.8 Properties of modified graphite-containing MgO-M_2S-C (3) castables

Carbon source	EG	EG-Si	CG1	CG2	Gmix
MgO	Mf	Mf	Mf	Mf+Mc	Mf
SiO_2, %	3	3	3	1	3
Water, %	6.0	6.0	6.0	5.3	6.0
Flow value, mm	179	176	182	170	170
B.D., g/cm^3					
110°C × 24h	2.73	2.72	2.74	2.80	2.70
1100°C × 3h	2.74	2.68	2.71		2.67
1500°C × 3h	2.73	2.71	2.74	2.77	2.68
A.P., %					
110°C × 24h	10.34	10.57	12.65	12.41	14.16
1100°C × 3h	17.17	17.47	16.03		19.03
1500°C × 3h	18.10	18.24	17.67	17.57	19.62
CMOR, MPa					
110°C × 24h	12.66	11.59	14.19	11.51	9.89
1100°C × 3h	7.20	7.16	10.01		4.34
1500°C × 3h	11.50	11.72	10.00	10.54	5.86
PLC, %					
1100°C × 3h	-0.1	-0.06	-0.19		-0.04
1500°C × 3h	-0.33	-0.11	0.04	0.02	-0.29

In addition, the proper use of magnesia fine and silica fume can reduce the water demand to 5.3% and improve the overall properties of MgO-M_2S-C castables.

Considering the possible high content of magnesia in the castable, good properties of MgO-M_2S-C castable (see sample CG2 in Table 5.8) was obtained with only 1% silica fume input, together with 2% metal silicon addition. The PLC of all castables were controlled within ± 0.5%.

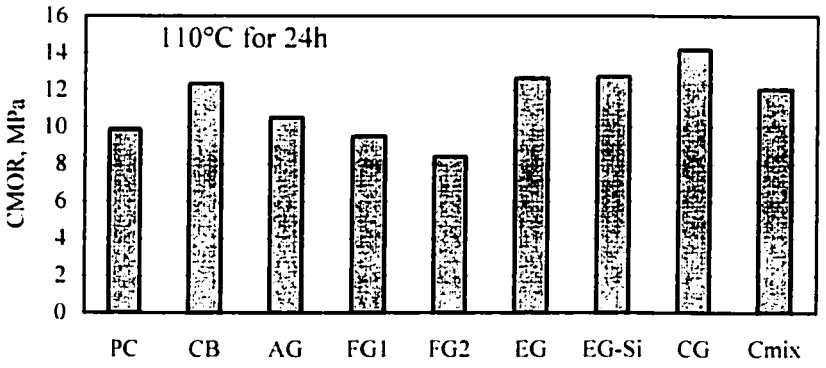

Figure 5.10a CMOR (110°C) vs. carbon sources in MgO-M_2S-C castables

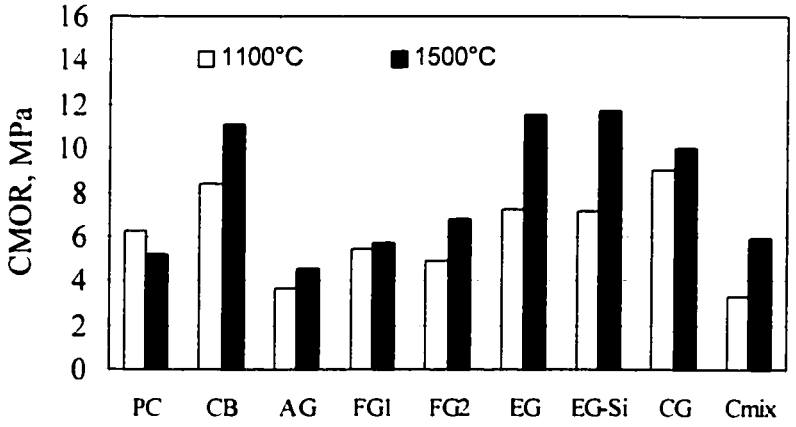

Figure 5.10b CMOR (1100/1500°C) vs. carbon sources in MgO-M_2S-C castables

5.4.3 Fracture Behaviour of Graphite Containing Castables

The influence of graphite materials on fracture behaviour of the castable was measured by the wedge-splitting test, see Appendix 5.1, where the work of fracture and thermal shock parameter were calculated. MgO-M_2S castables without carbon addition or with three different graphites with total carbon content of 6% were compared. The results are shown in Table 5.9 and Figure 5.11.

Table 5.9 Influence of graphite materials on fracture behaviour of MgO-M_2S-C castables (Wedge splitting test*)

Samples	WSP-1	WSP-2	WSP-3	WSP-4	WSP-5
Graphite	0	FG	AG	EG	EG
Si		2	2	2	2
SiO_2	1.5	2	2	2	2
C	0	6	6	6	6
Water, wt.%	5	8	6	6	6
Apparent porosity, %	13.8	19.7	14.8	18.2	12.3
CMOR, MPa	13.20	6.25	5.85	10.50	12.66
$\sigma_{max.}$ MPa	9.3	4.86	4.80	5.24	10.43
γ_{wof}, J/m^2	113	75	130	124	98
R"", mm	45	98	123	158	62

*Samples WSP 1-4 fired at 1500°C × 3h in coke, *WSP-5 after drying)

Table 5.9 and Figure 5.11 illustrate that introduction of flake graphite reduces the mechanical properties of the material. MgO-M_2S-C castable containing extruded graphite demonstrates better properties over AG and FG containing castables in terms of the modulus of rupture, the maximum rupture strength σ_{max}, the work of fracture and thermal shock parameter.

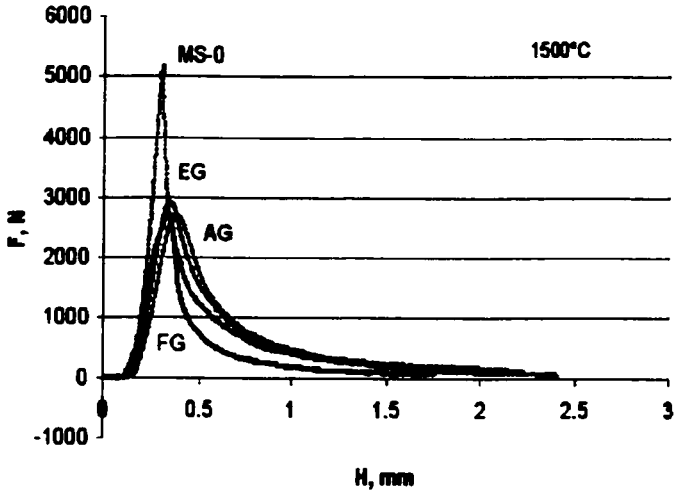

Figure 5.11 Wedge-splitting tests on MgO-M_2S-C castables

The work of fracture γ_{wof} of EG and AG containing castables are higher than that FG-containing castable. The modification of flake graphite by extrusion process helps to lower the water addition and improve flowability of EG-containing castable and therefore contribute to an improvement of mechanical properties of the castables. The R'''' values calculated based on the wedge-splitting test data represent the thermal shock resistance of the refractory material in a condition of stable crack propagation. It

can be seen that the EG-containing castable exhibits considerable higher R'''' (158) than FG and AG containing castables (98 and 123 respectively). All graphite containing castables have much higher thermal shock parameter R'''' as compared to castable without any graphite input (R''''= 45).

The sample with extruded graphite containing castable WSP-4 (1500°C) has higher mechanical property than AG and FG containing castables. Its fracture surface exhibits more extent of cleavage in magnesia aggregates.

5.4.4 Pore Size Distribution of Castables Using Modified Graphite

After heat treatment at 1400°C for 3 hours, the pore size distribution and the median pore diameter of MgO-M_2S-C castables containing different graphite materials were measured and illustrated in Figures 5.12-13.

FG containing castable has the highest cumulative intrusion volume as compared to AG, EG and CG containing castables since it needs high water addition which leads to high porosity over other carbon input. The pore size in a range of 0.1 to 10 μm was reduced by incorporating modified graphite pellets into castables as compared with the direct addition of flake graphite. AG-containing castable has lower water addition, lower porosity, lower cumulative intrusion compared to FG-containing castable, but the pores sizes are bigger than FG, EG and CG flake graphitic materials containing castables.

More pores of AG containing castable are concentrated in the range of 0.5 to 10μm compared to other graphitic materials.

To reach 80% cumulative intrusion, the pores are in the range of 10-1.5μm for AG-containing castable, 10-0.5μm for FG-containing castable, 10-0.3μm for EG-containing castable and 15-0.2μm for CG-containing castable, as shown in Figure 5.12.

The median pore diameters of MgO-M_2S-C castables with modified graphite EG and CG are smaller than that of castable with FG addition, as shown in Figure 5.13. The castable with AG has the highest median pore size compared with three other flake graphite containing castables (with FG, EG and CG).

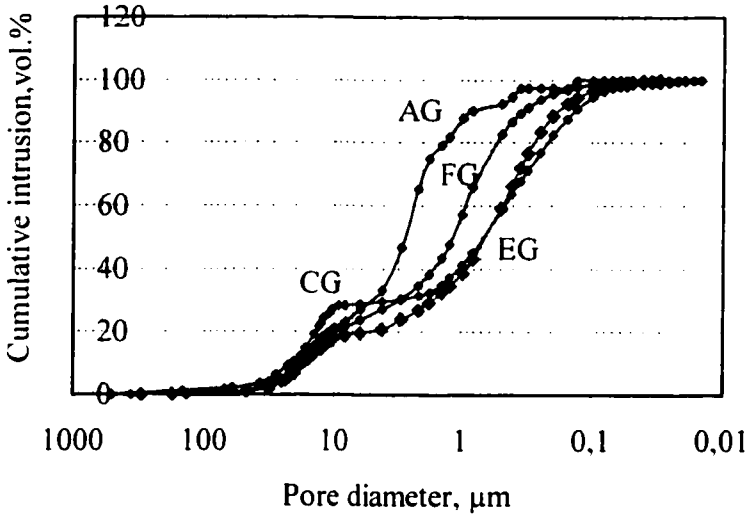

Figure 5.12 Pore size distribution of different graphites in MgO-M_2S-C (3) castables

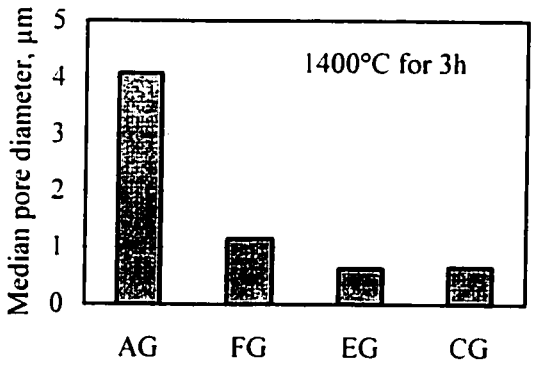

Figure 5.13 Median pore diameter vs. different graphites in MgO-M_2S-C (3) castables

Carbon source plays an important role in improving basic properties of carbon-containing castable. Modified graphite demonstrates good properties over directly use of flake graphite in terms of flowability, bulk density and apparent porosity, mechanical property, the work of fracture, thermal shock parameter and pore size.

5.5 OXIDATION RESISTANCE OF MgO-M_2S-C CASTABLES

5.5.1 Influence of Carbon Source on Oxidation Resistance

The influence of different carbon sources on oxidation resistance of MgO-M_2S-C castables is illustrated in Figure 5.14. Here, the oxidation index was calculated in which pitch-coke containing castable was taken as a reference. It indicates that the nature of a carbon has a direct influence on oxidation. Flake graphite containing castable results in higher water addition and higher porosity of the castable than other carbon source

containing castables, but still holds higher oxidation resistance than pitch-coke and carbon-black containing castables, and stands similar oxidation resistance as amorphous graphite containing castable. Therefore, the surface modification on flake graphite was expected to further improve the performance of flake graphite in castable since around 2% of water addition was reduced for modified flake graphite pellets containing castables. In fact, the modified graphite EG and CG containing castables demonstrate higher oxidation resistance than all other carbon sources as shown in Figure 5.14.

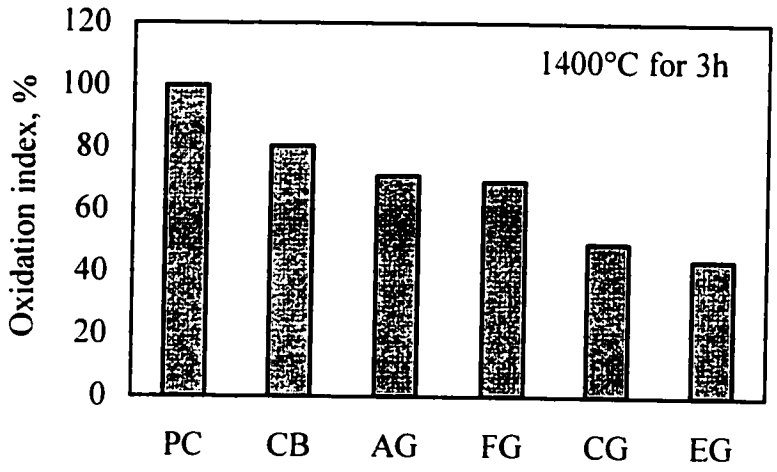

Figure 5.14 Oxidation of different carbon sources in MgO-M_2S-C (3) castables

(Oxidation Set-up B, sample 50×50×50 mm)

The increase of the oxidation resistance of the modified graphite containing castables benefits from the pellets not only being made of flake graphite but also offering better flowability of the castable with lower water addition and smaller size as compared to the case of directly using flake graphite. Coated graphite containing castable has demonstrated better flowability than that of extruded graphite pellets. However, its

oxidation resistance is slightly lower than that of extruded graphite containing castable at the same water addition because of coated graphite CG containing 30% pitch, which exhibits low oxidation resistance. Thus the nature of the carbon source and a dense texture of the castable itself are important factors to oxidation resistance of the castables.

5.5.2 Intruduction of Antioxidants into Extruded Graphite Pellets

Extruded graphite pellets have demonstrated better oxidation resistance than other carbon sources in MgO-M_2S-C castables. The further efforts were made to improve extruded graphite pellets themselves by incorporating antioxidants and oxides into the pellets.

The Oxidation resistance of extruded graphite pellets with different additive for forsterite bonded material system ($(EG\text{-}A.O.)_{MS}$) was evaluated by mass spectrometer on CO_2 gas evolution, as illustrated in Figure 5.15. There are two peaks in each oxidation curve. The first peak is due to the oxidation of the binder. With different additives and their combination, the relative intensity of CO_2 gas of extruded graphite pellets was reduced and the oxidation temperature was increased as compared to that of EG-0 pellets. With the addition of silicon carbide, higher oxidation temperatures and lower CO_2 gas relative intensity were obtained over other additives. The additional peak from EG-SiC represents the nature of SiC, which offers different carbon source. The results from EG-SOB and EG-SiB are very similar in terms of relative intensity of CO_2

gas and oxidation temperature. The improvement of oxidation resistance of extruded graphite pellets by incorporating antioxidants and oxides into the pellets benefits from the positive change of the microstructure of the pellets concerning the pore size and in-situ new compounds formation inside of the EG pellets.

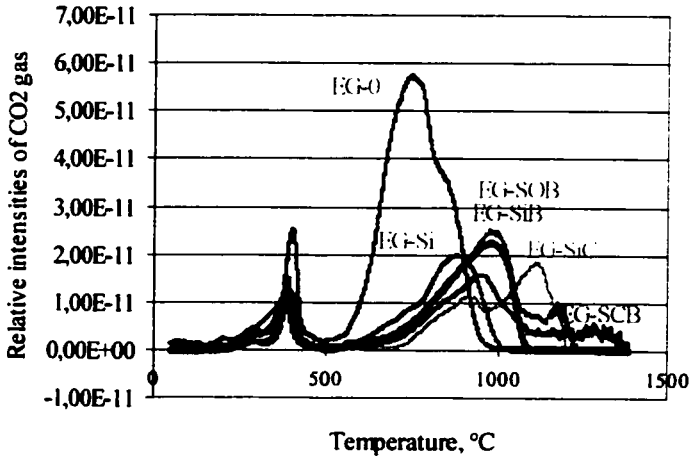

Figure 5.15 Oxidation behaviour of extruded graphite pellets $(EG\text{-}A.O.)_{MS}$ by evaluating relative intensity of CO_2 gas vs. temperature

5.5.3 Performance of $(EG\text{-}A.O.)_{MS}$ pellets in MgO-M_2S-C Castables

The oxidation resistance of upgraded extruded graphite pellets containing different antioxidants and/or oxides was tested in MgO-M_2S-C castables, as shown in Figure 5.16. EG-00 refers to no antioxidants in both the pellets and in the matrix. EG-0 and $(EG\text{-}A.O.)_{MS}$ containing castables contains 2% Si in the matrix. The oxidation resistance of

$(EG\text{-}A.O.)_{MS}$ containing castables were further improved as compared to EG-0 containing castable. Extruded graphite pellets with silicon addition exhibit the highest oxidation resistance at the given temperature. EG-SB and EG-SOB pellets have higher oxidation temperature but also a higher relative intensity of CO_2 gas evolution, higher median pore size than EG-Si, and here show lower oxidation resistance than that of EG-Si in related castable. Again, EG-SC has a higher oxidation temperature and not as efficient as EG-Si in improving oxidation resistance of its containing castable at the given temperature. EG-SC and EG-SCB containing castables illustrate lower oxidation resistance than castable containing EG-Si pellets. EG-SCB pellets have smaller median pore size than EG-SC pellets, and this contributes to a slightly higher oxidation resistance of its containing castable than EG-SC containing castable.

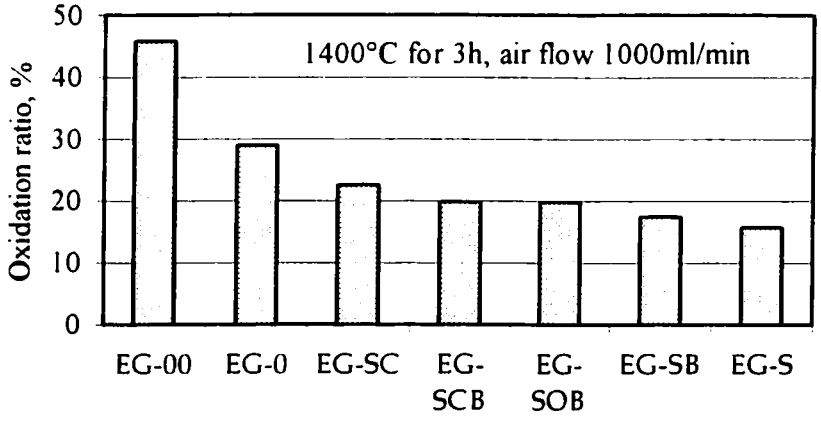

Figure 5.16 Oxidation of $(EG\text{-}A.O.)_{MS}$ pellets in $MgO\text{-}M_2S\text{-}C$ (3) castables

(Oxidation set-up D, sample 50×50×50 mm)

As a result, the distribution of antioxidant in a matrix is more efficient than that only in an extruded graphite pellets since the overall texture improvement of the material by putting antioxidant into the matrix is more functional than locally in extruded graphite pellets, see sample EG-00 and EG-0. The combinations of antioxidant in extruded pellets and in matrix give the best oxidation resistance of the castable.

5.5.4 Effects of Antioxidants in MgO-M_2S-C (4) Castables

Based on selected metallic additives and carbides, the influences of antioxidants on flowability and mechanical properties of green body were studied in MgO-M_2S-C castables, in which different antioxidants and their combination were chosen. Amorphous graphite was used in each castable. The carbon content is 6%. The results are shown in Table 5.10.

Table 5.10 shows that good casting properties and essential mechanical properties of the green body of MgO-M_2S-C (4) castables, with or without selected metals or carbide additives, were obtained. At a water addition of 6%, all castables containing different antioxidants reach flow value of over 175mm and CMOR over 7MPa after drying at 110°C for 24 hours.

The influences of Si, SiC and their combinations on the oxidation resistance of MgO-M_2S-C (4) castables were tested at 1200°C and 1400°C, as shown in Figure 5.17. This

reveals that the oxidation resistance was greatly improved with addition of Si, SiC or their combinations.

Table 5.10 Influence of antioxidants on properties of MgO-M_2S-C (4) castables (wt.%)

Code	S0	S2	S4	S6	SC2	SC4	SC6	S2SC2	S2SC2*	S2B
SiO_2	3	2	2	2	2	2	2	2	1	2
Carbon	6	6	6	6	6	6	6	6	6	6
Si	0	2	4	6				2	2	2
SiC					2	4	6	2	2	
B_4C										0.5
Water	6	6	6	6	6	6	6	6	6	6
Flow value, mm	188	183	184	179	194	202	181	192	191	185
CMOR, MPa	10.54	9.80	7.85	7.10	9.50	9.10	8.95	10.50	9.20	9.40

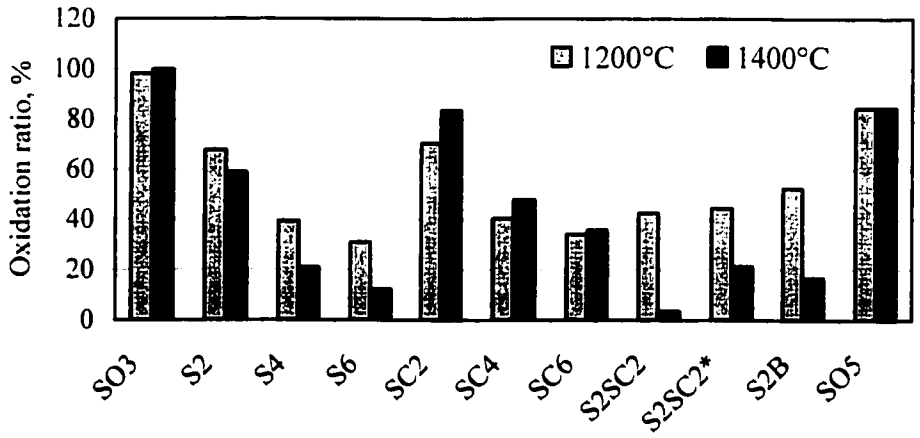

Figure 5.17 Influence of antioxidants on oxidation resistance of MgO-M_2S-C (4) castables (Unidirectional oxidation, Set-up B)

When addition of Si or SiC increases, the oxidation resistance increases. In the sample without the addition of antioxidants, oxidation increases with temperature. In contrast, samples with silicon additions, oxidation decreases with temperature since silicon exhibits good protection of carbon from oxidation at high temperature. Metallic Si is more effective than SiC on improving oxidation resistance at given temperatures. The combination of Si and SiC becomes more pronounced at high temperature. The combination of silicon and silicon carbide (sample S2SC2) offers higher oxidation resistance than that of S2 and SC2 at 1200°C. The oxidation resistance of S2SC2 is effectively enhanced as compared to samples S2, SC2, S4 and SC4 at 1400°C. Sample S2SC2 exhibits higher oxidation resistance than the combination of Si and B_4C (sample S2B). Oxide silica also affects oxidation resistance. Higher content of silica improves oxidation resistance, especially at higher temperature, see sample S2SC2 and S2SC2*, where silica content was 2% and 1% respectively. In the case of no antioxidant addition, oxidation resistance of castable with 5% silica fume is higher than that of castable with 3% silica fume.

The influence of antioxidant Si, SiC, and B_4C as well as the effect of their combination on mechanical property of the castable is presented in Figure 5.18. It reveals that mechanical property was increased with addition of silicon as well as its combination with silicon carbide or boron carbide.

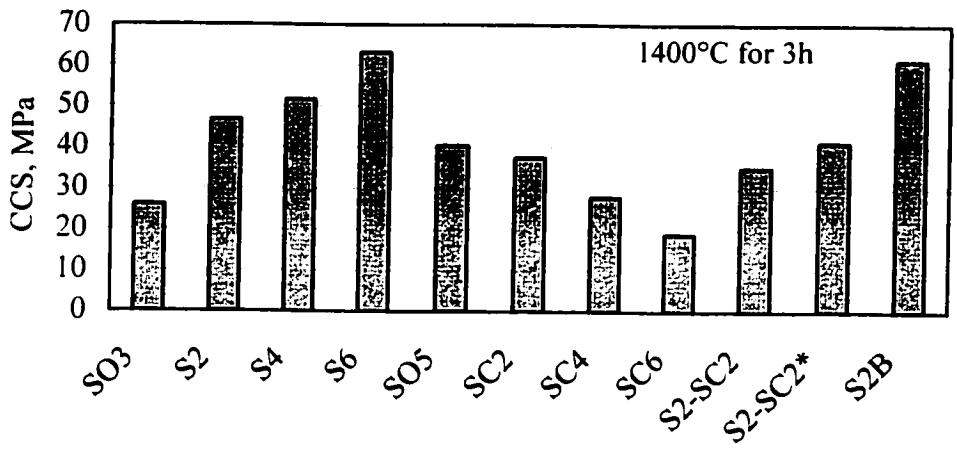

Figure 5.18 Improvement of antioxidants on mechanical property (CCS values) of MgO-M_2S-C (4) castables

Table 5.11 X-ray diffaction results

Code	S03	S2	S4	S6	SC2	SC4	SC6	S05
MgO	>>>	>>>	>>>	>>>	>>>	>>>	>>>	>>>
Mg_2SiO_4	*	****	*****	*****	**	*****	****	****
$MgSiO_3$	***	*			***	****	*****	*
SiC	*	***	****	****	***	*****	******	*
C	**	**	**	**	**	**	**	**

From X-ray diffraction results (Table 5.11), the intensity of in-situ formed forsterite increases with the addition of silicon. Silicon carbide was found in sample containing silicon. With silicon carbide alone, however, the mechanical property was not improved at a given temperature. X-ray diffraction results show that except in-situ formation of Mg_2SiO_4, new compound $MgSiO_3$ also exists in the sample with SiC addition at given temperature. Without antioxidants, higher silica-fume additions, higher amounts of

forsterite and less amount of $MgSiO_3$ form, therefore higher mechanical properties provides, as seen in samples SO3 and SO5 in Table 5.11.

CHAPTER 6 INTERPRETATION AND DISCUSSION OF THE RESULTS

The aims of this project were to study oxidation behaviour of carbon and graphite containing castables and the roles of carbon sources and antioxidants. The general objectives were:

(1) To improve flake graphite package in order to be able to insert such a valuable source of carbon in castables.

(2) To produce magnesia-based graphite containing castables having good flowability and promising properties.

(3) To select effective antioxidants with the proper combination and distribution, to further restrict oxidation of the graphite's packages at elevated temperatures.

(4) To uncover the roles of graphite and antioxidant additives in magnesia-based graphite containing castables and to identify the oxidation resistance's mechanism at high temperatures.

Two important factors regarding carbon containing castables are the nature of the carbon material and the role of the antioxidant. The challenges to be tackled are the difficulties of inserting graphite into castables, the limitation of using antioxidant in castables and the minimization of the porosity.

In this chapter the principle results presented in chapters 3 to 5 will be interpreted, along two themes: the role of carbon sources and the role of antioxidants.

6.1 ROLE OF CARBON SOURCES

The carbon source plays an important role in increasing the oxidation resistance and the overall properties of carbon-containing castables. In this thesis, pitch-coke, carbon black and amorphous graphite, were primarily studied for their reactivity with oxygen, as compare to flake graphite, as well as how their hydrophilic property influence the overall properties of the castables. Then, three agglomeration methods for flake graphite, by extruding, coating and granulating, were conducted to improve the wettability of flake graphite and reduce segregation during the mixing of graphite-containing castables. Furthermore, packaging the extruded graphite pellets by incorporating antioxidants and/or oxide fillers was studied to improve the oxidation resistance of the graphite pellets. At the final approach, a combination of modified graphite with fine carbon was achieved to improve the overall properties of the castables.

6.1.1. Flake Graphite Over Other Carbon Sources in Castables

Depending upon the properties being considered, such as water addition, flowability, physical and mechanical properties, pore size and oxidation resistance, each carbon source has its advantages and disadvantages. The experimental results show that non-

flake graphite carbon sources have granular particle shape and require around 2 to 2.5% less water than what is needed when flake graphite is used in castable, therefore provide better flowability, physical and mechanical properties to green body of the castables when compared to flake graphite. However, the mechanical properties of castables containing those carbon sources were strongly affected by the nature of the carbon after heat treatment at high temperature. Firstly, the volatilised phases in those carbons create large pores as illustrated in Figures 5.12 and 5.13 and reduce mechanical properties at high temperature, see Tables 5.7 and 5.8 in chapter 5. Secondly, the nature of the carbon, especially its crystallization, greatly influences the oxidation resistance, As shown in Figure 5.14 in chapter 5, amorphous graphite shows better oxidation resistance than pitch-coke or carbon black in its castable, even though carbon black has a higher content of carbon and high purity but without graphitic crystallization structure. It can be further explained if AG or CB containing castable is compared to flake graphite containing castable. Even if flake graphite containing castable requires higher water addition, it still presents a comparable oxidation resistance, which is beneficial to its high crystallization. Obviously, higher water addition by straight addition of flake graphite causes the degradation of the castable in terms of its physical and mechanical properties (Table 5.7). Therefore, incorporating flake graphite to utilize its inherent high oxidation resistance and trying to improve its hydrophilic behaviour in castables were expected to be greatly beneficial.

6.1.2. Improvements on Properties of Castables Using Modified Flake Graphite

To tackle the problems caused by straight addition of flake graphite into castables in terms of its hydrophobicity, high water addition, low density and mechanical property as well as oxidation resistance, applied countermeasures have demonstrated the effectiveness of surface modification of flake graphite through the following techniques:

1) To reduce the specific surface area by agglomerating graphite flakes together, either by extrusion (EG), coating (CG) or granulation (GG); 2) to optimize modified flake graphite pellets in terms of distribution, densification, new compounds formation, pore size distribution and oxidation resistance by adding antioxidant and oxide fillers into the pellets; 3) to perform hydrophilic treatment by using binder and wetting agent; 4) to improve the dispersion state of flake graphite in the castables thus maintain better bonding strength; and 5) to improve oxidation resistance of the modified flake graphite pellets by incorporating antioxidant into the pellets.

The modification of flake graphite by agglomeration practices either extruding, coating or granulating methods has brought out very positive results on flowability, physical and mechanical properties, pore size and oxidation resistance in both MgO-MA-C and MgO-M_2S-C material systems, as presented in chapters 4 and 5.

The hydrophilic property of the modified flake graphite has been effectively improved with different binders and production processes being used. The wetting angle of water on the surface of pressed sample of EG and CG are 49° and 48°, respectively, which were lower that of pressed sample of FG (76°). This contributes to 2 to 2.5% less water addition for modified graphite pellets to reach similar flowability for the magnesia-based castables tested. The efficiency of improving flowability of castables using EG, CG and GG is in the order of CG, EG and GG. The CG pellets perform the best in improving flowability since it has better wettability due to the hydrophilic treatment and spherical particle shape, which is beneficial to better flowability. In the case of EG, no hydrophilic treatment was performed on the pellets before being used into castables. As described in chapter 3, the hydrophilic treatment on EG pellets using a wetting agent effectively reduces wetting angle of a water drop on the surface of the pressed sample of EG pellets and improves the wettability of the EG pellets. This shows a direction to work for further improvement on wettability of the EG pellets through selecting the proper wetting agent.

The physical and mechanical properties of EG or CG containing castables were effectively improved as compared to FG containing castable. EG and CG had similar performance in both MgO-MA-C and MgO-M_2S-C castables. It benefits from reduced water addition and improved microstructure.

An important finding provides that EG and CG effectively reduce pore size of the castable as compared to FG and AG containing castables. The median pore diameters of using CG, EG, FG or AG in castable is 0.45, 0.5, 1.2 and 4.2μm, respectively (Figure 5.13). FG pellets results in highest cumulative intrusion volume because of high water demand, but smaller median size as compared to AG containing castable. AG leads to the biggest median pore diameter comparing with other graphitic materials. This may be explained that the volatilised phases in AG cause bigger pores within the material. CG has lower total cumulative intrusion than EG in castable since it has better hydrophilic property and more spherical particles and use less water. However, CG results in around 30% pores over 10μm, which is 10% higher than that of EG containing castable, see Figure 5.12. It may be from the 30% of pitch used in CG pellets.

For oxidation resistance, EG exhibits better results than CG since EG contains only flake graphite and CG contains flake graphite and pitch. In addition, even though CG leads to better flowability and smaller total cumulative intrusion volume, the median pore diameter of CG containing castables is closed to that of EG containing castables.

GG pellets did not perform as expected. It is less efficient in improving flowability, mechanical property and oxidation resistance of the castable as compared to EG and CG pellets.

As can be seen, the modified graphites are efficient in improving overall properties of the castables. The agglomeration technique leads to modified graphites having varied pellet size, shape and hydrophilic property, which have different contribution to its performance on flowability, pore size, physical and mechanical properties of the castables. Considering only flake graphite as carbon input, to improve oxidation resistance of the pellets, the optimization of extruded graphite pellets was further conducted by incorporating antioxidant packages into the pellets.

6.1.3. Characteristics of $(EG\text{-}A.O.)_{MA}$ and $(EG\text{-}A.O.)_{MS}$ Pellets

Incorporating antioxidant package and oxide fillers into extruded graphite pellets leads to very encouraging results. The optimized extruded graphite pellets demonstrate improved distribution of flake graphite, densification, pore size distribution and oxidation resistance, and in-situ new compounds formation within the system. These extruded graphite pellets (EG-A.O.) exhibit enhanced oxidation resistance. Their performances in castables are more pronounced on oxidation resistance rather than on physical and mechanical properties. Through further optimization of the pellets, $(EG\text{-}A.O.)_{MA}$ and $(EG\text{-}A.O.)_{MS}$ pellets, it is not only possible but also efficient to produce good castables, in terms of flowability, physical and mechanical properties, pore size and oxidation resistance.

6.1.4 Combination of Different Carbon Source in Castables

As discussed above, each carbon source has its own characteristics. It may have good hydrophilic property and spherical particles, but low purity, less graphitic structure and low oxidation resistance, such as pitch-coke or amorphous graphite. In contrast, when it has a good graphite structure and shows high resistance to oxidation, it is poorly wetted and distributed in a castable.

Considering the distribution of carbon and properties of the castables, EG in combination with coated graphite pellets in castables exhibits a higher oxidation resistance than FG. A combination of modified graphite EG or GG with 1% fine carbon CB, with a size less than 5μm, exhibits good overall properties concerning flowability, physical and mechanical properties and oxidation resistance. However, using additional flake graphite fine (1% FGf, <5μm) in Gmix castable, which contains 4%EG, 1%CG, 1%CB and 1% FGf, decreases the bulk density and CMOR after heat treatment at 1000°C and 1500°C. Additional flake graphite fine with size less than 5μm may prevent the sintering and the development of the strength.

Since both oxidation resistance and flowability are important factors in graphite containing castables, the combination of EG (3-5%) with CG (1-2%) as well as fine carbon CB (1%), is the best compromise.

6.2 ROLE OF ANTIOXIDANTS

Antioxidants were added either in the pellets or in the matrix of castables or of course in both EG pellets and the matrix. To interpret the results obtained, some thermodynamic calculations were carried out using FACT system [109]. Different systems have been considered, such as MgO-C, MgO-C-Al-N-O and MgO-C-Si-N-O systems.

Many reactions may be identified when MgO-C-Al refractories are being heated in air (oxygen plus nitrogen). In Figure 6.1 possible reactions are shown. They are influenced by the prevailing conditions, in terms of partial pressure and temperature, as well as texture (porosity, distribution of phases) of the refractories [16,21,56-61].

The equilibrium calculations on the M-C-Al-O system shows that the main stable phases, at 1600°C, are MgO and $MgAl_2O_4$, with P_{O2} varying from 0.2atm to 10^{-16}atm and P_{CO}=1atm, here neglecting the effect of P_{N2}.

In the M-C-Al-O system, our experimental results show that Al_4C_3, Al_2O_3, and $MgAl_2O_4$ (melting point 2135 °C) have been found in samples depending upon temperatures. Al_4C_3 and Al_2O_3 were found in the sample after firing at 1000°C and disappeared after firing at 1400°C. In-situ spinel was confirmed in samples (EG-A.O.)$_{MA}$/matrix fired at 1400°C for 3 hours (chapter 3) and matrix samples (MCA1/A2, MCA1B1) fired at 1000°C, 1200°C and 1400°C for 3 hours (chapter 4).

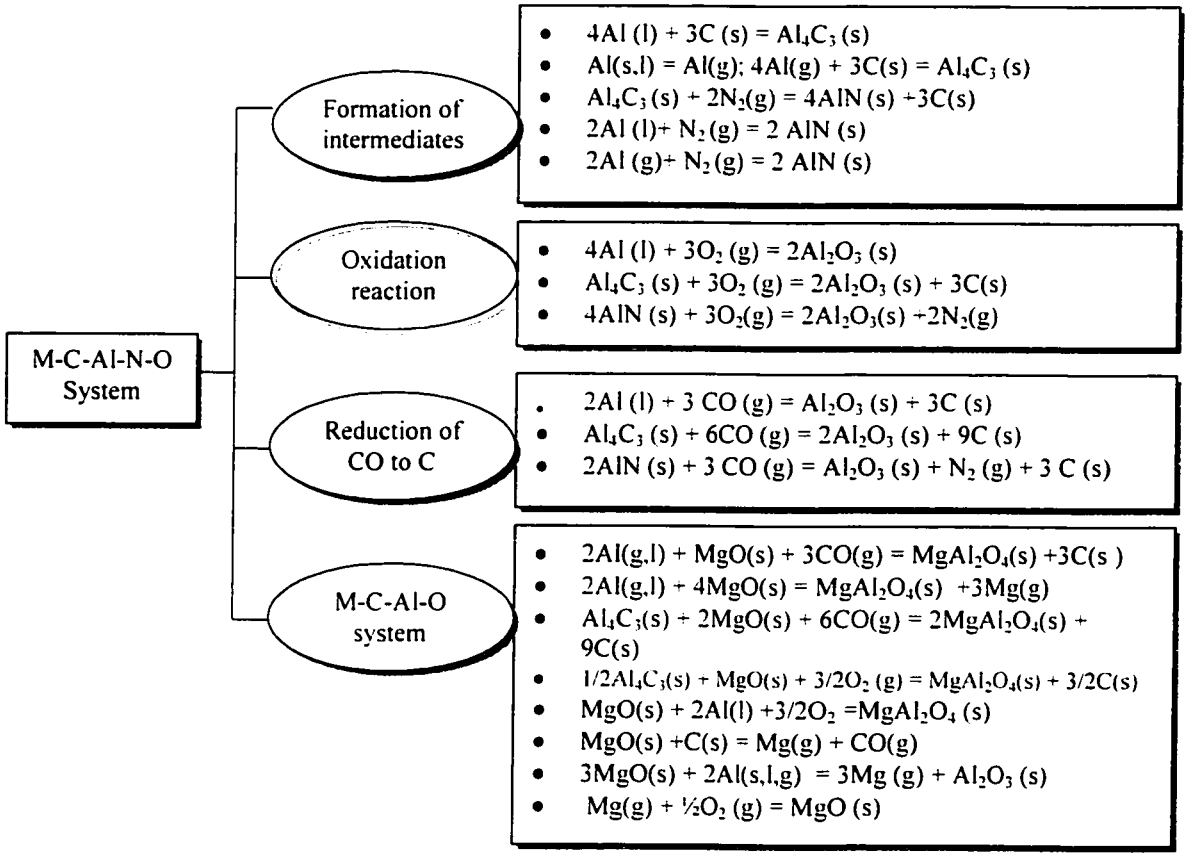

Figure 6.1 Possible courses of reactions in M-C-Al-N-O system [16, 21, 56-61]

From equilibrium calculations for the M-C-A-B-O system, it can be deduced that simultaneous additions of Al+B_4C lead to the formation of $MgAl_2O_4$ and $Mg_3B_2O_6$, when P_{O2} =0.2 to 10^{-16} atm, P_{CO} = 1atm, without considering N_2 influence. Compound $Mg_3B_2O_6$ has a low melting point and could block pores, acts as mineralizer to promote MA spinel formation, prevent inward oxygen diffusion and improve oxidation resistance of carbon-containing refractories. This is illustrated in sample MCA1B1, where a very

thin protected layer is found on the top of the oxidation surface and a dense spinel layer is formed close to the oxidation zone.

In the MgO-C-Si refractories, the possible reactions in the system are listed in Figure 6.2 [59-63]. The equilibrium calculations on the M-C-Si-O system in air, at T>1200°C, shows that SiC and Mg_2SiO_4 (melting point 1890 °C) are prevailing. In this thesis, this was confirmed in cylindrical samples (EG-A.O.)$_{MS}$/matrix (chapter 3) and in MgO-M_2S-C castable samples with antioxidant Si and SiC (chapter 5).

The mechanism of protecting carbon from oxidation with Al addition may be explained as follows. The reaction products, like Al_4C_3, AlN, Al_2O_3 and $MgAl_2O_4$, lead to a volume expansion (Figure 4.22) and reduce pore size (Figure 4.24), which enhance the microstructure and prohibit the inward diffusion of oxygen. In addition, many reactions leading to the reduction of CO to C and decreases carbon loss (section 6.2.4). Consequentially, AlN, Al_4C_3 crystals and high melting spinel formed in the refractories contribute to the development of the strength. Similarly in the case of Si addition, new compounds, SiC and Mg_2SiO_4, have high melting points, lead to volume change and reduce pore size. This contributes to the same way as Al addition to higher mechanical property and oxidation resistance. In addition, a cloud of gaseous phases may diffuse toward the hot face and prevent oxygen inward diffusion and therefore prevent the oxidation of carbon (section 6.2.1).

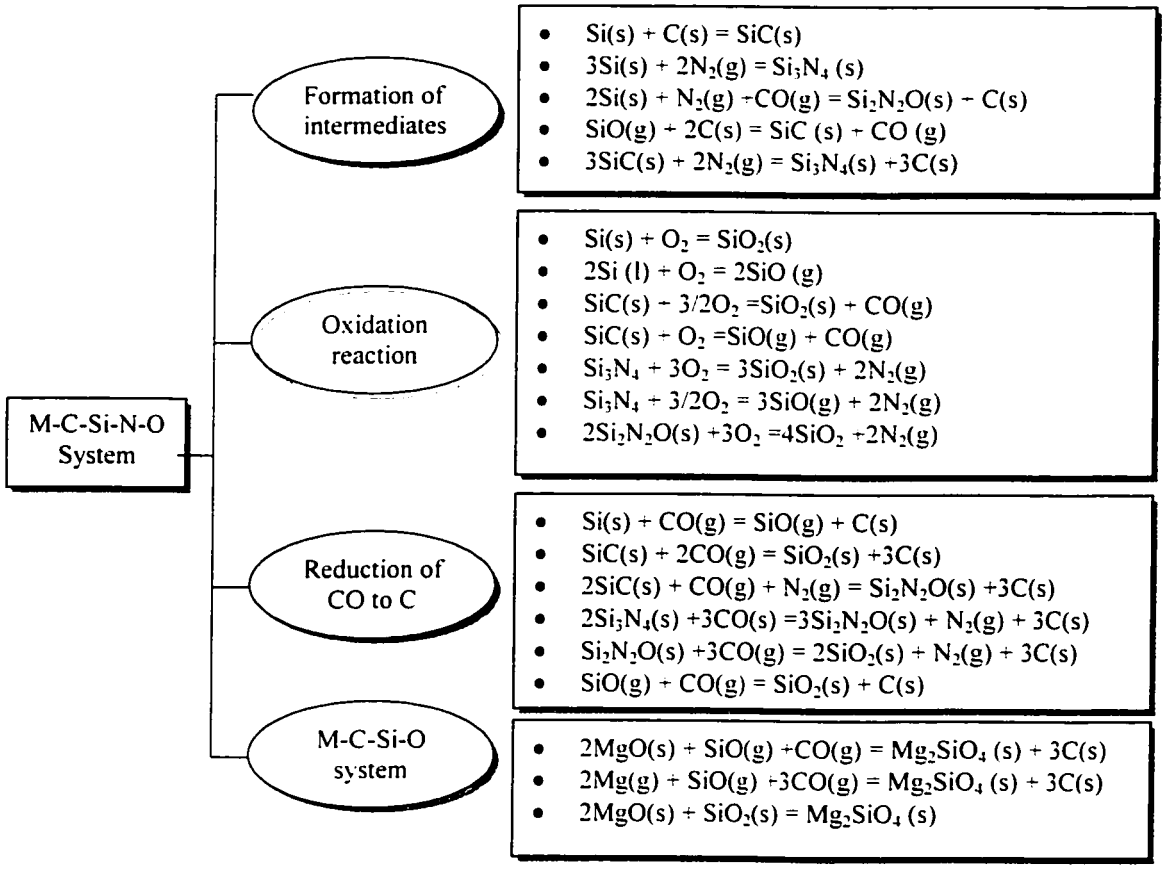

Figure 6.2 Feasible reactions in M-C-Si-O-N system [59-63]

6.2.1 Mg (g) Vapor and Gaseous Phases by Antioxidants

The influence of antioxidants on gaseous phases formation at different temperatures are calculated and illustrated in Figure 6.3 for M-C-Al-CO system and Figure 6.4 for M-C-Si-CO system.

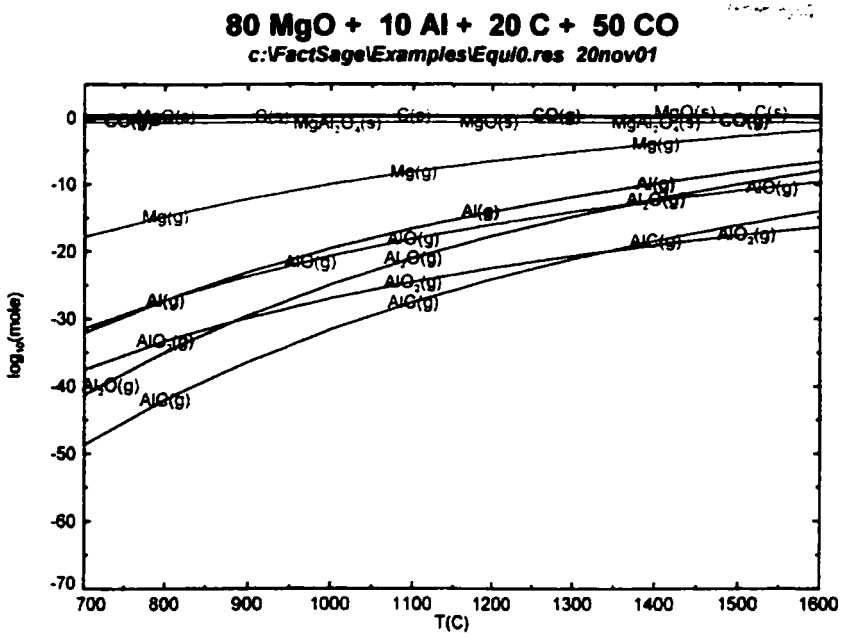

Figure 6.3 Influence of antioxidant Al vs. temperature on gaseous phases formation in M-C-Al-CO system (by FACT)

In the M-C-Al-CO system, the stable phases are MgO, spinel and carbon. Magnesia vapor is predominant over other gaseous phases, such as Al (g), AlO (g), Al_2O (g) and et al. In the M-C-Si-CO system, magnesia vapor and SiO(g) are the two dominant gaseous phases. Therefore, magnesia vapor is the dominant phase in both M-C-Al-CO and M-C-Si-CO systems.

Our experimental results illustrate that the reactions involve the participation of Mg (g) phase between the EG graphite pellets and the surrounding magnesia-based matrix, as

shown in extruded graphite pellets EG-A, EG-AB, EG-AOB, EG-SOB in Figures 3.10-12, where spinel was formed within the pellets which contains no magnesia. In cylindrical samples MCA1 and MCA1B1 in Figures 4.19-21, it shows that well developed spinel formation distributed in the place close to the hot face.

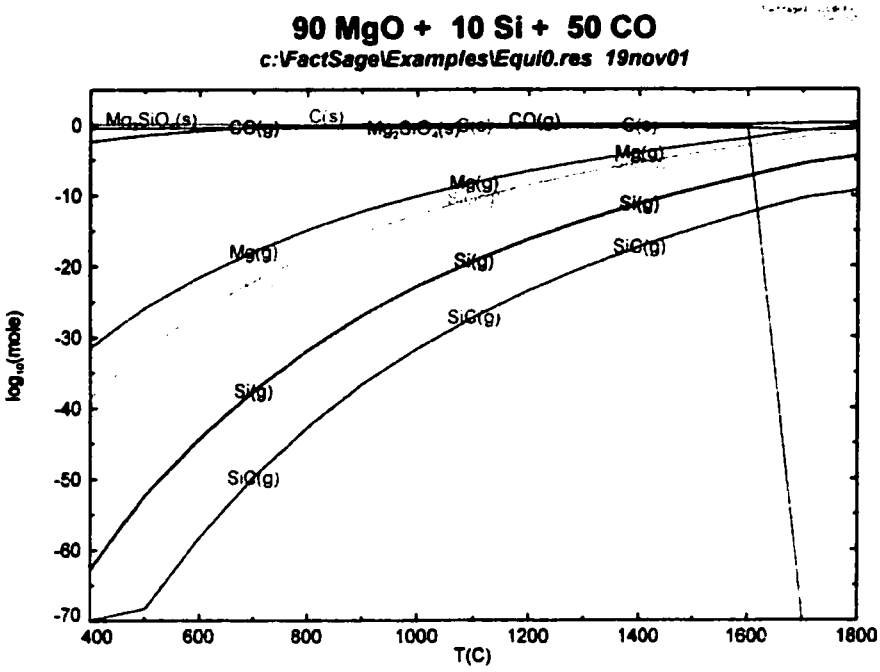

Figure 6.4 Influence of antioxidant Si vs. temperature on gaseous phases formation in M-C-Si-CO system (by FACT)

Figure 6.5 may show the situation inside a MgO-C material and the course of the reactions, involving reactive gaseous products such as magnesium vapor, SiO and AlO, and so on, depending on the total pressure and partial pressures in the system. These reactive gaseous phases can diffuse towards the hot face and reduce the partial pressure of the oxygen and therefore decrease the oxidation of the carbon containing materials.

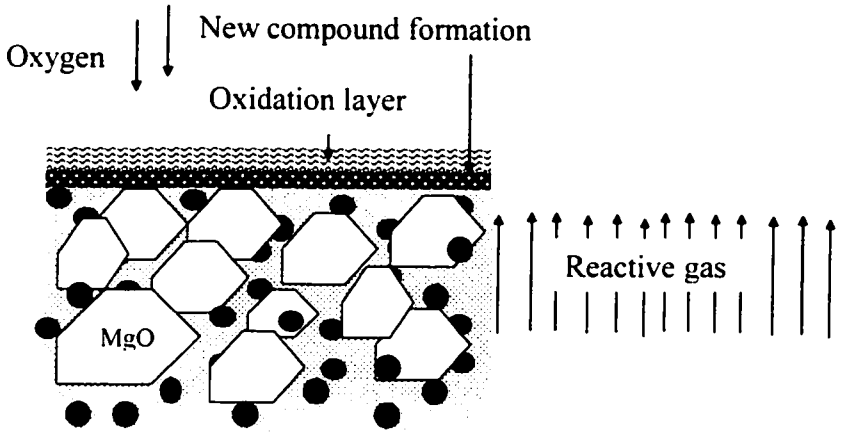

Figure 6.5 Possible courses of reactions within a MgO-C material

Other visible observations to illustrate magnesium vapour transport from our experiments have been the detection of MgO whiskers, which were found on top of samples or within samples. Such magnesia whiskers are shown in Figures 6.6 and 6.7. The SEM/EDS observations show the crystal structure of the MgO whiskers and confirm that the content of magnesia reaches up to 99.7% of MgO.

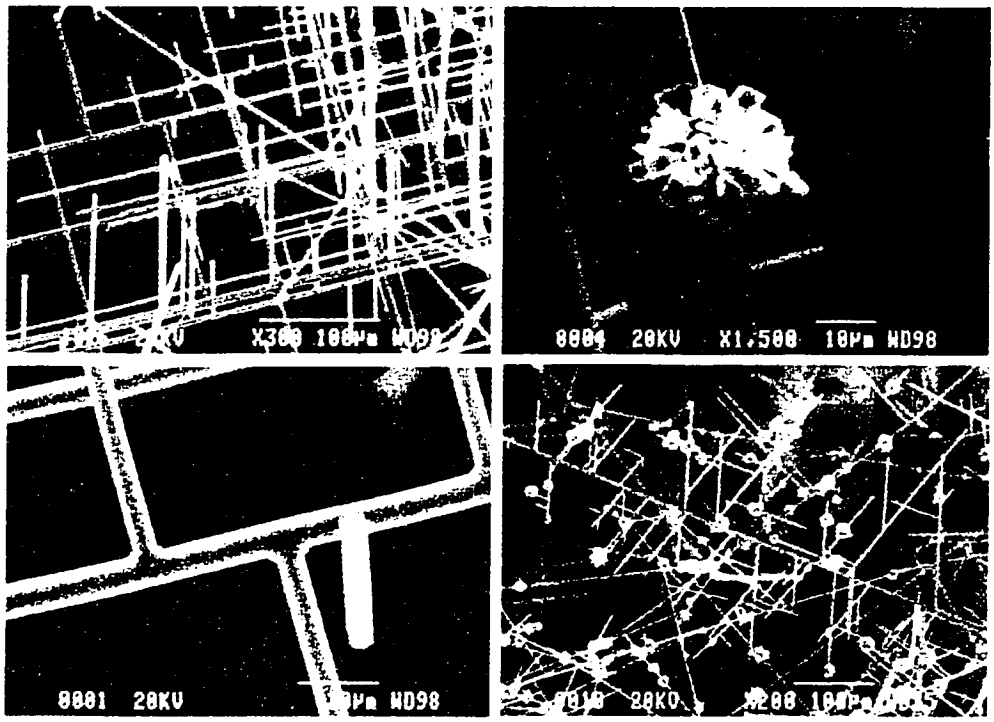

Figure 6.6 Magnesia whiskers formed during the oxidation test

from MgO-M_2S-C castable, fired at 1400°C×3h with air flow 1000ml/min

Mg (g) comes from the reduction of MgO by carbon or antioxidants, as reactions listed in Figures 6.1 and 6.2. In fact, the combination of graphite and antioxidants together in the matrix is more effective than only graphite in stimulating Mg (g) vapor formation. More spinel formations are observed in sample EG-AB/MABC than in sample EG-AB/MC, see Figures 3.10 and 3.11, where sample EG-AB/MC contained no antioxidant in matrix, and sample EG-AB/MABC contained antioxidant aluminium and boron carbide in matrix.

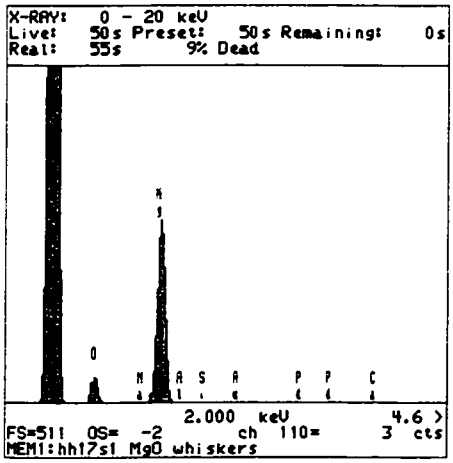

MgO 99.71%

Figure 6.7 Magnesia whiskers confirmed by SEM/EDS

MgO dense layer formation is another observation related to the Mg (g) phase transport. When magnesium vapor diffuses towards to the hot face, it oxidizes there and form a MgO dense layer depending on the local conditions, which are very complex in terms of densification, temperature, partial pressure, and presence of impurities. In fact, there are many oxygen sources at the hot face (T=1550-1600°C) to oxidize magnesium vapor due to the presence of slag ($P_{O2}=10^{-4}$), steel ($P_{O2}=10^{-6}$atm) and oxidizing atmosphere ($P_{O2}=0.2$atm). The dense layer becomes a major shielding factor to improve oxidation resistance as well as corrosion resistance in practical conditions.

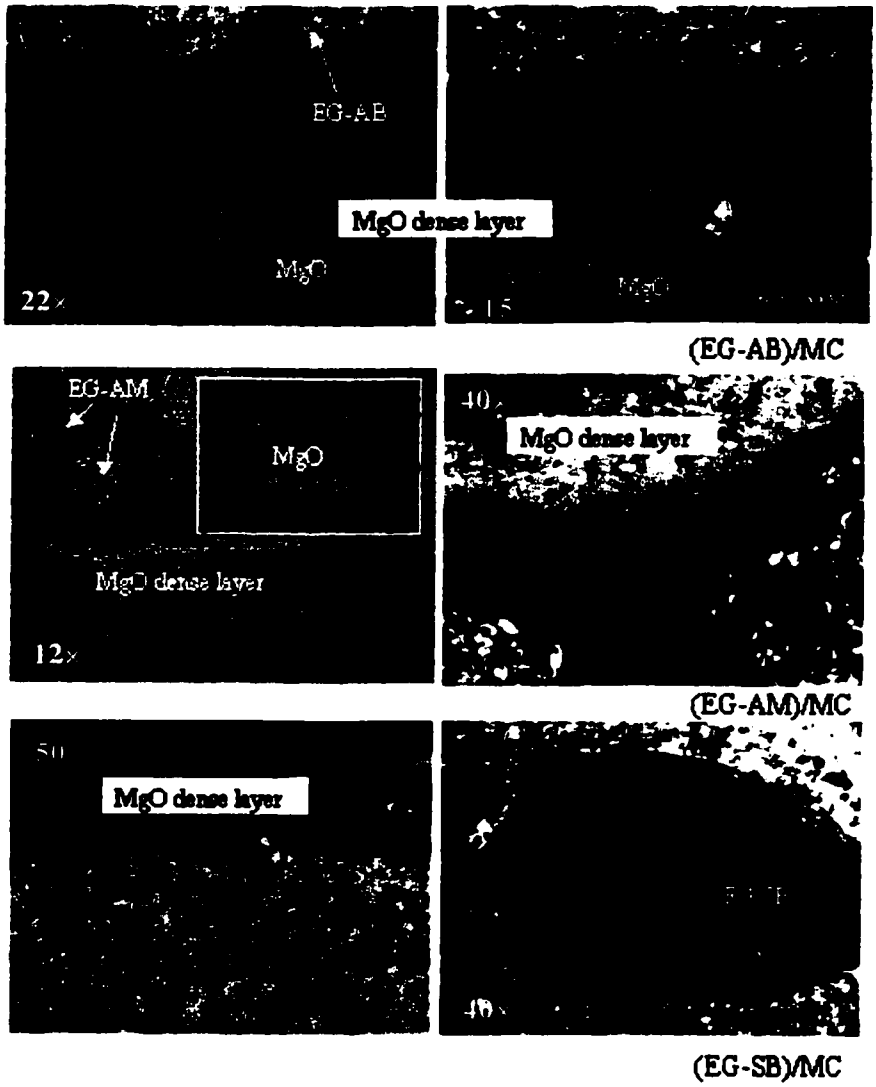

Figure 6.8 MgO dense layer formation in cylindrical samples of

EG-AB/MC, EG-AM/MC and EG-SB/MC

(after unidirectional oxidation at 1400°C for 3 hours)

In this work, MgO dense layer formations were found in cylindrical samples containing EG-AB, EG-AM and EG-SB pellets within the matrix containing magnesia and fine

carbon, as shown in Figure 6.8. From these three groups, the dense layer with EG-AM is the most effective one, where metallic alloy AlMg is more reactive than metallic powders Al and Si.

6.2.2 Pore Size Evolution

Oxidation of carbon involves the reaction of solid carbon with gaseous oxygen. To improve oxidation resistance, higher resistance to oxygen inward diffusion is expected to be beneficial. Permeability and pore size measurements are then important parameters to control. In this thesis work, our results indicate that antioxidants have a strong effect to reduce the pore size of the material. As shown in chapters 3, 4, 5, the effect of antioxidants on pore size distribution was studied in extruded graphite pellets (EG-A.O.)$_{MA}$ and (EG-A.O.)$_{MS}$ as well as in magnesia-based matrixes through the measurement of pore size by the mercury intrusion method.

From Figures 3.5a,b, c, and Figures 3.6a,b, c, it can be observed that the median pore size of the pellets changes from 8.75μm for EG-0 to 2.26-1.13μm for (EG-A.O.)$_{MA}$ and 4.93 to 0.50μm for (EG-A.O.)$_{MS}$. Comparing the pore size distribution with 80% of cumulative volume intrusion, sample EG-0 has pores distributed in the ranges of 20 to 4μm, samples (EG-A.O.)$_{MA}$ in the ranges of 20 to 0.2μm and samples (EG-A.O.)$_{MS}$ in the ranges of 20 to 0.50μm. For pore sizes over 4μm, EG-0 reaches 80% of cumulative

intrusion, $(EG\text{-}A.O.)_{MA}$ pellets have less than 20% of cumulative intrusion and $(EG\text{-}A.O.)_{MS}$ pellets have less than 50 % of cumulative intrusion.

Incorporating antioxidants and oxides into the pellets effectively reduces the pore sizes of the pellets. The pore sizes are shifted to the smaller pore range. This positive change of the structure contribute to a higher resistance to oxygen inward diffusion and therefore higher oxidation resistance, see Figures 4.17 and 5.15.

In pressed samples of the matrix containing MgO, graphite and antioxidant, as shown in Figure 4.24, the pore sizes are distributed in the range of 7-0.03μm for MC0 and 1-0.02μm for the samples with antioxidants. To reach the 80% cumulative intrusion value, pore sizes are in a range of 7-0.5μm for MC0 and 2-0.07μm for the samples with antioxidants (Figure 4.24b). The median pore size has decreased from 1.58 μm for sample without antioxidant (MC0) to 0.34 μm (MCA1), 0.29 μm (MCA2) and 0.27 μm (MCA1B1), respectively, in Figure 4.24c. The results illustrate that antioxidants effectively reduce the pore size of the materials. The formation of big open pores is prevented and the oxidation of carbon-containing materials is inhibited by incorporating antioxidants, see Figures 4.17-21.

The bulk density has increased and the apparent porosity has decreased for all $(EG\text{-}A.O.)_{MA}$ pellets as compared to EG-0 pelelts. In $(EG\text{-}A.O.)_{MS}$ pellets, not all upgraded pellets get effectively improved on bulk density and apparent porosity. Some data are

very close to that of EG-0, but the pore sizes of all optimized extruded graphite pellets, both $(EG\text{-}A.O.)_{MA}$ and $(EG\text{-}A.O.)_{MS}$, have indeed greatly decreased. Hence the pore sizes seem more important regarding oxidation resistance.

The bulk density may be decreased and the apparent porosity may be increased by adding antioxidant into the matrix if the in-situ formation of spinel causes a volume large expansion. However, an interesting finding is that the mechanical property and the oxidation resistance are effectively improved by incorporating antioxidants into the material at all temperatures (section 4.5). Understandably, this contributes to the positive changes on microstructure with decreased pore size and formed new compounds, which provide higher resistance to oxygen inward diffusion and higher mechanical properties.

6.2.3 Distribution and Combination of Antioxidants

The optimization of antioxidants in magnesia-based carbon containing castables has been conducted, by selecting the type, the addition, the combination and the distribution of the antioxidants in two different material systems. Antioxidants, such as Al, Al-Mg, Si, SiC and B_4C, behave differently in spinel-bonded MgO-MA-C materials and forsterite-bonded MgO-M_2S-C materials. The distribution of the antioxidants, both locally inside the extruded graphite pellets and overall inside the basic carbon-containing material system, provides different approaches in improving oxidation resistance.

6.2.3.1 Antioxidants in Spinel-bonded Material System

The effect of antioxidants on improving oxidation resistance was firstly studied in (EG-A.O.)$_{MA}$ pellets, where the single antioxidant Al, AlMg, B_4C and the combination (AB) as well as the combinations with refractory oxide MgO or Al_2O_3 (MAB, MAOBC, AOB) were used in such EG-A.O. pellets. Then, antioxidants were incorporated into the magnesia-based matrix, where metallic aluminium and its combination with boron carbide were considered. In MgO-MA-C castables, coated metallic aluminium as well as its combination with boron carbide or silicon was investigated.

The in-situ spinel formation occurs under proper conditions. For spinel formation, the magnesia sources are the magnesia fines and the magnesia vapor resulting from the reduction of MgO by carbon and antioxidants. Alumina sources come from either the alumina fine or the antioxidants Al and AM. The antioxidants not only act as additives to protect carbon from oxidation but also act as phase modifier to promote new compound formation, fill in pores and reduce pore size. In this work, boron carbide was used as a mineralizer to stimulate spinel formation in MgO-C-Al–O system, and to form magnesia borate liquid to block pores. Based on the concept of a denser structure and small pores of the materials, some oxide fillers, such as magnesia, alumina and silica fume, were used to form new compounds and the reduce pore size of the pellets, and thus act as "antioxidant" to protect carbon from oxidation.

Incorporating antioxidant packages into EG pellets effectively improves the oxidation resistance of $(EG\text{-}A.O.)_{MA}$ pellets and upgrades the quality of the pellets. The packages can be a single antioxidant and their combination. The total addition of antioxidant package is 5-20%, which exhibits good results. The EG-AB pellets contain a combination of antioxidant aluminium with boron carbide and exhibit the highest oxidation resistance regarding its CO_2 gas intensity, oxidation starting temperature and median pore size.

Magnesia vapor is a dominant gaseous phase in MgO-C-Antioxidant system. Even without magnesia fines as a constituent in the pellets, spinel can form easily and be homogeneously distributed in the pellets due to Mg(g) formation. This contributes to closed pores, reduced pore sizes and therefore increased oxidation resistance. The addition of magnesia inside pellets may not be necessary in terms of quantity of production since magnesia replaces flake graphite and more EG pellets are used to reach same carbon content. Fine carbon causes higher oxidation of the pellets and should not be considered as an addition into the pellets.

Aluminium is very effective in protecting carbon from oxidation and increasing the mechanical property of the material. Antioxidant not only has a higher affinity for oxygen than carbon, but also efficiently reduces pore size and promotes new compounds

formation, such as Al_4C_3, Al_2O_3 and MA spinel, as well as Mg (g) and possibly Al_xO_y gaseous phases.

Each antioxidant works most effectively at different temperatures. The combination of antioxidant demonstrates good oxidation resistance in a wider temperature range. The further study of aluminium or its combination with boron carbide on oxidation resistance of the matrix of the castables reveals that the oxidation resistance is improved with an increased amount of metallic aluminium. The combination of aluminium with boron carbide exhibits the best oxidation resistance because of reduced pore sizes, magnesia borate liquid formation and the dense spinel layer formation, which contributes to a higher resistance to inward oxygen diffusion. Boron carbide alone is not as efficient as when combined with aluminium. Since boron carbide's special effect on liquid formation, its addition is minimized to 0.5% in castables. A good oxidation resistance is achievable with a combination of 2% aluminium and 0.5% boron carbide or 2 % aluminium with 1% silicon in MgO-MA-C castables.

The reaction of aluminium in magnesia-based castables is very strong and cannot be directly used in castable dues to its violent reaction with water. To tackle this problem, for a limited aluminium amount, it is possible to incorporate it into extruded graphite pellets. This protects graphite from oxidation locally. To protect graphite and carbon from oxidation overall in castables, coated aluminium has to be used in the matrix of the castables. In this work, pitch-coated aluminium powders with particle sizes less than

1mm was proved to be effective to prevent metallic aluminium powder from violent reaction in varied magnesia based mixes. The good oxidation resistance was obtained with the addition of 2% coated aluminium in MgO-MA-C castable. With higher additions up to 4% of coated aluminium powder, the oxidation resistance was decreased. As presented here, aluminium faces more challenges when used in castables rather than in bricks.

The results show that oxide Al_2O_3 might replace Al to increase oxidation resistance because of its effect on promoting spinel formation homogeneously within the graphite pellets and on reducing the pore size of the pellets. In fact, the median pore size, CO_2 gas intensity and oxidation starting temperature of EG-AOB pellets are slightly higher than EG-AB pellets.

6.2.3.2 Antioxidants in Forsterite-bonded Material System

In forsterite-bonded magnesia-based material system, the in-situ forsterite formation occurs under given condition. For forsterite formation, the magnesia sources are magnesia fines and the magnesia vapor resulting from the reduction of MgO by carbon and antioxidant. The silica sources come from either the silica fume or the antioxidants Si and SiC. The study on influences of Si, SiC and their combination on oxidation resistance and mechanical property of the MgO-M_2S-C castables reveal that oxidation resistance was greatly improved with the addition of Si, SiC and a combination of the

both. When the addition of Si or SiC increases from 2% to 6%, the oxidation resistance increases. The metallic silicon is more effective than silicon carbide on increasing oxidation resistance and mechanical property at given temperatures. The combination of Si and SiC becomes more pronounced on improving oxidation resistance at high temperature. It was found that the mechanical property is not directly corresponding to the amount of forsterite formation. Different magnesia silicates, $MgSiO_4$ or $MgSiO_3$, formed from different additives of antioxidants, such as silicon and/or silicon carbide, affect the mechanical properties of the castables, as shown in Figure 5.18 and Table 5.11.

The distribution of antioxidant plays an important role in increasing oxidation resistance. For flake graphite containing castables, the distribution of antioxidants in both extruded graphite pellets and castable matrix are efficient in improving oxidation resistance. To protect graphite from oxidation locally within the pellets contributes to more choices of higher quality of graphitic material for castables. The distribution of antioxidants in the matrix is more effective than in extruded graphite pellets since a dense protected layer can be formed in the area closed to the oxidation zone of the castables. The combination of antioxidant in both extruded pellets and in matrix gives the best oxidation resistance.

Antioxidants efficiently protect carbon from oxidation. It not only has higher affinity for oxygen than carbon, but also leads to microstructural changes, pore size distribution and in-situ new compound formations.

Acting as phase modifier in magnesia-based systems, antioxidants produce intermediate products, promote new compound formation, effectively reduce pore size, and therefore oxidation resistance and mechanical property can be essentially improved. Antioxidant additives also influence physical property, such as bulk density and apparent porosity, volume expansion or shrinkage positively or negatively, depending on its type and addition. The overall considerations need to be given to balance the properties of the materials.

6.2.4 Complementary Tests on Secondary Carbon Formation

Antioxidants change the microstructure of the material and lead to the formation of intermediate solids, liquid or gaseous products, which hinder the inward diffusion of oxygen and protect the carbon from oxidation. Furthermore, antioxidants or together with the intermediate products may possibly reduce CO to C and lead to secondary carbon formation and reduce carbon loss. In addition, the secondary carbon may become fine carbon supply in the matrix and contribute to improving the slag penetration resistance. To complete the thesis work so far presented, specific new tests have been performed to illustrate those two points.

The possible courses of reactions involving antioxidant in the material system for secondary carbon formation are as follows.

$$A.O. + CO\ (g) \rightarrow Oxide\ (s,l,g) + C(s) \qquad (6.1)$$

$$Carbide\ (s) + CO\ (g) \rightarrow Oxide + C(s) \qquad (6.2)$$

$$Nitride\ (s, l) + CO\ (g) \rightarrow Oxide\ (s, l) + C\ (S) + N_2\ (g) \qquad (6.3)$$

The experimental design on secondary carbon formation has been carried out on the pressed sample made from the mixtures of magnesia fines with or without antioxidant Al or Si additives. The compositions of the samples are listed in Tables 6.1 and 6.2.

Table 6.1 Compositions of the samples for secondary carbon formation (group 1), wt. %

Code	M	M-Al-1	M-Al-2	M-Si-1	M-EG	M-EG-Al
MgO(Mf)	100	86	93	86	75	67
EG					25	22
Al		14	7			11
Si				14		

Table 6.2 Compositions of the samples for secondary carbon formation (group 2), wt. %

Code	M	M-Al	M-Si
MgO(Mf)	100	90	90
Al		10	
Si			10

All mixtures were compressed into cylindrical samples with a diameter of 19mm and height of 25mm at a pressure of 70MPa. Each sample was placed into a small alumina crucible and covered with coke. Each small alumina crucible was then placed into a big alumina crucible. Then, coke was filled into the big alumina crucible and a cover was placed on its top. During the firing, the samples were in a CO gas atmosphere for secondary carbon formation. The experimental set-up for secondary carbon formation is shown in Figure 6.9.

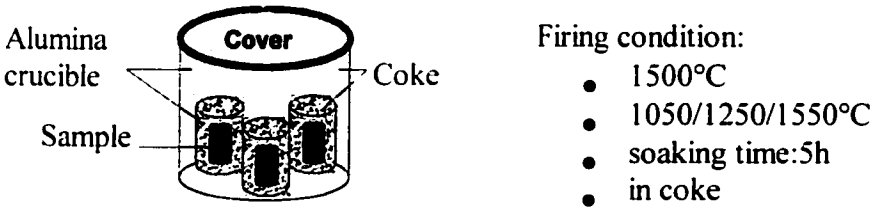

Figure 6.9 Experimental set-up for secondary carbon formation

In group 1, different antioxidants were considered in order to observe if the secondary carbon formation occurs in macro scale. All samples were fired at 1500°C for 5 hours in coke. Based on the results from group 1, further systematic study was performed on group 2, where the samples were fired at different temperatures (1050°C, 1250°C, 1550°C) for 5 hours. The chemical analysis on secondary carbon formation, microscopy observations by OM, CLM and SEM as well as X-ray diffraction were conducted in order to understand and confirm secondary carbon formation as well as other new compounds formation. The observations on secondary carbon formation are displayed in Figure 6.10.

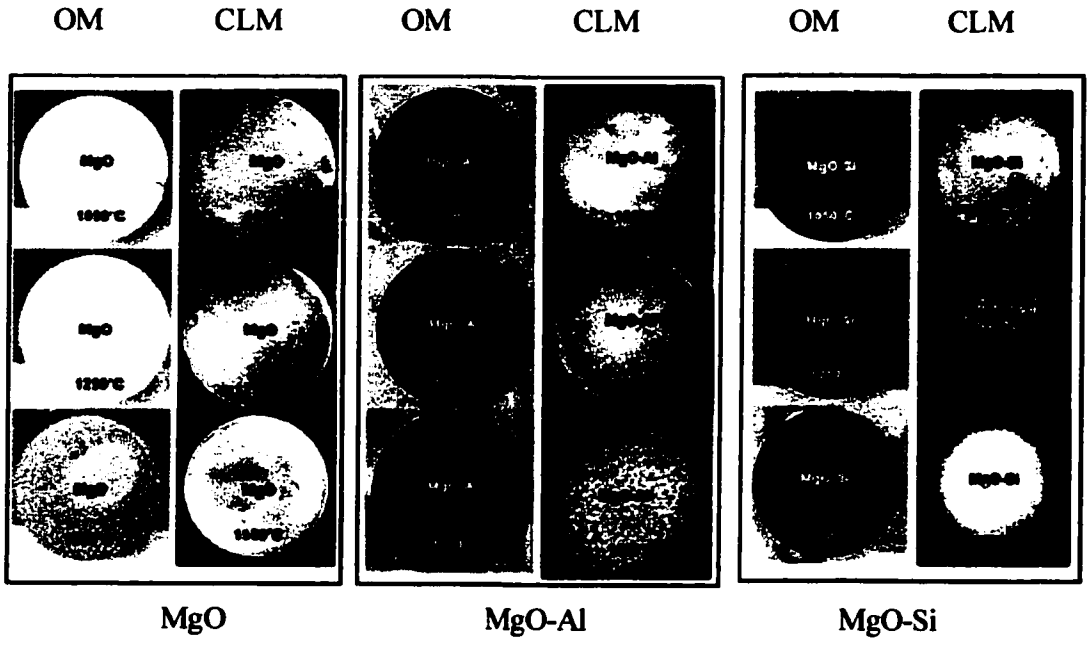

Figure 6.10 Secondary carbon formation in samples MgO-Al and MgO-Si after firing at 1050°C, 1250°C and 1550°C for 5h in coke

It is assumed that the secondary carbon formation can start at temperature of 1050°C since the colour of the samples with the antioxidant becomes black, and the samples without antioxidant remain of the same light colour. New compounds have been identified in different samples from CLM/SEM images and X-ray diffraction analysis. The distribution of the new compounds may be different from the surface of the sample to the inside of the sample since the layers with specific colors were observed

The secondary carbon formation in the sample containing antioxidant was examined by SEM, as shown in Figure 6.11. It shows that secondary carbon, new compounds spinel and MgO whiskers have been detected in sample MgO+Al.

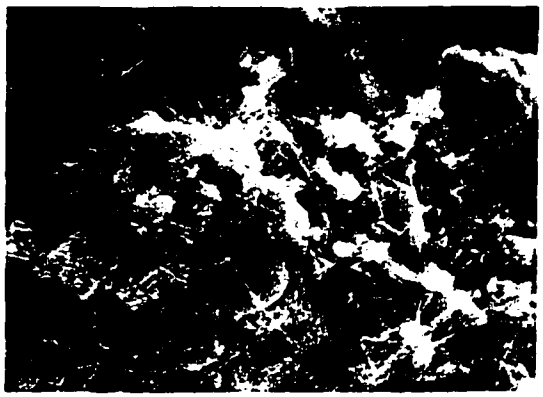

SEM observation:
MgO, MA spinel, C

Fracture surface also showing fine whiskers of secondary periclase developed in the matrix

Figure 6.11a New compounds formation in sample MgO-Al after firing at 1550°C for 5 hours in coke

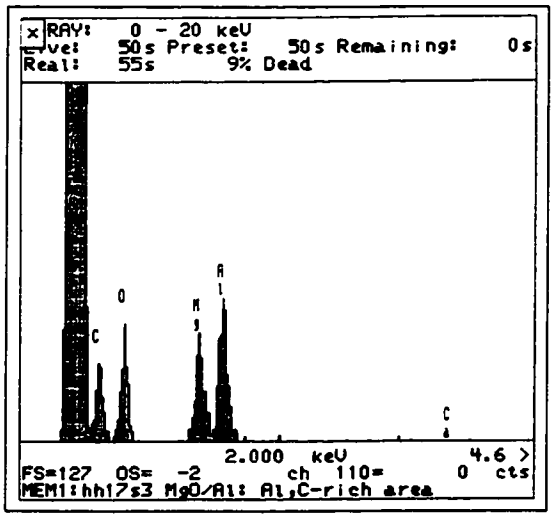

SEM observation:
MgO, MA spinel
Secondary carbon

Figure 6.11b New compounds formation in sample MgO-Al after firing at 1550°C for 5 hours in coke

The new compounds formations in samples M-Al and M-Si in group 2 were examined by X-ray diffraction, as shown in Figures 6.12 and 6.13. In the case of aluminium addition, MgO, Al_4C_3, Al_2O_3, Al and spinel were found at 1050°C. At 1250°C, main stable phases are magnesia and MA spinel. The amount of spinel increases with temperature up to 1550°C, as shown in Figure 6.12. For sample MgO with silicon addition, it shows that there are still the phases MgO and Si and nothing occurs at 1050°C. New compound forsterite M_2S starts to form at temperature 1250°C and its amount increases with temperature up to 1550°C, as shown in Figure 6.13.

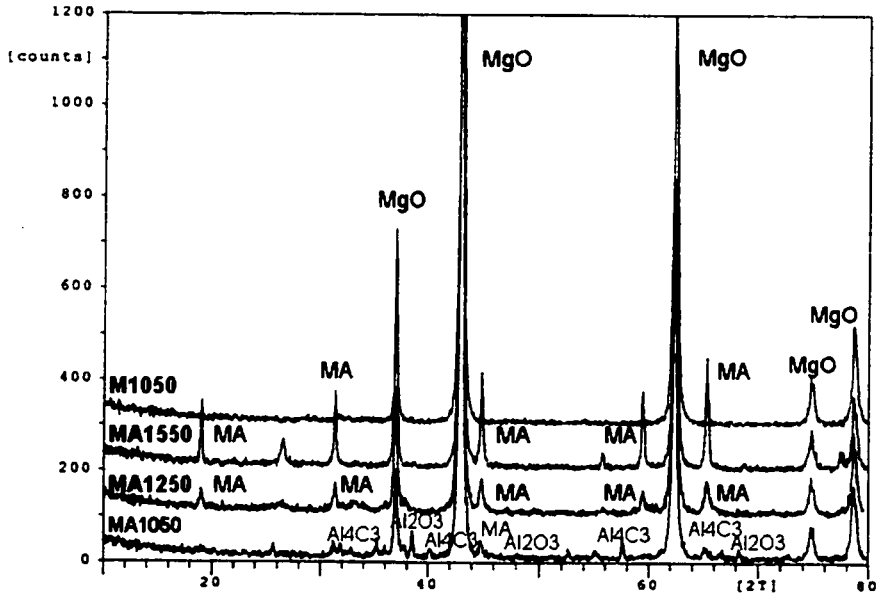

Figure 6.12 X-ray diffraction on magnesia with or without aluminium

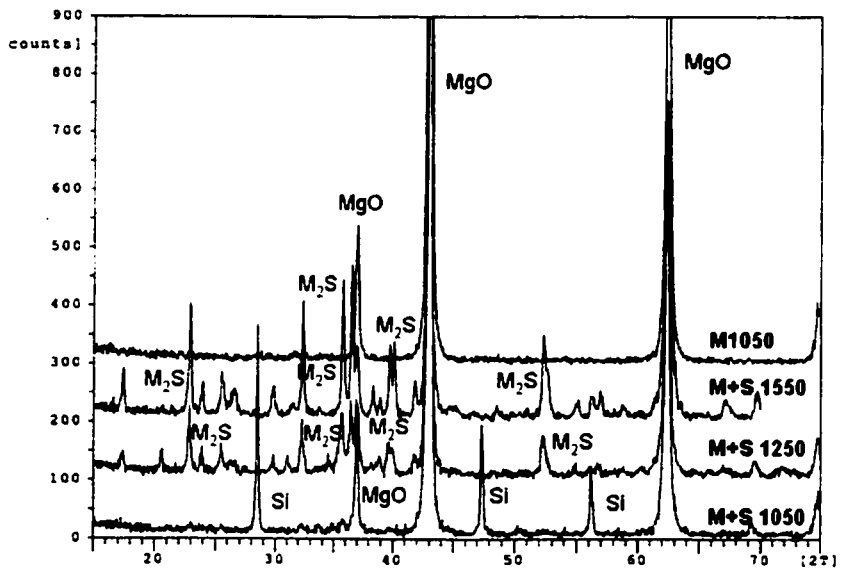

Figure 6.13 X-ray diffraction on magnesia with or without silicon

From the microscopy observation in Figure 6.14a, Al still exists and Al_2O_3 forms around Al particles at 1050°C. SEM observation confirms that Al_4C_3 was found in the matrix, and not around Al particle. It may be understood that Al_4C_3 was formed through gaseous phases. When temperature increases, spinel starts forming and developing within the matrix and toward the surface of the sample.

As can be seen, for secondary carbon formation by aluminium, the effect of Al on reducing CO to C starts at low temperature around 1050°C, where Al_4C_3 has formed in sample MgO-Al. The chemical analysis on secondary carbon formation shows that the highest amount up to 3.75% CO_2 is obtained after the sample was fired at 1050°C for 5 hours. With the increase of the temperature up to 1250°C and 1550°C, the amounts of detected CO_2 gas has greatly decreased down to 0.66% and 0.33%, respectively. It may

be explained that aluminium is very active at lower temperature. Al_4C_3 decreases with higher temperature and gradually disappears after 1250°C. After Al and Al_4C_3 disappear, there is no further protection for secondary carbon from oxidation by antioxidant. The fine carbon formed from reducing CO to C may be partially oxidized with further higher temperature and longer holding time.

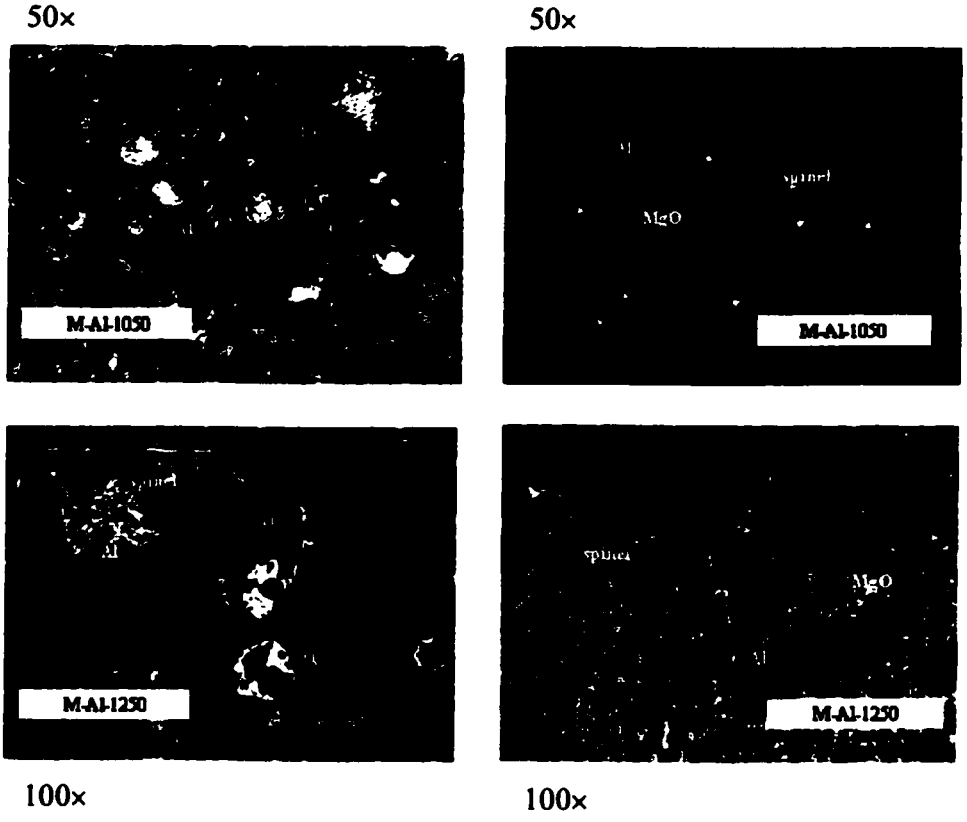

Figure 6.14a Microstructure and new compounds formation in sample MgO-Al after firing at 1050°C and 1250°C for 5 hours in coke (OM/CLM)

In Figure 6.14b, the magnesia dense layer, with spinel locally distributed, has formed on the surface and well developed. This shows that magnesia vapour is favored through reduction of MgO by antioxidant Al or CO (g) in the system. In addition, spinel has also formed at low temperature, and then developed into crystallized spinel from Al particles and distributed homogeneously within the sample after firing at temperature 1550°C, as seen in Figure 6.14b.

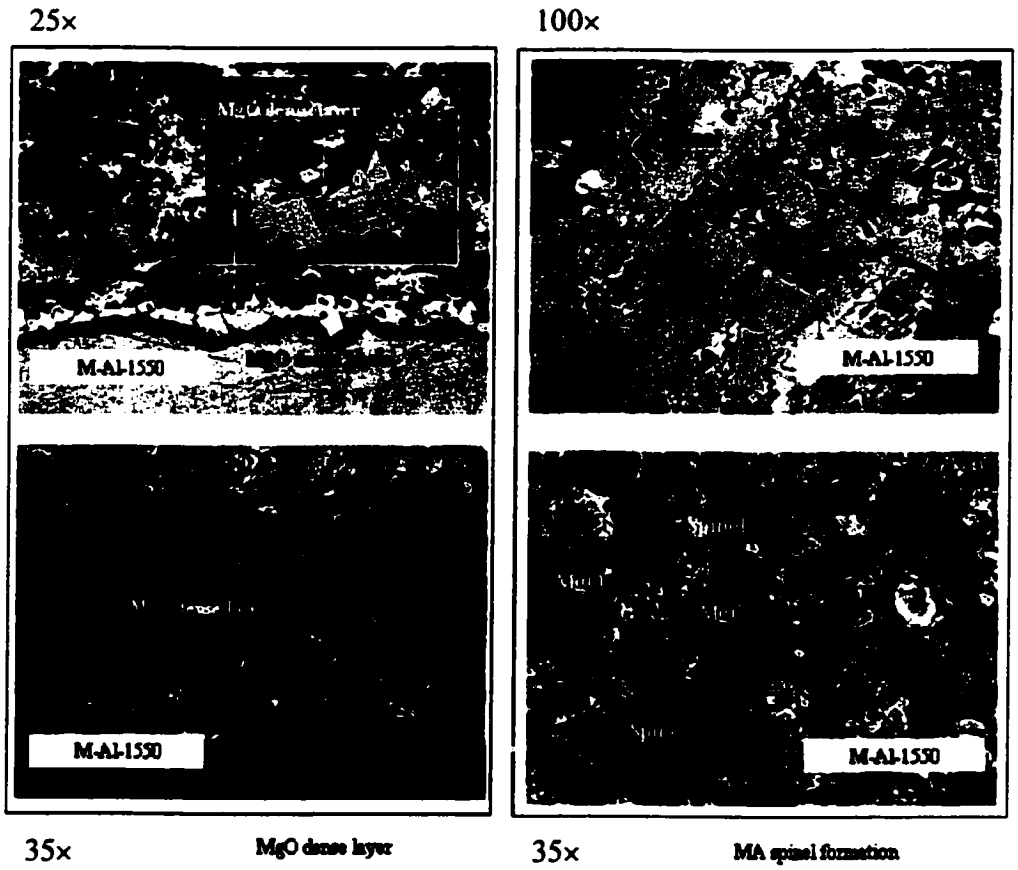

Figure 6.14b Microstructure and new compounds formation in sample MgO-Al after firing at 1550°C for 5 hours in coke (OM/CLM)

To explain these new compounds formation and possible gaseous phases in the system, the thermodynamic calculation on the MgO-Al-CO system is given in Figure 6.15.

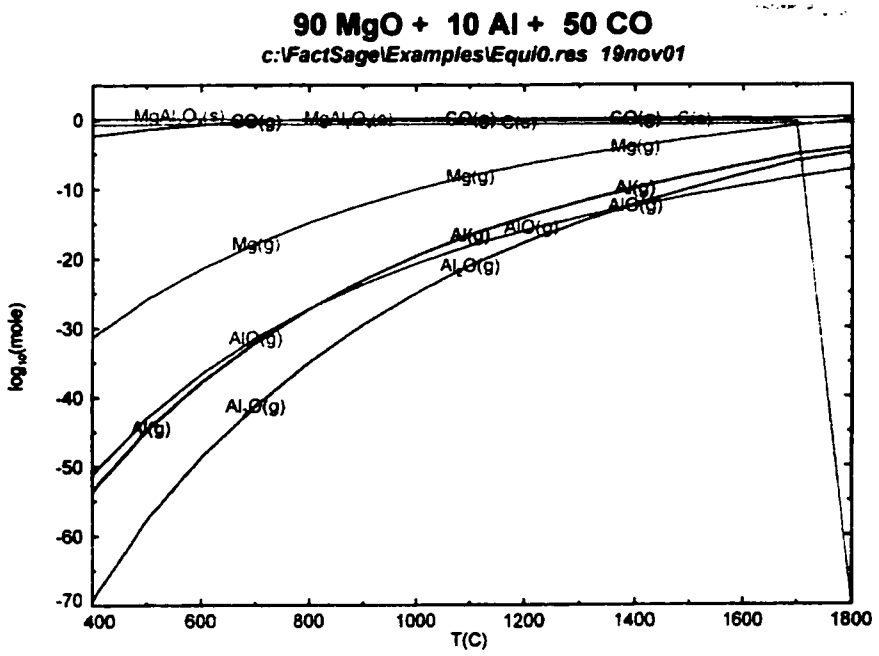

Figure 6.15 Thermodynamic calculation on secondary carbon formation and various gaseous phases in MgO-Al-CO system (by FACT)

The stable phases are magnesia, magnesia alumina spinel and carbon in a wide range of temperature. The gaseous phase Mg (g) becomes more pronounced than other gaseous phases and its amount increase with temperature. From temperature 1400°C to 1600°C, the partial pressure of magnesia vapour could reach around $P_{Mg}10^{-5}$ to 10^{-2} mole. It means that P_{Mg} is strong enough to supply Mg (g) to form spinel and MgO dense layer. In addition, it can be seen that various A_xO_y gaseous phases, such as Al (g), AlO (g) and Al_2O (g), may be involved in reactions and act as an alumina source for spinel

formation. As described above, spinel was well developed and distributed homogeneously in the matrix when just metallic aluminium is locally distributed in the matrix. It is believed that the A_xO_y gaseous phases acting as reactants take part in the reactions.

In Figure 6.16 metallic silicon is still in the matrix after firing at 1050°C. No new compound formation is observed at this temperature. With increased temperatures, forsterite starts to form at 1250°C and then further develops at a higher temperature of 1550°C. The amount of CO_2, which refers to the secondary carbon formation, was detected as 0.26% to 0.81% after firing the samples MgO-Si at 1050°C and 1550°C, respectively. Thus, secondary carbon formation by Si in the system is obvious.

Figure 6.16 illustrates that the texture of the sample exhibits differently from the surface to inside of the sample. A dense layer was formed in the place close to the surface, which was confirmed as forsterite by SEM/EDS. This indicates that the experimental condition did not reach its equilibrium. The partial pressure of the oxygen was unknown and different from the surface to the inside of the sample. SEM observation shows that silicon was found inside the sample after firing at 1550°C. It seems that a dense layer or magnesia silicate compound may lead to liquid formation during heating condition and the silicon was well protected and sealed inside of the sample.

The thermodynamic calculation on the MgO-Si-CO system is given in Figure 6.17. The stable phases are MgO, Mg_2SiO_4 and carbon in a wide temperature range. Magnesia vapour and SiO are more dominant than other gaseous phases. The microscopy observation on phase changes with temperature shows that a dense layer containing magnesia and silica was formed in the place close to the surface of the sample. It is believed that the reactants are from pre-set constitutes and gaseous phases by antioxidant in reducing atmosphere.

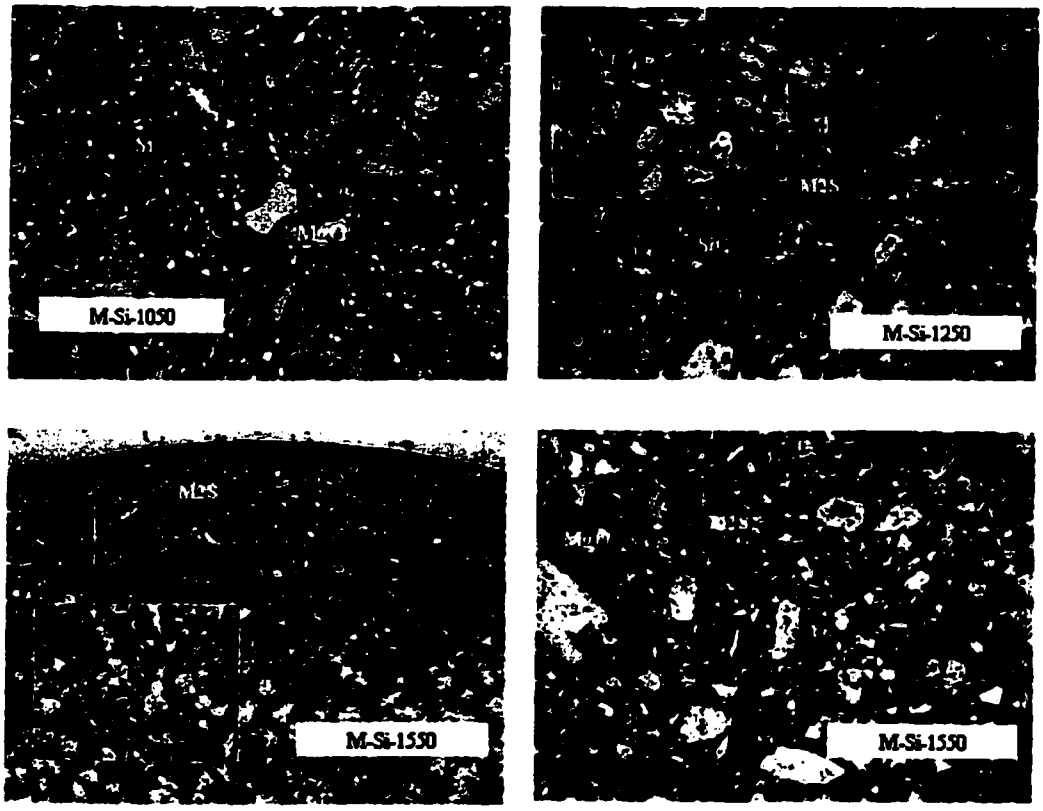

Figure 6.16 Microstructure and new compounds formation in sample MgO-Si after firing at 1050°C, 1250°C and 1550°C for 5 hours in coke (OM/CLM)

As can be seen, antioxidants are efficient to promote new compounds formation, which involve solid, liquid and gaseous phases formation and have different performance in the system. The transfer effect of gaseous phases by antioxidants is visible. Secondary carbon formation is obvious, especially in the case of using aluminium at low temperature 1050°C, where around 1% secondary carbon was formed and distributed in the matrix.

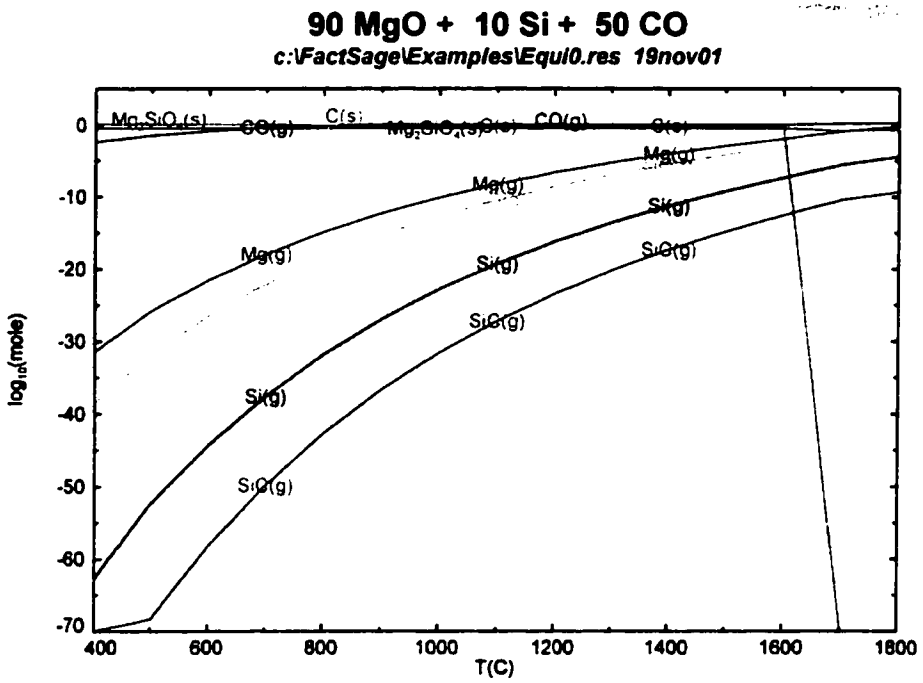

Figure 6.17 Thermodynamic calculation on secondary carbon formation and various gaseous phases in MgO-Si-CO system (by FACT)

The results confirms that antioxidants Al and Si reduce CO to C and lead to secondary carbon formation as well as new compounds spinel and forsterite formation as compared to sample MgO with samples MgO-Al or MgO-Si at designed test condition. This secondary carbon becomes a supplement of fine carbon in the matrix. Thus, the effect of antioxidant in magnesia-based materials on preventing slag penetration has been further studied.

For comparison purpose, the samples MgO, MgO-Al and MgO-Si were submitted to a static slag test. The slag composition is listed in Table 6.3.

Table 6.3 Slag composition (wt. %)

	CaO	SiO_2	Fe_2O_3	MgO	Al_2O_3	MnO	TiO_2	K_2O	Na_2O	P_2O_5	Cr_2O_3
Slag	36.3	19	1.04	7.24	33.7	0.72	0.3	0.36	<0.1	0.02	0.67

The configuration of the set-up is illustrated in Figure 6.18. The cylindrical sample, after firing at 1500°C for 5 hours for secondary carbon formation, was placed in a crucible made from a MgO-Cr_2O_3 brick. The inner surface of the crucible was painted with graphite coating to prevent slag penetration into the brick. After putting the sample into MgO-Cr_2O_3 crucible, slag with weight 25 gram was put into the gap between the sample and the crucible. Then, graphite powder was filled on top of the sample and then a cover was used to separate the sample from the filling coke. After that, the MgO-Cr_2O_3 crucible was put into a big alumina crucible with coke protection. The heating condition of the slag test was 1550°C for 1 hour with a heating rate of 5°C/min.

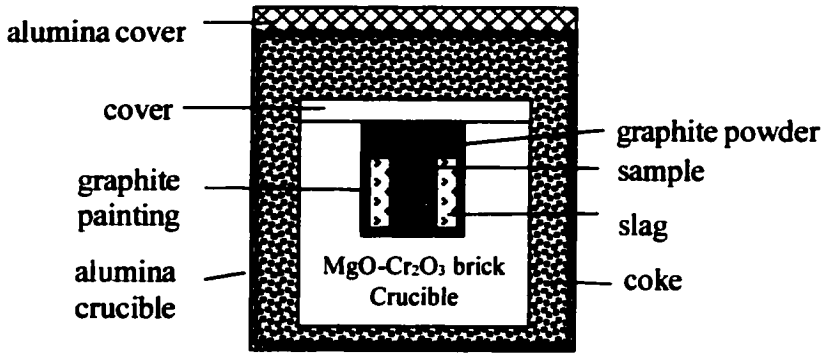

Figure 6.18 Set-up for static slag test

The results from the slag test are given in Figures 6.19-21. From cathodoluminiscence microscopy (CLM) observation on the unpolished sample MgO, the slag penetration layer was deeply formed and clearly visible, as Figure 6.19a. The elements detected from the edge to the centre of the sample by SEM/EDS were Mg-Al-Si-Ca-O. This shows that the slag penetrated totally into the whole sample under such condition, as shown in Figure 6.19b.

Figure 6.20 illustrates the slag test result on sample MgO-Al. The in-situ spinel formed distributes homogeneously within the sample MgO-Al. After slag test, no clear slag penetration depth is observed. It is believed that spinel and secondary carbon prevent the slag penetration.

OM

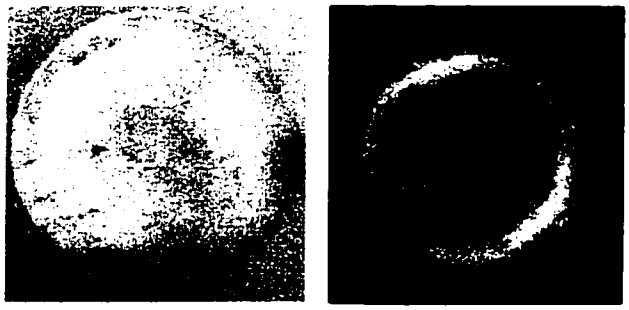

CLM

Figure 6.19a Slag test on sample with only magnesia (CLM)

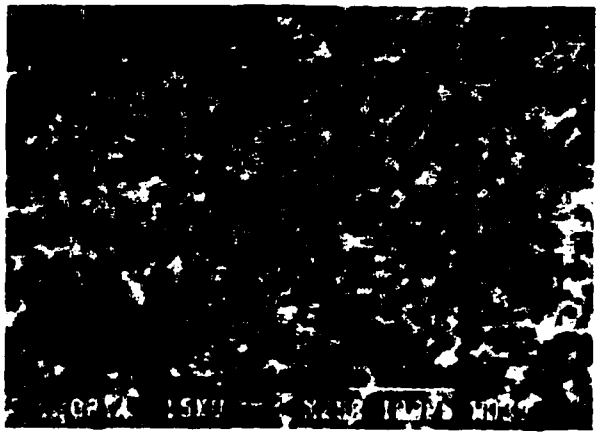

SEM

Dark gray :MgO
White : slag
Black : pores

Figure 6.19b Slag totally penetrated into the sample containing only magnesia (CLM)

(after slag test at 1550°C×1h in coke)

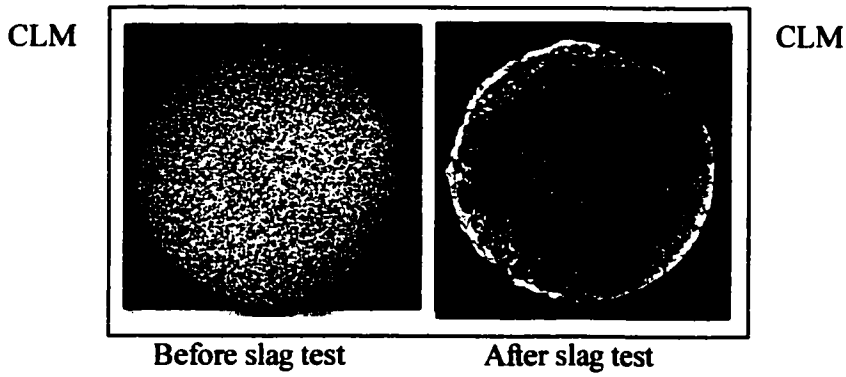

Figure 6.20 Static slag test on sample MgO-Al at 1550°C×1h in coke

In the case of the addition of antioxidant Si (sample M-Si), a sharp thin layer of penetration was formed. The penetrated zone has several different fine layers with different colours under CLM observation (see Figure 6.21a). In order to see how deeply the slag has penetrated into the sample, the polished microscopy sample was observed by SEM and CLM, see Figures 6.21b, 6.21c and 6.21c. Penetrated elements from the edge to the centre of the sample were also tested. The results are given in Table 6.4.

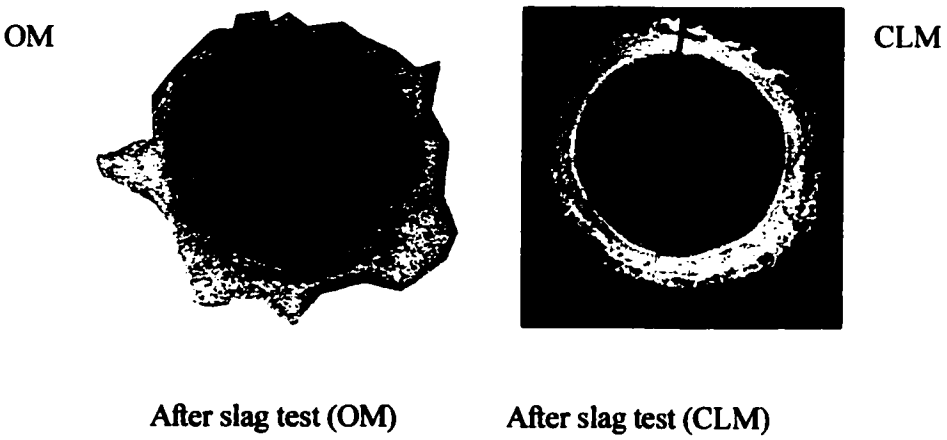

6.21a OM and CLM observations on sample MgO-Si after slag test at 1500°C×1h

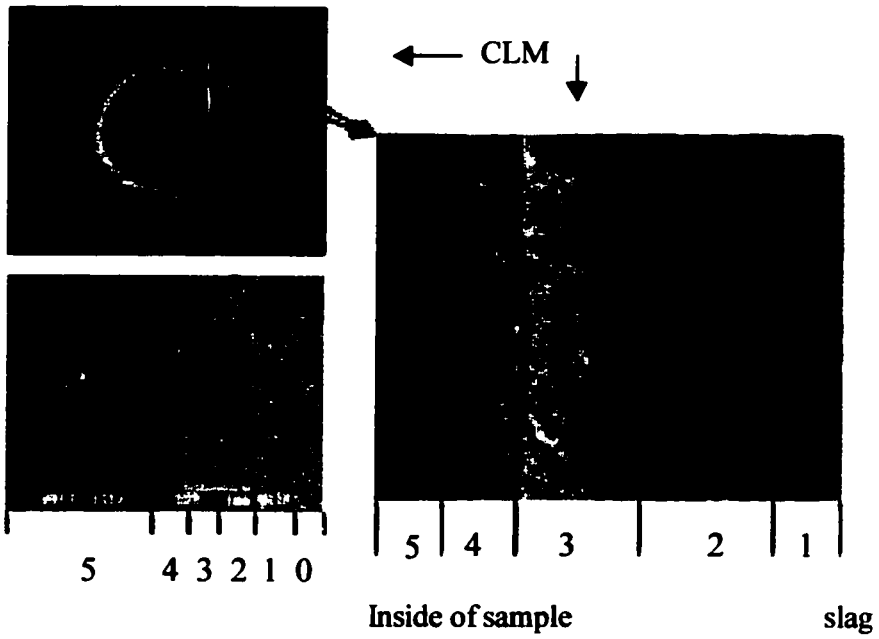

6.21b Penetration layers of sample MgO-Si after slag test

at 1500°C×1h in coke (SEM/CLM)

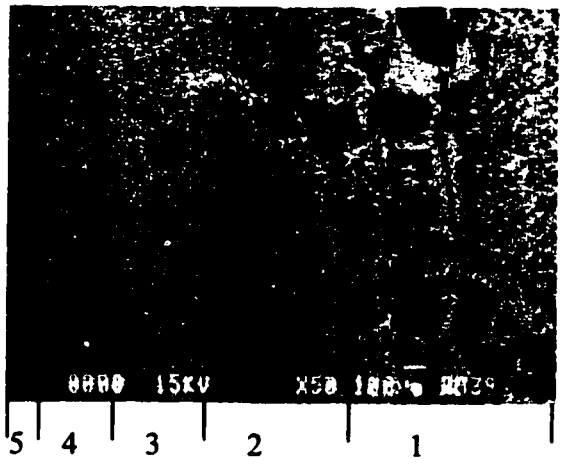

6.21c Penetration layers showing different textures (area 1-5) on sample MgO-Si (SEM)

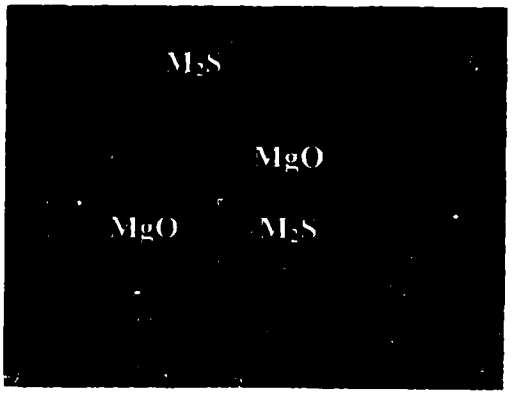

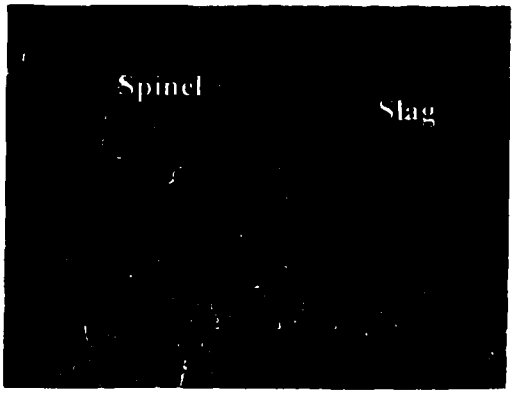

Non penetrated zone (Area 5) Crystal shaped spinel in Area 1

6.21d Details on non-penetrated area 5 and spinel layer in area 1

in sample MgO-Si after slag test at 1500°C×1h (CLM)

Table 6.4 Elements detected from the edge to the centre of the sample M-Si

after slag test at 1550°C×1h

Area	MgO-Si
0	Al-Ca-Si-O
1	Al-Mg-O
2	Al-Mg-O, Ca-Si-Mg-O
3	Mg-O, Mg-Si-Ca-Al-O
4	Si-Mg-Ca-O
5	Mg-Si-O

area 0, there is only slag composition. A well-developed crystal shaped spinel layer was formed between slag and penetrated zone (area 1). This explain that Mg (g) diffuses toward the surface of the sample and catchs Al_2O_3 from the slag composition to form spinel. It is more porous in area 2, which mainly contains Ca-Si rich slag with some spinel distributed in it. Area 3 contains magnesia and slag. A sharp edge separates the sample from slag between area 3 and area 4. Area 4 still contains a little Ca. It can be seen that the element Ca is the most aggressive one to penetrate into the material and the element Al is caught to form a dense spinel layer. A totally non-penetrated zone starts from area 5. It shows that the slag penetration was totally inhibited within area 5. Within the sharp edge (area 4), it reaches 88% of the total area. The non-penetrated zone (area 5) is around 78% of the total area. Therefore, the slag penetration resistance has improved, as compared to sample MgO

As discussed here, new compounds spinel and forsterite as well as secondary carbon formation, by incorporating antioxidant into the material, effectively reduce slag penetration as compared with the sample without antioxidant additives. Further testing on slag corrosion resistance would be required to truly understand the role of secondary carbon formation on slag penetration. But this was considered to fall outside the scope of this thesis.

6.3 Promising Properties of the Castables

To obtain good properties of graphite containing castables, a good starting castable is required. Castable's workability was investigated as the first step since it involves the study on flowability and flow decay of the castables. Selecting a proper carbon source is an important step to decrease water addition and to improve flowability and other properties. Deflocculant also plays a big role in reducing water demand, increasing mechanical property and obtaining a dense structure of the castables. Among the five deflocculants investigated in a magnesia based castables, sodium hexametaphosphate (S6P) is more efficient in reducing water addition in magnesia-based matrix. Galoryl (G) works well with a carbon material. Sodium dihydrogenecitrate (SD) can be used to adjust the setting time. The combination of sodium hexametaphosphate (S6P), galoryl (G) and sodium dihydrogenecitrate (SD) (D9) performs the best result with respect to water addition, flowability, mechanical property and setting time. There are many factors influencing flow decay, in which magnesia fine is the most pronounced one. The combination of magnesia fines with different size is possible to give better control of the flow decay.

To obtain promising properties of magnesia-based graphite containing castables, overall consideration on deflocculant, magnesia fine, binder and bonding systems are highly needed. Selecting a proper carbon source, upgrading the quality of the graphite pellets and optimizing antioxidant packages are important parameters to tackle.

CHAPTER 7 CONCLUSIONS AND RECOMMENDATIONS

7.1 CONCLUSIONS

This thesis work has demonstrated that the selections of the proper carbon source and antioxidants as well as controlling the good compactness of the material play decisive roles in minimizing the oxidation of carbon containing castables. By using the proper deflocculants and magnesia fines, modifying flake graphite through the appropriate packaging technique and optimizing the antioxidants and their combinations in every case, it has been possible to produce samples with high standards of performance.

The carbon source plays a significant role in improving the oxidation resistance and the overall properties of carbon-containing castables. Selection of the proper carbon source and incorporation of different carbons into the matrix and in the aggregates part have been studied in this work, and described as following four steps.

As the first step, non-flake graphite materials, such as pitch coke, amorphous graphite, were selected, and performed well in castables in terms of water addition, flowability, bulk density and apparent porosity. However, these carbons exhibit lower oxidation resistance and CMOR after high temperature firing due to their greater susceptibility to oxidization, which cause large pores, as compared to flake graphite. The straight addition of flake graphite offers higher oxidation resistance even if the castables require

higher water demand. It reveals that the nature of carbon source directly affects the oxidation of carbon containing materials.

The second step was to agglomerate flake graphite together by extruding (EG), coating (CG) and granulating (GG) methods to improve the wettability of flake graphite and reduce the segregation during the mixing of graphite containing castables. The problems caused by directly adding flake graphite into castables have been significantly minimized using EG, CG and GG pellets in terms of water addition, flowability, physical and mechanical properties in both MgO-MA-C castables and MgO-M_2S-C castables. This shows that the mode of inserting graphite plays a decisive role in improving the overall properties of the castables.

The third step was to further improve the extruded graphite package by incorporating antioxidants and/or oxide fillers into the EG pellets to densify the pellets, improve the distribution of the flake graphite within the pellets, reduce the pore size and increase the oxidation resistance of the EG pellets. In total, fifteen different extruded graphite pellets, divided into two different material systems: $(EG\text{-}A.O.)_{MA}$ with in-situ spinel formation as bond and $(EG\text{-}A.O.)_{MS}$ with in-situ forsterite formation as bond, have been compared. The extruded graphite pellets were evaluated by oxidation test through TGA and CO_2 gas analysis, pore size distribution measurement by mercury intrusion method as well as microscopy observation by optical microscopy (OM), scanning electronic microscopy

(SEM) and cathodoluminiscence microscopy (CLM). The oxidation resistance of the pellets and of the castables containing them is effectively improved. The optimized flake graphite pellets by incorporating antioxidants and oxides are more pronounced in improving oxidation resistances than other properties, such as physical and mechanical properties.

In the final step, the combination of modified graphite with fine carbon was studied in order to improve the distribution of carbon and balance the overall properties of the castables. Around 1% fine carbon with a size less than 5μm was used in combination with EG or CG graphite pellets and good overall properties have been achieved.

As an important constitutes of carbon containing castables, antioxidants face more challenges to be used in castables. Their role in increasing oxidation resistance of the materials has been studied thermodynamically and kinetically. Five different antioxidant additives were selected in the two magnesia-based material systems. In order to study the oxidation behavior of aluminium as an antioxidant in a castable, its reactivity in water-based mixes was duly documented. Antioxidants were studied in terms of their type, addition, and combination in both extruded graphite pellets and in castables for both spinel-bonded and forsterite-bonded material systems. Antioxidants, such as metallic Al, alloy AlMg, boron carbide B_4C, oxide Al_2O_3 and MgO, have been used in extruded graphite pellets, the matrix and the castable for spinel-bonded system.

Antioxidant additives, such as silicon Si, silicon carbide SiC, boron carbide B_4C and silica SiO_2, have also been inserted into extruded graphite pellets and then into the forsterite-bonded castables. The effects of antioxidants on oxidation resistance of the materials were evaluated by TGA, CO_2 gas analysis and the depth of decarbonized layer of the samples. Microscopic observations were performed through OM, SEM, EDS and CLM. In addition, X-ray diffraction was used to identify the mineral changes.

The oxidation resistance and mechanical properties of these materials are effectively improved by using such antioxidants due to the reduced pore size and in-situ spinel bond and forsterite bond formations, both locally in extruded graphite pellets and overall in the matrix of the castables. The proper combinations of antioxidants for better oxidation resistance are aluminium with boron carbide in MgO-MA-C system and silicon with silicon carbide in MgO-M_2S-C system.

Antioxidant additives are very effective to reduce pore size, stimulate magnesium vapor and other gaseous phase formation, act as phase modifier for in-situ spinel and forsterite formation and reduce CO to C for secondary carbon formation. Their addition, distribution and combination strongly influence the overall properties of the castables.

Obtaining promising properties of magnesia-based graphite containing castables requires using the proper deflocculants and magnesia fine, designing binding and bonding

systems, selecting the proper carbon source and optimizing antioxidant packages. Castable's workability is a premier target to work on since it is governed by its flowability and flow decay. Using the proper carbon source can sufficiently reduce water addition and improve flowability and mechanical property. In addition, the deflocculant is another important factor to improve flowability and mechanical property, and obtain a low porosity castable. Five different deflocculants were investigated in magnesia-based castables. The combination of different deflocculants, sodium hexametaphosphate (S6P), galoryl (G) and sodium dihydrogenecitrate (SD), exhibits the best result in terms of water addition, flowability, mechanical property and setting time of the castables. furthermore, magnesia fine strongly affects flow decay. The finer the magnesia fine is, the faster the flow decay acts. The proper use of magnesia fines with different size provides better flow decay control and better workability of the castables.

As a summary, the justifications derived from basic knowledge, the original contributions made in this thesis and the evaluation of the innovative experimental methods which has been used, also in this thesis, are to be presented.

7.1.1 Justifications Derived From Basic Knowledge

The direct oxidation of carbon is: $C+O_2 \rightarrow CO \rightarrow CO_2$. It involves solid-gas reaction, which is controlled by chemical reactions and oxygen inward diffusion. To reduce

access of the oxygen into carbon or graphite and to increase the resistance to the oxygen inward diffusion has constituted the main effort of this thesis and is highlighted. In addition, thermodynamic calculations on new compounds formation have been carried out using FACT computer program, together with combined microscopy observations by newly developed CLM with commonly used OM and SEM methods.

The main approaches to improve the oxidation resistance of carbon containing materials include the following aspect.

1) Reduce the surface areas of flake graphite by agglomeration through extruding, coating and agglomerating, to reduce water addition and porosity of magnesia-based castables. This contributes to less exposure of graphite to oxygen, therefore higher oxidation resistance. (Extruding method firstly done by N. Zhou mainly focus on improving the properties of alumina-based castables.)

2) Enhance the approach to reduce oxygen access to graphite by incorporating antioxidant and oxide fillers into the pellets. From the thermodynamic point of view, antioxidants have higher affinity for oxygen than carbon and therefore protect carbon from oxidation. Kinetically, antioxidants effectively reduce the pore size and increase the resistance to oxygen inward diffusion. Adding antioxidants and oxides

also sufficiently densifies the pellets and reduces the exposure of graphite to oxygen. Therefore, oxidation resistance of the pellets is effectively increased.

3) Incorporate antioxidants and very fine oxides in both extruded graphite pellets and the matrix of the castables through dense packaging techniques and in-situ compounds formation to reach the following purposes:

(1) Reduce pore size (in pellet and matrix)

(2) Densify the material (in pellets and matrix)

(3) Promote dense later formation (MgO or MA spinel dense layer)

(4) Form a few liquid phase to block pores (combination of Al+B_4C)

(5) Produce in-situ compounds filling in pores (Al_2O_3, Al_4C_3, SiC, MA and M_2S)

These microstructure changes of the material decrease the exposure of carbon and graphite to oxygen and increase the resistance to oxygen inward diffusion. Therefore, the oxidation resistance is increased. In fact, the combination of antioxidant in both pellets and the matrix of the castables give the best result of minimizing the oxidation of graphite locally in pellets and overall in castables.

4) Understand the importance of measuring the pore size distribution of the material regarding to oxidation resistance of the materials. The results of oxidation resistance

reveal that not only apparent porosity is important, but also the pore size is important since pore size plays an important role in increasing the resistance to oxygen inward diffusion.

5) Uncover the role of gaseous phases existed in the systems by thermodynamic calculations and microscopy observations. The results show that the gaseous phases by antioxidants not only play important role in the intermediate reactions but also move towards the hot face and reduce partial pressure of oxygen, and thus increase the oxidation resistance of the castables.

6) Use the combination of three different deflocculants to reduce water addition and apparent porosity. This is beneficial to reducing the exposure of carbon to oxygen and thus to improving the oxidation resistance of the castables.

7) To use ultra-fine silica fume and very fine active alumina as binder, and to obtain good flowability with less water addition and smaller pore size. These again contribute to improving oxidation resistance of the castables.

7.1.2 Contributions to Be Underlined

1. Apply Gas-Solid Reaction Theory and Thermodynamic Calculation by FACT Computer Program into Practical Development of Magnesia-Based Graphite Containing Castables.

2. Demonstrate What Carbon And Graphite Can Be Used And How They Can Be Used In Castables As Well As Their Influences On The Overall Properties Of The Castables.

Enhance the agglomeration of flake graphite by the packaging technique and provide more choices of using flake graphite into castables.

Point out the microstructure changes of the pellets within the specific system and giving an overall characterization of the graphite pellets in terms of densification, pore size distribution, new compounds formation and oxidation resistance.

Exhibit an overall view of using different carbons and graphites into castables and their influences on flowability, physical and mechanical properties, pore size, thermal shock resistance and oxidation resistance of the MgO-based castables.

Display the secondary carbon formation by antioxidants and show that the secondary carbon formation can be fine carbon supply in the material and is beneficial to the slag penetration resistance.

3. Take Different Approaches to Uncover The Role Of Antioxidant

Take the challenge to make metallic aluminium usable in castables. Document the danger of using un-coated metallic aluminium into magnesia-based Material. Describe how to make metallic aluminium usable in castables. Practically use coated aluminium up to 4% in castables. Give the resolution of using metallic aluminium in pellets and in matrix to minimize the problem.

Point out the gaseous phases involved in the system and their role in participating intermediate reactions, through thermal dynamic calculations by FACT computer program and microscopy observations on MgO whisker, MgO dense layer, in-situ spinel and forsterite formations.

Highlight the role of antioxidant on improving the oxidation resistance from the following aspects, regarding to decreasing access of oxygen to carbon and graphite as well as increasing the resistance to oxygen inward diffusion:

(1) Reduce pore size

(2) Gaseous phases toward to hot face

(3) Block pores by liquid

(4) Intermediate compounds filling the pores

(5) Densify the material

Uncover the role of antioxidants on reducing CO to C and to form secondary carbon, which becomes a fine carbon supply in the material, therefore to improve the slag penetration resistance of the materials.

Optimize the antioxidant not only on its type, addition and combination but also its distribution to maximum the oxidation resistance. Their effects on the physical and the mechanical properties and the volume change of the materials should not be neglected.

4. Achieve Promising Properties Of Magnesia-based, Cement-free Castables

Combine three different deflocculants to reduce water addition and increase flowability and mechanical property of the castables.

Exhibit how to select proper carbon materials for castables. Demonstrate how carbon or graphite plays a decent role in developing carbon-containing castables.

Show how difficult it is to use metallic aluminium into castables and how antioxidants influence physical and mechanical properties, the pore size distribution and the oxidation resistance of the materials.

Combine the optimized deflocculants, oxide fines, proper choice of carbon and graphite and antioxidants into the castables to demonstrate that the promising properties of the castables can be achieved.

7.1.3 Innovation Experimental Methods Used

1) CO_2 gas analysis was selected and employed newly on materials containing both carbon and antioxidant, instead of the commonly used TGA method in literature. The reason of doing so is that carbon oxidation displays weight loss, and antioxidant oxidation exhibits weight gain.

2) The combination of newly employed CLM method with the commonly used OM and SEM methods gave a better view of new compounds formation and mineral changes within the material system. This CLM method effectively demonstrates the newly formed compounds and their distribution and helps to explain the in-situ intermediate products involved in the solid-gaseous reactions.

3) To improve the oxidation resistance, the importance of measuring the pore size distribution of the material was highlighted, instead of just measuring the apparent porosity, which is commonly used by other researchers.

4) The fracture behavior of the graphite-containing castables was employed by wedge-split-test (WST), which is newly developed method for refractory, especially first approach on graphite-containing castables. The results show that it is possible to measure the fracture behavior of graphite-containing castables by the WST method.

7.2 RECOMMENDATIONS

The results so far are highly satisfying, and the main recommendations to be made are:

1. To PRODUCE EXTRUDED GRAPHITE PELLETS ON A PILOT-SCALE, with heavier equipments, to increase the productivity to a ton or so a day. For each working lining of a 250 ton-ladle, close to 200kg of EG pellets would be needed (3 tons of carbon containing castables, with 6 to 7% of the EG pellets).

2. TO PRODUCE A MAGNESIA BASED CASTABLE MIX TO BE TESTED IN A STEEL MAKING LADLE, under careful monitoring to fully document this in-plant trial. The first system to privilege would be the MgO-SiO_2-EG system, but trials with

the $MgO-Al_2O_3$-EG system could easily be justified, based upon our thesis results. These two recommendations fall outside the scope of the present work. There are still many opportunities to explore to continue the present work.

3. TO PURSUE THE OPTIMIZATION OF PACKAGING GRAPHITE FLAKES, with the objectives of improving the density and the shape of the pellets. Approaches to obtain spherical particles, by other methods, should be tempted, like spray drying or briquetting. Other binders to substitute for molasses could also be envisaged: pitches, tars, resins, etc. The opportunities to launch new researches are plenty. This work should be considered as a good starting reference.

4. TO COMPLETE THE CHARACTERIZATION OF THE MIXES SO FAR OBTAINED, in terms of slag corrosion, spalling resistance and thermomechanical properties, at 1400°C. Further efforts on the kinetic study would be required to cover more carefully some specific fundamental aspects.

REFERENCES

1. KREBS, K. (1999). Modern solution of refractory problems with unshaped refractories. Proceedings of UNITECR'99, Sep. 6-9, Berlin, Germany, 1-5.

2. NAKAGAWA, H. (1999). Monolithic refractories for the iron and steel industry. Taikabutsu Overseas, Vol. 19 (3), 56-57.

3. YORITA, E. (1999). Monolithic refractories in Japan--history and recent trend. Taikabutsu Overseas, Vol. 19 (3), 3-6.

4. KAMEI, S. (1989). Progress of monolithic refractories for recent 10 years in Japan. Proceedings of UNITECR'89, Nov. 1- 4, Anaheim, USA, Vol.1, 46-86.

5. PARR, C. and BIER, T.A. (1999) The design Fundamentals of High Technology Castables-An Understanding for Steelmakers, Steelmaking Conference Proceedings, 237-249

6. RIGAUD, M. and XING, C. (1997). Basic castables for ladle's steel making applications: A review, Journal of Canadian Ceramic Society, Vol. 66 (3), 206-209.

7. RIGAUD M. (1999). Magnesia-Carbon Castables: A Review. 82th Steelmaking Conference Proceedings, Chicago, 251-255.

8. NAKAMURA, R. and KANESHIGE, T. (1999). The current status of casting steel ladles in Japan. 82th Steelmaking Conference Proceedings, March 21-24, Chicago, USA, 267- 278.

9. ITOSE, S., ISOBE, T. and FURUKAWA, K. (1997). Optimum castable lining for steel ladle in Japan, Proceedings of UNITECR'97, Nov 4-7, New Orleans, USA, Vol.1, 165-174.

10. TAWARA, M., FUJII, K. and TANIGUCHI, T. (1996). Application of alumina-magnesia castable in high temperature steel ladle, Takabutsu Overseas, Vol.16 (2), 17-19.

11. HENRY, F.W. J. and STENDERA, J.W. (1998). Recent development in spinel forming castable use in steel plants, Proceedings of 1998 Electric Furnace Conference, Nov. 15-18, New Orleans, USA, Vol. 56, 221- 228.

12. OHISHI, I. and EBIZAWA, R. (1991). Application of alumina-spinel castable refractories to steel ladle, Proceedings of UNITECR'91, Sep. 23-26, Aachen, Germany, 148-151.

13. LI, N. and WEI, Y. (1999). Properties of MgO castables and effects of reaction in microsilica-MgO bond system, Proceedings of UNITECR'99, Beriin, Germany, 97-101.

14. SANDBERG, B. and MYHRE, B. (1995). Castable in the system $MgO-Al_2O_3-SiO_2$, Proceedings of UNITECR'95, 173-179.

15. RIGAUD, M., XING, C. and BLANCHAR, M. et al. (1998). Basic castables for steel-making applications, Proceedings of 1998 Electric Furnace Conference, 213-220

16. LI, N. and ZHANG, W. J. (1990). Carbon Containing Refractories, published by Science Press, China

17. TABATA, K. (1992). Recent progress and future trend of carbon bearing refractories in Japan, Proceedings of the second International Symposium on Refractories, Oct. 30-Nov. 2, Beijing, China, 22-33.

18. ZHU, B.Q. (2000). The present progress and problems of carbon-containing castables, China's Refractories, Vol. 9, No. 1, 8-11.

19. KAWASAKI, H., YOSHITOMI, J., SHIKANO, H. and HAYASHI, T. (1991). Surface treatment of graphite for monolithic refractories, Taikabutsu Overseas, Vol. 11 (4), 46-47.

20. COOPER, C.F. (1984) Refractory application of carbon-flake graphite, its function in modern refractories, Refractory Application of Carbon in Sheffield

21. RIGAUD, M. (1997). New additives in carbon-bonded refractories, CIREP-Ecole Polytechnique of Montreal

22. URE, A. (1843). Manufactures and mines, Dictionary of Arts, Longmens, Brown and Longmens, London, 1004

23. PERCY, J. (1875), Metallurgy, John Murray, London

24. KARHUT, G. and JUNGER, H.J. (1997). Research and development of refractories to meet the future demands, The Refractories Engineer, April, 26-31

25. TORIGO, A. and TADA, H. and NOMURA, O.(1998). Environmentally friendly MgO-C brick for steel ladles, Taikabutsu Overseas, Vol.18 (4), 48-51.

26. KEISUKE, H. (1985). Corrosion of various basic bricks by CaO-SiO_2-Fe_2O_3-MgO slag, Taikabutsu Overseas, Vol.5 (1), 12-20.

27. JHUNJHUNWALA, R., SAHU, M. M. and PADHI, P.C. (1993). Advance in Magnesia-Carbon Brick Application, Proceedings of UNITECR'93, 391-400

28. WANG, X.Z., LI, Y.Q., LI, Q.H., ZHANG, Y.M. and LIN Y.L. (1992). The use of Al_2O_3-MgO-C bricks for 300 ton steel ladle, Proceedings of the 2nd International Symposium on Refractories, Oct. 30-Nov. 2, Beijing, China, 349-355.

29. BANERJEE, S.(1998). Monolithic Refractories. The American Ceramic Society, Westerville, Ohio, USA

30. FRANKLIN, S.A. and WARMAN, M.O. (2000). Where have all the bricks gone? The Refractories Engineer, No. 1, 2000, 2-11.

31. YE, G.T. and LI, Z.G. (1999). Trend in monolithic refractories technology, China's Refractories, Vol. 8 (3), 15-18.

32. MORI, J., WATANABE, N., YOSHIMURA, M., OGUCHI, Y. and KAWAKAMI, T. (1990). Material design of monolithic refractories for steel ladle, The American Ceramic Society Bulletin, Vol. 69 (7), 1172-1176.

33. NAGAI, B., MATSUMOTO, O. and ISOBE, T. (1991). Development of monolithic refractory linings for B.O.F. ladle in Japan mainly for the last decade, Proceedings of UNITECR'91, Sep. 23-26, Aachen, Germany, 116-122.

34. Flavia, N., RICHARD, C. and BRADT, C. (1999). Reactions of constituents for in-situ bonds of $MgAl_2O_4$, Mg_2SiO_4 and $3Al_2O_3 \cdot 2SiO_2$ in refractories, Proceedings of 1999 Electric Furnace Conference, 143-152.

35. LEE, W.E. and MOORE, R.E. (1998). Evolution of in situ refractories in the 20th century, Journal of the American Ceramic Society, Vol. 81(6), 1385-1410.

36. RIGAUD, M., KOVAC, V., XING, C., PALCO, S. and RYBAR, A. (1998). Spinel and forsterite bonded magnesia castables for steelmaking applications, 81st Steelmaking Conference Proceedings, Toronto, Canada, March 22-25, 477-486.

37. Matsui K. Saihi, (1995). Effects of impurities on the hydration of magnesia clinker, Proceeding of UNITECR'95, Kyoto, Japan, 513-520.

38. KANEYASU, A., YAMANOTO, S. and WATANABLE, T.(1995). MgO raw material improved hydration resistance, Proceedings of UNITECR'95, Kyoto, Japan, 533-540.

39. RIGAUD, M. and LANDY, R.A. (1996). *Pneumatic steelmaking*: Volume three on Refractories. A publication of the iron & Steel Society, 81

40. NAKAGAWA, Z., ENOMOTO, N., YI, I.K. and ASANO, K. (1995). Effect of corundum/periclase sizes on expansion behavior during synthesis of spinel. Proceedings of UNITECR'95, Nov. 19-22, Kyoto, Japan, Vol. 1, 379-386

41. NAKAGAWA, Z., ITOH, T. and ENOMOTO, N. (1996). Effect of compositional variation on expansion behavior of MgO/Al_2O_3 compact during spinel formation. Proceedings of 35th Annual Conference of Metallurgists, Aug. 24-29, Montreal, Canada, 257-268.

42. XING, C. (1999). Optimization of magnesia based, cement-free, spinel bonded castables, Ph. D. Dissertation, Ecole Polytechnique de Montreal, Canada, November 1999.

43. RIGAUD, M., PALCO, S. and WANG, N. (1995). Spinel formation in the MgO-Al_2O_3 system relevant to basic castables, Proceeding of UNITECR'95, Nov. 19-22, Kyoto, Japan, 387-394

44. PALCO S., FELICE, F. and PETERS, D., (1998). Castables with improved spalling and thermal shock resistance, Proceedings of 1998 Electric Furnace Conference, 245-251.

45. KENAN, W.M. (1989). Hidden properties of graphite, Proceedings of UNITECR'89, Nov. 1- 4, Anaheim, USA, Vol.2, 1463-1470.

46. KENAN, W.M. and ALLERA, E. (1994). Graphite. Ceramic Bulletin, Vol. 73(6), 101-104.

47. C.F.COOPER. (1994). Graphite, nature's unique raw material, J. Can. Cerm. Soc., Vol.63 (3), 197-208.

48. MOCHIDA, I. (1988). Roles of carbons in Composite Refractories for Better Properties, Taikabutsu Overseas, Vol 8, (4), 36-47

49. YAMAGUCHI, A. (1997). Affects of oxygen and nitrogen partial pressure on stability of metal, carbide, nitride and oxide in carbon-containing refractories, Taikabutsu Overseas, Vol.7 (1), 4-13.

50. LI, X. and RIGAUD, M. (1995). Oxidation kinetics of graphite phases in magnesia-carbon refractories, J. Am. Ceram. Soc., Vol.78 (4), 965-971.

51. J.SZEKELY J.W.EVANS and H.Y.Sohn, (1976). *Gas-Solid Reactions*. Academic Press, New York

52. Li, X.M. and RIGAUD, M. Effect of graphite quality on oxidation and corrosion resistance of magnesia-carbon refractories. Advances in refractories for the metallurgical industries II, Quebec City, Canada, 95-108

53. COOPER, C.F. (1980). Graphite containing refractories. Refractories Journal, Vol. 55(6), 11-21.

54. SAKAGUCHI, M., ISHII, H., ARATANI, K. and OGUCHI, Y. (1993). Effect of graphite particle size on properties of MgO-C bricks, Taikabutsu Overseas, Vol. 13 (1), 27-29

55. YAMAGUCHI, A. and ZHANG, S. (1996). Behaviour of various kinds of carbon in carbon-containing refractories. Advances in refractories for the metallurgical industries II, Montreal, Canada, 59-71

56. YAMAGUCHI, A. (1987). Thermochemical analysis for reaction process of aluminium and aluminium-compounds in carbon-containing castable, Taikabutsu Overseas, Vol.7 (2)

57. NAGAI, B., MATUMURA, T. and UTO, S. (1986). Behaviour of magnesia carbon bricks containing aluminium under vacuum at high temperature. Taikabutsu Overseas, Vol.6 (2), 51-56.

58. ICHIKAWA, K., NISHIO, H. and NOMURA, O. (1995). Suppression effects of aluminium on oxidation of MgO-C bricks, Taikabutsu Overseas, Vol.15 (2), 21-24.

59. YAMAGUCHI, A. (1984). Behavior of Si and Al added to carbon-containing refractories, Taikabutsu Overseas, Vol. 4 (3), 14-18.

60. P.O.R.C. BRANT and B. RAND, (1991). Reaction of silicon and aluminium in MgO-graphite composites I-Effects on porosity and microstructure, Proceedings of UNITECR'91, 247-253.

61. WATANABE, A., TAKAHASHI, H. and TAKANAGA, S. (1997). Behaviour of different metals added to MgO-C brick, Taikabutsu Overseas, Vol.7 (2), 17-23.

62. TAFFIN, C. and POIRIER, J. (1994). The behaviour of metal additives in MgO-C and Al_2O_3-C refractories, Interceram. Vol. 43, 354-360.

63. HEUER, H. and LOU, V. L. K. (1990). Volatility diagrams for silica, silicon nitride, silicon carbide and their application on high-temperature decomposition and oxidation, J. Am. Ceram. Soc.., Vol.73 (10), 2783-3128.

64. BREWSTER, A. J. and EVANS, D. (1999). Development in European monolithic ladle repair techniques, 1999 Steelmaking Conference Proceedings, 257-264

65. RYMON-LIPINSKI, T.., FICHTNER, R. and BENECKE, T. (1992). Study of the oxidation protection of MgO-C refractories by means of boron carbide, Steel Research, Vol.63 (11), 493-495.

66. RYMON-LIPINSKI, T. and SCHMEIZER, B. and ULITZKA, S. (1994). Tests on the oxidation-inhibiting effect of CaB6 in refractory MgO-C materials, Steel Research, Vol.65 (6), 234-237.

67. RYMON-LIPINSKI, T and WOLF, P. (1993). Reaction processes In the interior of an MgO-carbon with boron carbide additive, Steel Research, Vol. 64 (12), 123-127

68. HUMOLD, K., OLLIG, M. and POTSCHKE, R. (1997). The effect of B_4C and CaB_6 additions in MgO-C bricks, Proceedings of UNITECR'97, 789-797.

69. KLAUS, H. and JURGEN, P. (1999). Effect of boron-containing antioxidants on the reaction between MgO-C bricks, molten steel and slag. Proceedings of UNITECR'1999, 316-319.

70. HAYASHI, S., TAKANAGA, S., TAKAHASHI, H. and WATANABLE, A. (1991). Behavior of boric compound added in MgO-C bricks, Taikabutsu Overseas, Vol. 11(3) 12-19

71. PALCO, S., LI, X. and RIGAUD, M. (1994). Synergetic effects of boron-based antioxidant combined with aluminium additive in magnesia-carbon refractories. J.Can.Ceram.Soc., 63 (4) 261-265

72. HIRAI, S., MURAKAMI, H. and KATAYAMA, H. G. (1991). Effects of antioxidants on the formation of MgO-Al_2O_3 from MgO and Al_2O_3. J. Japan Inst. Metals, Vol.55 (2), 166-171

73. RIGAUD, M., BOMBARD, P., LI, X. and GUEROULT, B. (1995). Phase evolution in various carbon-bonded basic refractories. Proceedings of UNITECR'95, Nov. 19-22, Kyoto, Japan, 341-348.

74. YAMAGUCHI, A., ZHANG, S. and YU, G., etc. (1995). Behaviour of Antioxidants Added Carbon-Containing Refractories, Proceedings of UNITECR' 95, 341-348

75. BARTHEL, H. and KALTNER, E. (1983). The effect of carbon in carbon-containing magnesia bricks on the wear in basic oxygen furnaces, The first international conference on refractories, Nov. 15-18, Tokyo, Japan, 91-104

76. DIPL, P., MOSSER, J., KARHUT, G. and HAMMERER, W. (1995). Refractories for modern ladle lining, Proceeding of UNITECR'95, Nov. 19-22, Kyoto, Japan, 195-202

77. MAPIRAVANA, J., ARGENT, B. B. and RAND, B. (1991). Reactions of silicon and aluminium in MgO-graphite composites: II-Reaction products, Proceedings of UNITECR'91, Sep. 23-26, Aachen, Germany, 252-153

78. YAMAGUCHI, A. and ZHANG, S. (1997). A comparison of Al, Si and Al_4SiC_4 added to Al_2O_3-C refractories. Proceeding of UNITECR'97, 861-869.

79. WANG, T. and YAMAGUCHI, A. (2001). Oxidation protection of MgO-C refractories by means of $Al_8B_4C_7$, J. Am. Ceram. Soc., Vol. 84 (3), 577-582

80. TERANISHI, H., KAWAMURA, T., YASUI, K. and IMAI, I. (1998). Application of MgO-C castable to ladle furnace slag line, Taikabutsu Overseas, Vol. 18, No. 1, 38-42.

81. SAKAMOTO, S., ONO, Y. and ONO, T. (1995). Graphite containing unshaped refractories. Proceedings of UNITECR'95 , Nov. 19-22, Kyoto, Japan, Vol.2, 189-196.

82. YU, J., UENO, S. and HIRAGUSHI, K. (1997). Modification of Raw Refractory Materials by TiO_2 Coating. Proceedings of UNITECR'97, 1019-1026

83. LI H. YU J., HIRAGUSHI K., MIZOTA Y., (1998). Surface modification of graphite with in-situ reaction formed ZrO_2-Al_2O_3 composite powder. The 3rd international symposium on refractories, Beijing, China, 198-300.

84. YOSHIMATSU, H., FUJIWARA, S., KONISHI, R., MIYAWAKI, M. and MIURA, T. (1995). The water wettability and oxidation resistance of Al_2O_3-coated graphite. Journal of the Ceramic Society of Japan, Vol. 103 (6), 929-934.

85. YU, J., UENO, S. and HIRAGUSHI, K. (1996). Improvement in flowability, oxidation resistance and water wettability of graphite powders by TiO_2 coating. Journal of the Ceramic Society of Japan, Vol. 104 (6), 481-485.

86. ISOMURA, K., KUMAGAI, M., TAKAGI, M., GOTO, S., NOMURA, M., JONO, K, TIRITANI, Y. and TANAKA, S. (1998). Development of graphite containing

alumina castable and its application to BF trough. Proceedings of the 3rd International Symposium on Refractories, Nov. 3-6, Beijing, China, 51-56.

87. ZHOU, N. and RIGAUD, M. (1998). Different approaches to incorporating natural flake graphite into Al_2O_3-SiC-C castables, Proceedings of the 3rd international symposium on refractories, Nov. 3-6, Beijing, China, 291-297

88. HE, H., KOVAC, V. RIGAUD, M. and CHABRY, P. (1999). Oxidation behaviour of graphite materials usable in monolithic refractories, Advances in refractories for the metallurgical industries III, Quebec, Canada, 69-77.

89. GODA, K., TSUJI, Y. (1996). The effect of metal addition on carbon-containing castables, Taikabutsu Overseas, Vol. 16(4)

90. OUCHI, T., SASAKI, T. (1998). Development of a joint packing material containing surface-coated aluminium powder, Taikabutsu Overseas, Vol. 18 (4), 56

91. PEARLSTEIN, F., AGARWALA, V.S. (1994). Trivalent chromium solutions for applying chemical conversion coating to aluminium alloys or for sealing anodized aluminium, Plating and Surface Finishing, July, 50

92. ICHIKAWA, K., NISHIO, H. and HOSHIYAMA, Y. (1994). Oxidation test of MgO-C bricks, Taikabutsu Overseas, Vol. 14 (1), 13-19

93. GRIFFIN, D. J., LOEFFELHOLZ, M. D., MILLER T. G., (1991). Considerations for the measurement and improvement of oxidation resistance in dolomite-carbon and magnesia-carbon refractories. Proceedings of UNITECR'91, Sept. 23-26, Aachen, Germany, 253-256.

94. TSUCHIYA, I., TANAKA, S. and OGUCHI, Y. (1995). Effects of metallic additives on the oxidation-reduction reaction in MgO-C bricks under vaccum at elevated temperature. Proceedings of UNITECR'95, 156-163.

95. RIGAUD, M. and LI, X. (1996). Methods to characterize oxidation resistance for magnesia-carbon refractories, China's refractories, Vol.5 (3), 13-22.

96. HE, H. Q. (2000). Role of antioxidants in carbon-bonded refractories, Report for pre-doctoral examination, École Polytechnique de Montréal

97. SATOSHI, H. (1997). Techniques for evaluating carbon-containing refractories. Taikabutsu Overseas, Vol.17 (4), 23-30.

98. ZHOU, N. (2000). Elaboration of Al_2O_3-based graphite containing castables, Ph.D. Dissertation, Ecole Polytechnique de Montreal, August, 2000

99. PoreSizer 9320 system Manual book, 1991, Micromeritics

100. FUNK, J.E., and DINGER, D.R. (1994). Particle Size Control for High-Solids Castable Refractories. Am. Ceram. Soc. Bull., Vol. 73(10), 1994, 66-69.

101. MYHRE, B. and HUNDERE, A. M. (1996). The use of particle size distribution in development of refractory castables. the 25th ALAFAR Congress, San Carlos de Bariloche, Argentina, Dec. 1-4, 1996.

102. BJORN, M. (1996). Particle size distribution and its relavance in refractory castables, Elkem a/s Refractories.

103. ASTM C860-91 (1999): Practices for determining and measuring consistency of refractory concretes. Annual Book of ASTM Standards, Vol.15.01.

104. ASTM C830-93 (1999): Test methods for apparent porosity, liquid absorption, apparent specific gravity, and bulk density of refractory shapes by vacuum pressure. Annual Book of ASTM Standards, Vol.15.01.

105. ASTM C1407-98 (1999): Practice for calculating areas, volume and linear change of refractory shapes. Annual Book of ASTM Standards, Vol.15.01.

106. ASTM C133-97 (1999): Test methods for cold crushing strength and modulus of rupture of refractories. Annual Book of ASTM Standards, Vol.15.01.

107. HARMUTH, H. and TSCHEGG, E.K. (1997). A fracture mechanics approach for the development of refractory materials with reduced brittleness. Fatigue & Fracture of Engineering Materials & Structures, Vol. 20 (11), 1585-1603

108. PARANSKY, E., PALCO, S. and RIGAUD, M. (2001). Fracture testing of carbon-containing refractories. 2001 Steelmaking Conference Proceedings, 429-435

109. BALE, C. W. and PELTON, A. D. (1999). FACT Text book, École Polytechnique of Montréal

110. RYMON-LIPINSKI, T. (1994) The use of metal powders in carbon-containing refractories, Refractories for the Steel Industry, Elsevier Applied Science, 236-245

APPENDIX 1 WEDGE SPLITTING TEST

Wedge splitting tests has been performed on a variety of shaped refractories to evaluate fracture behaviour of the material. It enables stable crack propagation even for relatively large specimen dimensions that are necessary to eliminate the size effect [100]. It is schematically illustrated in Figure A1 and A2. In this set-up load transmission equipment consisting of a wedge, two roll bodies and two loads transmission pieces is inserted into the groove. For small angles of the wedge, the machine force F_M of the testing machine causes a far large horizontal force F_H of the splitting force acting to separate the specimen into two pieces. The WST tests were carried out on an Instron testing machine with a speed of 0.5mm/min during the loading.

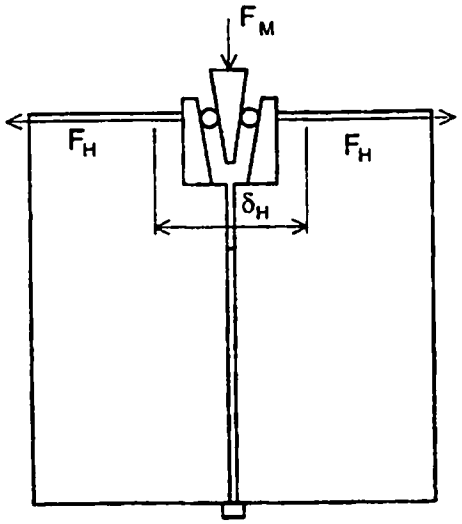

Figure A 1 Schematic view of the wedge-splitting tests set-up [100]

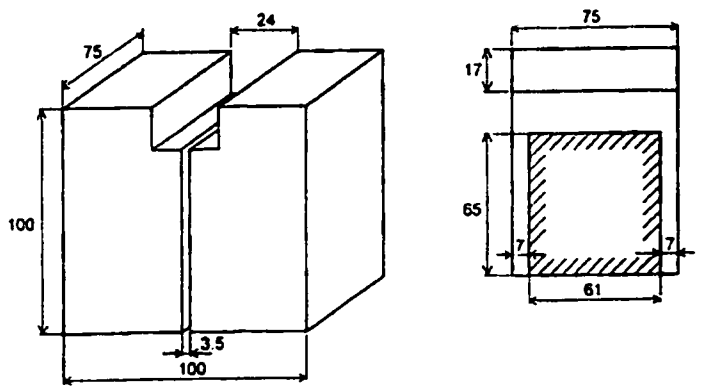

Figure A2 The specimen's shape and dimensions for WST [100]

The force F_H was calculated by [100]

$$F_H = F_M / (2\tan\frac{\beta}{2}), \text{ where } \beta \text{ is } 10^o \qquad (A.1)$$

Based on the recorded load-displacement curves for the specimen, work of fracture was calculated as follows [100, 101]:

$$\gamma_{wof} = \frac{\int_\delta F d\delta}{2A} \qquad (A.2)$$

where is $\int_\delta F d\delta$ the total area under the load-displacement curve, 2A is total projected fracture area. Modulus of elasticity was determined from the sloppy of the loading curve in the initial segment of CMOR tests. The thermal shock resistance parameter, R'''', is given as follows:

$$R'''' = (E. \gamma_{wof}) / \sigma_{max}^2 \qquad (A.3)$$

Where E is modulus of elasticity, σ_{max} is maximal fracture stress.